



Aalborg Universitet

AALBORG UNIVERSITY
DENMARK

Studies on Mobile Terminal Energy Consumption for LTE and Future 5G

Lauridsen, Mads

Publication date:
2015

Document Version
Peer reviewed version

[Link to publication from Aalborg University](#)

Citation for published version (APA):
Lauridsen, M. (2015). Studies on Mobile Terminal Energy Consumption for LTE and Future 5G. Department of Electronic Systems, Aalborg University.

General rights

Copyright and moral rights for the publications made accessible in the public portal are retained by the authors and/or other copyright owners and it is a condition of accessing publications that users recognise and abide by the legal requirements associated with these rights.

- ? Users may download and print one copy of any publication from the public portal for the purpose of private study or research.
- ? You may not further distribute the material or use it for any profit-making activity or commercial gain
- ? You may freely distribute the URL identifying the publication in the public portal ?

Take down policy

If you believe that this document breaches copyright please contact us at vbn@aub.aau.dk providing details, and we will remove access to the work immediately and investigate your claim.

Studies on Mobile Terminal Energy Consumption for LTE and Future 5G

Ph.D. Dissertation
Mads Lauridsen

Dissertation submitted November, 2014

Thesis submitted: November, 2014
PhD Supervisor: Prof. Preben Mogensen, Aalborg University
PhD Co-Supervisor: Assoc. Prof. Troels B. Sørensen, Aalborg University
PhD Committee: Senior Lecturer Simon M.D. Armour, University of Bristol
Prof. Frank Fitzek, Aalborg University (chairman)
Prof. Christian Wietfeld, Technische Universität Dortmund

Published papers:

- Reducing LTE Uplink Transmission Energy by Allocating Resources; **Lauridsen, M.**, Jensen, A. R. and Mogensen, P.; IEEE VTC Fall 2011
- Fast Control Channel Decoding for LTE UE Power Saving; **Lauridsen, M.**, Jensen, A. R. and Mogensen, P.; IEEE VTC Spring 2012
- LTE UE Power Consumption Model: For System Level Energy and Performance Optimization; Jensen, A. R., **Lauridsen, M.**, Mogensen, P., Sørensen, T. B. and Jensen, P.; IEEE VTC Fall 2012
- LTE UE Energy Saving by Applying Carrier Aggregation in a HetNet Scenario; **Lauridsen, M.**, Wang, H. and Mogensen, P.; IEEE VTC Spring 2013
- Empirical LTE Smartphone Power Model with DRX Operation for System Level Simulations; **Lauridsen, M.**, Noël, L. and Mogensen, P.; IEEE VTC Fall 2013
- An Empirical LTE Smartphone Power Model with a View to Energy Efficiency Evolution; **Lauridsen, M.**, Noël, L., Sørensen, T. B. and Mogensen, P.; Intel Technology Journal. 18, 1, p. 172-193, March 2014
- Ensuring Energy Efficient 5G User Equipment by Technology Evolution and Reuse; **Lauridsen, M.**, Berardinelli, G., Sørensen, T. B. and Mogensen, P.; IEEE VTC Spring 2014
- Centimeter-wave concept for 5G ultra-dense small cells; Mogensen, P., Pajukoski, K., Tiirola, E., Vihriälä, J., Lähetkangas, E., Berardinelli, G., Tavares, F. M. L., Mahmood, N. H., **Lauridsen, M.**, Catania, D. and Cattoni, A. F.; IEEE VTC Spring 2014
- An Efficient Rank Adaptation Algorithm for Cellular MIMO Systems with IRC Receivers; Mahmood, N.H., Berardinelli, G., Tavares, F.M.L., **Lauridsen, M.**, Mogensen, P., Pajukoski, K.; IEEE VTC Spring 2014
- LTE HetNet Mobility Performance Through Emulation with Commercial Smartphones; Jensen, A.R., Pedersen, K.I., Faaborg, J., **Lauridsen, M.**, Mogensen, P.; IEEE VTC Spring 2014
- Power-Consumption Measurements for LTE User Equipment: Keysight Application Note; **Lauridsen, M.**, June 2014 Keysight Technologies.
- Achieving low latency and energy consumption by 5G TDD mode optimization; Lähetkangas, E., Pajukoski, K., Vihriälä, J., Berardinelli, G., **Lauridsen, M.**, Tiirola, E. and Mogensen, P.; IEEE ICC 2014
- Current Consumption Measurements with a Carrier Aggregation Smartphone; Sanchez-Mejias, R., **Lauridsen, M.**, Guo, Y., Ángel Maestro Ruiz de Temino, L. and Mogensen, P.; IEEE VTC Fall 2014
- Deployment and Implementation Strategies for Massive MIMO in 5G; Panzner, B., Zirwas, W., Dierks, S., **Lauridsen, M.**, Mogensen, P., Pajukoski, K. and Miao, D.; IEEE GLOBECOM 2014

During the PhD study 3 patent applications have been filed and another 3 have been drafted.

© Copyright by Mads Lauridsen

This thesis has been submitted for assessment in partial fulfilment of the PhD degree. The thesis is based on the submitted or published scientific papers which are listed above. Parts of the papers are used directly or indirectly in the extended summary of the thesis. As part of the assessment, co-author statements have been made available to the assessment committee and are also available at the Faculty. The thesis is not in its present form acceptable for open publication but only in limited and closed circulation as copyright may not be ensured.

Abstract

Smartphones have become an essential device for many, but they are limited by short battery life due to high data rates, big displays, and diverse applications. In this study we examine how to improve the battery life by optimizing the smartphone's cellular subsystem, as well as the cellular network, without compromising performance.

At the start of this study in 2010 there were no cellular subsystem power consumption models available for the newly introduced 3GPP Long Term Evolution (LTE) standard. Therefore an LTE model, based on power consumption measurements on commercial smartphones, has been established. The model depends on receive and transmit power and data rates, and shows that the cellular subsystem being ON and transmit powers above 10 dBm are the primary power consumers, while high data rates are more than 10 times more energy efficient than low data rates in LTE. The Discontinuous Reception (DRX) method is included in the model and is shown to provide significant energy savings due to low-power sleep mode. However, improvements are needed in the time period between entering and leaving the sleep mode. The model, with amendments and updates since its first publication in 2012, has proved useful for both academia and industry.

In this study we use the model to propose an uplink resource allocation scheme, where a TDMA-like scheduling is preferred, and to develop the micro sleep concept, which targets the LTE control-data frame structure that leads to unnecessary buffering for unscheduled users. The model is expanded to Carrier Aggregation, which we demonstrate to be an energy saving feature for high data rate applications, and this has been confirmed by our later measurements on commercial smartphones.

The second part of this study deals with the design of a future Fifth Generation (5G) Radio Access Technology. It targets 10 Gb/s peak data rate, 1 ms latency, and flexible uplink/downlink by use of advanced Multiple Input Multiple Output receivers in an Ultra-Dense Small Cell, high bandwidth, Centimeter Waves network. We examine selected features such as Time Division Duplexing, control-data structure, and Orthogonal Frequency Division Multiplexing to determine if and how they improve the energy efficiency. We also simulate how 5G DRX due to a short, optimized frame improves the battery life 5-15 times as compared to LTE DRX.

With respect to the feasibility of 5G we study how the increased bandwidth, dynamic range, data rate, and number of Radio Frequency components affect the power consumption, and how the performance of the components evolves over time. This results in a performance and power consumption forecast for 2020 and 2030, which predicts that the hardware will be able to handle the 5G requirements. However, we identify

the following to be key challenges; baseband processor power consumption due to the higher data rate, coexistence issues due to the use of multiple carriers to achieve sufficient bandwidth, and low Power Amplifier efficiency at high carrier frequencies. Finally we propose an event-based pre-paging method for 5G, which allows mobile terminals to power down the main receiver, and listen for pre-paging signals from other nodes via simple, low-power hardware.

Resumé

Smartphones er blevet en uundværlig enhed for mange, men de er begrænset af kort batteritid pga. høje datahastigheder, store skærme og forskelligartede applikationer. I dette studie undersøger vi, hvordan batteritiden kan forbedres ved at optimere smartphonens mobiltelefoni-delsystem såvel som det mobile netværk uden at kompromitere ydeevnen.

Da dette studie blev indledt i 2010 var der ingen effektforbrugsmodel for mobiltelefoni-delsystemet for den nyligt introducerede 3GPP LTE standard. Derfor er der etableret en LTE model baseret på effektforbrugsmålinger på kommercielle smartphones. Modellen afhænger af modtage- og sendeeffekt og datahastigheder, og viser at de primære effektforbrugere er det at delsystemet er tændt og sendeeffekter over 10 dBm, hvorimod høje datahastigheder er mere end 10 gange så energieffektive sammenlignet med lave hastigheder i LTE. DRX metoden er inkluderet i modellen, og det er vist, at den medfører signifikante energibesparelser pga. en lav-effekts dvaletilstand. Dog er det nødvendigt med forbedringer i den tidsperiode, der er imellem indgang og udgang af dvaletilstanden. Modellen, som har fået tilføjelser og opdateringer siden første publikation i 2012, har vist sig at være brugbar for både den akademiske verden og industrien.

I dette studie bruger vi modellen til at foreslå en resource-allokerings-mekanisme, hvor en TDMA-lignende metode foretrækkes, og til at udvikle et mikrodvale-koncept, som er målrettet LTE's kontrol-data rammestruktur, der leder til unødvendig lagring af data for brugere, der ikke er skeduleret. Modellen er udvidet til CA, som vi viser er en energibesparende egenskab for applikationer med høje datahastigheder. Dette er senere bekræftet vha. vores målinger på kommercielle smartphones.

Den anden del af studiet omhandler design af et fremtidigt 5G mobiltelefonsystem. Systemet sigter efter 10 Gb/s tophastigheder, 1 ms forsinkelse og fleksibel uplink & downlink vha. avancerede MIMO modtagere i et UDSC, høj båndbredde, CmW netværk. Vi undersøger udvalgte egenskaber som TDD, kontrol-data struktur og OFDM for at afgøre om og hvordan de kan forbedre energieffektiviteten. Vi simulerer også, hvordan 5G DRX pga. en kort og optimeret rammestruktur forbedrer batteritiden 5-15 gange i forhold til LTE DRX.

Mht. gennemførligheden af 5G undersøger vi, hvordan den øgede båndbredde, dynamiske rækkevide, datahastighed og antal RF komponenter påvirker effektforbruget, og hvordan komponenternes ydeevne udvikler sig over tid. Dette resulterer i en forudsigtelse af ydeevnen og effektforbruget i 2020 og 2030 om at hardwaren kan håndtere 5G kravene. Dog identificerer vi følgende hovedudfordringer: baseband processor effektforbrug pga. højere datahastigheder, problemer med sameksistens pga. brugen af flere bærere til

at opnå tilstrækkelig båndbredde, og lav effektivitet for effektforstærkeren ved høje frekvenser. Til slut foreslår vi en eventbaseret pre-paging metode til 5G, som tillader enhederne at slukke deres hovedmodtager og lytte efter pre-paging signaler fra andre enheder vha. simpel laveffekt hardware.

Contents

Abstract	iii
Resumé	v
Preface	xi
List of Abbreviations	xiii
1 Introduction	1
1.1 Power versus Energy	7
1.2 Research Questions	8
1.3 Applied Methods	9
1.4 Thesis Outline	10
2 System Level Analysis of Power Consumption in LTE User Equipment	15
2.1 Power Modelling	16
2.2 Paper Contributions	23
2.3 The LTE Smartphone Power Consumption Model	24
2.4 Measurement Method & Setup	27
2.5 Selected Power Consumption Results	30
2.5.1 Discontinuous Reception Measurement Results	33
2.6 Summary	37
3 Energy Saving in LTE User Equipment	39
3.1 Paper Contributions	40
3.2 Fast Control Channel Decoding	41
3.3 Energy Saving by Uplink Scheduling	46
3.4 Carrier Aggregation Energy Saving	51
3.5 Measurements on Carrier Aggregation Power Consumption	54
3.6 Summary	56
4 Fifth Generation Radio Access Technology	59
4.1 Duplexing	62
4.2 Bandwidth & Carrier Frequency	64
4.3 Waveform and Multiple Access scheme	65

4.4	Frame Structure	68
4.5	Multiple Antennas and Advanced Receivers	72
4.6	Sleep mode	74
4.7	LTE-like Features	77
4.8	Summary	78
5	Power Consumption Challenges in 5G	81
5.1	Analog RF Evolution	82
5.2	ADC Evolution	92
5.3	Digital Processing Evolution	96
5.4	Estimation of Receiver Power Consumption	100
5.5	Notes on Transmission	104
5.6	Summary	106
6	DRX and Aperiodic Sleep Modes in 5G	109
6.1	Examples of 5G User Scenarios	109
6.1.1	Video Streaming	110
6.1.2	Machine Type Communications	113
6.2	DRX in 5G	115
6.3	Event Based Pre-Paging Concept	126
6.4	Summary	134
7	Conclusion	135
7.1	System Level Analysis of Power Consumption in LTE User Equipment	135
7.2	Energy Saving in LTE User Equipment	136
7.3	Fifth Generation Radio Access Technology	136
7.4	Power Consumption Challenges in 5G	137
7.5	DRX and Aperiodic Sleep Modes in 5G	137
7.6	Main Conclusion	137
7.7	Future Work	138
	Bibliography	139
A	Smartphone Details	157
B	Power-Consumption Measurements for LTE User Equipment	159
C	LNA Survey Details	169
D	Limited Functionality Mode Concept	187
E	LTE UE Power Consumption Model - For System Level Energy and Performance Optimization	197
E.1	Introduction	199
E.2	UE Model Design	200
E.3	LTE UE Measurements	201
E.4	Model Fitting	204

E.5	Verification	206
E.6	Discussion	208
E.7	Conclusion	209
F	Empirical LTE Smartphone Power Model with DRX Operation for System Level Simulations	211
F.1	Introduction	213
F.2	Design of the Smartphone Power Model	214
F.3	Conducted Smartphone Measurements	216
F.4	The Smartphone Power Consumption Model	222
F.5	Discussion	223
F.6	Conclusion	224
G	An Empirical LTE Smartphone Power Model with a View to Energy Efficiency Evolution	227
H	Fast Control Channel Decoding for LTE UE Power Saving	251
H.1	Introduction	253
H.2	Applying FCCD to Save Energy	254
H.3	Simulation Results	260
H.4	Verification	261
H.5	Conclusion	262
I	Reducing LTE Uplink Transmission Energy by Allocating Resources	265
I.1	Introduction	267
I.2	Simulation Results	271
I.3	Conclusion	276
J	LTE UE Energy Saving by Applying Carrier Aggregation in a HetNet Scenario	279
J.1	Introduction	281
J.2	Downlink CA UE Power Model Design	281
J.3	The HetNet Scenario	284
J.4	Simulation Assumptions and Energy Consumption Results	285
J.5	Energy Break-Even	290
J.6	Conclusion	290
K	Current Consumption Measurements with a Carrier Aggregation Smartphone	293
K.1	Introduction	295
K.2	Carrier Aggregation in LTE	296
K.3	Measurement Setup	297
K.4	Measurement Results	299
K.5	Discussion	303
K.6	Conclusion	304

L	Ensuring Energy Efficient 5G User Equipment by Technology Evolution and Reuse	307
L.1	Introduction	309
L.2	Energy Efficiency of existing RATs	310
L.3	Recommendations for EE 5G	317
L.4	Conclusions and future work	320

Preface

This PhD thesis is the outcome of the research I have performed since summer 2010 in the Radio Access Technology Section, now the Wireless Communication Networks Section, at the Department of Electronic Systems, Aalborg University, Denmark. The work was carried out in parallel with the mandatory courses required to obtain the PhD degree.

The PhD study was made under the supervision of Professor Preben Mogensen and co-supervised by Associate Professor Troels B. Sørensen. The study was financially supported by the Fourth Generation Mobile Communication and Test Platform (4GMCT) project, which is a collaboration between Aalborg University, Keysight Technologies (former Agilent Technologies), and Intel Mobile Communications (former Infineon Technologies). The project was partly funded by the Danish National Advanced Technology Foundation and was conducted from Fall 2009 to Fall 2014.

In this thesis the power consumption of the cellular subsystem in Long Term Evolution User Equipment is measured and modelled, and the obtained knowledge is used to propose energy optimizations for Long Term Evolution and for a future Fifth Generation Radio Access Technology. In addition the power consumption of a future Fifth Generation mobile terminal is estimated. Due to the focus on multiple mobile communication systems the reader is expected to be familiar with the basics of Long Term Evolution, Radio Access Technology features for the PHY and MAC layers, and cellular subsystem design.

I would like to express my gratitude to my supervisors for their guidance and assistance in developing and interpreting concepts and results, and in writing papers. My weekly Friday meeting with Preben has always left me with something new to think about, not always technical but always thought-provoking.

Initially the topic of my PhD study was to emulate drive tests in the lab, but after a long and painfully slow period of analysis Preben and I fortunately decided it was time to shift focus. We decided to study the power consumption of smartphones, something I had definitely not expected and was not prepared for, and after another lengthy period we finally got on track. I have an M.Sc.EE in Applied Signal Processing and Implementation and thus the world of Wireless Communication was new to me, but after 5 years in this position I have gained useful technical knowledge in the area and a much stronger ability to perform research and disseminate my knowledge.

During the project both Preben and I sometimes had to admit that we were approaching areas out of our expertise, and therefore I am grateful for the opportunities

I have had to discuss methodologies and technologies with the project partners at Intel and Keysight, especially Janus Faaborg who has always been a great facilitator for my measurements. I am also grateful for the discussions with Stacy Ho of Mediatek; RFMD in Aalborg; and last but not least colleagues in Nokia Networks in Aalborg, Munich, Oulu, and Irving. Many thanks to Frank Frederiksen of Nokia Networks for always being prepared to discuss new ideas and the most detailed subclauses of a 3GPP standard, and for teaching me about the world of patents. I would also like to thank my colleagues Hua Wang and Huan Cong Nguyen for reading parts of the thesis and provide useful comments.

Now is the time to extend a very special thank you to a person I have never met; Laurent Noël of Vidéotron, Canada. Laurent contacted me via e-mail in January 2012 and offered his generous help because I had applied a WCDMA measurement of his in my very first article. Since then we have been in regular e-mail contact, exchanging ideas on how to measure and analyse power consumption, and Laurent with his background in cellular subsystem design has been an invaluable help. In addition his employment at the Canadian mobile operator Vidéotron has allowed him to measure the power consumption of the state of the art smartphones and share it with me such that we in collaboration have been able to update the power model, which judging from about 20 combined citations and more than 2800 downloads from the university database and IEEE is useful to our colleagues in academia and industry.

I would also like to thank my friends and colleagues in the old Radio Access Technology Section, and my friends and former fellow students now spread across the Department of Electronic Systems and Denmark. You have all contributed to a good working environment that has made me enjoy these years of the PhD study. For some years I shared an office with Anders R. Jensen and I learned a lot from the discussions we had on measurements and energy saving.

Finally I would like to thank my family for always being supportive and showing interest no matter what I do. Without you this PhD study would not have been completed.

To conclude this preface I would like to state that I believe my work affected the 5G concept design such that it can become an energy efficient Radio Access Technology, providing improvements as compared to previous generations and thus improve the user experience. We will however not know if this is true before 2020!



Mads Lauridsen
Aalborg University, November 2014

List of Abbreviations

16QAM 16 Quadrature Amplitude Modulation

256QAM 256 Quadrature Amplitude Modulation

3GPP Third Generation Partnership Project

5G Fifth Generation

64QAM 64 Quadrature Amplitude Modulation

ACK Acknowledgement

ACLR Adjacent Channel Leakage Ratio

ADC Analog-to-Digital Converter

AGC Automatic Gain Control

AP Access Point

APT Average Power Tracking

ARQ Automatic Repeat Request

AS Access Stratum

BB Base Band

BLER Block Error Rate

BT Bluetooth

CA Carrier Aggregation

CC Component Carrier

CCE Control Channel Element

CDMA Code Division Multiple Access

CMOS Complementary Metal–Oxide–Semiconductor

cmW Centimeter Waves

CP	Cyclic Prefix
CPU	Central Processing Unit
CRC	Cyclic Redundancy Check
CSI	Channel State Information
CW	Code Word
D2D	Device-to-Device
DAC	Digital-to-Analog Converter
DCH	Dedicated Channel
DCI	Downlink Control Information
DFT	Discrete Fourier Transform
DFT-s-OFDM	Discrete Fourier Transform spread OFDM
DMRS	DeModulation Reference Symbol
DRX	Discontinuous Reception
DRX LP	DRX Long Period
DTX	Discontinuous Transmission
DUT	Device Under Test
DwPTS	Downlink Pilot Timeslot
EE	Energy Efficiency
eNB	Evolved Node B
ENOB	Effective Number of Bits
EPDCCH	Enhanced Physical Downlink Control Channel
ET	Envelope Tracking
EVM	Error Vector Magnitude
FACH	Forward Access Channel
FBMC	Filter Bank Multi Carrier
FDD	Frequency Division Duplexing
FDMA	Frequency Division Multiple Access
FEC	Forward Error-Correcting Code

- FFT** Fast Fourier Transform
- FoM** Figure of Merit
- FPC** Fractional Power Control
- FTP** File Transfer Protocol
- GMSK** Gaussian filtered Minimum Shift Keying
- GP** Guard Period
- GPS** Global Positioning System
- GSM** Global System for Mobile Communications
- HARQ** Hybrid Automatic Repeat Request
- HetNet** Heterogeneous Network
- HS-DSCH** High-Speed Downlink Shared Channel
- HS-SCCH** High-Speed Shared Control Channel
- HSPA+** Evolved High-Speed Packet Access
- IC** Integrated Circuit
- ICIC** InterCell Interference Coordination
- ICT** Information and Communications Technology
- IP3** Third-Order Intercept Point
- IRC** Interference Rejection Combining
- ITU** International Telecommunication Union
- KPI** Key Performance Indicator
- LNA** Low Noise Amplifier
- LOS** Line of Sight
- LTE** Long Term Evolution
- LTE-A** Long Term Evolution Advanced
- MA** Multiple Access
- MCS** Modulation and Coding Scheme
- MIMO** Multiple Input Multiple Output
- MIPS** Million Instructions Per Second

MME	Mobility Management Entity
mmW	Milimeter Waves
MNO	Mobile Network Operator
MRC	Maximum Ratio Combining
MTC	Machine Type Communication
NACK	Negative Acknowledgement
NAS	Non-Access Stratum
NF	Noise Figure
NLOS	Non-Line of Sight
OBO	Output Back-Off
OFDM	Orthogonal Frequency Division Multiplexing
OFDMA	Orthogonal Frequency Division Multiple Access
OOB	Out-of-Band
OOK	On-Off-Keying
OS	Operating System
OTA	Over-the-Air
PA	Power Amplifier
PAPR	Peak-to-Average-Power Ratio
PBCH	Physical Broadcast Channel
PC	Personal Computer
PCell	Primary Cell
PCFICH	Physical Control Format Indicator Channel
PCH	Paging Channel
PDCCH	Physical Downlink Control Channel
PDSCH	Physical Downlink Shared Channel
PGC	Programmable Gain Control
PMU	Power Management Unit
PRB	Physical Resource Block

PSS	Primary Synchronization Signal
PUCCH	Physical Uplink Control Channel
PUSCH	Physical Uplink Shared Channel
QoS	Quality of Service
QPSK	Quadrature Phase-Shift Keying
RAT	Radio Access Technology
RE	Resource Element
REG	Resource Element Group
RF	Radio Frequency
RNTI	Radio Network Temporary Identifier
RRC	Radio Resource Control
RRH	Remote Radio Heads
RS	Reference Signal
RTT	Round Trip Time
Rx	Receive
SC FDMA	Single Carrier FDMA
SCell	Secondary Cell
SIC	Successive Interference Cancellation
SIM	Subscriber Identity Module
SINR	Signal to Interference + Noise Ratio
SNDR	Signal to Noise and Distortion Ratio
SNR	Signal to Noise Ratio
SSS	Secondary Synchronization Signal
TCP	Transmission Control Protocol
TDD	Time Division Duplexing
TDMA	Time Division Multiple Access
TPC	Transmit Power Control
TTI	Transmission Time Interval

Tx Transmit

UDSC Ultra-Dense Small Cell

UE User Equipment

UpPTS Uplink Pilot Timeslot

V2V Vehicle-to-Vehicle

VCO Voltage Controlled Oscillator

WCDMA Wideband Code Division Multiple Access

WuRx Wake up Receiver

ZT DFT-s-OFDM Zero-Tail Discrete Fourier Transform spread OFDM

Chapter 1

Introduction

When Gartner in 2007 noted [1] that the Information and Communications Technology (ICT) sector accounted for 2 % of the worlds CO₂ emissions it led to numerous research projects in academia and amongst equipment vendors to limit the energy consumption. Furthermore the International Telecommunication Union's Study Group number 5 under the Telecommunication Standardization Sector started focusing on the environment and climate change in the following study period (2009-2012 and onwards) [2].

One example of the research projects is the founding of the Centre for Energy-Efficient Telecommunications at the University of Melbourne which together with Alcatel-Lucent have projected that the ICT sector will comprise 5 to 15 % of the world's energy consumption in 2025 depending on the improvement in equipment energy efficiency [3]. The GreenTouch consortium [4], which is constituted by both ICT industry partners and academia, predicts the ICT CO₂ emissions will double from 2010 to 2020 and account for about 4 %. There is great uncertainty in terms of the amount of CO₂ generated by ICT partly due to difficulty to assess

- the possible improvements in equipment energy efficiency
- the number of ICT users
- what type of ICT equipment will be used
- the amount of data to be transferred
- the energy consumption of transferring data and other ICT tasks

Therefore the European Commission has initiated a project with 27 industry partners to determine a unified methodology for measuring the ICT sector's CO₂ emission [5]. Even without the unified methodology it is however clear that all parts of the ICT sector must improve. Figure 1.1 shows an estimate of the CO₂ emission contribution by certain subsectors of ICT. The mobile telecommunication was a rather small component (9 %) when the data was published in 2007, [6] but this may change as the number of mobile phones and the amount of data transferred continues to increase. For example Cisco [7] has predicted the mobile data traffic will increase 11-fold from 2013 to 2018 while the number of devices will exceed 10 billions in 2018. In addition Ericsson has published a report [8], predicting the ICT electricity consumption increases 60 % from 2007 to 2020 due to the aforementioned increasing device count and network expansion. The data is

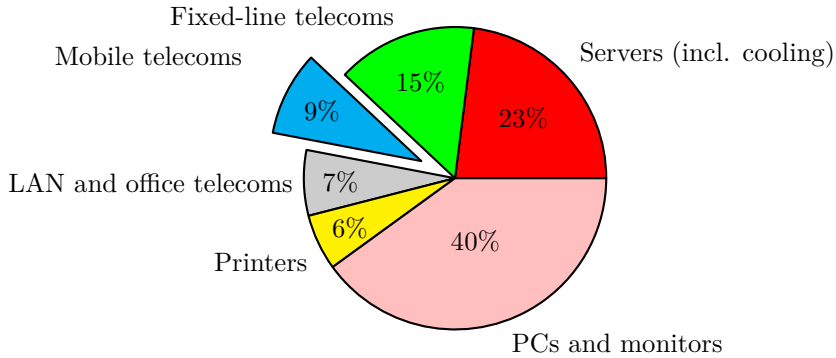


Figure 1.1: Distribution of ICT CO₂ emissions. Based on [6].

shown in figure 1.2. The figure illustrates that the mobile telecommunication, which in

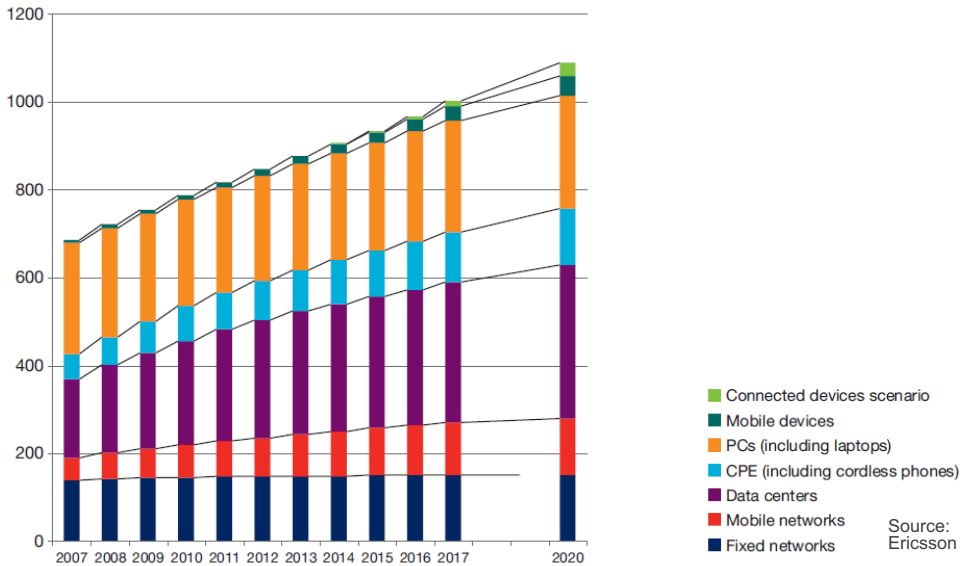


Figure 1.2: Electricity consumption in TWh. The data covers the electricity consumed while operating the equipment i.e. the power required to manufacture it is not included. [8, Edited Figure 10].

the figure is split into devices and networks, will have an increasing influence from 2007 to 2020 especially because the number of connected devices increases. Even though the total share is only about 10% it is important to **reduce the CO₂ emissions caused by mobile networks and devices**, and that is the starting point for this thesis. Many researchers have already examined the mobile network power consumption, one example being the work by Micallef [9]. Because this work is partly funded by the mobile chipset manufacturer Intel Mobile Communications and the mobile device measurement vendor Keysight Technologies the scope is **limited to mobile devices**.

According to Gartner [10] the smartphone sales share (51.8%) exceeded the share of feature phones (48.3%) for the first time in the second quarter of year 2013. The total number of sold smartphones in the second quarter was 225 million, an increase of 46.5% compared to the same quarter in 2012. In the third quarter of 2013 [11] the number had increased to 250.2 million (a 54.9% share) and it is not expected to decrease. Because of the smartphones' increasing market share the thesis' focus is **limited to smartphones** and not the basic and feature phones. Another reason for this limitation is that in a survey by Qualcomm [12] in 2013 60% of the consumers stated battery life was the most requested smartphone feature to be improved, while another smartphone satisfaction survey by J.D. Power and Associates [13] showed battery performance was the attribute with the lowest rating. Furthermore the survey indicated that the Long Term Evolution (LTE) users were more dissatisfied than 3G users, and that the satisfaction with smartphone's battery life before a recharge is needed has not improved from year 2007 to 2012. The fact that the LTE networks were scarcely deployed, when the survey was made, has some effect on the battery life due to poorer downlink reception power and higher uplink transmit power, but the smartphones' bigger display, faster processor, higher throughput and more diverse applications leading to increased usage certainly also affect the battery life negatively [14]. Therefore this thesis will focus on **the energy consumption of smartphones**.

The smartphones' high energy consumption is a problem for

- the owner of the smartphone because of the short battery life
- the manufacturer because the dissatisfied user may not choose the same smartphone brand again
- the network operator because the user may generate less traffic to save power
- the environment because charging is equivalent with CO₂ emission

The issue can in general terms be improved either by increasing the available battery capacity or by reducing the power consumption. A third method is to harvest energy, [15], from the surroundings for example by use of kinetic or solar elements. The latter method is however not examined in further detail in this work.

The battery capacity evolution for four well-known series of smartphones is illustrated in figure 1.3. The data used to generate the plots is presented in appendix A. The trends for the Google, Nokia, and Samsung smartphones are very similar: with every new generation of the smartphone series the battery capacity increases 10-20%, while the Apple smartphones' battery capacity evolve at a slower pace.

The increased battery capacity could be expected to have a positive effect on the users satisfaction level, but as stated previously surveys [12, 13] have shown this has not been the case. During the same period of time the smartphones' screen size has also increased, as the printed numbers illustrate in figure 1.3. This may be one reason why the increased battery capacity has not improved the battery life. The increased screen size is often related with an increase in screen resolution, which Qualcomm has noted to increase $\sim 25x$ from 2006 to 2012 [12], and this entails increased graphic processing requirements leading to higher power consumption [16, 17]. Furthermore the users now tend to perform many more activities (75%) such as web browsing, gaming, and video streaming, where the screen is ON as opposed to old-fashioned telephone calls (25%) where the screen may be OFF [14, Chapter 14].

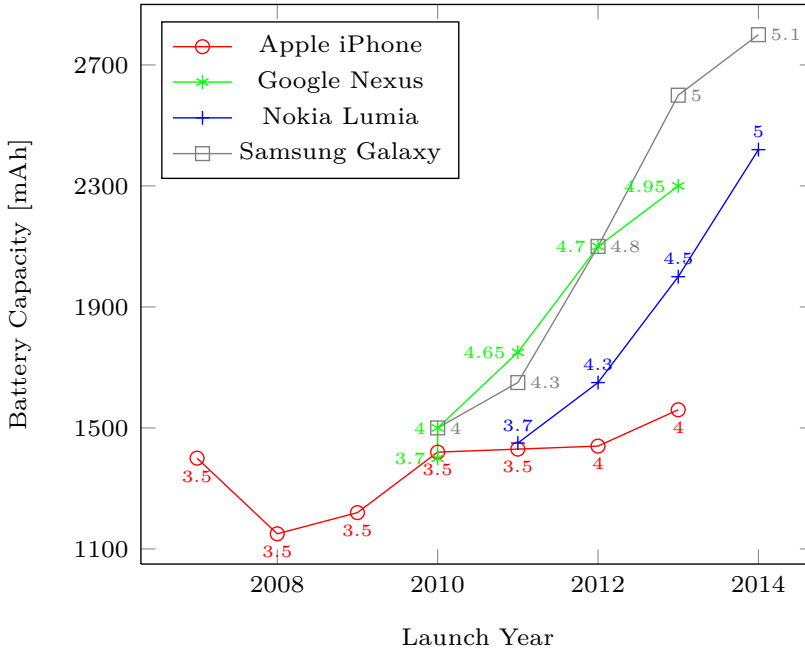


Figure 1.3: Battery capacity and screen size evolution for selected smartphone series. The printed numbers are the screen sizes in inches.

The increased screen size obviously entails the smartphone's physical dimensions also increase, and this may be one of the reasons why the battery capacity has improved in addition to the energy density of the battery itself. The average annual improvement of energy storage density has only been in the order of 3% for more than 100 years, [18], while Li-Ion batteries have improved 4.5-5% [19, 20] the last 20 years and almost 7% according to [21]. To examine this hypothesis figure 1.4 shows the battery capacity normalized with the screen area. The area is used under the assumption that the batteries' width do not vary much, and because the volume metric was not available for all the examined smartphones. The figure shows that there is very little improvement in the energy density, and therefore the conclusion is that the battery evolution is not sufficient to improve the user satisfaction.

The other approach to improve battery life is to lower the power or energy consumption of the smartphone, and this is the main research area for this study. When optimizing the battery life, by reducing the power consumption, it is important to be aware of the user experience in terms of performance such as download data rate and application speed. The performance cannot degrade significantly because it is also one of the top requirements of users [12]. Thus the study must examine the trade-off between perceived user experience and battery life.

A modern smartphone is not just a combination of the cellular subsystem, connecting the device to the network, and an interface towards the user. Today the smartphone can instead be considered to be a mobile Personal Computer (PC), which has multiple wireless connections to the internet, an application processor, a graphics processor, an

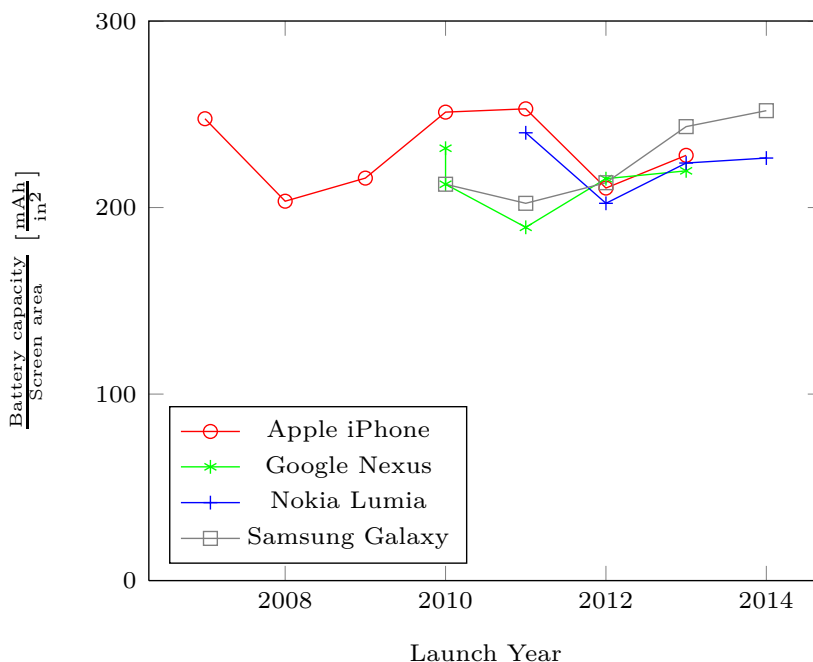


Figure 1.4: Energy density metric based on battery capacity evolution normalized to screen area for selected smartphone series.

audio codec, various types of memory, and an interface towards the human user as illustrated in figure 1.5.

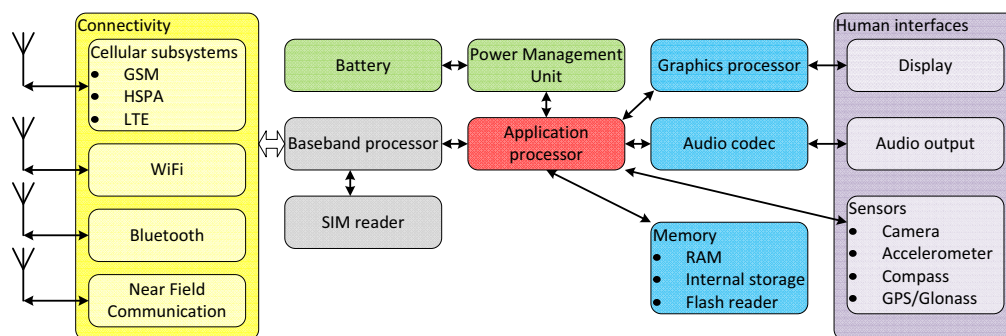


Figure 1.5: Typical smartphone components.

Therefore the optimization for low power consumption can be performed on multiple layers as described in table 1.1. On the *Application* layer power can be saved if the smartphone's performance is adjusted to the current needs of the running applications. For example the clock speed of the Central Processing Unit (CPU) can be adjusted as in a normal desktop CPU.

On the *Transport* layer it may be possible to combine data packets from multiple appli-

Table 1.1: Power optimization options on different telecommunication layers. The layers are based on [22].

Layer	Optimization
Application	Adjust display brightness, CPU speed etc. to what the application requires
Transport Network	Combine data from multiple applications into one transfer Ensure low overhead
Physical + data link	Adjust network-controlled parameters such as scheduling and transmit power control Use low power components Apply power management

cations/protocols on the upper layer into one. In this way the smartphone only needs to carry out one data transfer even though the data has multiple end points. One example is [23] where the authors show energy savings of up to 43 % by bundling multiple Instant Messaging transmissions into one packet, where the cost is an increased transfer delay. The *network* layer is also known as the internet layer, and it is taking caring of routing packets. This layer basically consists of the Internet Protocol and there are no obvious techniques to optimize the smartphone’s energy consumption for this protocol besides efficient use of header information and acknowledgements, and fast routing in the core network.

The final layers are the *physical and data link* layers. Considering the latter it is important that the Radio Access Technology (RAT) is setup to ensure low power consumption. This could for example imply the use of an energy aware scheduler and Transmit Power Control (TPC). On the physical layer the smartphone’s instantaneous power consumption is directly related to the hardware components comprising the smartphone. Savings can for example be achieved by using the lowest possible Complementary Metal–Oxide–Semiconductor (CMOS) technology node, because switched capacity and short-circuit power decreases while the leakage power increases with decreasing technology node [24, Chapter 38]. Choice of Transmit Power Amplifier (PA), display size and technology and so forth will also have a major effect. Finally it is important to have a Power Management Unit (PMU) which makes sure to power OFF unused components and scale the performance of the components, which are currently ON. In this work the focus is therefore on **physical and data link layers**.

Before the research questions for this PhD study is defined it is necessary to define the parameter to optimize: lower power consumption, lower energy consumption or a combination of both.

1.1 Power versus Energy

A battery is usually stated to have a certain capacity in Ampere-Hours at a specific supply voltage. Hence it contains energy:

$$U \cdot I \cdot t = P \cdot t = E \quad [\text{J}] \tag{1.1}$$

where: U is the battery supply voltage [V]
 I is the current drawn from the battery [A]
 t is the time of use [s]
 P is the instantaneous power drawn from the battery [W]
 E is the energy drawn from the battery [J]

Given the battery’s specifications the first thing the designer will need to ensure is that the amount of current drawn by the smartphone does not exceed a certain limit defined by the battery’s internal resistance. If the current is too high it may entail a battery voltage drop, which may cause the PMU to power down the smartphone to prevent unexpected behaviour. The current draw is typically at its peak when many components are powered ON at once, and therefore the PMU can apply a power-ON-sequence [16]. Provided that this fundamental requirement is fulfilled the designer can start optimizing the components to achieve longer battery life.

The instantaneous power consumption is important to keep at a minimum, both to avoid the battery voltage drop and to improve the battery life. However it may sometimes be beneficial to accept a high instantaneous power consumption if it entails the ON time of the User Equipment (UE) is reduced. The increased OFF time may then be substituted with a low-power sleep mode. This will for example be the case if a single data transfer is scheduled. Figure 1.6a illustrates the case where the power consumption scales 1:1 with the data rate and the area of each block corresponds to the total energy consumption required to transfer the specific amount of data. In this case the total energy consumption and the number of bits transferred is the same whether the data rate is low and the transfer time is long or the data rate is high and the transfer time is short. However a more realistic case is depicted in figure 1.6b, where the double data

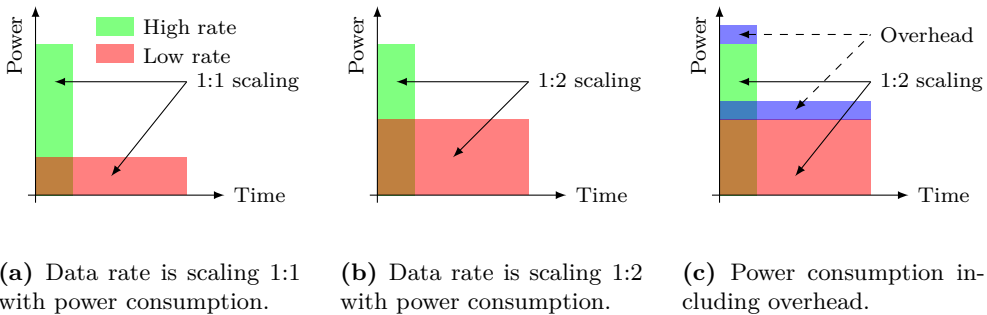


Figure 1.6: Power consumption as a function of data rate scaling. Note the same amount of bits is transferred in each case.

rate does not entail a doubling of the power consumption. The reason is that there will be a certain *base* power consumption due to the data rate-independent components being on, for example the Radio Frequency (RF) front end. Furthermore if the data transfer is related to a user browsing a web page there may be an additional overhead, which for example includes the display being ON. If the page is loaded faster the user will also turn OFF the display faster. This is illustrated in figure 1.6c.

To summarize figure 1.6 illustrates it is important not only to optimize for low power consumption, but also low energy consumption, because the method to achieve the latter may be to increase the first. Otherwise the smartphone may have with low power consumption, but also low performance and therefore also short battery life due to increased ON time. For this chain of arguments to be valid the smartphone will obviously need to enter a very low power mode when it has finished the data transfer. One important metric, which relates the instantaneous power consumption to a data transfer is the Energy Efficiency (EE), which is defined as:

$$EE = \frac{R}{P} = \frac{b}{P \cdot t} \quad \left[\frac{\text{bit}}{\text{J}} \right] \quad (1.2)$$

where: EE is the energy efficiency [J/bit]
 R is the data rate [bit/s]
 P is the power consumption [W]
 t is the time to transfer [s]
 b is the number of bits transfered [bit]

Comparing figures 1.6a and 1.6b it is clear that the EE is constant for 1.6a while it increases for increasing data rate in 1.6b.

1.2 Research Questions

Based on the discussion in the previous sections the thesis' focus is the smartphone's short battery life, and more specifically how the energy consumption can be reduced to improve the user experience. The scope limitation is illustrated in figure 1.7. This has

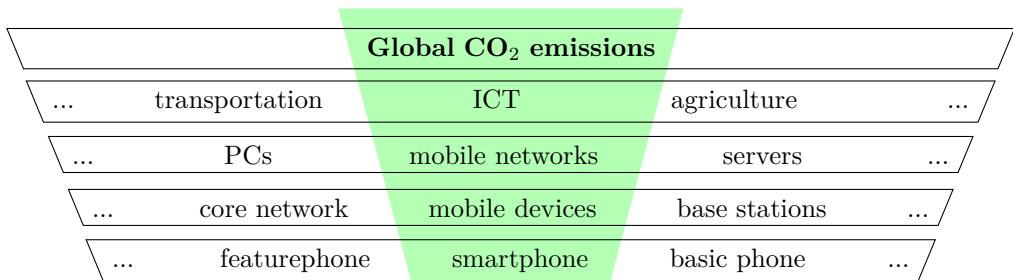


Figure 1.7: The thesis' scope (marked with green color).

lead to the following research questions:

1. What is the power consumption of an LTE smartphone's components?
To determine how to save energy in the smartphone it is necessary to identify the most power consuming components (illustrated in figure 1.5)
2. How can the power consumption of an LTE smartphone be reduced while maintaining the performance?
Improving the battery life should not affect the user experience and therefore it is important to maintain the performance of the smartphone.
3. How can a future Fifth Generation (5G) RAT be designed to significantly improve the mobile terminal battery life as compared to current RAT generations?
Ideas & suggestions for a future RAT should be based on what was learned when answering questions 1 & 2

The latter question is included because research on a future 5G RAT is ramping up and targeting deployment around 2020. By analysing and answering questions 1 & 2 it will be possible to provide input on which mobile terminal and RAT features 5G must re-use, replace and update to ensure the battery life. The term mobile terminal and Access Point is used for 5G because the nomenclature is not yet defined as opposed to the use of UE and Evolved Node B in the standardized language of LTE.

In addition the 5G also targets to include Machine Type Communication (MTC) devices, which also require long battery life, and therefore the smartphone term does not cover the target of research question 3.

1.3 Applied Methods

There are multiple methods available for analysing the aforementioned research questions including a theoretical analysis possibly based on a mathematical model, Monte Carlo simulations where random values are used in repeated computer simulations to obtain a numerical value, deterministic modelling where simulation parameters are assigned specific values and the computer simulation is used to obtain a numerical value, and empirical measurements. In this subsection a brief overview of the applied methods are provided.

Research questions 1 & 2, defined in the previous section, rely on knowledge about LTE smartphones' instantaneous power consumption. When the thesis work was started such information was not available with sufficient detail and therefore empirical measurements were made. The measurements followed a methodology which was designed to be able to separate the power consumption of each component.

Based on the measurements, and the power model which was developed using the results, it became possible to define a hypothesis stating how a specific parameter could be adjusted to lower the power consumption and then evaluate and accept/reject it using system level computer simulations and the power model i.e. the method is a combination of empirical measurements and simulation, which can be both Monte Carlo and deterministic.

During the study the empirical measurements have been repeated, when a new generation of LTE smartphones became available. This has provided a view on the evolution,

which combined with a review of previous RAT generations formed the basis for suggestions for an energy efficient 5G RAT thus a combination of theoretical models and empirical measurements.

Finally the obtained knowledge is also used to solve specific issues of the 5G concept, e.g. an optimized sleep mode and frame structure, by use of theoretical analysis and computer simulations.

1.4 Thesis Outline

This thesis is twofold due to the research questions presented in section 1.2, which are focused on either LTE or 5G. The first part of the thesis therefore deals with LTE power consumption modelling and energy saving, i.e. research question 1 and 2.

Chapter 2: System Level Analysis of Power Consumption in LTE User Equipment

First the development of an LTE UE power model is described. The model covers the cellular subsystem and is divided into functional blocks based on a breakdown of how specific parameters such as transmit power and data rate affect the power consumption. The model has been updated continuously throughout the project to evaluate how the LTE devices' mature and therefore the work concludes with a view on the evolution in LTE power consumption.

The main contribution is the publication and updating of an empirical LTE UE power model, which has enabled academia and industry to evaluate power consumption in system level simulations. Relevant publications [25, 26, 27].

Chapter 3: Energy Saving in LTE User Equipment

Next the power model is applied to examine how energy can be saved in LTE while maintaining the performance based on research question 2. First it is examined how energy can be saved in cases where the UE is not scheduled but connected to the Evolved Node B. Since the transmit PA is the most power consuming component in the cellular subsystem the work also examines how transmission energy can be reduced by allocating uplink resources. Finally potential energy savings are examined when using Carrier Aggregation (CA) in the downlink.

The main contribution is the simulation results which show how resource allocation, utilization of low power sleep mode and high data rates may provide energy savings. Relevant publications: [28, 29, 30, 31].

In the LTE research area multiple articles have been published and therefore the first part is structured as a *collection of papers* where the key messages from each article is presented and discussed ¹.

¹It must also be noted that the decision to apply this structure is partly due to the financial situation at the Department of Electronic Systems, Aalborg University, because it has introduced a strict time limitation on the thesis work.

The second part of the thesis deals with the design of the future 5G answering research question 3:

Chapter 4: Fifth Generation Radio Access Technology

In this chapter a future 5G RAT concept is described, and it is examined whether technology features of 2G, 3G, and 4G can be reused to improve the energy efficiency. Among the examined features are the waveform, duplexing scheme, transmit power control, frame structure, sleep mode design, and interference management.

The main contribution is the analysis of how each technology feature affect the energy efficiency. Relevant publications: [32, 33].

Chapter 5: Power Consumption Challenges in 5G

In this chapter the performance and power consumption evolution of Low Noise Amplifiers (LNAs), Analog-to-Digital Converters (ADCs), and Base Band (BB) processors are examined and estimated for 2020, where 5G is targeted to be deployed. Using the estimates power consumption challenges are then identified due to increased bandwidth, data rate, number of Multiple Input Multiple Output (MIMO) streams and dynamic range. It is also studied how the transmit PA is affected by the 5G requirements and especially the need for higher carrier frequencies to obtain sufficient spectrum.

The main contribution is the literature survey and study of LNA evolution, using a Figure of Merit (FoM) to predict ADC performance, and finally the estimation of receiver power consumption in 2020 and 2030. Relevant publications: [34].

Chapter 6: DRX and Aperiodic Sleep Modes in 5G

In this chapter sleep modes for 5G are studied with the specific use cases video streaming and MTC because they will be dominant traffic types in the future. It is examined and simulated how Discontinuous Reception (DRX), which is periodic, can be applied in 5G and how it will differ from LTE due to a new short frame. Finally an event based pre-paging concept is presented to solve issues related to aperiodic MTC traffic, which may not fit DRX.

The main contribution is the simulation of DRX performance in 5G, and the proposal of the event based pre-paging concept. The concept has been disclosed in multiple patent applications, but references cannot be provided due to confidentiality requirements. Relevant publication: [35].

The work on 5G has mainly been documented in internal concept documents and patent applications and therefore it is structured as a *monograph*. Figure 1.8 provides an overview of how the papers and patent applications are used in the thesis' two main parts.

The third and final part of the thesis contains the conclusion together with suggested future work. The thesis also contains a bibliography and the following appendices:

- Appendix A
An overview of the smartphones used in this chapter

- Appendix B
A re-print of [36], which is a detailed description of the measurement setup, which was used in the UE power consumption measurements. The appendix is an application note written for Keysight Technologies.
- Appendix C
The details and the bibliography for the Low Noise Amplifier study
- Appendix D
A new limited functionality mode concept is presented in relation with Device-to-Device (D2D) to allow devices to transfer certain types of data without establishing a connection with the network core. The concept is described in a patent application, but not included in the main thesis.
- Appendix E-L
Re-print of the relevant papers [25, 26, 27, 28, 29, 30, 31, 33, 32, 34]

During the PhD study the following papers have also been co-authored in addition to three patent applications that are not discussed in this thesis:

[37] NH. Mahmood, G. Berardinelli, FML. Tavares, M. Lauridsen, P. Mogensen, and K. Pajukoski. “An Efficient Rank Adaptation Algorithm for Cellular MIMO Systems with IRC Receivers”. In: *VTC Spring, IEEE 79th* (May 2014)

[38] AR. Jensen, KI. Pedersen, J. Faaborg, M. Lauridsen, and P. Mogensen. “LTE HetNet Mobility Performance Through Emulation with Commercial Smartphones”. In: *VTC Spring, IEEE 79th* (May 2014)

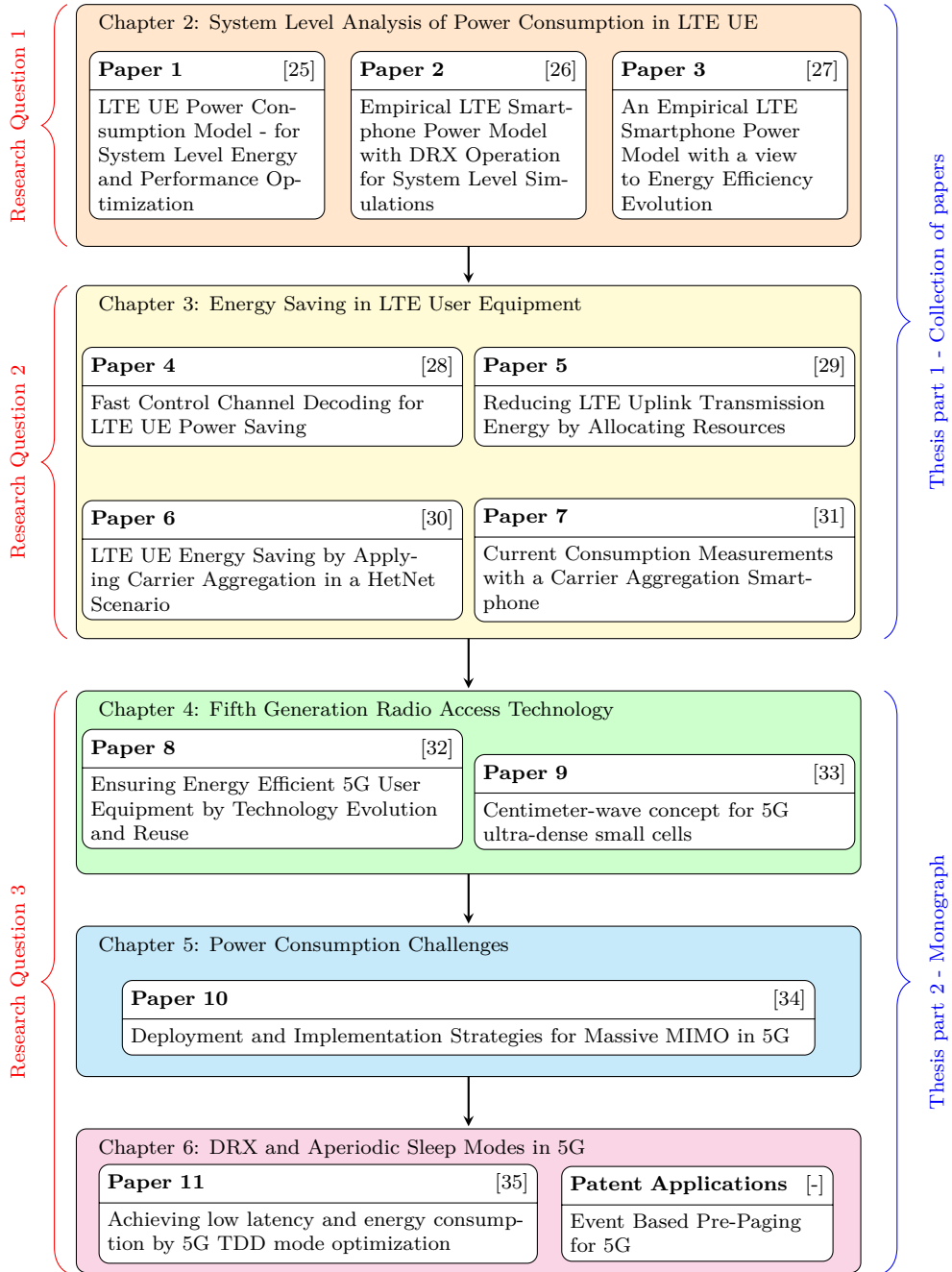


Figure 1.8: Overview of and dependency between the chapters and the publications.

List of relevant papers from figure 1.8:

1. [25] A. Jensen, M. Lauridsen, P. Mogensen, T. Sørensen, and P. Jensen. “LTE UE Power Consumption Model - for System Level Energy and Performance Optimization”. In: *VTC Fall, IEEE 76th* (Sept. 2012)
2. [26] M. Lauridsen, P. Mogensen, and L. Noël. “Empirical LTE Smartphone Power Model with DRX Operation for System Level Simulations”. In: *VTC Fall, IEEE 78th* (Sept. 2013)
3. [27] M. Lauridsen, L Noël, T. Sørensen, and P. Mogensen. “An Empirical LTE Smartphone Power Model with a view to Energy Efficiency Evolution”. In: *Intel Technology Journal* 18 (1 Jan. 2014)
4. [28] M. Lauridsen, A. Jensen, and P. Mogensen. “Fast Control Channel Decoding for LTE UE Power Saving”. In: *VTC Spring, 75th* (May 2012)
5. [29] M. Lauridsen, A.R. Jensen, and P. Mogensen. “Reducing LTE Uplink Transmission Energy by Allocating Resources”. In: *VTC Fall, IEEE 74th*. Sept. 2011
6. [30] M. Lauridsen, H. Wang, and P. Mogensen. “LTE UE Energy Saving by Applying Carrier Aggregation in a HetNet Scenario”. In: *VTC Spring, IEEE 77th*. 2013
7. [31] R. Sanchez-Mejias, Y. Guo, L.A.M.R.D Temino, M. Lauridsen, and P. Mogensen. “Current Consumption Measurements with a Carrier Aggregation Smartphone”. In: *VTC Fall, IEEE 80th* (2014)
8. [32] M. Lauridsen, G. Berardinelli, T. Sørensen, and P. Mogensen. “Ensuring Energy Efficient 5G User Equipment by Technology Evolution and Reuse”. In: *VTC Spring, IEEE 79th*. 2014
9. [33] P. Mogensen, K. Pajukoski, E. Tiirola, J. Vihriälä, E. Lähetkangas, G. Berardinelli, FML. Tavares, NH. Mahmood, M. Lauridsen, D. Catania, and AF. Cattoni. “Centimeter-wave concept for 5G ultra-dense small cells”. In: *VTC Spring, IEEE 79th* (May 2014)
10. [34] B. Panzner, W. Zirwas, S. Dierksy, M. Lauridsen, P. Mogensen, K. Pajukoski, and D. Miao. “Deployment and Implementation Strategies for Massive MIMO in 5G”. in: *Globecom Workshops, IEEE*. Accepted. 2014
11. [35] E. Lähetkangas, K. Pajukoski, J. Vihriälä, G. Berardinelli, M. Lauridsen, E. Tiirola, and P. Mogensen. “Achieving low latency and energy consumption by 5G TDD mode optimization”. In: *IEEE International Conference on Communications* (2014)

Chapter 2

System Level Analysis of Power Consumption in LTE User Equipment

One of the main goals of this thesis is to reduce the Long Term Evolution (LTE) smartphone energy consumption, because the users are not satisfied with the battery life [12, 13]. In order to determine how the energy consumption can be reduced research question 1 is examined. The purpose is to determine how energy can be saved by identifying the main power consuming components of the smartphone and then study how the components' power consumption depends on relevant parameters e.g. how the Base Band (BB) processor power consumption depends on downlink data rate. One method to achieve this is thus to define a power consumption model. To obtain a model a proper measurement method is required and therefore previous work is examined to identify suitable methods. Besides inspiration for the measurement method the previous work also provides insight to what other researchers find to be important power model parameters. As illustrated in figure 1.8 the chapter is based on the contributions in [25, 26, 27].

A modern smartphone resembles a Personal Computer (PC) with interfaces towards the human user and connectivity, see figure 1.5 for an illustration. To achieve this functionality a large number of components are integrated in the smartphone, and in [26] we presented a comparison of the power consumption in the key components and it is repeated in figure 2.1. A user's average daily power consumption depends a lot on the user behaviour in terms of applications executed and connectivity methods used, but based on the measurement in figure 2.1 it is evident that the LTE cellular subsystem is a major contributor. The cellular subsystem consists of the LTE compliant transmitter, receiver, and interface towards the rest of the User Equipment (UE), and it is often referred to as the modem though this is not exactly accurate because it would then only cover MOdulation and DEModulation, and not the Radio Frequency (RF) components.

The cellular subsystem power consumption can be optimized on multiple fronts; e.g. chipset design & layout including component choice, power management, which is

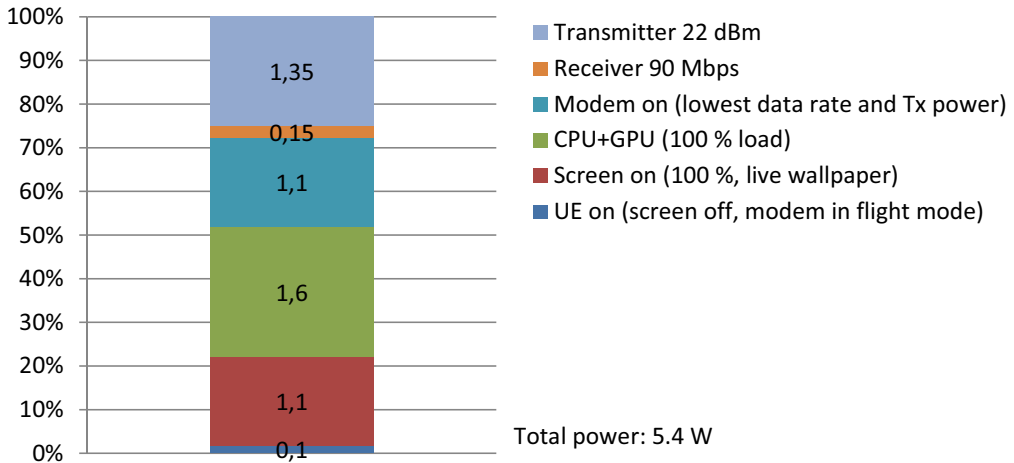


Figure 2.1: Power consumption of selected components in an LTE smartphone, [26, Figure 9].

controlled by the operating system and user interaction, and Radio Access Technology (RAT) design, scheduling, power control, mobility management and so forth.

Due to the multiple adjustment possibilities and the fact that the PhD study was performed within the Wireless Communications area and in cooperation with Intel Mobile Communications and Agilent Technologies the power consumption modelling and investigation was **limited to the LTE cellular subsystem**.

In the next sections we discuss why a power model is needed, what it must include and how it can be applied by performing a review of previous work.

2.1 Power Modelling

Before we describe our proposed power model it is important to answer why a new model is needed?

First of all LTE is not 3G! There are fundamental differences in the technological features: for example the use of Orthogonal Frequency Division Multiple Access (OFDMA) instead of Code Division Multiple Access (CDMA) affects baseband processing complexity and Transmit Power Control, while the different frame structure and the positioning of control and data channels affect UE sleep mode possibilities [32].

A good power model will in general be beneficial to both academia and industry. It allows academia to evaluate new ideas such as scheduling and transmit power control algorithms, while it allows Mobile Network Operators (MNOs) to estimate users' battery life when they adjust network parameters. Finally it can give chipset manufacturers insight into how the rival perform, and where they need to spend extra effort to be competitive. In 2010, when the study was initiated, such a LTE cellular subsystem model was not available because LTE was just being launched.

Before a useful measurement method can be identified it is necessary to identify the

model parameters. The power model is supposed to cover the LTE cellular subsystem and therefore the following parameters are important:

- Transmit and receive power levels: The transmit power level is determined by the transmit Power Amplifier (PA), which is known to affect the power consumption significantly. The receive power level will affect the gain levels of the Low Noise Amplifiers (LNAs) and possibly also mixer performance requirements.
- Downlink and uplink data rate: Decoding and encoding the data affects the base-band processor power consumption because the complexity increases with data rate.
- State change: The power consumption of the cellular subsystem changes when state is changed i.e. from RRC Idle to RRC Connected. Furthermore it is also important to note how fast the changes occur.
- Discontinuous Reception (DRX): The length of the DRX periods determine the sleep mode power level.
- Scanning & measuring: Scanning and measuring neighbor cells e.g. in preparation for handover also impacts power consumption.
- Cell bandwidth: The cell bandwidth will affect Analog-to-Digital Converter (ADC) and Digital-to-Analog Converter (DAC) power consumption.

In a real network the aforementioned parameters will vary and therefore it is important that the power model reflects this behaviour.

When measuring smartphone power consumption it is of interest to compare the LTE cellular subsystem power consumption with other components and their related parameters such as the following: display brightness & activity (may also depend on wallpaper type), Central Processing Unit (CPU) activity & clock frequency, memory usage (both internal and flash cards), other RATs, camera, Global Positioning System (GPS), audio volume, and flight mode (for baseline comparison). It is interesting to compare the cellular subsystem power consumption with these components because it is important to focus on the components where the biggest savings can be achieved without harming the user experience. The comparison has already been done by multiple researchers, but the aforementioned components are not essential for functionality of the cellular subsystem and therefore it is important to keep their impact as low and constant as possible while measuring.

Previously a large amount of papers have been published on 2G, 3G, and WiFi power consumption and tables 2.2, 2.3, and 2.4 provide an overview of selected power models. The target is to observe the measurement methodology and which model parameters the authors selected. Therefore the parameters in table 2.1 are of interest and listed in the following tables' columns.

Examining the listed papers in tables 2.2, 2.3, and 2.4 in detail it is clear that most of the measurements were carried out by connecting a commercial smartphone to a commercial cellular network [39, 42, 43, 45, 46, 52, 53, 58]. Using a commercial smartphone as the Device Under Test (DUT) is a common choice because the smartphone is easy to

Table 2.1: Key measurement parameters and methods.

Parameter/method	Value
Radio Access Technology	2G, 3G, LTE, and WiFi
UE type	Prototype, dongle, feature-, and smartphone
Type of network connection	Commercial, emulated, and local
Power logging method	Application based and supply/battery logging
Parameter logging method	Application based and network based

obtain, it provides the real performance experienced by users, and if the Operating System (OS) allows it, to deploy a measurement and/or logging application. Other options are to measure on a laboratory prototype [51] or USB dongles [45, 57]. Using a prototype may give the researcher more control of the device, leading to a more detailed and thorough analysis, but it also does not reflect the real performance experienced by users. Measuring on a USB dongle, and basing a power model on it, may also not provide the real performance because the USB dongles are not as optimized power consumption wise as a smartphone since they are not battery operated. Using a simple USB dongle will however entail that less overhead is measured as opposed to the smartphone where the CPU and memory always will contribute. Based on this discussion the **preferred DUT is a commercial smartphone**.

When a DUT has been selected the next task is to determine how to connect it to the network of interest. There are multiple types of networks, each associated with different costs of establishing the connection and with different levels of control, and therefore with different constraints on how the power model can be made. Connecting the DUT to a commercial network has been the preferred method when the RAT is of the cellular type (2G, 3G, and LTE). When the RAT has shorter range, e.g. WiFi, Bluetooth, and ZigBee, a local network is most often used [42, 46, 41, 44, 47, 48, 55]. Two less used options are full connectivity control by a local PC [51] and connecting the DUT to a base station emulator in the laboratory [57].

The commercial network connection is easy to set up, because the researcher only needs a valid Subscriber Identity Module (SIM) card and coverage before he can start transferring data etc. to measure the power consumption. The problem is that e.g. the downlink data rate depends not only on the channel between the DUT and the base station, but also the overall network load and the backhaul of the base station. Therefore it can be challenging to stabilize the data rate and even more challenging to vary it to determine the power consumption as a function of the data rate. Furthermore the DUT power consumption in e.g. DRX mode is highly dependent on the network settings, which the researcher often has no possibility of adjusting. Therefore the researchers often only report average values for parameters, which actually are functions of a variable [42, 45, 46, 52, 40, 49, 50, 56]. This can partly be circumvented by gathering measurements from multiple users as discussed later in this section.

The local network connection is easy to set up for WiFi, BT and so forth, because either a PC or simple access point hardware can be used. In this type of network the researcher may control both ends and therefore it is easier to ensure that the variables

Table 2.2: Selected power models presented in literature, part 1.

Ref.	Year	RAT	UE type	Network	Power logging	log-Parameter logging	Power model	Other
[39]	2010	WiFi, 3G	HTC Dream and Magic smartphones	Commercial network	Measurement at supply	Wifi and 3G is measured by uploading packets to a local server	WiFi is a function of number of packets and UL rate. 3G has a constant value for FACH and DCH states	Other components' activity is kept low to minimize impact. Includes power as a function of CPU utilization and clock frequency, display brightness, audio state, GPS state.
[40]	2010	GSM, GPRS, WiFi	Openmoko Neo Freerunner smartphone	Commercial network	Sensing component level + total power at battery terminal	at 2G and WiFi is measured by downloading a file	Fixed values for 2G & WiFi DL + a value for strongly attenuated signal. Includes overall comparisons with two other 3G smartphones	Power as function of display brightness, CPU & RAM frequency, GPS activity, flash and SD memory activity
[41]	2010	ZigBee	TI CC2480	Local network	Measurement at battery terminal	Both network ends are controlled and logged	Start up, scanning, sleeping, transmission power and duration	Includes a data sheet based comparison with 6 other commercial ZigBee chips
[42]	2011	WiFi, 2G, 3G, BT	Nokia N95	Commercial 2G & 3G networks, local WiFi & BT networks	Nokia Energy Profiler application	Nokia Energy Profiler application captures signal strengths and CPU activity	Values are given for fixed 2G & 3G DL rates (a plot shows data rate variations). Fixed values for handover, voice, idle mode, video call and SMS.	The accuracy of the Nokia app is controlled by using a measurement supply. The authors also include display, memory and CPU usage.
[43]	2011	LTE, 3G	HTC Thunderbolt	Commercial network	Measurement at battery terminal	Traffic characteristics are logged in the phone	Measurement plots showing power traces for LTE connected and idle mode, but no values or model is given	User generated & background traffic is compared in terms of packet size and interarrival times
[44]	2011	WiFi	HTC Nexus One	Local network	Measurement at battery terminal	Video stream via WiFi and the UE's memory	Fixed values for streaming low & high quality video, but no details of channel power levels etc.	Power as a function of display brightness, audio volume and CPU activity
[45]	2012	LTE, 3G, WiFi	HTC Android phone & USB modem	Commercial network	Measurement at supply	The packet and CPU trace is logged using a program on the phone. The UE is connected via TCP to a local server	LTE promotion & tail, short & long DRX (parameters not varied because they are network-controlled), uplink & downlink data rate	The authors also deployed a logging app among real users to measure LTE network performance and CPU usage

Table 2.3: Selected power models presented in literature, part 2.

Ref.	Year	RAT	UE type	Network	Power logging	log-Parameter logging	Power model	Other		
[46]	2012	WiFi, 3G	Nokia N95	Local commercial 3G network	WiFi, Nokia Energy profiler application	En-Profiler application. Data is transferred via a local PC	UL and DL data transfer, but independent of rate. Idle and in-active mode.	The authors examine power up and down times in detail		
[47]	2012	WiFi 802.11n	Google Nexus smartphone	Local network	net-Measurement supply	Android application logs battery level & packet data rate. The network was controlled and used to generate data traffic	DL data rate is logged via iperf, which establishes a connection between a local PC and UE	Functions of DL data rate and DL channel quality	Run at night to minimize interference	
[48]	2012	WiFi	Google Nexus One	Local network	net-Android application	Android application logs battery level & packet data rate. The network was controlled and used to generate data traffic	A combined power consumption function is given for UL & DL data rate	Power consumption as a function of display brightness and RGB settings, CPU activity and audio level		
[49]	2012	N/A	HTC Dows 7.5	Win-Phone network	Commercial network	On-board power sensor and measurement supply	None, but power is compared for 10 hours	No specific parameters, but two measurements on average power for a 10 hour use case	The on-board power sensor is accurate within 2% of the power supply measurement	
[50]	2012	WiFi and GSM	Nokia N8 and C7	Commercial network	Commercial network	Nokia Energy profiler application	En-Profiler application	Nokia Energy profiler application	Each RAT is divided into 4 power states each with a time duration i.e. no dependency on data rates and power levels	None
[51]	2013	LTE	Lab type	proto-type	The UE is controlled by a PC	Measurement supply	The transmitted output is examined on a spectrum analyzer, a PC logs the UE state	A function of transmit power and cell BW are shown in graphs, but model parameters are not provided	None	
[52]	2013	LTE, WiFi	Samsung Galaxy HD LTE	Commercial network	Commercial network	Measurement supply	Logging of normal and sleep mode, but no details on what they cover	Normal and sleep average values are provided for LTE, WiFi, flight mode, and power save mode	Active applications during the measurements are noted	

Table 2.4: Selected power models presented in literature, part 3.

Ref.	Year	RAT	UE type	Network	Power logging	log-Parameter logging	Power model	Other
[53]	2013	WiFi, 3G	HTC Nexus One, Motorola Atrix, Sony Xperia S	Commercial network	Measurement at battery terminal	The UE downloads data from a local PC. RSSI is logged using an UE application and varied by moving the UE	WiFi and 3G as a function of signal strength for receive, transmit, and tail states (one submodels per UE). Measurements are made at night to minimize interference	Traces from 3785 Android devices are analyzed using an app which logs battery level, 3G and WiFi signal strength and transferred data
[54]	2013	N/A	Android devices	Commercial network	Android application	Android application logs battery level, location, and network parameters (state, amount of data transferred, link speed)	The model parameters can be varied, but no values are presented	The power required to run the app cannot be excluded, and therefore the sampling time was set to 10 s.
[55]	2013	ZigBee	TI CC2530 SoC	Local network	Measurement at battery terminal	Both network ends are controlled and logged	Scanning, sleeping, and data transfer but only for a specific scenario, i.e. independent of the amount of data and the scanning period	None
[56]	2013	N/A	Android devices	Commercial network	Android application	Android application logs battery level & applications activities	Average values for a phone call, playing Angry Birds and using SinaWeibo	Includes a comparison with a Tianyu W806 smartphone, but without measurement details
[57]	2013	LTE	4 modems & HTC Velocity smartphone	USB Base station emulator connected with RF cables	Measurement at battery terminal	Uplink rate is fixed, transmit power is varied by use of LTE TPC commands	LTE transmission power and carrier frequency	None
[58]	2014	LTE, 3G, WiFi	Android smartphone	Commercial network	Android application	The app logs applications' activities & battery percentage. No information on how the RATs are exercised	UL & DL data rate, but not all required values to model the power consumption are provided.	The power model is used to develop an application, which can estimate the power consumption of UEs

are exercised properly. One issue is that the frequency bands, which are contention based, may be used by other users as well and therefore some researchers perform the measurements at night [53, 47].

In [57] a base station emulator is used to connect the DUT. This setup provides full control of the network side, allowing the researchers to examine how the DUT power consumption depends on each network-defined parameter. The problem with this setup is that the emulator is expensive and in addition the connection between the emulator and the DUT is often established using wires, which bypasses the DUT's antennas, and therefore the measured performance may not correspond exactly with what can be measured over-the-air. A minor issue is how to set up the emulator with realistic parameters, which match the settings used in commercial networks.

Based on this discussion it is clear that researchers can choose between an easy and cheap measurement setup, based on commercial networks which provide limited possibilities for parameter exploration, and an expensive but controllable laboratory setup using either a base station emulator or access points, depending on the RAT type. For a full examination of DUT power consumption the **preferred network connection is based on a base station emulator**.

When a DUT and a network connection has been selected the next step is to select a power consumption logging method, because it defines the measurement accuracy, the type of parameters that can be logged, the number of samples and the sampling frequency that can be used to generate the power model. In previous work either a measurement supply [39, 43, 45, 51, 52, 53, 57], an application [42, 46, 58], or sensing on the circuit board [40, 49] has been used. The latter may be the most accurate in determining the power consumption of individual components, but it also requires detailed knowledge about the circuit board layout and the pin connections of the on-board chips. The measurement supply is used to either replace the battery or provide power at the battery terminal. Replacing the battery is not a trivial task, because a modern battery has multiple pin connections which is used by the phone to determine the charge level, temperature and other battery health metrics. If the supply is instead connected at the battery terminal the measurement will include both DUT power consumption and possibly power used for charging the battery. No matter how the measurement supply is connected it provides good resolution both in time and power, and easy transfer to further processing on a PC.

Power logging with an application is mainly performed either by use of the Nokia Energy Profiler [42, 46, 50] or Android applications [48, 53, 54, 56, 58], made specifically for the measurement by the researchers. The Nokia application and some of the Android applications are made to run on a single phone after which the logged data is transferred to a PC, whereas some Android applications are published on the Android Market Place and used to obtain measurements from multiple users which are then uploaded to a central server. Both types of applications will affect the measured power consumption, and furthermore the sampling time plays a major role. In the Nokia Energy Profiler it is set to 250 ms as a compromise between measurement resolution and application power consumption, while [54] reported a 10 s sampling time to limit the application power consumption. Besides the applications' very slow sampling time, which for measurement supplies may be up to 5 kHz [39, 45], the applications have less

accurate power consumption readings, because the OS often only provides a reading of the current battery level in percent. One convenient feature of the applications is their ability to log both power consumption and other relevant parameters such as data rate. Because the applications are slow and inaccurate the **preferred power logging method is the measurement supply, which replaces the battery.**

Besides logging the power consumption it is also necessary to log the relevant parameters such as transmit power and downlink data rate listed previously in this section, because they affect the power consumption. The number and type of parameters depend on the selected RAT and the overall target with the model. Some studies examine multiple RATs but only obtain average values [39, 42, 52, 40, 50], while others only exercise a few parameters in detail and do not cover the whole cellular subsystem [46, 53, 57]. Another issue is that the selected network type in combination with the parameter logging tool may entail the researchers are not able to vary the variables or study them in detail [45, 44, 55, 49]. Finally some researchers actually perform the detailed logging but do not share all the details necessary to implement a model, [43, 51, 58, 54]. Several researchers have also included measurements on other smartphone components such as the display and CPU activity [39, 42, 40, 44, 48].

Similar to the power logging method the parameters are either logged using an application on the phone or some type of external equipment, and therefore similar pros and cons can be listed: the application affects power consumption and has low accuracy and sampling rate, but is easy to deploy amongst users, while the external equipment has better accuracy, but only allows measurement at a single DUT. Previously the base station emulator was selected as the preferred network connection, and because it is also able to provide parameter logging the **preferred parameter logging method is the base station emulator.**

To summarize the power model shall be based on measurements on a commercial smartphone using a measurement supply, which replaces the battery, while being connected to a base station emulator, which provides both the network connection and parameter logging.

In the next section a list of the published power consumption model papers is given highlighting the contribution and novelty of each. After that the proposed LTE cellular subsystem power consumption model is presented and followed by an overview of how the measurements are made to parametrize it.

2.2 Paper Contributions

In this section the contributions from relevant papers are highlighted. Re-prints are available in appendix E, F, and G.

[25] LTE UE Power Consumption Model - for System Level Energy and Performance Optimization

In this paper the novel LTE power model design was presented and the functional blocks were defined based on a discussion of how the cellular subsystem components would contribute to the total power consumption. Based on the block division a measurement

campaign was designed to exercise the relevant parameters, and carried out using an LTE USB dongle, a measurement supply replacing the battery, and a base station emulator. The paper has 15 individual citations, excluding self-citations, as of November 2nd 2014.

[26] Empirical LTE Smartphone Power Model with DRX Operation for System Level Simulations

In this paper the model and measurement campaign from [25] was reused on 3 LTE smartphones. Furthermore the paper includes measurements on DRX, cell bandwidth and other smartphone components. The main contribution is the comparison between the cellular subsystem and other smartphone components, which showed that the LTE connection may contribute up to half of the total power consumption. The paper also contains the first comprehensive LTE DRX measurements, which showed that 3GPP's widely used model is inaccurate. The paper was made in external collaboration with Laurent Noël, Vidéotron, Canada.

[27] An Empirical LTE Smartphone Power Model with a view to Energy Efficiency Evolution

In this paper the measurements from [26] was compared with the latest smartphone chipset in terms of the model parameters and DRX, providing one of the first studies on how the power consumption of LTE evolves over time/with each chipset generation. In addition the article presented a review of how the Energy Efficiency (EE) has evolved in the cellular generations, WiFi, Bluetooth (BT), and ZigBee. The article concluded with an overview of some of the energy saving techniques, which had been presented in [28] and [30]. The paper has more than 1250 downloads on vbn.aau.dk at the end of October 2014 after publication in January 2014.

2.3 The LTE Smartphone Power Consumption Model

In this section the LTE smartphone power consumption model is presented. The first version of the model was presented in [25] and later updated in [26, 27, 31].

The power consumption model is defined as follows using the Radio Resource Control (RRC) states [59] of LTE :

$$P_{\text{cellular}} = m_{\text{con}} \cdot P_{\text{con}} + m_{\text{idle}} \cdot P_{\text{idle}} + m_{\text{DRX}} \cdot P_{\text{DRX}} \quad [\text{W}] \quad (2.1)$$

where: P_{cellular} is the power consumption of the cellular subsystem [W]
 m_{con} is a binary variable describing whether the UE is RRC_connected [-]
 P_{con} is the power consumption in RRC_connected mode [W]
 m_{idle} is a binary variable describing whether the UE is RRC_idle [-]
 P_{idle} is the power consumption in RRC_idle mode [W]
 m_{DRX} is a binary variable describing whether the UE is in DRX [-]
 P_{DRX} is the power consumption in DRX mode [W]

The power consumption in RRC_connected mode P_{con} is partitioned into multiple functional blocks such that the contribution from each parameter can be determined and studied. The blocks cover Transmit (Tx) and Receive (Rx) BB and RF, which depend on power levels (S) and data rates (R) as illustrated in figure 2.2. The reason for this

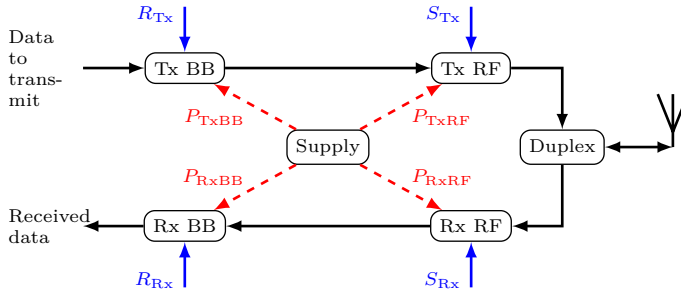


Figure 2.2: LTE smartphone cellular subsystem power consumption model.

partitioning is given in [25], but the idea is that each functional block has one specific parameter which is the main reason for power consumption variations within the block. The partitioning also makes separate power consumption measurements easier as will be discussed later.

The RRC_connected mode power consumption P_{con} is (refer to figure 2.2):

$$P_{\text{con}} = P_{\text{on}} + m_{\text{Rx}} \cdot (P_{\text{Rx}} + P_{\text{RxBB}}(R_{\text{Rx}})) + P_{\text{RxRF}}(S_{\text{Rx}}) + m_{\text{Tx}} \cdot (P_{\text{Tx}} + P_{\text{TxBB}}(R_{\text{Tx}}) + P_{\text{TxRF}}(S_{\text{Tx}})) \quad [\text{W}] \quad (2.2)$$

where:	P_{on} is the base power consumed when the cellular subsystem is ON	[W]
	m_{Rx} is a binary variable indicating active reception	[-]
	P_{Rx} is the base power consumed by the active receiver	[W]
	R_{Rx} is the DL data rate	[Mb/s]
	P_{RxBB} is the Rx BB power consumption	[W]
	S_{Rx} is the DL receive power	[dBm]
	P_{RxRF} is the Rx RF power consumption	[W]
	m_{Tx} is a binary variable indicating active transmission	[-]
	P_{Tx} is the base power consumed by the active transmitter	[W]
	R_{Tx} is the UL data rate	[Mb/s]
	P_{TxBB} is the Tx BB power consumption	[W]
	S_{Tx} is the UL transmit power	[dBm]
	P_{TxRF} is the Tx RF power consumption	[W]

The second part of equation (2.1) covers the RRC_idle mode power consumption in which the UE periodically performs neighbor cell measurements and check for incoming paging messages from the network. In between the active periods the UE is in a low power sleep mode, whose length is defined by the network using the paging cycle parameter t_{pc} . This periodic switching between active and sleep mode is similar to the third part of equation (2.1) which covers the RRC_connected DRX mode. In LTE the DRX Long Period (DRX LP) t_{LP} is 10-2560 ms [60] and therefore it can be matched well with many types of traffic. Furthermore the ON duration t_{onD} of each period is also adjustable such that the network can accommodate larger data transfers if needed and the network may even specify that the UE after successful decoding of data remains ON for an extra period to await further traffic. Figure 2.3 illustrates the timing and power consumption states of a DRX long period. The wake-up phase, synchronization

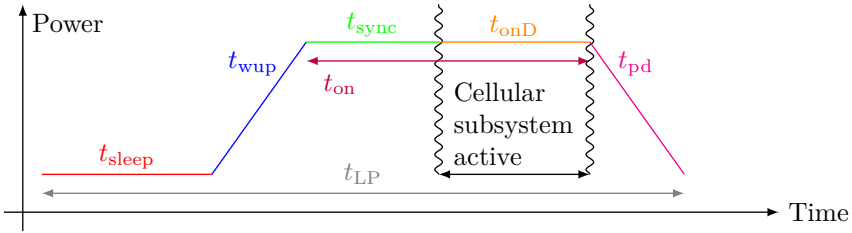


Figure 2.3: UE states in a DRX long period.

phase, and power down phase all depend on the t_{LP} setting and the cellular subsystem design and therefore the sleep time is defined as

$$t_{\text{sleep}}(t_{\text{LP}}, t_{\text{onD}}) = t_{\text{LP}} - (t_{\text{wup}}(t_{\text{LP}}) + t_{\text{sync}}(t_{\text{LP}}) + t_{\text{pd}}(t_{\text{LP}}) + t_{\text{onD}}) \quad [\text{s}] \quad (2.3)$$

where: t_{sleep} is the sleep time [s]
 t_{LP} is the DRX Long Period [s]
 t_{onD} is the DRX On Duration [s]
 t_{wup} is the wake-up time from sleep to active [s]
 t_{sync} is the synchronization time after sleep [s]
 t_{pd} is the power down time from active to sleep [s]

Excluding the power consumed in the t_{onD} phase the average DRX power consumption is

$$P_{\text{DRX}}(t_{\text{LP}}, t_{\text{onD}}) = \frac{t_{\text{sleep}}(t_{\text{LP}}, t_{\text{onD}}) \cdot P_{\text{sleep}}(t_{\text{LP}}) + E_{\text{wup+sync+pd}}(t_{\text{LP}})}{t_{\text{LP}} - t_{\text{onD}}} \quad [\text{W}] \quad (2.4)$$

where: P_{DRX} is the average DRX power consumption [W]
 P_{sleep} is the sleep mode power consumption [s]
 $E_{\text{wup+sync+pd}}(t_{\text{LP}})$ is the energy consumed during the wake up, synchronization and power down phases [J]

By summing the result of equation (2.4) and the power consumed in the active mode during t_{onD} (using equation (2.2)) the total power of a DRX period may be calculated. If t_{LP} is replaced with t_{pc} the power consumption of RRC_idle may be approximated.

Note that average power is used and therefore the equations covering DRX cannot be applied in Transmission Time Interval (TTI) simulations, but only system level simulations made with a slower time perspective. This is however not the case for the RRC_connected model in equation (2.2) which can be applied in TTI simulations.

2.4 Measurement Method & Setup

In this section the measurement method developed to parametrize the power model is presented together with an overview of the equipment setup and the examined UEs. For further details on the setup and the used equipment refer to [36].

Based on the discussion in section 2.1 the measurement setup consists of a base station emulator connected to a UE, which is powered by a measurement supply that replaces the battery as illustrated in figure 2.4. In principle the setup can be made conducted using cables or Over-the-Air (OTA), but because the cable-based setup is easier to calibrate and less expensive it was the choice for all measurements. The conducted measurements entail the UE's antennas are bypassed and thus the circuit which tunes the antenna and PA to have matching impedances is not challenged and therefore the power consumption may be a bit lower than in real OTA measurements, [16].

As mentioned in sections 2.1 and 2.3 the power model must cover the following parameters: 1. transmit and receive power levels, 2. downlink and uplink data rate, 3. cell bandwidth, 4. state change, 5. scanning & measuring, and 6. DRX. The first 3 set of parameters in the list directly affect the power consumption of an individual block in figure 2.2 while the latter 3 deal with the power consumption of the entire cellular

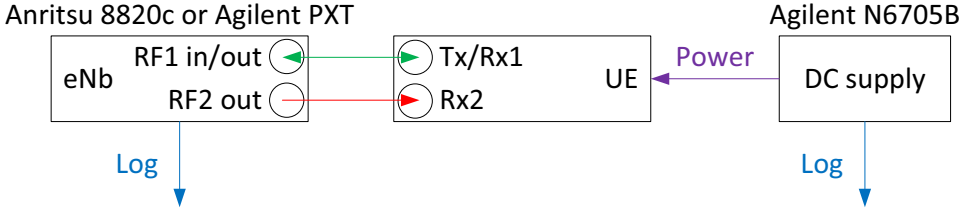


Figure 2.4: Measurement setup for power consumption modelling of UEs. [27, Figure 4]

subsystem. All measurements are made with all applications terminated, other wireless peripherals OFF and the display OFF as well to minimize the impact.

It is assumed that each of the functional blocks in figure 2.2 only depend on one parameter and thus the power consumption of the block can be examined by keeping the other parameters constant while varying the target parameter. The reason behind this independence assumption is detailed in [25], and an example is that the Turbo decoder complexity scales linearly with downlink data rate but is independent of the receive power level, and all transmit related parameters. The measurements for parameter sets 1 and 2 may be repeated for various cell bandwidths, depending on UE and emulator support as was done in [26]. To parametrize the functional blocks at least one test case was therefore designed per block, and the specific test settings are given in table 2.5. Note how the impact of the other parameters are kept low, when they are not varied i.e. a low transmit power, a high receive power and low data rates.

The power consumption was measured over a period of at least 30 seconds, while the examined parameter was kept constant. Then the parameter was increased one step and another recording of 30 seconds was performed. When the parameter was fully exercised the data was post-processed in Matlab, and an average value extracted per 30 seconds measurement. Note that the test cases are designed to have an overlapping point such that the 3 constants in equation (2.2) may be calculated, [25]. Appendix B and [27] provides a discussion on the number of measurement points per test case needed to update the model.

Table 2.5: Measurement test cases. Downlink tests are made for 1 & 2 Code Words (CWs).

Test case	DL parameters			UL parameters		
	MCS [-]	PRB [-]	S_{Rx} [dBm]	MCS [-]	PRB [-]	S_{Tx} [dBm]
Rx BB 1	[0,28]	100	-25	6	100	-40
	0	[0,100]	-25	6	100	-40
Rx RF 3	0	100	[-25,-90]	6	100	-40
Tx BB 4	0	3	-25	6	[0,100]	-40
	0	3	-25	[0,23]	100	-40
Tx RF 6	0	3	-25	6	100	[-40,23]

Measurement on state change power consumption and timing is made by sending paging requests and release commands from the base station emulator to the UE. Fur-

thermore it is also of interest to capture the UE’s base power consumption, which is done by activating “flight mode”. When the UE is sent to RRC_idle mode it will perform neighbor cell measurements and check for paging messages (parameter set 5 in the list) based on the paging cycle, which is set by the Evolved Node B (eNB). Therefore this measurement can be completed in conjunction with the previous measurements by recording the power over a time duration, which is a multiple of the paging cycle. Afterwards the data is post-processed by dividing the data into chunks each one cycle long, and then calculating the average of each sample point in the cycle, resulting in one average cycle.

The final parameter set covers DRX. The used base station emulators were unable to schedule data in the ON periods of the DRX cycle and therefore the UE would only be scanning the control channels for a scheduling grant, but never receive data. Due to this issue the DRX parameter set was reduced to exercising the period length (10 ms to 2560 ms) and the duration of the ON time (1 ms and 6 ms). As with parameter set 5 the measurements are performed over a multiple of the period, after which the average over one period is calculated.

In the following section selected results are presented, which compare the power consumption of measurements from [26] and [27] and unpublished material. The measurement UEs are Android smartphones, but they differ in terms of component Complementary Metal–Oxide–Semiconductor (CMOS) technology node and generation as shown in table 2.6. Decreasing the CMOS node entails the chip occupies a smaller area and because the supply voltage can also be scaled the dynamic power consumption can be reduced. Refer to section 5.3 for further details on CMOS scaling.

Note that UE5 power consumption was only measured as a function of uplink transmit power because of limited support for higher order Modulation and Coding Scheme (MCS) in the provided DUT.

Table 2.6: User Equipment (UE) main physical characteristics.

	UE1	UE2	UE3	UE4	UE5	UE6
Android OS version	2.3.6	4.0.4	4.1.2	4.4	4.4.2	4.4.2
Launch date	May '12	Jun. '12	Apr. '13	Oct. '13	Apr. '14	Sep. '14
Modem & CPU - CMOS node	Part #A 45 nm	Part #B 28 nm	Part #C 28 nm	Part #D 28 nm	Part #E 28 nm	Part #F 28 nm
RF transceiver - CMOS node	Part #G 65 nm	Part #H 65 nm	Part #I 65 nm	Part #I 65 nm	Part #J 65 nm	Part #K 65 nm
Band 4 PA LTE bands	Part #L 4,17	Part #L 4,17	Part #M 1,2,4,5,17	Part #N 1,2,4,5,17, 19,25,26	Part #O 1,2,3,4,5, 7,8,17	Part #P 2,4,7,17
UE category	3	3	3	4	4	4

Appendix B and [27, 36] provides a discussion on measurements uncertainties and model verification.

2.5 Selected Power Consumption Results

In this section power consumption measurements as a function of uplink transmit power, downlink data rate and DRX parameters are shown. For a complete set of measurement results refer to [27]. The cell bandwidth is 20 MHz and the carrier frequency is 2145 MHz because this was supported by all UEs listed in table 2.6.

The power consumption as a function of uplink transmit power is shown in figure 2.5 for the selected UEs. The uplink transmit power was chosen because it dominates the cellular subsystem's total power consumption when the PA operates in the high power region (>10 dBm).

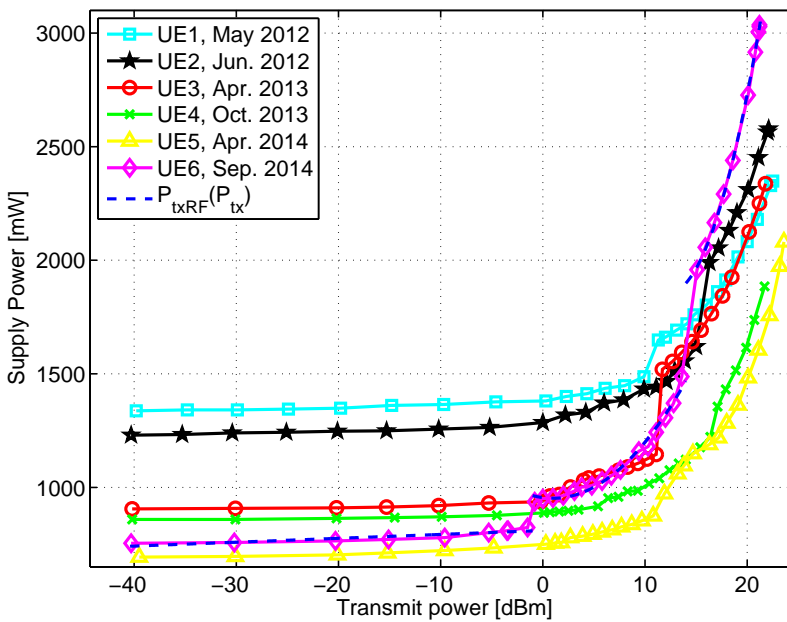


Figure 2.5: Power consumption as a function of transmit power. Quadrature Phase-Shift Keying (QPSK) modulation is used.

Examining the low power region (<0 dBm) it is clear that the power consumption decreases with each UE generation. For example the CMOS node was lowered from UE1 to UE2 and this entailed 8-10% lower power consumption, but examining the high power region where the external PA is activated it is clear that UE2's advantage is lost even though it uses the same PA as UE1. The reason may be different gain settings and Adjacent Channel Leakage Ratio (ACLR) performance, but this was not examined in further detail because it requires knowledge about chip design and setup that is only available to the manufacturer. The CMOS node of UE3 and UE4 is the same as UE2, but the chipsets have been updated and therefore the step from UE2 to UE3 shows an impressive 27% power saving in the low power region. The step from UE3 to UE4 only leads to 5% savings because they use the same RF transceiver. UE4 is one of the first commercial smartphones to utilize Envelope Tracking (ET), which entails the

supply voltage is scaled to the transmit power level currently needed by tracking the signal amplitude using a high bandwidth supply. Therefore the PA can operate closer to its saturation point where the efficiency peaks as opposed to the commonly used Average Power Tracking (APT) PA which instead adjusts the supply voltage at TTI level. Unfortunately the APT technique is not efficient at high transmit powers and for high Peak-to-Average-Power Ratio (PAPR) signals. The savings of the ET PA are in the order of 20% for this first generation. UE5 also uses an ET PA and combined with the newer transceiver, which saves 20-24% at low transmit powers, it is currently the most energy efficient UE maintaining about 10% lower power consumption at high transmit powers as compared to UE4. UE6 is also of the newest generation in terms of transceiver and baseband modem, but only a mid-end smartphone as compared to the other smartphones which are expensive high-end editions. The use of the newest chipset provides power saving benefits at low transmit powers where 10-14% is saved as compared to UE4. However UE6 uses a simpler multi-band APT PA and consumes almost 20% more power than the two year older UE2. For budget smartphones the manufacturers clearly need to make a trade-off between transmit power consumption and cellular subsystem power consumption in general. This point is also illustrated in figure 2.6 which shows the same power consumption measurement but having the power consumption at the -40 dBm transmit power subtracted. Note that UE1 has a very favourable high-power setup but that the base power consumption is almost double of UE5 and UE6.

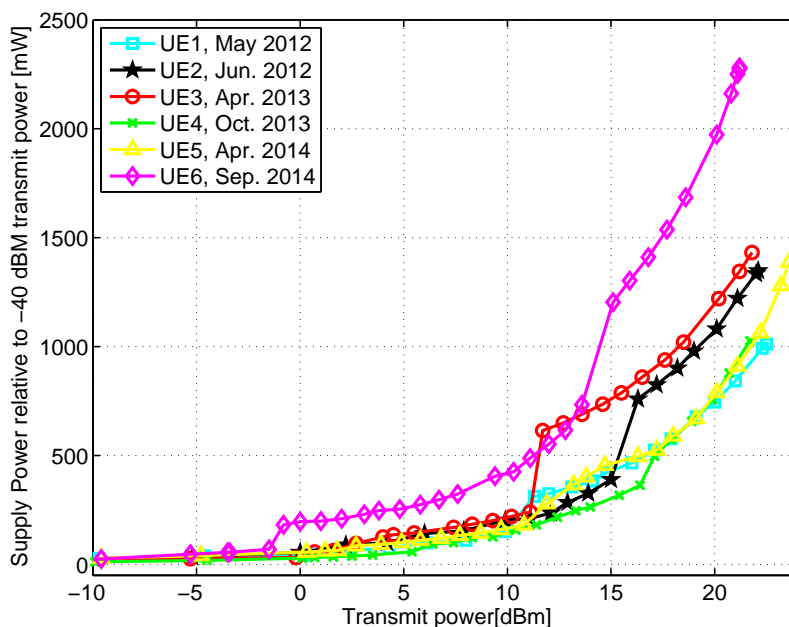


Figure 2.6: Power consumption as a function of transmit power using -40 dBm as reference. QPSK modulation is used.

The main message based on the measurements in figures 2.5 and 2.6 is therefore

to avoid transmit powers above 10 dBm, but also that improving CMOS node and PA technology will continue to enhance the energy efficiency.

The power consumption as a function of uplink data rate is almost constant, and thus not presented here, besides a minor increase in some UEs due to adjustments when switching from QPSK to 16 Quadrature Amplitude Modulation (16QAM). The reason may be the increased PAPR which forces the PA to adjust the tradeoff between ACLR and power consumption.

The second selected result, shown in figure 2.7, is the power consumption as a function of downlink data rate. As in figure 2.5 it is possible to observe decreasing power consumption of 8 %, 25 %, 5 %, and 10 % for each generation respectively. This is also the case when using 2 CWs to increase the data rate, but because it only adds a constant offset to the power consumption those results are not shown here.

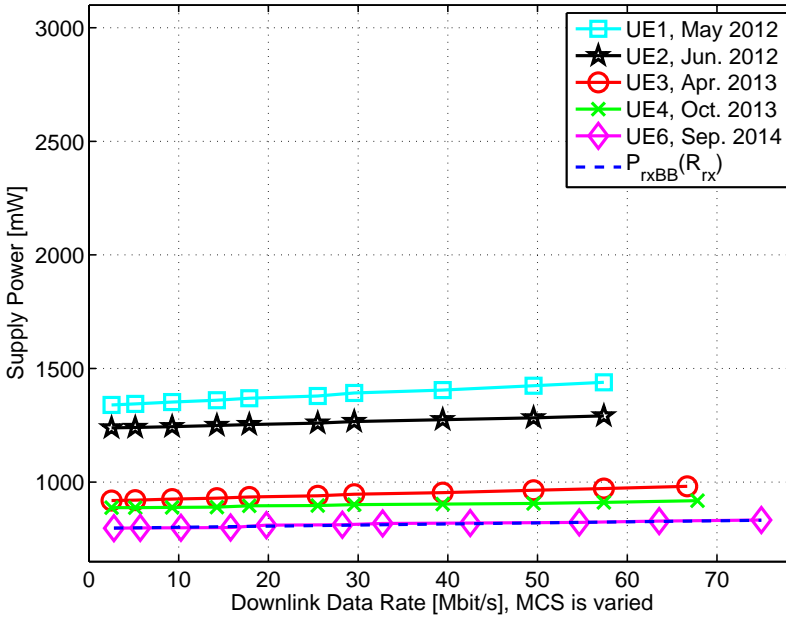


Figure 2.7: Power consumption as a function of downlink data rate for 1 CW.

What is more interesting to note is the EE, defined in equation (1.2) as data rate divided with power consumption, which is 15-25 times higher for the high data rates. This result is illustrated in figure 2.8, where minimum EE is based on the lowest data rate and maximum on the highest data rate measured. The spread in EE entails that MNOs should use a scheduler which allocates many resources to a single user in a round robin like fashion to boost the data rates instead of allocating a few resources to many users. The feasibility of such a scheduler depends on the delay and data rate requirements, but it would certainly improve the EE for the individual user.

The power consumption as a function of downlink receive power is not shown here,

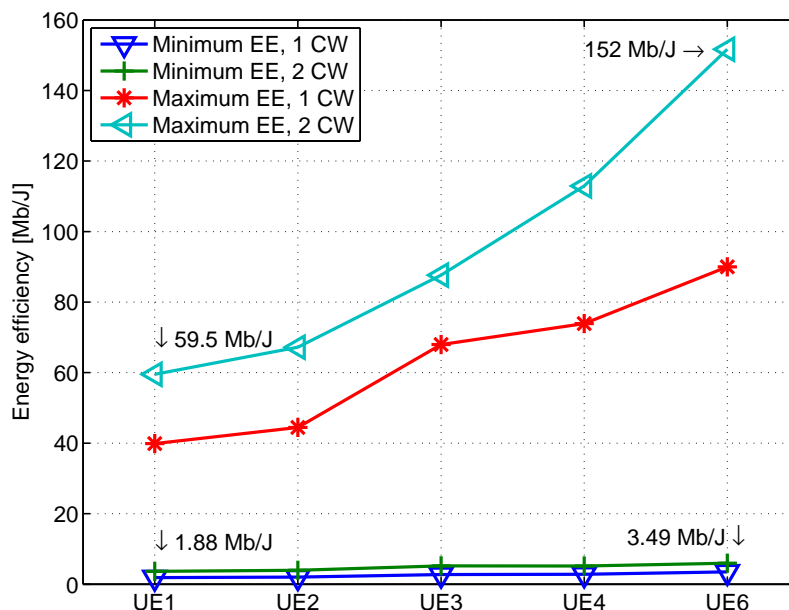


Figure 2.8: Downlink energy efficiency for the 4 UEs.

because the same overall power savings between UEs can be observed. The power consumption is almost independent of the receive power, but it shows 1-2 distinctive jumps in power consumption whenever the UE changes gain settings due to increased/decreased receive power level. The gain change mechanism was observed to employ hysteresis such that the baseband processing is not affected by switching issues.

To summarize the RRC Connected mode measurements figure 2.9 shows the average power consumption of each UE relative to their launch date. The figure includes two fits to the data and they show that the average UE power in 2015 will be less than 700 mW.

2.5.1 Discontinuous Reception Measurement Results

In this subsection the DRX power consumption is examined ¹. This feature allows the cellular subsystem to power down specific components for a certain amount of time, which depends on the implementation and period length as illustrated in figure 2.3 and described in [27]. If the period is long the cellular subsystem can reach a deep sleep mode, where the power consumption is close to the base power (measured in flight mode), but if the period is shorter the light sleep mode is used. The advantage of the light sleep mode is that the power up and down time is much shorter. The two modes are illustrated in figure 2.10a and 2.10b, which are averaged measurements on UE3 and UE4.

Both the sleep power level and the state-change time improves from UE3 to UE4,

¹Measurement data is not available for UE1, UE5, and UE6

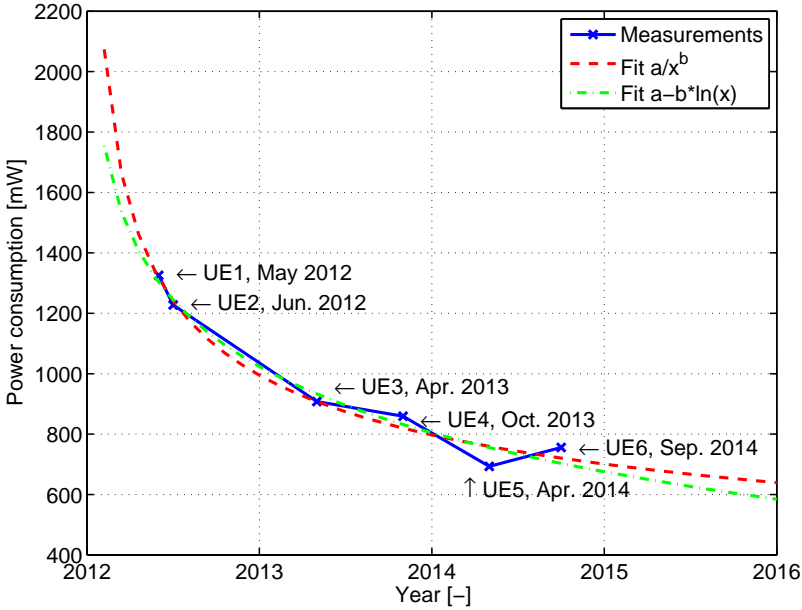


Figure 2.9: Power consumption evolution with two fits. Data is for the common point where DL MCS 0, DL PRB 3 or 4, receive power -25 dBm, UL MCS 5 or 6, UL PRB 100, transmit power -40 dBm. Found in test case 2, 4, 5, and 6 and averaged.

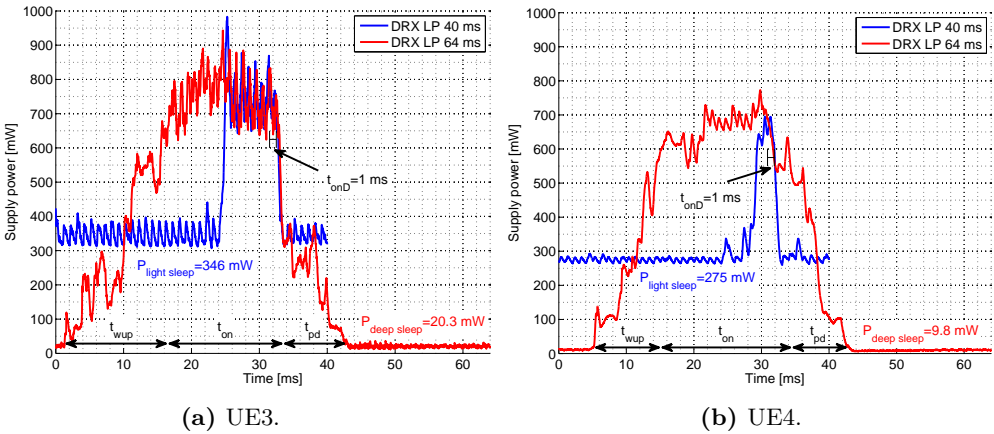


Figure 2.10: Discontinuous Reception power consumption measurements.

and this is also illustrated in figure 2.11a, which shows that the power consumption in both light and deep sleep has been reduced by more than 50 % from UE2 to UE4. In [27] we analyzed the total energy consumption in light and deep sleep mode as a function of DRX Long Period length and the result showed that the switching point between the two modes is carefully selected such that the total energy consumption is as low as

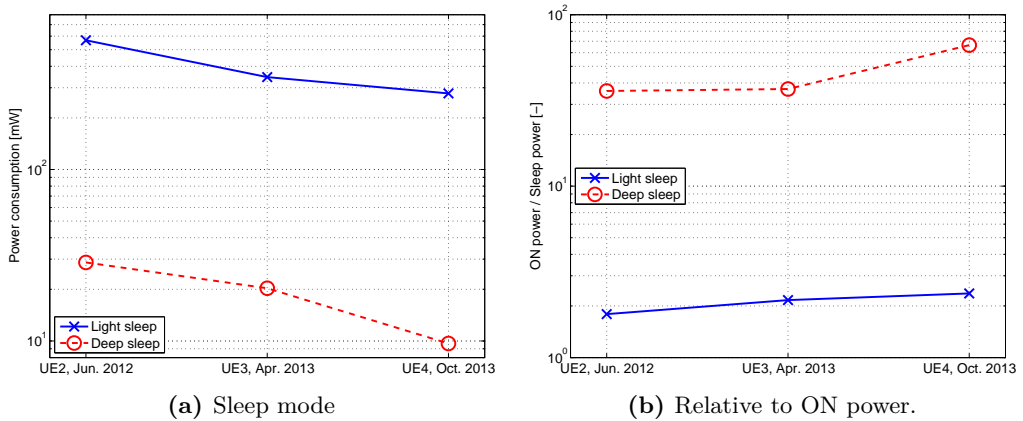


Figure 2.11: Power consumption evolution for Discontinuous Reception sleep mode.

possible.

The published DRX measurements [26, 27], which to the author’s knowledge were the first detailed LTE DRX examinations, are in contrast with the widely used model proposed by Nokia in Third Generation Partnership Project (3GPP) in early 2007 [61]. The model assumes that deep and light sleep is $1/50$ and $1/2$ of active mode power consumption, respectively, and this corresponds well with the performance of UE4 as illustrated in figure 2.11b. The issue is that the model estimates the transition from light sleep to active mode takes 1 TTI i.e. 1 ms while exiting deep sleep takes another TTI. The transitions are however not executed that fast in the current devices as can be seen in figures 2.12 and 2.13, which show the times for long and short periods respectively. Therefore estimations, which are based on the old model [61] are too optimistic in terms of how fast the UE can enter and exit the sleep mode, and also in estimating the total energy consumption because the power consumption in the transition phase is higher than in the sleep mode and because the time durations is longer.

Figure 2.12 furthermore illustrates that the wake up and power down times have improved with each UE generation, while the ON time is more static. One reason is the structure of LTE’s Primary Synchronization Signal (PSS) and Secondary Synchronization Signal (SSS), which only are broadcasted every 5 ms. Therefore the UE cannot go below this system boundary without using a more accurate clock to avoid synchronizing via PSS and SSS, which would lead to higher power consumption.

Examining the results for the short period ², shown in figure 2.13, it is evident that a different approach has been take in the chipset design, because UE3 shows a dramatic improvement in state change time while the ON time is almost the same as UE2. On the other hand UE4 provides a significant reduction of the ON time while transition times are longer than UE3. The latter option however proves to be the most efficient because the power consumption in the ON phase is higher than in the transition phases. This can be seen in the total energy consumption $E_{\text{wup+sync+pd}}$, which is almost reduced to half.

²Note that none of the UEs enter DRX sleep modes when the period is shorter than 32 ms

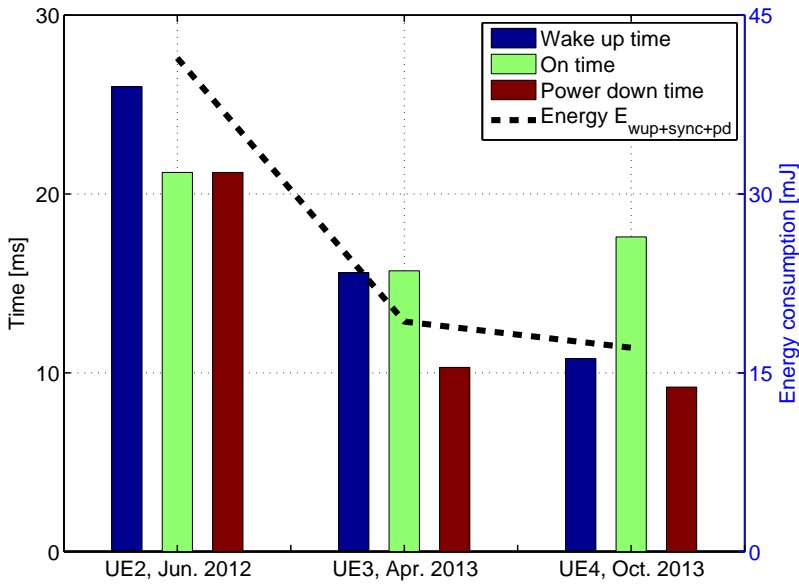


Figure 2.12: Evolution for DRX time parameters for long periods (80 ms for UE2 and 64 ms for UE3 and UE4).

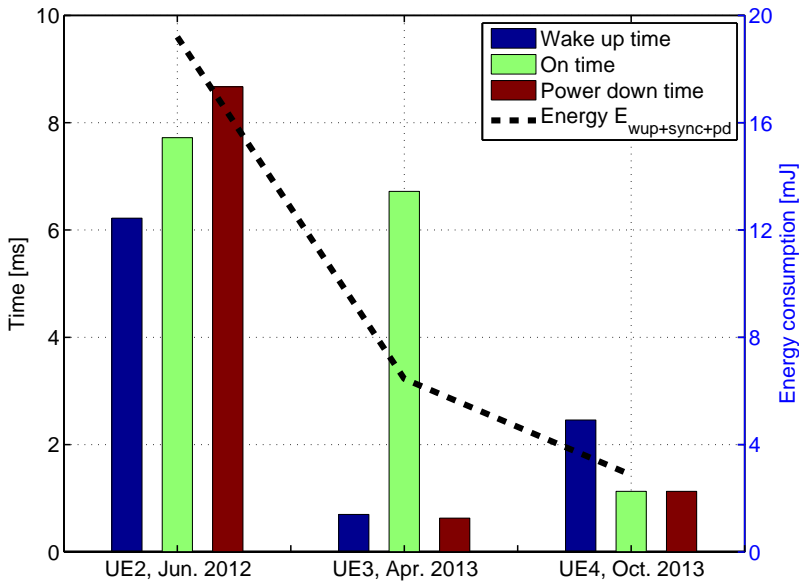


Figure 2.13: Evolution for DRX time parameters for short periods (40 ms for all UEs).

2.6 Summary

In this chapter the proposed LTE UE power consumption model was presented together with the applied measurement methodology. The chapter was based on the contributions in [25, 26, 27].

The methodology, which uses a base station emulator and a measurement power supply at the battery terminal, was selected based on a review of existing power consumption models and the related methodologies. A set of test cases were then developed to separately measure the power consumption of specific components of the cellular subsystem. The model covers power consumption as a function of receive and transmit power levels and data rate, and also includes DRX light and deep sleep modes.

Selected measurement results were presented to illustrate that turning the cellular subsystem ON and using high transmit powers (≥ 10 dBm) are the most power consuming features of current LTE smartphones. The benefits of LTE was noted to be high EE at high data rates and low power consumption in DRX sleep mode.

The chapter also showed how the UE power consumption has evolved since the first LTE capable smartphones were launched in Spring 2012. The base power consumption of the cellular subsystem has almost been reduced by half, but some vendors loose this advantage due to the choice of a less efficient PA solution. The comparison also illustrated that the new supply technique Envelope Tracking can provide significant improvements for the high transmit power region where Average Power Tracking is less efficient. In addition to the decreased base power consumption the DRX sleep mode has also evolved such that both the power up and down times are shorter and the sleep power is lowered by approximately half.

In the next chapter the model is applied to optimize LTE smartphone power consumption while maintaining the performance experienced by the user.

Chapter 3

Energy Saving in LTE User Equipment

Due to the user demand for longer smartphone battery life, discussed in chapter 1, this study also focused on how energy may be saved in Long Term Evolution (LTE) User Equipment (UE). In this chapter the main results of four published articles, dealing with energy saving, is presented together with an overview of the contributions. The details are available in the re-print of the papers located in appendix H, I, J, and K.

The measurement results presented in chapter 2 showed that the most power is consumed when the cellular subsystem is ON and when the transmit power exceeds 10 dBm. On the contrary high data rates in uplink and downlink provides the most energy efficient means for data transfer, while Discontinuous Reception (DRX) especially for periods longer than 40 ms is the optimal state for unscheduled UEs. Thus this knowledge can be applied when designing features for LTE. However some of the work presented in this chapter was made and published before the LTE UE power model was developed because commercial UE were not available at that time. Fortunately the work deals with some of the key problems later identified by the model, and furthermore the overall trend observations and conclusions are still valid even though the absolute values have changed given the updated power model.

During the standardization phase and around the launch time of LTE most research in the area of UE energy saving focused on efficient DRX sleep mode, low power components, and energy aware scheduling.

The DRX papers often proposed their own power model e.g. in the work [62] assume 75 % energy is saved in the sleep mode as compared to the active mode while not specifying the time it takes to switch mode. Another [63] only calculated the percentage of time the UE can sleep without including the switching time. Finally some DRX analysis [64] was based on Nokia's power model [61], which uses light and deep sleep power levels and swiatching times that are quite far from what is currently achievable because deep sleep is estimated to be 0 mW while light sleep is 11 mW. The transition time is also set to just 1 ms.

Clearly much research was devoted to the DRX sleep mode, but actually the UE may also sleep when in active mode due to the channel allocation structure. This concept was explored in [28] and is discussed in section 3.2.

Besides the studies on configuration and possible benefits of DRX, work was also done to examine how to power ON and OFF the cellular subsystem components [65]. Related to that the power consumption of the individual components was studied, for example the Power Amplifier (PA) [66] and the Turbo decoder [67]. In addition to the physical UE components the network settings were also studied to ensure long battery life. For example the Fractional Power Control was introduced [68] to ensure limited intercell interference at cell edges, but it was not considered how it could be combined with a scheduler to improve the battery life. Some articles did consider the power consumption when designing the scheduler, but often the transmit power was used instead of a proper power model, reflecting the PA efficiency, to calculate the consumption [69]. Therefore the work published in [29] and presented in section 3.3 was made to link the Transmit Power Control (TPC) with a scheduler to examine energy consumption using a power consumption model.

The initial release of the LTE standard does not fulfil the data rate requirements of 1 Gb/s [70], defined for the International Mobile Telecommunications-Advanced system, and therefore the use of Carrier Aggregation (CA) was implemented in release 10 to boost the data rate. It was thus an open issue how the UE energy consumption would be affected by the increased hardware and processing complexity. This was addressed by [30] and later verified by [31] as presented in sections 3.4 and 3.5.

In the next section the contributions of the papers are highlighted after which the main concept and results of each paper are presented.

3.1 Paper Contributions

In this section the contributions from the published papers are highlighted. Re-prints are available in appendix H ,I , J, and K.

[28] Fast Control Channel Decoding for LTE UE Power Saving

In this paper it is analysed how unscheduled, but RRC_connected UEs may apply fast control channel decoding to determine whether they are scheduled and then power down until the next subframe to save 5%-25% energy. The cost is a degraded channel estimate leading to a minor throughput loss of 1-4%. The paper also discusses the sleep method's feasibility, which later was confirmed to be applicable by the 4GMCT project partner Intel Mobile Communications, and how it can complement DRX.

[29] Reducing LTE Uplink Transmission Energy by Allocating Resources

In this paper uplink scheduling is discussed using UE power consumption as a metric. The target is to evaluate, using a power consumption model, whether it is most energy efficient to upload a video using a few resource blocks over a long period or many resource blocks during a short period. The preferred scheme is Time Division Multiple Access (TDMA)-like i.e. allocating many frequency resources to a single user. The paper has 18 individual citations, excluding self-citations on November 2nd 2014.

[30] LTE UE Energy Saving by Applying Carrier Aggregation in a HetNet Scenario

In this paper the measurements from [25] were used to develop a CA UE power consumption model. Using a simulated Heterogeneous Network (HetNet) and the model it was concluded that CA may provide energy savings if the data rate is increased at least 20% as compared to single carrier UEs. The paper presents the first CA power model applied in a realistic HetNet and the assumptions were later confirmed by [31].

[31] Current Consumption Measurements with a Carrier Aggregation Smartphone

In this paper the CA model from [30] was compared with the first publicly available CA power consumption measurements on a commercial smartphone. The measurements include DRX and various traffic types. The results verified that for a transfer of large files the use of CA is more energy efficient than single carrier LTE because the UE may enter a low-power sleep mode faster. The paper was made in collaboration with Nokia, Irving, USA, which connected the UE to a commercial Evolved Node B (eNB) Over-the-Air (OTA)

3.2 Fast Control Channel Decoding

The DRX sleep mode has been extensively studied [62, 63, 64] in connection with the launch of LTE, and the measurements presented in section 2.5.1 also confirmed that it is an important method for UE energy saving. The issue with DRX is however that it requires the downlink traffic to be periodic or resilient to delays because the UE can only be scheduled periodically as illustrated in figure 2.3. Because the eNB can only deliver data in these periodic ON instances it complicates the scheduling and increases the eNB buffer requirements. Finally overhead is also introduced because the eNB needs to inform the UE about the DRX parameters such as the duration of the DRX Long Period (DRX LP) and the ON time. These disadvantages may entail that the eNB chooses not to apply DRX sleep mode to a specific UE if the traffic pattern is less suitable. This has a negative effect on the UE energy consumption because the UE is required to buffer and decode every subframe to check if it is scheduled. In [28] it was thus examined if the UE can enter a micro sleep mode when it is not scheduled and what the cost would be

of not receiving the specific frame.

In LTE the 10 ms frame is composed of 10 subframes. Each subframe, which is structured as illustrated in figure 3.1, is split into two slots and some of those are allocated special channels, for example the Physical Broadcast Channel (PBCH) only appears in the second slot of the first subframe while the Primary Synchronization Signal (PSS) and Secondary Synchronization Signal (SSS) are allocated in the first slot of subframe 1 and 6 [71].

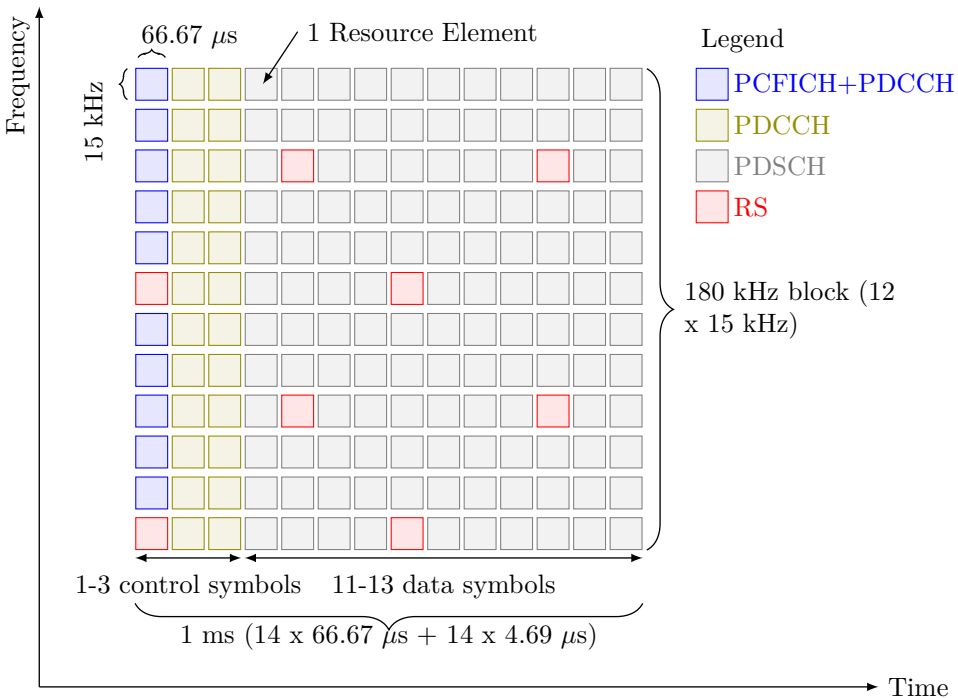


Figure 3.1: An LTE subframe with normal cyclic prefix ($4.69 \mu\text{s}$) ahead of each symbol. Note not all possible channels are shown. [71].

Every downlink subframe is primarily occupied by the Physical Downlink Shared Channel (PDSCH), which contains the individual user data. Based on channel feedback and the scheduling algorithm the eNB will allocate data for each user in time and frequency in chunks known as a Physical Resource Block (PRB) which in LTE is constituted of 1 subframes in the time domain and 180 kHz wide in the frequency domain. The eNB will use the Physical Downlink Control Channel (PDCCH) to inform the UE where the data is located and what Modulation and Coding Scheme (MCS) is used. This information is conveyed via the Downlink Control Information (DCI), which may also contain updates on TPC, Hybrid Automatic Repeat Request (HARQ), uplink grants etc., [72]. Multiple PDCCHs can exist in the same subframe and each uses 1, 2, 4, or 8 Control Channel Elements (CCEs) to contain the DCI. Furthermore the PDCCH may span the first 1, 2, or 3 Orthogonal Frequency Division Multiplexing (OFDM) symbols

depending on the control channel load. By decoding the Physical Control Format Indicator Channel (PCFICH) the UE will know the number of symbols used for PDCCH in the current subframe. By applying the UE-specific Radio Network Temporary Identifier (RNTI) in the decoding process the UE can determine whether the DCI was intended for it by checking for Cyclic Redundancy Check (CRC) errors. If errors are observed the UE is not scheduled in the current subframe and it will thus await the beginning of the next subframe. The problem is that the PDSCH follows directly after the PDCCH, as illustrated in figure 3.1, and therefore the UE is forced to buffer the PDSCH across the whole channel bandwidth because it does not know if and where it is scheduled when the channel data starts to arrive. This reception and buffering is a waste of energy if the UE after decoding the DCIs learns it is not scheduled. In [28] it was therefore proposed to decode the PCFICH and PDCCH as fast as possible and then stop buffering the PDSCH and power down the receiver if the data is not intended for the UE. The first issue is thus whether the UE can decode the control channels as fast as needed.

Because LTE's wide bandwidth allows for many CCEs in the PDCCH two search spaces are introduced; a common containing for example DCI with information about TPC and a UE specific containing the PDSCH allocation. The common search space, defined in [72, Table 9.1.1-1] to cover 16 CCEs, may aggregate either 4 or 8 CCEs to transfer one DCI and therefore it can contain either 4 or 2 of those. Because the UE is blindly decoding it will attempt to decode the first CCE in each of the aggregated parts hence a total of 6 decoding attempts as illustrated in figure 3.2. The UE-specific search space also allows for aggregation levels of 1 and 2 and in

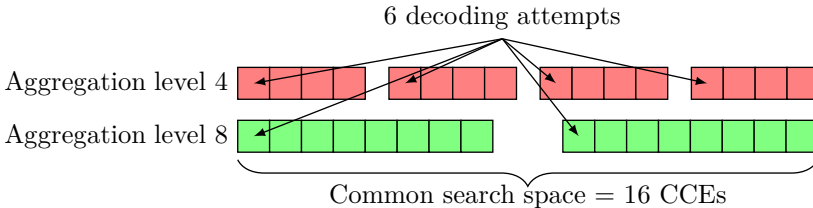


Figure 3.2: Locating PDCCH in common search space. Note that the search space may be spread across the frame in both time and frequency. [72].

total there are 16 possible locations. For each transmission mode there is always two DCI formats [72, Table 7.1-5] of individual size and therefore the UE has to decode $2 \cdot 6 + 2 \cdot 16 = 44$ CCEs in each subframe.

Each CCE is composed of 9 Resource Element Groups (REGs) and each REG contains 4 Resource Element (RE), which is the smallest component in LTE as illustrated in figure 3.1. The total number of bits per Quadrature Phase-Shift Keying (QPSK) modulated CCE is thus $9 \cdot 4 \cdot 2$ bits = 72 bits and therefore the UE needs to decode at least 72 bits $\cdot 44 = 3168$ bits per symbol duration. A category 3 LTE UE can receive up to 100 Mb/s [59] i.e. decode 100 kb per subframe and 7.1 kb per symbol duration and thus the control channel decoding of about 3 kb can be expected to complete fast.

The proposed concept in [28] was therefore to perform a fast channel estimation followed by fast decoding of the control channels to determine if the DCIs carry a scheduling grant. If this is not the case the UE shall proceed as illustrated in figure 3.3 and enter

a low power sleep mode for the rest of the subframe. Obviously it is only possible to

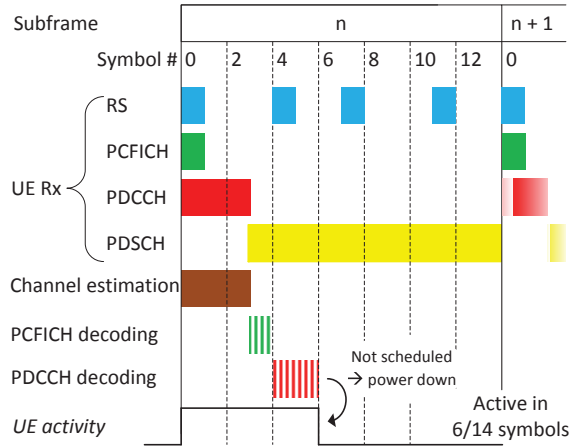


Figure 3.3: Applying the fast control channel decoding to power down in unscheduled subframes. [28, Figure 1]

power down components in Radio Frequency (RF) and Base Band (BB) which have a short wake-up delay such as buffer memory and throttling of processor frequency in the BB and Low Noise Amplifiers (LNAs) and Programmable Gain Controls (PGCs) in the RF, which were estimated to wake-up within $2 \mu\text{s}$ in [73]. The measurements in section 2.5.1 especially figure 2.13 have however shown that the wake-up and power-down times to light sleep DRX currently is in the order of 1 ms while the power consumption is reduced by a factor of 2 as illustrated in figure 2.11b. The time may be optimized by avoiding powering up/down components, which settle slow such as the synthesis, and optimizing the wake-up sequence.

The power saving potential of the fast control channel decoding concept, in short referred to as micro sleep [74], was evaluated by estimating the power consumption in subframes where the concept was applied. The power consumption was then compared with the power consumption in normal subframes with data reception and with subframes where the PDSCH is buffered but not processed, when the UE is unscheduled. The micro sleep concept was estimated to consume between 40% and 60% of the active power, while the less efficient concept where PDSCH is buffered but not processed was set to 70%-90%. Then a two-state Markov chain was used to calculate the activity factor i.e. the relationship between scheduled and unscheduled subframes and to simulate various traffic types such as voice and video, see [28, Table 3]. The potential savings when using the micro sleep concept instead of the full buffering method are illustrated in figure 3.4. Depending on the activity factor of the application the savings are 5%-25% for the case where the micro sleep concept saves 50% power and the full buffering method 70%.

Figure 3.4 also illustrates how DRX in theory can be applied for specific activity factors. For example DRX LP has a minimum periodicity of 10 subframes [60] and given that the UE is active in one of those subframes the maximum activity factor is 10%. Clearly the micro sleep concept is applicable for much higher activity factors

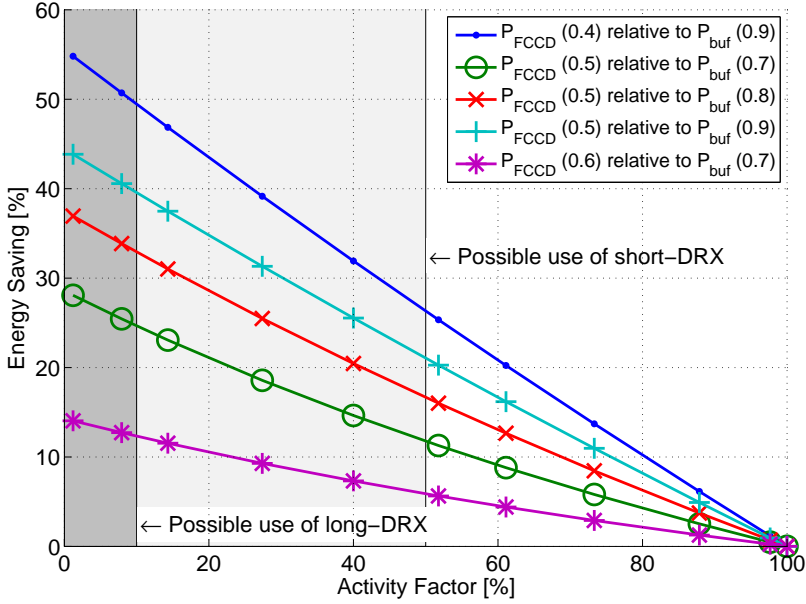


Figure 3.4: Potential energy savings when the micro sleep concept replaces the method where data is buffered. $P_{\text{FCCD}}(x)$ covers the micro sleep power consumption relative with $x\%$ to the active mode while P_{buf} covers the buffering method.[28, Figure 7]

and it can thus complement DRX when the traffic pattern is rapidly switching and/or aperiodic. Furthermore there is no control channel overhead when using the concept because it is applied individually by each UE, and in contradiction to DRX it does not affect scheduling.

The cost of using the micro sleep concept is evident, when examining figures 3.1 and 3.3 because if the UE is powered down after the 6th OFDM symbol it cannot receive the Reference Signal (RS) located in symbol 8 and 12. The RS are used to perform channel estimation and receiving them would entail the UE had an updated estimate available when the next subframe arrives. There are 8 RS per antenna port per PRB [71] and assuming that the UE is using half of the RSs from the previous frame for stabilization, the channel estimate will in the general single antenna case be based on 12 RS. When the UE applies the micro sleep concept in a frame the channel estimate for the following frame can only be based on the 8 RS within that frame thus the estimate is degraded, which may be interpreted as a lower Signal to Noise Ratio (SNR) using [75]

$$\text{SNR}_{\text{ch.Est}} = \frac{\text{SNR}}{1 + \frac{1}{d} + \frac{1}{d \cdot \text{SNR}}} \quad (3.1)$$

where: $\text{SNR}_{\text{ch.Est}}$ is the effective SNR based on channel estimation [dB]
 SNR is the SNR provided full channel information [dB]
 d is the number of RSs used for channel estimation [-]

Equation (3.1) is valid when the channel, in which the PRB is transmitted, is flat in time and frequency. In [28] this was calculated to be the case when the UE speed is below 27 km/h and because most UEs are indoor, thus having low mobility, the requirement is fulfilled.

The estimated SNR loss when using micro sleep is illustrated in figure 3.5. The low

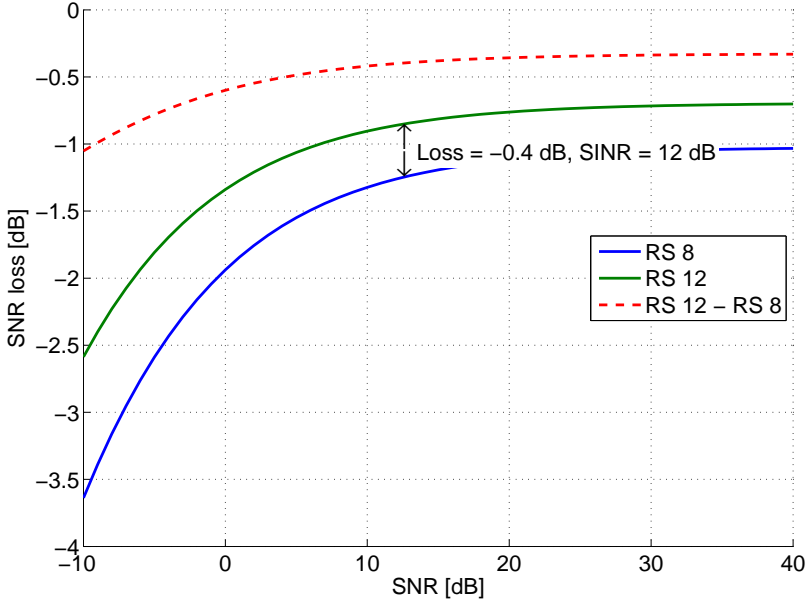


Figure 3.5: Estimated SNR reduction as a function of received RS.[28, Figure 3]

SNR loss was calculated to result in about 1% throughput loss on average and maximum 4% in [28] and thus the degradation is deemed negligible.

The conclusion is that the micro sleep concept can help reduce the energy consumption when UEs are RRC_connected but not scheduled, by performing fast control channel decoding and sleeping for parts of a subframe. The estimated savings are in the order of 5%-25% while a maximum throughput loss of 4% was observed due to a degraded channel estimate.

Refer to section H which is a re-print of [28] for simulation details and results.

3.3 Energy Saving by Uplink Scheduling

As explained in the beginning of this chapter researchers have studied how TPC and scheduling can be optimized to increase throughput and coverage, but with little emphasis on UE energy consumption. The work presented in [29] therefore examined how allocation of PRBs in uplink affect the instantaneous transmission power and the UE energy consumption of a file transfer.

The starting point is to determine the transmission power in the Physical Uplink Shared Channel (PUSCH), which is used for most UE data transfers. It is updated on a subframe basis using TPC [72] and includes both Fractional Power Control (FPC) and closed loop parameters:

$$P_{\text{Tx}} = \min(P_{\text{MAX}}, P_0 + PL \cdot \alpha + 10 \log_{10}(M) + \Delta_{TF} + f) \quad [\text{dBm}] \quad (3.2)$$

where:

P_{Tx} is the transmit power	[dBm]
P_{MAX} is the maximum transmission power	[dBm]
P_0 is a FPC power offset parameter	[dBm]
PL is the downlink path loss estimate	[dB]
α is a FPC path loss compensation factor	[-]
M is the number of allocated PRBs	[-]
Δ_{TF} and f are closed loop parameters	[dB]

The FPC relies on adjusting the factor $\alpha \in \{0, 0.4, 0.5, 0.6, 0.7, 0.8, 0.9, 1\}$ to compensate for the measured path loss [68], while the closed loop parameters depend on the selected MCS in order to achieve a certain Signal to Interference + Noise Ratio (SINR) according to interference [76] and load [77].

In [29] only FPC, with $\alpha = 0.6$, $P_0 = -54.5$ dBm, is used hence the transmit power depends on the path loss and the number of allocated resources. If the number of resources M is doubled the transmit power will also increase 3 dB provided that the maximum transmit power is not exceeded. The number of resources a UE can obtain depends on the channel bandwidth, which in this work was set to 10 MHz, the number of active UEs and the scheduling algorithm. The number of active UEs was varied from 6 to 10 while the scheduling algorithm relies on a round-robin equal opportunity principle where each UE is assigned PRBs turn-by-turn until P_{MAX} or maximum number of PRBs per user is reached or all PRBs are used. Each UE is assigned one path loss value as if located in the macro1 propagation scenario [76]. The instantaneous transmit power is then calculated using eq. (3.2) with the assigned M and PL after which the power consumption is calculated.

When the study was made a Wideband Code Division Multiple Access (WCDMA) based measurement [78] was the only model available. The model maps transmit power to total UE power consumption and includes the power consumption of not only the PA but also the BB and the Power Management Unit (PMU). The mapping is illustrated in figure 3.6 and the measurements presented in section 2.5 have confirmed that it is a reasonable assumption not to include the uplink data rate as a parameter because the power consumption is nearly independent of the encoding function. Figure 3.6 also includes the measurements on LTE UE4, refer to table 2.6 for detailed characteristics, because it is the most energy efficient UE where a complete model is available. The older WCDMA UE consumes less power, but the results from [29] are not updated because the two UEs show the same trend i.e. increasing energy efficiency when the transmit power increases above 0 dBm. Because most UEs in the macro1 propagation scenario use transmit powers above 0 dBm, see the transmit power distribution in [29, Figure 5], the conclusions are expected to be similar for the LTE UE4 even though the absolute numbers are different. The major difference in the power modelling is related

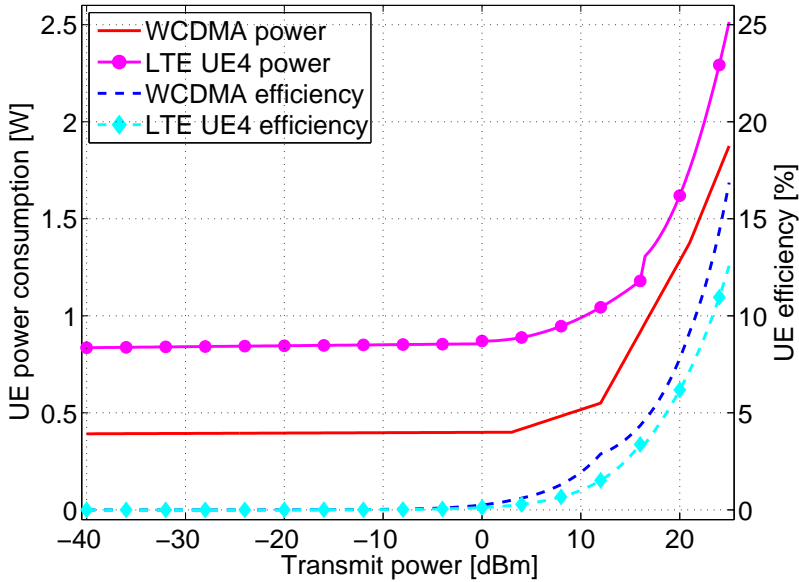


Figure 3.6: Transmit power consumption and energy efficiency for WCDMA and LTE UE4. The WCDMA model is a fit to [78, Figure 20.30]

to the RRC_connected, but not scheduled power and sleep mode power. In [29] the unscheduled UE was estimated to consume 35% less than when actively transmitting with sub zero power. This is in contrast to LTE UE4 which, according to the power model, saves less than 5% when awaiting scheduling grants. The incentive to finish the transmission fast is therefore greater for the LTE UE. In the simulations only uplink traffic is used and therefore the UEs can enter a combined Discontinuous Transmission (DTX) and DRX mode. The sleep mode power was set to 11 mW in [29] while the measurements in figure 2.10b report about 10 mW, but due to the difference in active mode power consumption the incentive to enter sleep mode fast is greater for the LTE UE. The sleep mode duration is calculated such that all users are compared over the same amount of time:

$$t_{\text{DTX},i} = \max_{j \in [1,N]} (t_{\text{tx},j}) - t_{\text{tx},i} \quad [\text{s}] \quad (3.3)$$

where: $t_{\text{DTX},i}$ is the time the i 'th user will be in DTX sleep [s]
 N is the total number of simulated users [-]
 $t_{\text{tx},j}$ is the transmission time for the j 'th user [s]

Note that the transition time from sleep to active and vice versa was not included in the simulations because it was based on the old Nokia model [61].

In the first simulation a single user was placed in a cell with limitations on the number of available PRBs. Because control signalling, such as the RSs, consumes up to

2 PRBs [79] the available resources are varied between 48 and 2 as illustrated in figure 3.7. Allocating many frequency resources in a short time frame resembles the TDMA scheme while the opposite strategy resembles the Frequency Division Multiple Access (FDMA).

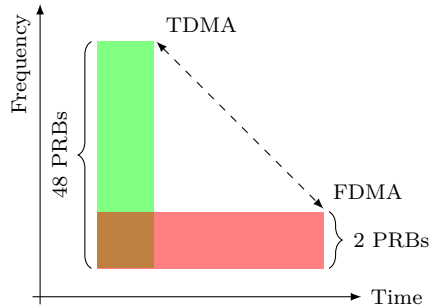


Figure 3.7: Allocation of PRBs in the time and frequency domain.

Allocating many resources to one UE will increase the delay before other UEs can commence their transfer, but in this study the upload of a video was not considered delay critical and furthermore the transfer will in theory finish as fast as the case where the UEs are allocated a few resources each Transmission Time Interval (TTI). The latter scheme may however increase the active time for each UE causing excessive power consumption. Furthermore the two Multiple Access (MA) schemes each provide diversity benefits in either time or frequency domain, but this requires feedback which limits the available resources.

The single user data rate is illustrated in figure 3.8 and the step-wise part of the curves clearly indicate how transmit power limited users are forced to reduce the number of PRBs and thereby also have their data rate reduced. The right-most part of each curve is determined by the UEs's SINR which determines the spectral efficiency per PRB. Using the mapping of figure 3.6 and equation (3.3) the total energy consumption of each UE was calculated and as expected the allocation of many resources to a single user proved to be most energy efficient. The reason is the related short transmit time and the fact that the transmit PA is most efficient at high transmit powers.

In the second simulation multiple users exist in the system and arrive with a probability such that 4 users on average are active in each TTI. The maximum number of simultaneous users is varied to examine how the UEs's energy consumption is affected by the increased scheduling delay due to the round-robin scheduler. The resource sharing limits the users' data rate, but again the TDMA like scheme is preferable and UEs who can utilize up to 48 PRBs finish the transfer 24 %-38 % faster than users limited to 8 PRBs [29, Table 2]. Therefore the total energy consumption is also lower for the UEs who are allocated many resources as illustrated in figure 3.9.

The conclusion is that the longest battery life is achieved if the scheduler allocates as many resources as possible to a single UE turn-by-turn instead of allocating a few resources to many UEs each TTI.

Even though the results were produced using a WCDMA based power model the

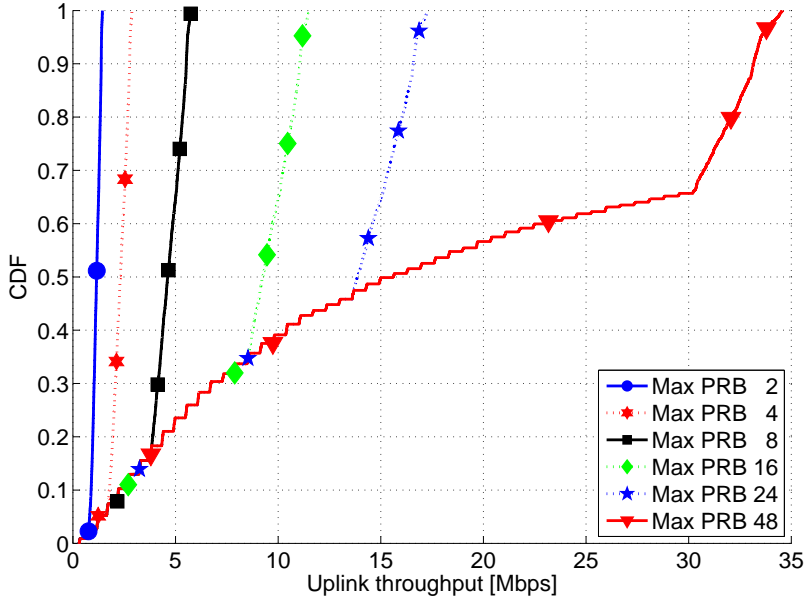


Figure 3.8: Single user uplink throughput [29, Figure 4].

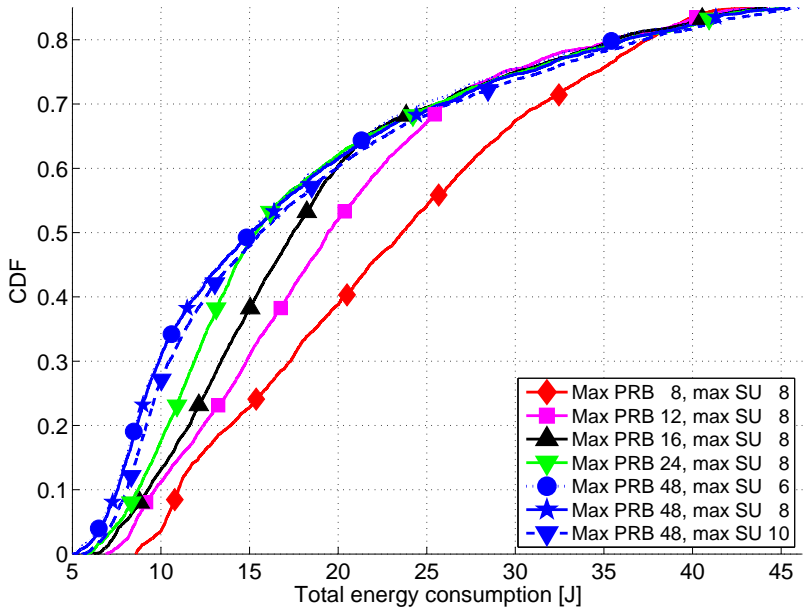


Figure 3.9: Simultaneous users' total energy consumption. *Max SU* refers to the maximum number of simultaneous users.[29, Figure 8]

results are also valid for LTE and as discussed earlier the gains of finishing the transfer faster will be even bigger because the ratio between active, unscheduled but active and

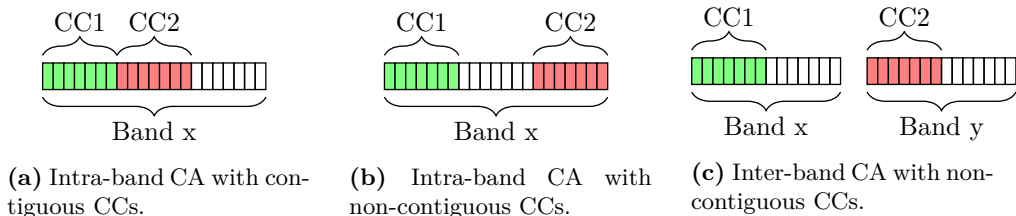
sleep mode are more advantageous in the WCDMA model.

Refer to section I which is a re-print of [29] for simulation details and results.

3.4 Carrier Aggregation Energy Saving

CA was introduced in LTE release 10 to improve the coverage and average throughput by allowing UEs to connect to multiple Component Carriers (CCs) in downlink. The benefits of the increased bandwidth in terms of frequency diversity and scheduling flexibility [80] are clear, but it was unclear how the UE power consumption would be affected by the increased component count and complexity. In [30] a CA power consumption model was therefore proposed to study the battery life in a HetNet scenario.

The Third Generation Partnership Project (3GPP) defined three band options [81] for CA; the intra-band CA with contiguous CCs illustrated in figure 3.10a, the intra-band CA with non-contiguous CCs illustrated in figure 3.10b, and the inter-band CA with non-contiguous CCs illustrated in figure 3.10c. The first CC the UE connects to will be configured as the Primary Cell (PCell) and the procedure follows the one of release 8. After a successful connection the UE will inform the eNB about its capabilities and possibly connect to one or more additional CCs configured as Secondary Cell (SCell). If the eNB decides to activate a SCell the UE has to follow the procedures related to monitoring a regular cell i.e. perform decoding of control channels and feedback Channel State Information (CSI), which are both power consuming tasks.



Due to the diverse CA configurations two types of UEs implementations were modelled in [30]; a single RF front end with a single wideband Analog-to-Digital Converter (ADC) and dual BB, and a dual RF front end with dual narrowband ADCs and dual BB. The first option is only applicable in the intra-band scenarios, and only if the cell bandwidth is equal to or smaller than the UE's bandwidth. The latter UE implementation is applicable in all scenarios, but also has a more complex receiver structure.

At the time of publication of [30] there was no commercial release 10 UEs available to develop an empirical model and therefore the LTE release 8 model, presented in section 2.3 was expanded to cover the envisioned designs. Referring to equation (2.2) as the release 8 model the wideband release 10 model was defined as [30, Equation 4]:

$$P_{R_{x,R10wb}} = P_{R_x} + P_{R_{xRF}}(S_{R_x}) + P_{ADC}(BW) + [q_{2CW, cc1} + q_{2CW, cc2}] \cdot P_{2CW} + P_{R_{xBB1}}(R_{R_{x1}}) + P_{R_{xBB2}}(R_{R_{x2}}) \quad [W] \quad (3.4)$$

where: $P_{\text{Rx,R10wb}}$ is the release 10 wideband UE power consumption [W]
 BW is the channel bandwidth [MHz]
 P_{ADC} is the ADC power consumption defined in [30, Figure 2] [W]
 $q_{2\text{CW, cc1}}$ is the probability of using 2 Code Words (CWs) in CC1 [-]
 P_{RxBB1} is the power consumption in the BB receiving CC1 [W]
 R_{Rx1} is the data rate of CC1 [Mb/s]

while the narrowband release 10 model was defined as [30, Equation 5]

$$\begin{aligned}
 P_{\text{Rx,R10nb}} = & 2 \cdot P_{\text{Rx}} + P_{\text{RxRF1}}(S_{\text{Rx1}}) + P_{\text{RxRF2}}(S_{\text{Rx2}}) + P_{\text{RxBB1}}(R_{\text{Rx1}}) \\
 & + P_{\text{RxBB2}}(R_{\text{Rx2}}) + P_{\text{ADC1}}(\text{BW1}) + P_{\text{ADC2}}(\text{BW2}) \\
 & + [q_{2\text{CW, cc1}} + q_{2\text{CW, cc2}}] \cdot P_{2\text{CW}} \quad [\text{W}]
 \end{aligned} \tag{3.5}$$

where: $P_{\text{Rx,R10nb}}$ is the release 10 narrowband UE power consumption [W]
 P_{RxRF1} is the power consumption in the RF front end receiving CC1 [W]
 S_{Rx1} is the received power in CC1 [dBm]
 BW1 is the bandwidth of CC1 [MHz]
 P_{ADC1} is the ADC power consumption for CC1 [W]

The models were made before the DRX power consumption measurements were published in [26] and therefore the RRC_idle mode power was used instead. This roughly corresponds to using the light sleep power instead of the deep sleep in the current power model and therefore the UEs which can enter the sleep mode fast will be able to save even more energy if the results were updated. The sleep time is defined as a function of the slowest receive time as in equation (3.3) in section 3.3. Furthermore the energy efficiency at high data rates have improved as illustrated in figure 2.8 and this will further improve the energy saving potential for UEs achieving the high data rates.

The proposed CA power models were used to analyze the power consumption and energy saving potential in a HetNet scenario where macro cells were carefully deployed to provide coverage and ensure limited intercell interference, while Remote Radio Headss (RRHs) were deployed to minimize coverage holes and improve the capacity in hotspot areas with many users. In the simulations one CC of 10 MHz was assigned to the macro cells while the RRHs were assigned another CC of 10 MHz. The release 8 UEs can only connect to one of the CCs while the release 10 UEs are assumed to always be connected to both such that fast load balancing can be performed. For further details on the propagation conditions, range expansion settings and scheduler implementation refer to [30].

The average throughput is illustrated in figure 3.10 and because the release 10 UE on average is allocated 95 PRBs as compared to the average 48 PRBs of the release 8 UE it experiences approximately 56 % larger throughput. The higher throughput and the use of more complex receivers entails the $P_{\text{Rx,R10nb}}$ on average is estimated to consume 20 % more power while actively receiving data, but due to the shorter receive time the release 10 UE actually consumes 25 % less total energy when receiving as illustrated in the three left-most curves, marked with *Active*, in figure 3.11. The overall savings

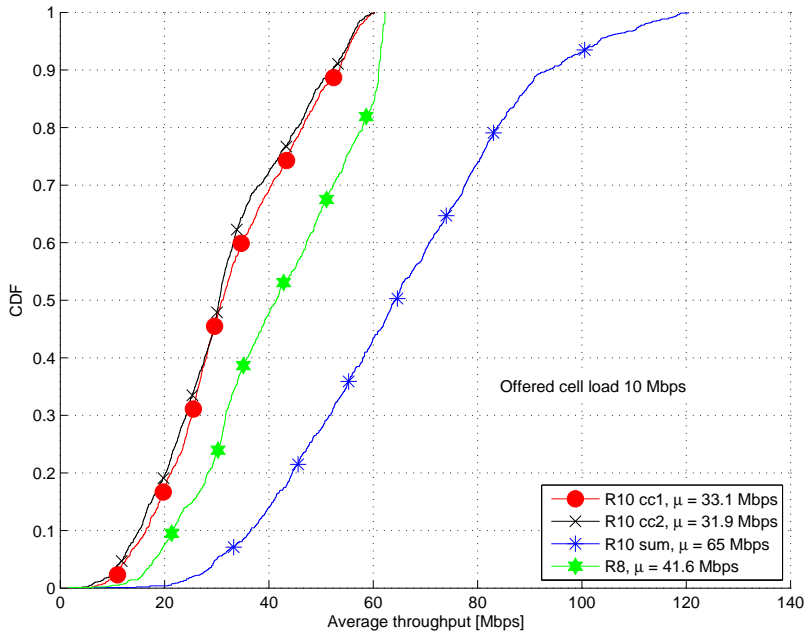


Figure 3.10: Throughput in the HetNet scenario, μ is the average. [30, Figure 6]

when using CA are however only 3%-4%, as marked with *Total* on the three right-most curves, because the total energy consumption is dominated by the sleep mode. This is evident in figure 3.11 where the two *sleep* curves are just left of the *total* curves. Given that the updated power consumption model provides improvements in terms of Energy Efficiency (EE) at high data rates and lower sleep mode power consumption the difference would be bigger if new simulations were made.

In [30] the offered cell load was varied and it was clear that when the throughput advantage of CA is lost due to higher cell loads the battery life may be penalized with up to 20%. Furthermore it was noted that the activity factor, which was discussed in relation to the micro sleep concept presented in section 3.2, is less than 50% for one of the release 10 CCs in high load scenarios. This is illustrated in figure 3.12 where the CC related to the macro cell is utilized much less than the RRH CC. Note there is potential energy savings if the micro sleep concept is applied. In addition to that the 3GPP has also proposed to deactivate the secondary CC (the SCell) if it is not used by the UE, [82].

The conclusion is that the use of CA can provide energy savings in the UE if the throughput is increased at least 20% according to the power model and the analyzed scenario. In the next section the first publicly available measurements on a commercial CA UE is presented and it is confirmed that a throughput increase can lead to longer battery life for certain traffic scenarios.

Refer to section J which is a re-print of [30] for simulation details and results.

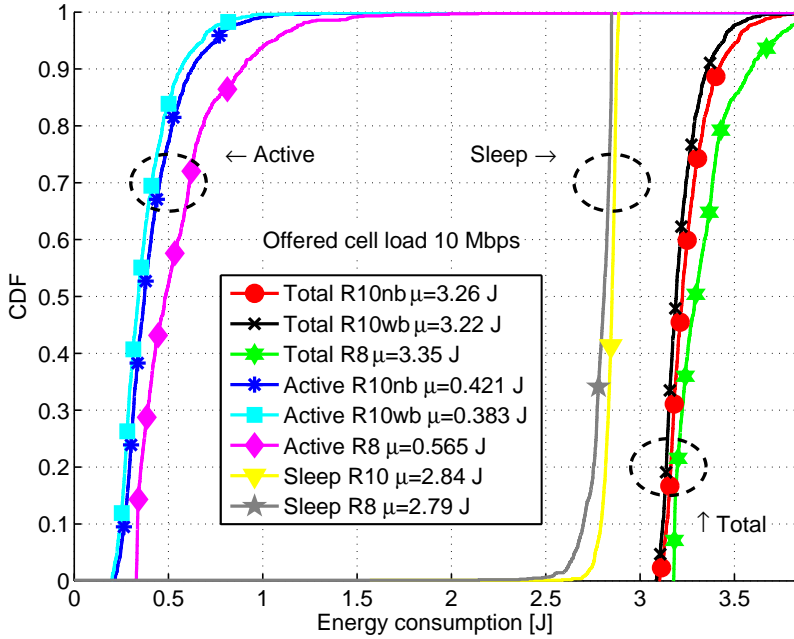


Figure 3.11: Energy consumption when using release 8 and 10 UEs. μ is the average. [30, Figure 8].

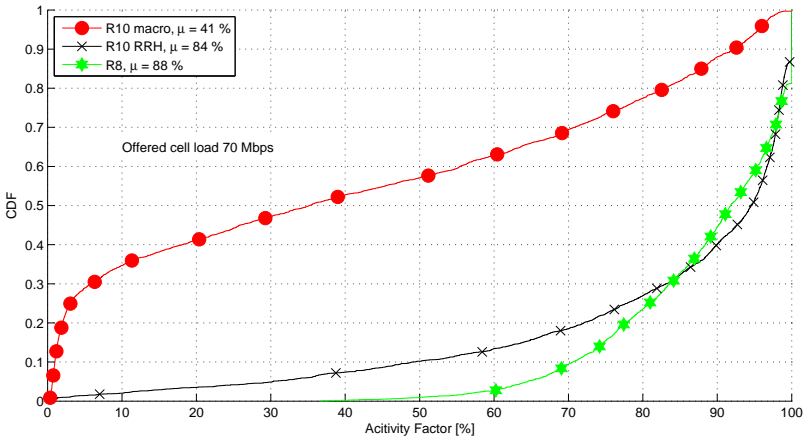


Figure 3.12: Activity Factor for an offered cell load of 70%. μ is the average. [30, Figure 6].

3.5 Measurements on Carrier Aggregation Power Consumption

In summer 2013 the first Long Term Evolution Advanced (LTE-A) UE supporting CA was launched commercially [83] and in [31] we published what we believe is the first

public power consumption measurements on a CA-capable UE. The UE utilizes inter-band CA with a 10 MHz CC in band 3 (at 1.8 GHz) and another 10 MHz CC in band 5 (at 850 MHz).

The measurements were made OTA in the laboratory using eNB equipment, where each band's power was controlled by a variable attenuator. The power consumption was measured using a measurement supply at the battery terminal. Using the eNB entails the level of control achieved in the previous measurements [25, 26, 27] was not possible, but a throughput log with subframe resolution was however obtained.

The first measurement focused on how the power consumption is affected by CA when it is either configured or activated, but no data transfer is occurring. When CA is activated the UE has to monitor the control channels and feedback CSI for both CCs, while in the configured mode the UE will only monitor the PCell. The measurements showed that activated 10+10 MHz CA increased the average current consumption with almost 80% for a 320 ms DRX LP as compared to the single carrier release 8 configuration and this will significantly reduce the benefits of DRX low power sleep. A second measurement showed that when CA is configured, but not activated, entailing only the PCell is monitored, the power consumption is still 65% higher and therefore this first CA implementation seems to switch on both CC receivers even though only monitoring of the PCell is required.

The next measurement dealt with reception of a 1 GB file via the File Transfer Protocol (FTP), and based on the release 8 LTE model, section 2.3, and the extended CA model, section 3.4 the expectation was that the higher data rates would benefit the CA EE. Figure 3.13 illustrates the current consumption when downloading the file for cases where the UE is connected to the single 10 MHz carrier, a single 20 MHz carrier and using 10+10 MHz CA. The red bars shows that the current consumption during the active data transfer is highest when CA is used, but only 4% higher than the 20 MHz single carrier case, which can be interpreted as if the number of PRBs and not the number of CC chains dominate the power consumption.

The CA UE achieves the highest average download speed of 97 Mb/s as opposed to 92 Mb/s and 51 Mb/s of the single carrier 20 MHz and 10 MHz respectively. Even though the current consumption, when using CA is also the highest, the energy efficiency for the reception is more than 20% better as compared to the single carrier case as illustrated with the blue line in figure 3.13. The higher download rate furthermore entails the UE can enter the low power DRX sleep mode faster and therefore the EE improves 13% as compared to the 10 MHz case, when the current consumption is averaged over the slowest download time as was done in equation (3.3) in section 3.3. The results in figure 3.13 therefore confirm the assumption presented in [30] that CA becomes the most energy efficient solution when it is used to improve the user throughput. The exact power consumption and throughput values do however not match between [30] and [31] and because the CA measurements did not follow the test case procedure specified in table 2.5 it is difficult to assess what causes the difference.

Besides testing the high data rate FTP the low data rate applications web browsing, Skype video call and YouTube video streaming were tested but the eNB rarely scheduled data on the SCell in good channel conditions. If channel conditions were bad or higher data rate was required, for example in High Definition YouTube videos the SCell was activated to utilize the gain of being able to schedule more resources on two different

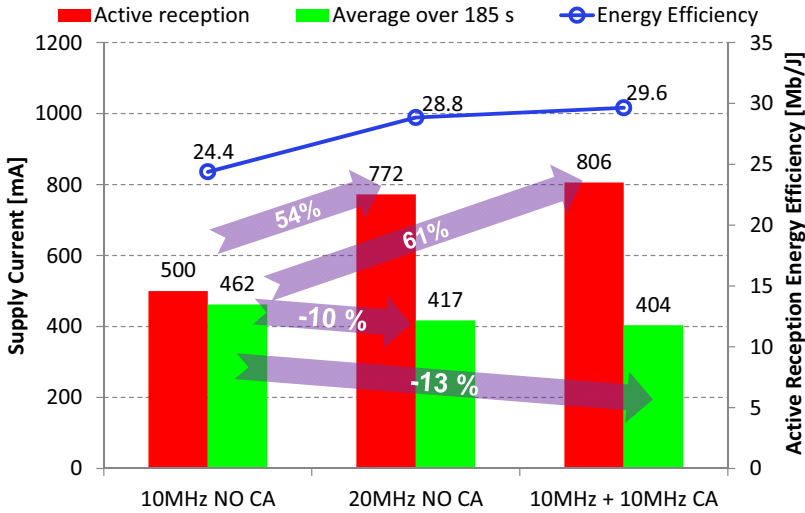


Figure 3.13: Average current consumption for a 1 GB FTP download, [31, Figure 4].

carrier frequencies, but with a cost of 12%-21% in increased power consumption [31]. In addition to the aforementioned low data rate applications the use of keep alive messages was also examined and if CA is configured it may reduce the battery life 3%-13% depending on the number of messages per hour.

The conclusion is that CA will have a positive effect on UE battery life for high data rate applications when the channel conditions and the number of resources are sufficient i.e. as predicted in the previous work [30] discussed in section 3.4. The results also showed that the PMU must be optimized to handle DRX sleep more efficient. Furthermore Mobile Network Operators (MNOs) must carefully consider whether to configure CA if the UE is unlikely to use high data rate applications because CA may not be activated at all and will eventually penalize the user when receiving keep alive messages.

Refer to section K which is a re-print of [31] for simulation details and results.

3.6 Summary

In this chapter research on how to save UE energy in the LTE Radio Access Technology (RAT) was presented using the published results from the articles [29, 28, 30, 31].

The research focused on 3 key areas: controlling the transmit power by resource allocation, ensuring as long low-power sleep as possible, and utilization of high data rates due to CA.

The conclusions are that by allocating many resources to a single UE it can finish a data transfer fast and enter low-power sleep mode, even though it leads to high instantaneous transmit power and therefore high power consumption. The same conclusion is valid for downlink, because the measurements in section 2.5 have confirmed that the EE increases with increasing data rate. However the control and data channel structure

of LTE is not efficient if the UE is not scheduled and therefore the micro sleep concept was presented. The idea is to decode the control channels fast, and if there are no incoming data, enter a low power sleep mode for the remainder of the subframe. Finally it was discussed how the data rates of LTE may be increased by the use of CA and by extending the theoretical power consumption model it was studied how energy may be saved if the data rates are boosted significantly. This was confirmed by measurements on a commercial LTE-A UE, but the results also showed that configuration of CA shall be avoided when low data rate applications and keep alive messages are used.

The conclusion is thus that LTE can be made energy efficient and help prolong the UE battery life if proper scheduling is applied by the MNOs and if UE manufacturers implement efficient DRX and micro sleep modes. In [27] we also noted LTE is currently the most energy efficient RAT.

In the next chapter a new Fifth Generation (5G) is presented to cope with increasing traffic demands. The target is to apply the knowledge obtained about LTE power consumption to ensure the next generation RAT provides long battery life to the users.

Chapter 4

Fifth Generation Radio Access Technology

Every decade since 1980 has been accompanied by the launch of a new mobile Radio Access Technology (RAT) [84, 85], the last one being Long Term Evolution Advanced (LTE-A) (also known as LTE release 10) standardized around 2010 [86], and thus it can be expected that a Fifth Generation (5G) RAT will be launched in 2020. The process of establishing the requirements, exploring design options, and agreeing on solutions via standardization followed by commercialization is a time consuming process and thus it is time to start 5G studies [87].

One reason for the launch of the new RAT every decade is user demand in terms of traffic growth, but the technological improvements also allow for more and more complex systems. In 2007 a study [18] was published on the general technological improvement over more than 100 years and the results showed that the annual improvement is 19-37% for Information and Communications Technology (ICT). It can therefore be expected that the technology will be between $1.19^{10\text{years}} \approx 6$ and $1.37^{10\text{years}} \approx 23$ times more powerful in 2020 as compared to 2010 when LTE-A was standardized. Thus there is a push-pull effect between the capability of technology and the requirements of the RAT.

As mentioned above another reason for implementing a new RAT is the increase in traffic, and a recent traffic forecast [7] by Cisco predicts that the amount of mobile traffic, of which 2/3 will be video, will increase more than 11 times between 2013 and 2018. The forecast also predicts there will be more than 10 billion mobile-connected devices in 2018, while Qualcomm has estimated there will be 25 billion connected devices in 2020 [85]. Thus it is necessary to introduce a new RAT with improved capacity, in terms of data rate and number of served users, and this was also noted in [88] as illustrated in figure 4.1. The figure shows how the number of users with a broadband connection is expected to reach 100% in 2030, but also that the traffic per user is increasing 25%-40% per year, which actually is in line with the general technology improvement [18]. Combining these numbers entails the total amount of traffic will be 130-360 times higher in 2020 as compared to 2010 and thus leading to need for more capacity. Assuming the growth estimates are also valid beyond 2020 the increase in traffic will be 2.300-14.200 times larger in 2030 as compared to 2010 thus a 5G concept must be able to be expanded after

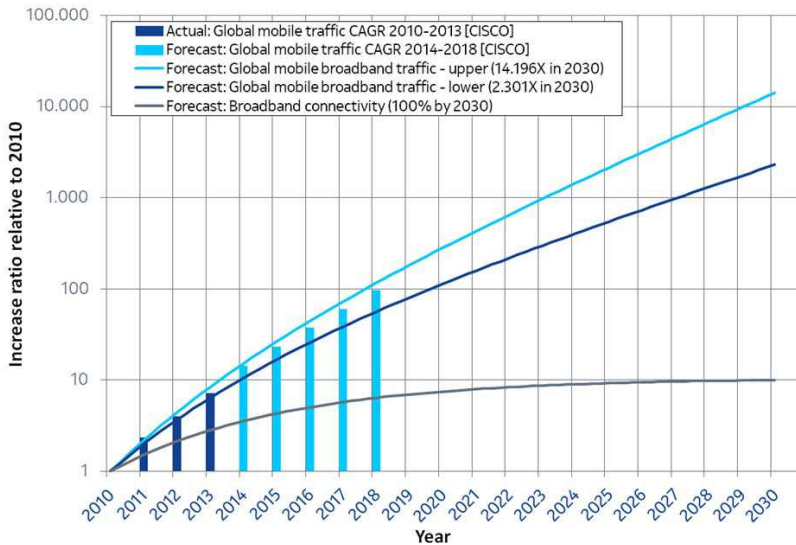


Figure 4.1: Traffic forecast for 2020 using 25 % and 40 % growth rates for individual user traffic. [88, Figure 13].

the expected deployment in 2020. The figure also shows that the actual observed mobile traffic (the bars) in the years 2010-2013 fit well with the curve. The 11 times increase, estimated by Cisco, between 2013 and 2018 will be approximately in between the two *global mobile broadband traffic* curves of figure 4.1 thus there is a common understanding of the need for capacity in terms of traffic volume.

The conclusion is that the general technology performance and the traffic volume increases 6-23 and 130-360 times, respectively in 2020 as compared to when the previous RAT generation was launched around 2010, and therefore the requirements to a new 5G RAT are also made significantly higher [87] than LTE-A:

- 10 Gb/s DL and UL peak data rate
- 100 Mb/s cell edge data rate (for the 5th percentile of the users)
- Round Trip Time (RTT) less than 1 ms
- Inactive to active mode transition within 10 ms

As mentioned earlier the 5G must also be able to support the need for capacity in 2030, which is estimated to be several thousand times larger than 2010 as illustrated in figure 4.1. Furthermore Machine Type Communication (MTC) devices, with small amounts of traffic, are expected to experience a battery life of approximately 10 years.

Currently there are no applications which can utilize the peak data rate, but industry expects this to change with the introduction of the successors to 4K video, holograms, and the emergence of other advanced user oriented features. The improvement in cell edge data rates will however directly improve the user experience for less demanding applications. The RTT may not be perceivable by humans, but it will be beneficial for MTC and this is also the case for the fast mode transition.

To fulfil the data rate requirements an increase in bandwidth, spectral efficiency and number of cells is needed. The spectrum resources are scarce and it is difficult to improve the spectral efficiency without increasing the number of antennas to a level where it is difficult to fit them all in a normal sized mobile terminal. Therefore the number of cells is expected to be the main driver, and thus the 5G RAT is also referred to as an Ultra-Dense Small Cell (UDSC) network [33]. Currently the research on 5G has branched into two separate parts focusing on Centimeter Waves (cmW), using frequency bands in the range 3-30 GHz, and Milimeter Waves (mmW), using frequency bands in the range 30 - 100 GHz [89]. In this work the focus is on the cmW, because the carrier frequencies are closer to what is used in the current cellular RATs, and therefore the learnings from Long Term Evolution (LTE) regarding Energy Efficiency (EE) can be reused. This is important because users demand better battery life, as discussed in chapter 1, and therefore mobile terminal EE was identified as a Key Performance Indicator (KPI) in [90, 91, 92, 93]. Note that in addition to the study on UDSC cmW work has also been initialized with focus on wide area 5G for frequencies below 6 GHz.

The standardization of 5G is expected to take place in the years 2016-2018, but certainly not before the International Telecommunication Union (ITU) World Radiocommunication Conference in 2015, where new spectrum is to be allocated [89]. The focus will however be on spectrum below 6-6.5 GHz, which will not provide enough free bandwidth to fulfil capacity and data rate requirements [94]. Spectrum above 10 GHz is however on the agenda for ITU World Radiocommunication Conference 2019 [94], but this entails the cmW concept is being developed for frequency bands that may not even be allocated when standardization starts. Furthermore there is an expectation in South Korea of prototypes being available for the Winter Olympics in 2018, while Japan is looking to test the new RAT at the Summer Olympics in 2020. No matter the launch date 5G must be able to cope with the traffic development and user requirements until at least 2030 where a sixth generation RAT may be introduced in accordance with the “rule” of a new RAT per decade.

One contribution of this chapter is to introduce a 5G concept, which is developed at Aalborg University and Nokia Networks among others, but is not yet finalized and therefore the currently selected features and nomenclature may change in the future. The proposed 5G concept includes a complete RAT design from the physical layer to the transport layer. In this chapter the focus is on the physical layer, because the technology features used here directly affect mobile terminal consumption. Figure 4.2 shows a mapping between the requirements and the features that are currently selected as facilitators. Some of the requirements have been discussed previously, but it is also worth noting that support for Device-to-Device (D2D), self-backhaul, localization, and self-optimization of the deployed Access Points (APs) are key requirements. In addition there is a requirement about simplicity and cost-effectiveness because it is important for the Mobile Network Operators (MNOs) to see a sound business case in the 5G RAT. As mentioned earlier the spectrum is scarce and thus 5G is required to be able to operate in unpaired bands and with support for flexible link directions due to varying loads. Finally there is a requirement about the mobile terminal being always ON, without draining the battery, which is also reflected in the inactive to active mode transition of 10 ms.

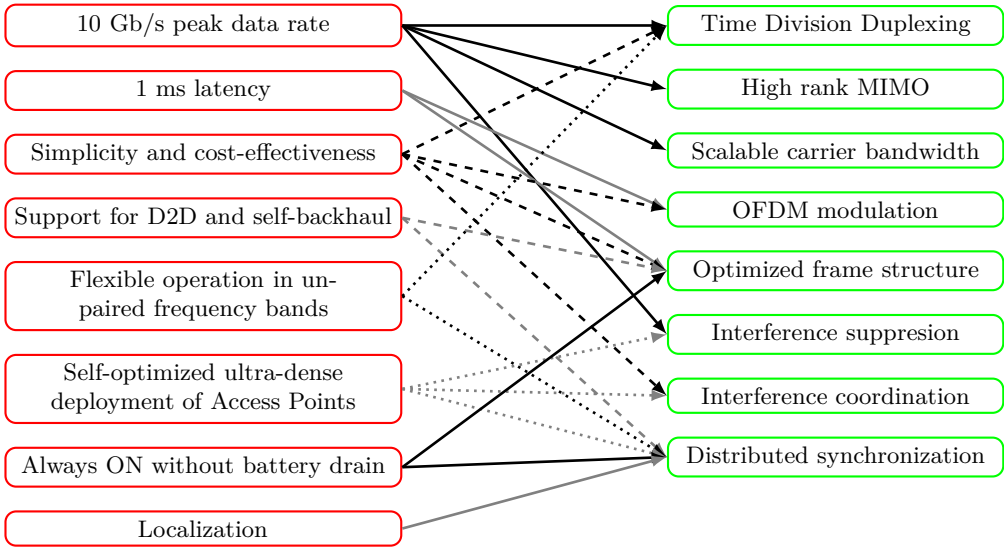


Figure 4.2: Mapping of requirements and selected features for 5G.

As indicated in figure 4.2 each requirement is expected to be affected by multiple features, and in the following sections selected features are discussed from a mobile terminal power consumption perspective using the publications [32, 34, 33], of which the first is also available as a re-print in appendix L. The selected features are compared with the existing Third Generation Partnership Project (3GPP) standards where Global System for Mobile Communications (GSM) release 7 is referred to as 2G, Evolved High-Speed Packet Access (HSPA+) release 8 as 3G and LTE release 11 as 4G [95]. The analogue first generations like Nordic Mobile Telephony (NMT) are not included.

After the concept has been presented specific power consumption challenges that arise due to the 5G design are discussed in chapter 5. Furthermore the performance evolution of the components, which are affected by the challenges, is evaluated using literature surveys and road maps to examine if the challenges can be handled in 2020.

Note that other companies and research institutions are also working on 5G concepts, for example 5GNOW [96] and Metis [93] which both are sponsored by the European Union. In fall 2013 the 5G-PPP [97] was signed by private partners and the European Union as the preliminary culmination on the many 5G concepts. For a more complete overview of 5G research refer to [84], which summarizes the ongoing developments in North America, Asia, and Europe.

4.1 Duplexing

Duplexing describes a point to point system where communication flows in both directions. Full duplexing entails the communication can flow simultaneously in both

directions while half duplexing only allows communication in one direction at a time. If two separate frequencies are used for the two directions the duplexing is called Frequency Division Duplexing (FDD), see figure 4.3a, and this can e.g. be used to achieve full duplexing if both frequencies are used simultaneously. If only one frequency is available Time Division Duplexing (TDD), see figure 4.3b, can be used to emulate full duplexing by strictly controlling when transmission and reception occurs. The two division duplexing methods both have advantages and disadvantages, and the duplexing method affects the energy consumption due to hardware requirements and impact on data rate and latency.

In previous cellular generations 2G used half duplexing FDD, while 3G used full

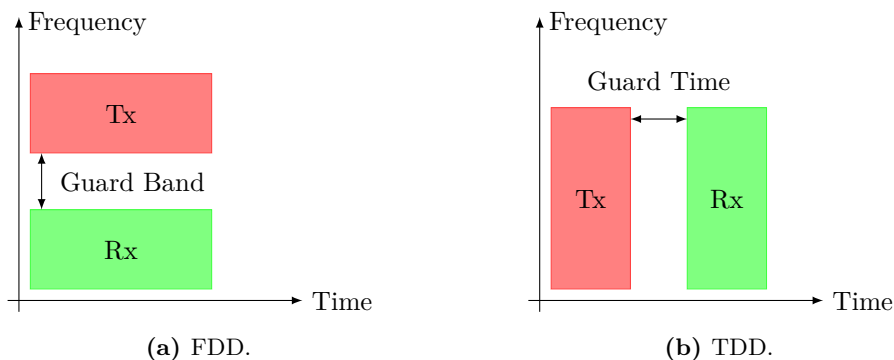


Figure 4.3: Duplexing methods.

duplexing FDD. The use of half duplexing entails the duplexer in the Radio Frequency (RF) front end can be avoided, resulting in a lower component cost and less attenuation between the antenna and the RF front end. The cost is the requirement for guard time in order to avoid transmit leakage into the receive slot. On the contrary the full duplexing solution requires a duplexer, but the guard time can be avoided. However the combination of FDD and full duplexing may lead to mixing of the mobile terminal's own transmit signal with external signals leading to a blocker in the receive band. Therefore good Third-Order Intercept Point (IP3) performance is required, and this is a power consuming feature as discussed later in section 5.1. In 4G both FDD and TDD have been specified to fulfil requirements from around the world.

The 5G concept is designed to use TDD. The reason is that TDD allows for a flexible spectrum assignment with no need for paired spectrum as in FDD, flexible duplexing of UL and DL, which is beneficial for asymmetric data and which does not waste expensive spectrum, and simple support for backhauling and D2D communication. The cost is the need for tight time synchronization to mitigate cross link interference that is not aligned with the agreed frame structure. Without having synchronized APs handover may also be more difficult.

The inter-AP synchronization is achieved using a distributed scheme [91], where the APs broadcast synchronization beacons in a contention based channel and update accordingly to received beacons. The network is expected to be an UDSC deployment, and because many of the APs will be placed indoor it is not possible to apply Global

Positioning System (GPS) or a similar system for synchronization. The local area network furthermore induces that the propagation delay between mobile terminal and serving AP is so small that it can be embedded in the Cyclic Prefix (CP). This leads to a faster connection time because the “timing advance” operation of 4G can be avoided. The cost is a slightly larger CP which equals increased overhead.

From an energy consumption perspective the TDD has several advantages. The duplexer can be replaced with an antenna switch, which should reduce the attenuation in the front end with up to 3 dB in both directions [32, 16], and furthermore the IP3 requirements can be relaxed. Other advantages of TDD are that the channel can be assumed to be reciprocal and thus avoid transmission of channel feedback. This will however require calibration because the front ends of mobile terminal and AP differ [87].

4.2 Bandwidth & Carrier Frequency

The bandwidth of the cellular RATs has increased with every generation from 200 kHz in 2G to 5 MHz in 3G and then 20 MHz in 4G [32]. The increased bandwidth entails more complex Base Band (BB) processing, because the data rate increases as well, and stricter requirements to the RF front end including the Analog-to-Digital Converter (ADC). However, in current 4G implementations the processing power consumption does not scale proportionally with the data rate as proved by the power consumption measurements illustrated in figure 2.7 and therefore it is more energy efficient to use the higher data rates.

The 5G concept also relies on increased bandwidth as compared to previous generations in order to fulfil the capacity requirements. As stated in the introduction of this chapter the 5G must deliver a peak data rate of 10 Gb/s. To achieve this target both the bandwidth, the number of spatial streams and the modulation order must increase. One example configuration is:

$$\begin{aligned} R_{5G} &= \text{BW} \cdot N_{\text{streams}} \cdot M \cdot \alpha && [\text{b/s}] \\ &= 400 \text{ MHz} \cdot 4 \cdot 8 \text{ b} \cdot 0.8 \approx 10.2 \text{ Gb/s} && (4.1) \end{aligned}$$

where: R_{5G} is the peak data rate [b/s]
 BW is the total channel bandwidth [MHz]
 N_{streams} is the number of spatial streams [-]
 M is the number of bits in the modulated symbol [b]
 α is the overhead [-]

Thus using an overhead of $\alpha = 0.8$, which is comparable with LTE [59], the mobile terminal must support 400 MHz per stream modulated using 256 Quadrature Amplitude Modulation (256QAM). In order to obtain 400 MHz of bandwidth it will most probably be necessary to apply Carrier Aggregation (CA) because even though TDD allows for use of unpaired spectrum it is difficult to find such a large continuous spectrum chunk in the cellular frequency range. Furthermore the modulation format includes 256QAM to increase the spectral efficiency.

To ensure multiple MNOs can provide such large bandwidths it is necessary to include new spectrum in the concept and therefore both cmW and mmW are envisioned. Using higher carrier frequencies impose new challenges to the cellular system because the path loss between transmitter and receiver does not only increase with distance, but also the carrier frequency as demonstrated in the free space path loss model [98, Equation 4.6]:

$$PL = -10 \cdot \log_{10} \left(\frac{c^2}{(4\pi)^2 d^2 f^2} \right) \quad [\text{dB}] \quad (4.2)$$

where: PL is the path loss [dB]
 c is the speed of light [m/s]
 d is the distance between transmitter and receiver [m]
 f is the carrier frequency [Hz]

Furthermore measurements at 38 GHz [99] have shown that the diffraction loss is very high and even though the reflection loss is lower it is still preferable to deploy the mmW in Line of Sight (LOS) conditions or favourable Non-Line of Sight (NLOS) conditions. In addition the penetration loss is determined to be much higher for high frequencies [99]. As opposed to that the cmW may be deployed in both LOS and NLOS, because the penetration, diffraction, and reflection loss is smaller.

The small wavelength of the mmW entails the antennas can be made much smaller and therefore the number of antennas which can be fitted into the same area of both AP and mobile terminal is much higher. Due to the LOS conditions with few if any multipaths it may not be possible to utilize the many antennas for high rank transmissions because there are a limited number of independent paths [100, 101]. Instead the massive Multiple Input Multiple Output (MIMO), which is the term for the use of many more antennas than users [34], can be used for beamforming to increase the Signal to Noise Ratio (SNR) at the receiver, [102], and to perform spatial cancellation of interference. The data rate can also be improved because the mmW domain entails much more spectrum is available and therefore the channel bandwidth may be several Gigahertz. Contrary to that the cmW has less bandwidth available and fewer large antennas, but due to the NLOS environment it is possible to exploit rich multipath fading to achieve a high rank transmission leading to increased capacity as well.

The conclusion is therefore that the 5G concept must rely on both mmW and cmW carrier frequencies to obtain the bandwidth needed to fulfil the capacity requirements. In chapter 5 the challenges caused by the increased bandwidth are discussed in further detail.

4.3 Waveform and Multiple Access scheme

A RAT's waveform (or modulation format) affects the amount of bits that can be transferred per spectral resource and with each new generation the spectral efficiency

has increased going from Gaussian filtered Minimum Shift Keying (GMSK) in 2G to 64 Quadrature Amplitude Modulation (64QAM) in 4G. The advantage of GMSK is the constant envelope, but the spectral efficiency is low [103], while the 64QAM has a varying envelope that is sensitive to distortion in the Power Amplifier (PA) and other RF components, but higher spectral efficiency. As calculated in equation (4.1) the use of 256QAM is needed in 5G to fulfil the data rate requirement.

The waveform is tightly coupled with the choice of Multiple Access (MA) scheme, which determines how multiple users can access the system's resources in time and frequency and thus the achievable data rate.

In 2G a combination of Time Division Multiple Access (TDMA) and Frequency Division Multiple Access (FDMA), illustrated in figure 4.4a and 4.4b respectively, is used and the mobile terminal may occupy one or more of the 8 time slots, which compose a TDMA frame [104]. Furthermore frequency hopping, where the carrier is changed once per frame, is applied to combat frequency selective fading and reduce intercell interference. In 3G the Code Division Multiple Access (CDMA), illustrated in figure 4.4c,

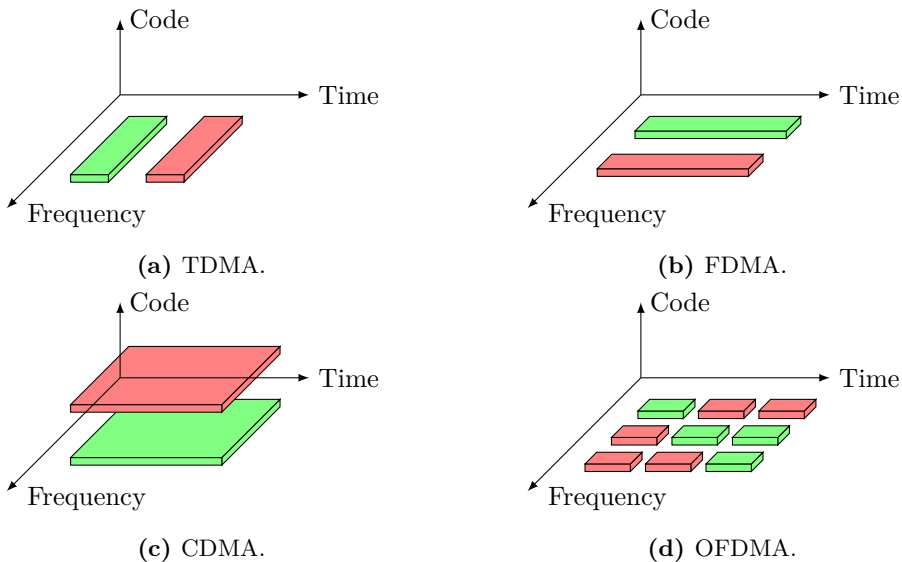


Figure 4.4: Selected multiple access methods.

is used and due to the near-far problem, where a mobile terminal close to the AP can “drown” the signal of a mobile terminal further away, a fast Transmit Power Control (TPC) is needed [78]. This entails the transmit power is adapted to the current path loss, but also a large overhead in terms of control signalling. In 4G the Orthogonal Frequency Division Multiplexing (OFDM) waveform is used for MA and the resulting Orthogonal Frequency Division Multiple Access (OFDMA) is illustrated in figure 4.4d. As opposed to the FDMA scheme in 2G the individual subcarriers are orthogonal hence they can be placed next to each-other without causing interference and thus eliminating the guard band. The OFDMA scheme also allows for resource allocation in the time domain, which entails users can be scheduled in both the most favourable channel fading

conditions and according to their resource needs. The cost of using the OFDM waveform is a large Peak-to-Average-Power Ratio (PAPR) due to the sum of sinusoids in the time domain. This is problematic because a high PAPR will force the PA to operate far from the saturation point, where the efficiency is at its peak as illustrated in figure 4.5. The reason is that the modulation formats include an amplitude component which will be distorted if the PA is operating in the non-linear region where the efficiency is best. This distortion adds to the Error Vector Magnitude (EVM) which will be discussed further in section 5.5. Therefore Output Back-Off (OBO) is used to lower the transmit power to the linear region after which the PAPR further reduces the average power as illustrated in figure 4.5. Besides distortion of the amplitude component the non-linear region may also entail increased Adjacent Channel Leakage Ratio (ACLR), which again will affect the capacity of the system due to interference in the neighbour channels. In 4G uplink a

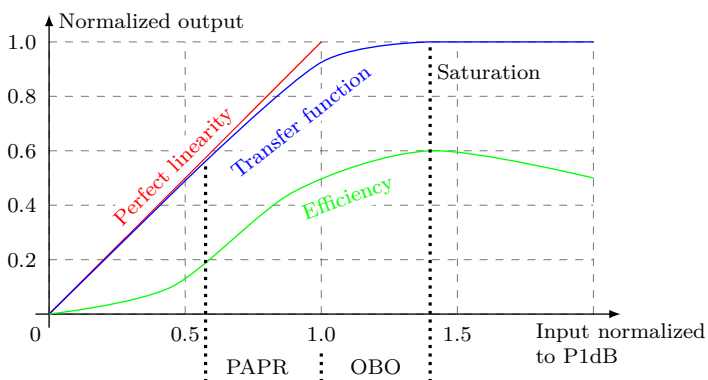


Figure 4.5: Power amplifier operation, based on [103, Figure 2.30].

special type of OFDMA is therefore used known as Single Carrier FDMA (SC FDMA). In one implementation a Discrete Fourier Transform (DFT) is applied to the modulating signal, and the resulting signal is known as Discrete Fourier Transform spread OFDM (DFT-s-OFDM). The purpose is to obtain a transmitted signal with lower PAPR (up to 4 dB [32]), but with the good properties of OFDMA. The cost is increased noise at the receiver, which may degrade the link performance [105]. For further information on how PAPR has evolved with the RAT generations and the increasingly spectrally efficient waveforms refer to [103, 32].

The currently preferred MA scheme for the proposed 5G concept is OFDMA because it has proved to be efficient in 4G. The use of multiple narrowband frequency resources leads to simple one-tap equalization because the individual channels are considered to have flat fading. In addition it is easy to combine with MIMO [87], which is one of the drawbacks of the competitor Filter Bank Multi Carrier (FBMC). This waveform replaces OFDM's square window at each subcarrier with a filter and allows for removing the CP and reduces Out-of-Band (OOB) emissions [32], but the computational complexity may be 10 times higher than OFDM [87]. Another scheme which was considered was Non-Orthogonal MA [106] which is a combination of Superposition Coding and OFDM. The drawback is that a complex Successive Interference Cancellations

tion (SIC) receiver is required to cancel the Superposition Coded signals targeted the other mobile terminals, and while the SIC receiver may also be used in OFDMA the Non-Orthogonal MA scheme requires the mobile terminal to decode intra- or inter-cell streams. Those streams are not intended for the mobile terminal as compared to decoding interfering spatial streams, also containing data intended for the mobile terminal, which it would decode anyway in OFDMA. This is also the case for Multiuser MIMO, where a SIC receiver is also forced to decode streams that are not intended for the mobile terminal. Furthermore the UDSC scenario entails the channel gain difference between mobile terminals is small and this limits the applicability of Superposition Coding.

The OFDM does also have its drawbacks, such as the aforementioned high PAPR, but it is expected that the use of new PA supply techniques such as Envelope Tracking (ET), which entails the PA can operate closer to the saturation region, will mitigate the problem. Refer to figure 2.5 for a measurement on ET PA power consumption in two 4G User Equipments (UEs) and section 5.5 for a review of ET evolution.

Another issue is system overhead caused by the predefined and hardcoded CP, which is inserted in front of each symbol to cope with intersymbol-interference caused by propagation delay and the channel's delay spread. Since the CP is a copy of the last part of the symbol it leads to a computational advantage because it allows for an interpretation of the channel as being circular convoluted with the symbol. This entails it can be transformed to a simple multiplication in the frequency domain. The CP problem becomes increasingly significant as the symbol time is expected to be shorter, and therefore the ratio between CP size and symbol time increases, which leads to larger system overhead. However a modification has been proposed [107] to DFT-s-OFDM where the CP is replaced with a low power tail by adding a variable number of zeros to the signal. The method is known as Zero-Tail Discrete Fourier Transform spread OFDM (ZT DFT-s-OFDM) and entails the length of the CP replacement can be adjusted to the channel conditions and furthermore the OOB emissions are reduced. For now the regular OFDM is used in the 5G concept.

4.4 Frame Structure

The frame size, i.e. the Transmission Time Interval (TTI), and structure plays an important role in terms of latency, power consumption, and overhead. The TTI has been reduced with the introduction of every new RAT going from 4.615 ms in 2G, to 2 ms in 3G and finally 1 ms in 4G. A short frame entails the latency is reduced and furthermore it reduces power ON time, which is the time the mobile terminal spends when transitioning from a low-power sleep state to being active, and other hand-shaking procedures such as exchange of parameters and handover. In addition the short latency will reduce the need for buffer memory and therefore size and cost of the mobile terminal. The proposed 5G frame structure is illustrated in figure 4.6. The frame is composed of 14 OFDM symbols and 3 Guard Periods (GPs). Each symbol is preceded with a 1 μ s CP to ensure the performance of the OFDM waveform is not degraded by intersymbol

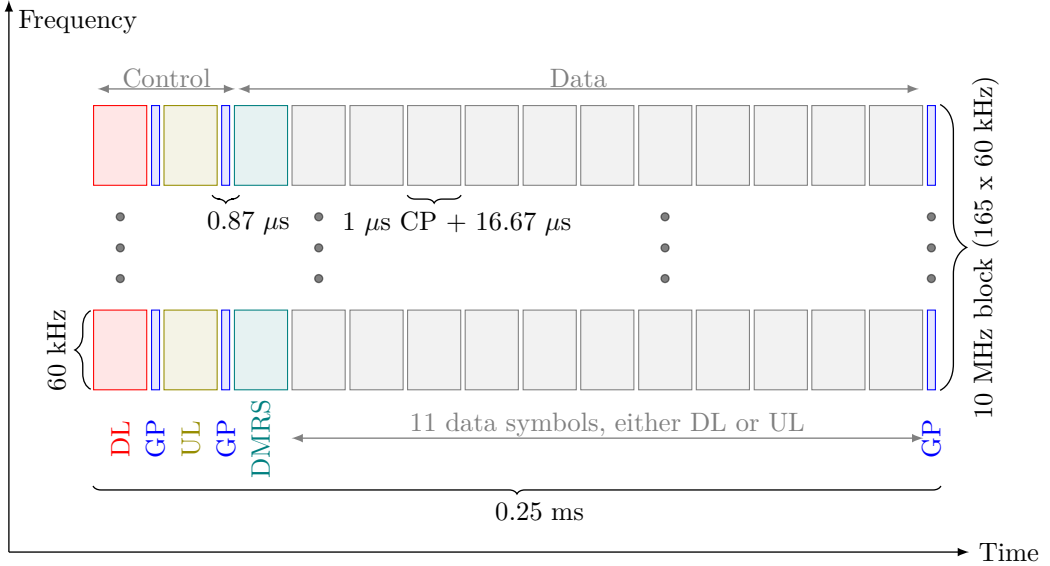


Figure 4.6: A single 5G frame.

interference. The total frame length is therefore currently set to

$$\begin{aligned}
 t_{\text{frame}} &= 14 \cdot (t_{\text{CP}} + t_{\text{symbol}}) + 3 \cdot t_{\text{GP}} \\
 &= 14 \cdot (1 \mu\text{s} + 16.67 \mu\text{s}) + 3 \cdot 0.87 \mu\text{s} = 250 \mu\text{s}
 \end{aligned}
 \tag{4.3}$$

where: t_{frame} is the total frame length [s]
 t_{CP} is the CP length [s]
 t_{symbol} is the symbol length [s]
 t_{GP} is the GP length [s]

and this ensures about 1 ms latency performance as discussed later in this section. The low latency is a major improvement as compared to the previous RAT generations.

The first two symbols are reserved for downlink and uplink control information, for example scheduling requests and grants, synchronization, and Modulation and Coding Scheme (MCS) information. The short frame and the frequent occurrence of synchronization and scheduling information (in the DL control channel) entails the mobile terminal can quickly perform the power ON procedure after sleep mode. This includes synchronization and decoding of the control channel, which was one reason for the longer latency of LTE as discussed in section 2.3. Therefore 5G mobile terminals can be made very energy efficient by enabling fast synchronization and data transfer, within a few frames, after which the device quickly can return to a low-power sleep mode.

The following 12 symbols are allocated for data and organized such that the transfer can only occur in one direction per frame i.e. either uplink or downlink. This helps

to stabilize the interference pattern in the frame, but also allows for a flexible and asymmetric allocation across frames. The variable link switching does however lead to difficulties in predicting the Signal to Interference + Noise Ratio (SINR) of the following frame and therefore either coordination between APs or novel rank adaptation techniques [37] are needed. Due to the high data rates the transfers may also finish and vary faster and therefore also affect the experienced interference. Finally the highly dynamic uplink-downlink frame allocation requires a redesign of the scheduler. In [33] a scheduler is proposed which decides the link direction based on a threshold using the head-of-line delay of the uplink and downlink buffers.

In between the control symbols and before the data part a GP is inserted to avoid power ON/OFF transients when link direction is switched. The allocated time is based on a prediction of how hardware switches evolve over time and that the transmit power in the UDSC scenario will be significantly lower than in current RATs.

As shown in figure 4.6 the first symbol of the data part may be used for a DeModulation Reference Symbol (DMRS) that can be applied to estimate the channel for example by use of orthogonal sequences with good auto- and cross-correlation properties.

Note that if the ZT DFT-s-OFDM is used instead of OFDM the CP will be both of variable size and incorporated into the following symbol. Therefore the frame nomenclature would have to be reconsidered as well. The circular properties would however be preserved thus not affect decoding complexity [107].

In the frequency domain each symbol is

$$bw_{\text{symbol}} = \frac{1}{t_{\text{symbol}}} = \frac{1}{16.67 \mu\text{s}} = 60 \text{ kHz} \quad (4.4)$$

wide and grouped in Physical Resource Blocks (PRBs) of 165 i.e. $165 \cdot 60 \text{ kHz} = 10 \text{ MHz}$ in a fashion similar to 4G. The division of the 400 MHz bandwidth into smaller PRBs allows for frequency reuse and coordination. In the control channel part of the frame the APs and mobile terminals use robust codes and separate PRBs to provide the required information to the receiver without destructive interference.

Examining the previous generations' frame structures it is evident that the voice-oriented 2G uses the TDMA frames in an inefficient manner because a certain number of resources is continuously dedicated for a transfer even though they may be unused. The latter RAT generations have switched to a frame-by-frame allocation, but still differ significantly in how the control and data channels are positioned in the frame. In 3G the High-Speed Shared Control Channel (HS-SCCH), which informs the mobile terminal how to demodulate the data, is located in slots n and $n+1$ as illustrated in figure 4.7a. The control in slot n details the MCS while slot $n+1$ has redundancy and retransmission information together with Automatic Repeat Request (ARQ) number. The data follows in the High-Speed Downlink Shared Channel (HS-DSCH) in slot $n+2$ and onwards and because the mobile terminal receives scheduling information in slot n it has a whole slot duration to decode the information and decide whether to receive and buffer slot $n+2$.

In the first release of LTE (release 8) the structure, illustrated in figure 4.7b is less efficient because the Physical Control Format Indicator Channel (PCFICH) and Physical Downlink Control Channel (PDCCH), which informs the mobile terminal how to demodulate the data, are followed directly by the Physical Downlink Shared Channel

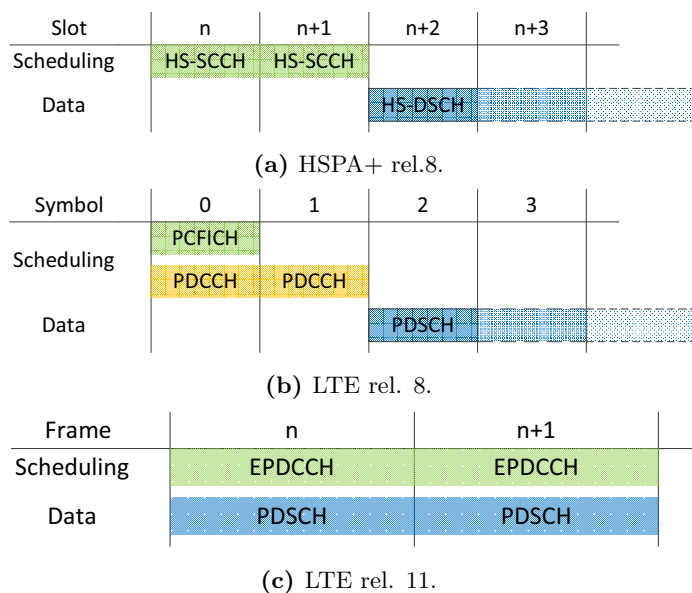


Figure 4.7: Positions of control and data channels in previous RAT generations' frames. [32, Figure 4.a-c]

(PDSCH), which contains the data. Therefore the mobile terminal is forced to buffer the PDSCH because it cannot decode the control channels instantaneously and determine if and where it is scheduled. This entails the mobile terminal wastes energy buffering data that it cannot decode because the data was not intended for the mobile terminal. This is the reason why the micro sleep concept was proposed [28], and presented in section 3.2, to decode the control channels as fast as possible and then sleep for the rest of the frame, when the mobile terminal is not scheduled. The cost is that the Reference Signals, which are spread across the frame are not all received and decoded, but it is estimated that the degraded channel estimate and related loss in throughput is minor [28]. The use of micro sleep is not possible in LTE release 11 because the Enhanced Physical Downlink Control Channel (EPDCCH) has been standardized. The target of EPDCCH is to obtain a frequency selective scheduling gain by spreading the channel in time across the most suitable subcarriers. Unfortunately this forces the mobile terminal to receive and buffer the whole frame before it can decode the scheduling information.

Based on the learnings from previous generations the 5G concept proposes that scheduling grants are sent one frame ahead of the data as illustrated for the downlink case in figure 4.8. This entails the mobile terminals can determine whether it is scheduled in due time and perform energy efficient pipelined processing. Thus the mobile terminal always needs to decode the downlink control channel, but it may then power down if there is no pending uplink transmissions or no scheduled downlink data. Due to the short frame length the time from a scheduling grant is received and until the Acknowledgement (ACK) is sent is approximately 0.75 ms.

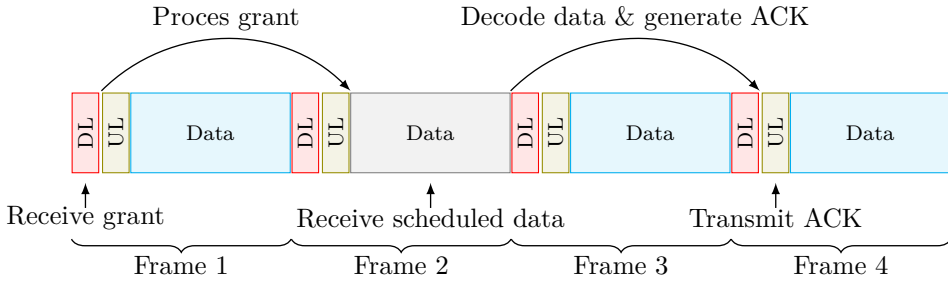


Figure 4.8: Procedure for receiving data in downlink.

Transmitting in the uplink is contention based in the sense that a mobile terminal first has to send a “request to transmit” in the uplink control channel and then await a positive feedback in the following frame after which it can transmit the data. The procedure is illustrated in figure 4.9 and the total time from request to ACK is about 1 ms and thus the requirement for RTT is fulfilled.

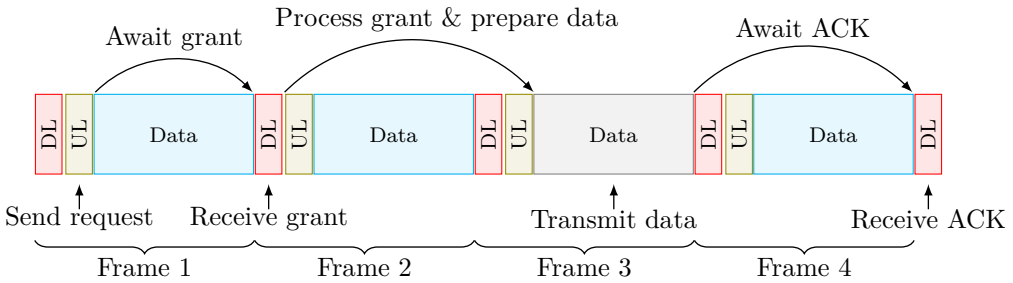


Figure 4.9: Procedure for transmitting data in uplink.

4.5 Multiple Antennas and Advanced Receivers

In previous RATs receive diversity has been exploited by requiring two receive antennas in the mobile terminal. Starting with 3G downlink dual stream spatial multiplexing was also standardized to boost the data rates and in 4G 4 receive antennas are in principle possible though not yet commercialized. This is also the case for uplink where 2G and 3G only support one transmitter while 4G has specified up to 4 uplink streams.

The minimum MIMO configuration for the cmW 5G concept is 4 Receive (Rx) and 4 Transmit (Tx) antennas. The reasons for this choice are the physical size of the antennas at cmW, the relatively slow improvement of RF power consumption, as discussed in section 5.1, whose component count scales directly with the number of antennas, and the larger overhead which is caused by the need of sending individual DMRS per antennas. Finally the 4x4 MIMO configuration can be combined with 400 MHz bandwidth and 256QAM to achieve the 10 Gbps target as shown in equation (4.1).

For the mmW case the use of Massive MIMO is considered because each antenna can be made much smaller, but other challenges such as the component count remains [34].

As discussed in the previous section the control channel symbols will be coded robustly and separated in the frequency domain, but this is not the case for the data symbols, which will be subject to intercell interference if frequency reuse is not applied. Therefore the use of advanced receivers is envisioned. Initially the Interference Rejection Combining (IRC) receiver has been compared with 4G's baseline Maximum Ratio Combining (MRC) receiver, and proved to result in significant gains when the interference is high [108, 33]. The reason is that the IRC receiver can estimate the interference+noise covariance matrix every frame using the DMRS and suppress the strongest interferers, because the interference is stable during the data part of the frame. Note that the source of the interference is irrelevant because all 5G devices are required to transmit the DMRS and are synchronized. Currently the use of SIC receivers is investigated [33]. This receiver type is more complex because the strongest stream is first decoded and subtracted from the remaining streams to cancel its interference contribution. Next the second strongest stream is decoded and so forth [102]. In order for SIC to work the receiver needs to know the MCS and the rank of the interfering streams and therefore it also adds to the complexity of the concept. Furthermore a decoding error in one of the strongest streams will propagate to all remaining streams.

The use of InterCell Interference Coordination (ICIC) between APs has also been considered because it can manage the frequency reuse scheme in a distributed and autonomous manner. The method needs to be autonomous because it is expected that the number of small cells will be 100 times the current level [87]. Due to the improved processing power in the mobile terminals the advanced receivers and the increased number of antennas are however the current choice to combat intercell interference. However there is another key area where intelligent APs are needed: rank coordination. The MIMO channel's rank, or degree of freedom, depends on the number of separable multipaths and the number of Tx and Rx antennas [102]. The degrees of freedom is the upper limit to the number of spatial streams, but if the number of streams is reduced the remaining degrees of freedom can be used for interference cancellation [37]. Thus there is a tradeoff between the number of spatial data streams and the number of cancellable streams, which is to be handled by a Rank Adaption algorithm. If one user selfishly increases the number of spatial streams that user will also increase the number of interference streams towards other users, often referred to as victims, and thereby limit their throughput. The target for a Rank Adaption algorithm is therefore to adjust the number of spatial streams for each user and be victim aware. To perform well the algorithm would operate based on reported Channel State Information (CSI) that includes the SINR of the previously received frame. This works fine in 4G, but in 5G the interference will vary much faster, because the data rate and link direction are varied, and therefore the CSI, in terms of experienced rank, will be outdated when received by the AP. Consequently a *chicken and egg* problem exist where the rank should be based on the CSI, but the CSI can only be estimated after the transmission using the selected rank has occurred. In [37] an algorithm is proposed that first makes the receiver estimate the SINR for all possible ranks. The receiver then calculates the achievable data rate for all ranks and feedbacks the rank, which maximizes the data rate, to the transmitter. Due to the processing time and the feedback transfer the SINR may also

be outdated, but in general the simulation results show good performance.

The use of CA is also envisioned for the 5G concept. The reason is that the spectrum needed to achieve the high data rates is not available in a contiguous chunk, but fragmented due to the many competing wireless technologies. Therefore the combination of TDD and CA is useful to obtain bandwidths of 400 MHz or more. Using CA entails that the number of RF front ends and possibly also ADCs increases linearly with the number of carriers and furthermore also with the number of spatial MIMO streams and therefore the chip size and power consumption may increase as well as discussed in chapter 5. Recent measurements on 4G CA, presented in section 3.5 and in [31] have however proved that the energy efficiency may improve due to the improved data rates. The effect on the ADC due to the increased bandwidth is analyzed in section 5.2.

4.6 Sleep mode

In the 5G concept an “always ON” behaviour is targeted, but it has to be combined with a low-power sleep mode to ensure the battery life. However there is a significant trade-off between the experienced delay and the achievable sleep mode power consumption as discussed in section 2.5.1.

In Wideband Code Division Multiple Access (WCDMA) and LTE the mobile terminal can be in either a connected or idle mode, when registered in the system [59] as illustrated in figure 4.10. In 3G there are two high power modes; the Cell_DCH using

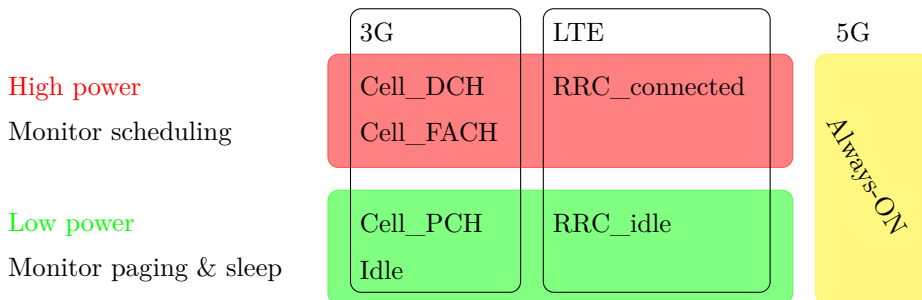


Figure 4.10: mobile terminal modes for 3G, LTE and 5G.

the Dedicated Channel (DCH) and the Cell_FACH using the Forward Access Channel (FACH). The DCH is a dedicated bi-directional channel where the mobile terminal is allocated resources continuously in both uplink and downlink. In release 6 the mobile terminal has to transmit the control channel even though there is no related data, while release 7 allowed for use of Discontinuous Transmission (DTX) [78]. The DCH is specifically targeted at transferring large amounts of data, and if the channel has not been used for a specific amount of time the mobile terminal will be moved to Cell_FACH. In the FACH the mobile terminal still has to monitor the downlink for scheduled data, but it can power off the transmitter and thus reduce the estimated current consumption from 200-400 mA for the DCH to 100-200 mA [78]. In addition release 7 introduced enhanced FACH where Discontinuous Reception (DRX) can be applied. This new mode resembles the Cell_PCH where the mobile terminal is using DRX while listening for a

Paging Channel (PCH) resulting in an estimated current consumption smaller than 5 mA, which is similar to the idle mode. The latter is not a preferred mode because it entails more signalling when the mobile terminal transfers to and from this mode.

In LTE the number of Radio Resource Control (RRC) modes has been reduced to two. In the RRC_connected mode the mobile terminal continuously has to monitor for scheduling grants and while this decreases the delay for the data transfer it also increases the power consumption. In RRC_idle mode the mobile terminal can enter a sleep mode and only perform periodic monitoring of the paging channel and measurements on neighbor cells for possible cell re-selection. If the mobile terminal is paged it will need to transfer to the connected mode before it can receive the incoming data and thus while the power consumption is lower the delay is higher. Changing modes takes time and consumes energy, but it also affects the system's overall capacity because there is a significant amount of signalling involved.

The time it takes to transfer from idle to connected and vice versa depends on the RAT design and the MNO's setup, and for example [45] measured the delay from idle to connected to be about 260 ms in LTE. This is significantly shorter than the tail delay, e.g. moving from connected to idle after a data transfer is finished, which is based on the expiry of an inactivity timer. In one LTE network [109] noted this takes 10.2 s, while [45] measured 11.6 s. In general [110] estimates the range to be a few seconds to a few tens of seconds for LTE while the inactivity timer in 3G is typically 2-10 s [78]. The reason for the long tail is that the MNO would like to avoid the mobile terminal leaves the connected mode and shortly thereafter reconnects, causing unnecessary signalling. This may happen more often due to the use of keep-alive-messages that make sure the connection between e.g. an Instant Messaging application and the server is not disconnected, and the use of push-email [110, 78]. In 3G the Fast Dormancy mode was introduced to allow mobile terminals to ask the network to disconnect, when the data transfer is completed, but before the inactivity timer has expired [78]. The UE will then move from DCH or FACH to PCH instead of moving to idle, which will cause significant signalling overhead the next time the UE wants to reconnect.

Table 4.1 summarizes the characteristics of the two general modes: connected and idle. The trade-off between power consumption and the delay to transfer, e.g. receive paging/scheduling message or data, is evident and depends on the choice of paging and DRX cycle length.

Table 4.1: Characteristics of general UE modes.

Parameter mode	Idle	Connected
Power consumption	Low	High
Delay to transfer	High	Low
Time to change mode	Short (<0.5 s)	Long (> 2 s)
Depends on	Paging cycle	DRX cycle

The challenge is thus how to proceed in 5G with the “always ON” requirement stating that the transition from inactive to active must be ≤ 10 ms. One option is to avoid the use of an inactivity timer and instead enable the mobile terminal to request a quick release i.e. similar to 3G's Fast Dormancy [110]. Another option is to avoid the

idle mode and rely on a connected mode strongly coupled with DRX, which then must allow for more flexible and much longer periods as compared to LTE where the upper limit is 2.56 s and the period length is not very adaptive with respect to the traffic type.

The advantage of the first option is that the tail time, i.e. time to go to idle, can be much shorter, but the amount of signalling for the mode change will still be high. The signalling will also be high for the DRX based mode if the mobile terminal is moving fast and performing many hand overs, but the main issue is the delay the network will experience when contacting the mobile terminal.

In the presented 5G concept the “connected mode only” design is selected. There are multiple reasons for this choice and one is that it simplifies the control signalling, because the mobile terminal will no longer change mode but only notify the network when it has entered the coverage area. Another reason is that the short frame structure entails the mobile terminal can quickly receive the channels necessary to synchronize and determine if it is scheduled as illustrated in figure 4.8. This entails the ON time of DRX can be made short while the sleep part can be long.

The challenge for the mobile terminal designer is that it takes a non-negligible amount of time to transfer from sleep to being active and vice versa and that the transfer time depends on the achievable sleep power level [27]. Section 2.5.1 presented LTE DRX measurements on 3 UEs and in the light sleep mode, i.e. a power level which in the best case is a little less than half of the active power, the transition time is significantly lower than for the deep sleep mode, where the power level however is less than 1/50 of the active power. Figure 4.11 show the energy consumption in DRX mode as a function of the DRX Long Period (DRX LP) for the examined UEs. The minimum period length is calculated as the sum of t_{onD} (set to 1 ms), t_{wup} , t_{sync} , and t_{pd} defined in equation (2.4).

For short DRX LP the mobile terminal cannot apply the deep sleep mode because it takes too long to power up and down the components, and this is reflected in the figure where the deep sleep mode is not applicable before the periods are longer than 40 ms. This is however not an issue because the light sleep mode is actually more effective for shorter periods. The reason is that the mobile terminal consumes a significant amount of energy when transferring to and from the deep sleep state. The improvement in sleep power levels, from UE2 to UE4, is evidently useful when targeting longer battery life, but it is even more important that the support for shorter power up/down and synchronization times is also improved with each new mobile terminal, the sum dropping from 22.6 ms to 9 ms to 6 ms and being dominated by the power up and synchronization procedures. In order to achieve significant energy savings while fulfilling the 10 ms requirement the overall time it takes to change state must however be improved further especially because the aforementioned sums are theoretical limits. In current LTE implementations the UEs do not apply sleep mode when the period is shorter than 32 ms.

It is thus a key challenge to achieve a fast power ON procedure and fast synchronization, which includes channel estimation. The latter will be reduced due to the 5G frames which are 4 times shorter than in LTE, but the power ON procedure is in principle independent of the RAT design. The procedure includes achieving phase lock in the synthesizer, stable gain control, configuration of filters, and calibration of RF components [27]. In addition the power ON procedure must be performed sequentially to

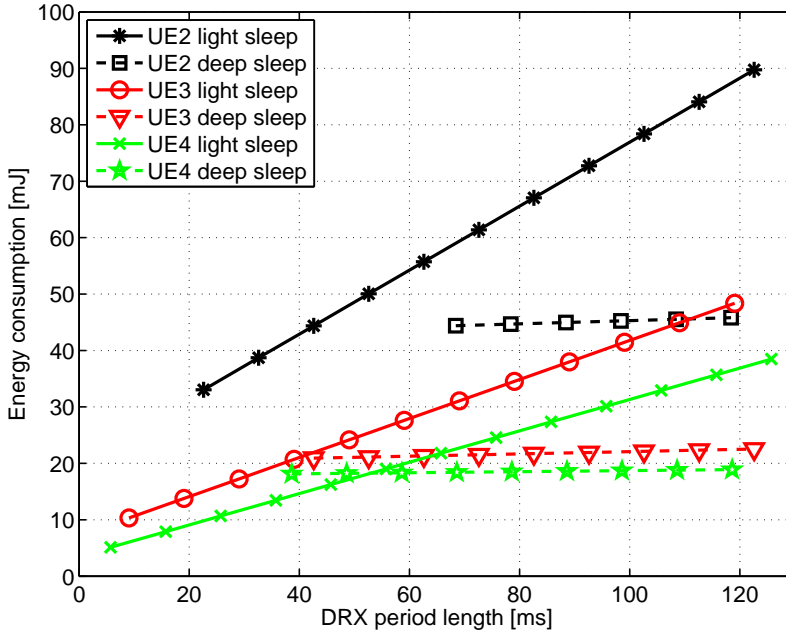


Figure 4.11: Energy consumption in LTE DRX mode as a function of DRX LP for UEs 2, 3, and 4 in section 2.5.1.

avoid the battery voltage dropping [16] thus increasing the power ON time.

To conclude the 5G concept targets to be “always ON” i.e. switching from a low-power mode to active data transfer within 10 ms. In this section it was discussed how it may be achieved by relying on the use of a single connected mode combined with adaptive DRX settings, which may have much longer periods than LTE’s 2.56 s. The challenges to achieve this are the time required to power ON the cellular subsystem after it has been in sleep mode in order to perform synchronization and channel estimation before the data transfer occurs. The short frame length will entail the procedures can be performed faster, but the power ON procedure itself is limited by how fast the components can be powered ON, stabilize and obtain the required settings, e.g. phase lock and a specific gain mode. Measurements on LTE DRX across 3 mobile terminal generations have however showed that the procedures are performed faster and faster and that the achieved sleep power levels are decreasing.

4.7 LTE-like Features

The 5G concept resembles 4G in the sense that it applies OFDM, but other features such as Hybrid Automatic Repeat Request (HARQ), [111], and link adaptation are also reused. In addition DRX is also applied as discussed in the previous section and analysed in chapter 6.

The HARQ is needed because the receiver may not decode the transmitted signal properly. Decoding errors can be caused by bad channel estimates, aggressive link adaptation, erroneous CSI decoding at the transmitter-side and outdated channel estimates. HARQ is a combination of ARQ and Forward Error-Correcting Code (FEC) used in both 3G and 4G. The ARQ method implies that error-detecting code is transmitted together with the data, and if the receiver detects an error it will send a Negative Acknowledgement (NACK) implying that the transmitter must resend the data. The ARQ method furthermore implies that if the transmitter has not received any feedback from the receiver within a certain time window it will also retransmit the data. Adding the FEC to the ARQ entails that the receiver may be able to correct the errors instead of sending a NACK, but at the cost of larger overhead. Currently the specific HARQ method has not been selected but due to the frame structure the delay will only be about 0.75 ms as illustrated in figure 4.12. Given the short and fixed HARQ RTT the

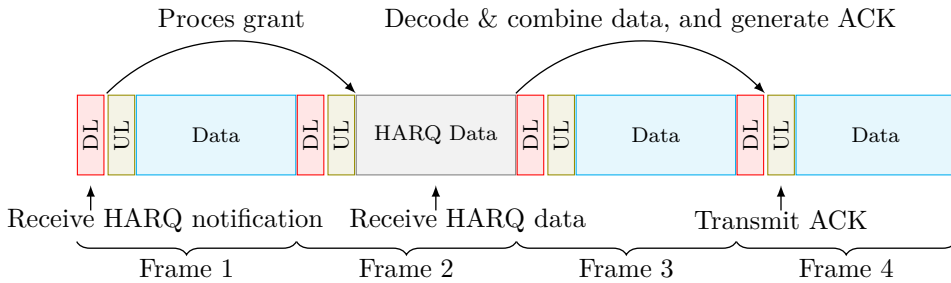


Figure 4.12: HARQ procedure in downlink.

number of parallel processes is limited to 4 and this entails major savings in terms of buffer memory as compared to the 15 processes of LTE-TDD [33].

In addition to the HARQ the 5G concept will also apply link adaptation, similar to 4G, together with the aforementioned Rank Adaption algorithm and an algorithm to decide the link direction [112]. The goal is to select the link direction and the MCS which can fulfil the desired Block Error Rate (BLER) target such that the optimal trade-off between the benefits of HARQ and selecting a too optimistic MCS is achieved.

4.8 Summary

This concludes the overview of the proposed cmW, 5G concept, which is targeting 10 Gb/s peak data rate, 100 Mb/s cell edge data rate, and short RTT of 1 ms in unpaired frequency bands using self-optimized, synchronized UDSC.

The 5G RAT is not expected to be deployed before 2020 and the battery capacity will not improve significantly until then because it only increases about 3-7% per year as discussed in chapter 1. On the contrary the technology improves 19-37% a year and therefore it is possible to exploit the improved hardware capabilities, discussed further in chapter 5, to optimize the cellular subsystem's energy consumption. The introduction of a new RAT furthermore entails low mobile terminal energy consumption can be included

as a KPI from the beginning of the concept design phase. In this chapter the following features were identified as having major influence on the battery life:

- OFDM: The waveform allows for efficient implementation in the mobile terminal and when used for MA also efficient resource allocation. It may also be combined with MIMO and advanced receivers to improve the data rate. The high PAPR drawback may be handled by improved PA techniques such as ET.
- Larger bandwidth: This is an essential feature for improving the data rate, which may lead to shorter transfer times and therefore longer sleep time. Furthermore LTE measurements show that the decoding process is most energy efficient at the highest data rates and thus they shall be applied as much as possible.
- CA and MIMO: Both increase the hardware complexity and also the instantaneous power consumption, but they also improve the data rate due to increased bandwidth, frequency diversity, and spatial multiplexing. As noted in section 2.5 the EE increases with the data rates and therefore the features may improve the battery life.
- TDD: This method entails the duplexer, causing about 3 dB loss, can be discarded and consequently the transmit power can be lowered to save transmit energy. Furthermore the IP3 requirements can be relaxed due to the absence of transmit signals when data is received. With proper calibration of the transceivers the channel may also be perceived as reciprocal and as a result the channel feedback is limited, saving transmit energy.
- Frame structure: The support for asymmetric data may decrease the time to transfer thus improving the sleeping opportunities. Furthermore the structure allows for pipelined processing such that unscheduled users do not receive and buffer data, which is not intended for the user. Finally the short frame entails the reference signals, needed for synchronization and channel estimation, occur often and thus allow for fast transfers between idle and active modes.

Besides the useful features the UDSC scenario may also result in lower path loss thus leading to lower transmit powers, which is a significant improvement because high transmit power is one of the main power consumers in current 4G UEs as shown in section 2.5.

In the next chapter some of the power consumption challenges that arise due to the increased system parameters are examined. Furthermore the power consumption of the affected components are estimated by analysing their performance evolution, and finally the power consumption of mobile terminal in 2020 and 2030 is estimated.

Chapter 5

Power Consumption Challenges in 5G

In this chapter the Fifth Generation (5G) system parameters' effect on mobile terminal power consumption is examined. First the performance evolution from approximately 1990 and until today of selected hardware components is modelled. Then the models are extended to 2020 and 2030, where 5G is expected to be deployed, to determine if they can handle the increased requirements and to estimate the power consumption.

As discussed in chapter 4 the 5G targets a peak data rate of 10 Gb/s in both uplink and downlink. In equation (4.1) it was calculated that one configuration which achieves this data rate could be the use of 400 MHz bandwidth per stream in a 4x4 Multiple Input Multiple Output (MIMO) setup using 256 Quadrature Amplitude Modulation (256QAM).

From a transceiver perspective these increased numbers will also affect the power consumption. The larger bandwidth directly leads to higher sampling frequency in the Analog-to-Digital Converter (ADC) and Digital-to-Analog Converter (DAC), and due to the use of higher carrier frequencies to obtain sufficient spectrum it also affects the analog Radio Frequency (RF). In the digital domain the larger bandwidth affects the complexity because the Base Band (BB) processor has to calculate the channel estimate and perform equalization across the whole bandwidth.

The dynamic range must also increase to support 256QAM and the advanced receivers. This affects the analog RF requirements in terms of gain and noise factor, the ADC and DAC's bit resolution and the number of bits used in the digital domain. The latter will increase the size and cost of the memory and the interconnecting buses, and also affect the power consumption of the digital processor because each calculation will be made with higher resolution.

The number of Component Carriers (CCs) used for Carrier Aggregation (CA) entails the mobile terminal need to implement a similar number of RF chains, ADCs, and DACs. This increases both the cost, size and power consumption. Moreover, the need for 4 spatial streams entails that 4 RF chains are needed per CC. Processing multiple spatial streams will also increase the BB power consumption both due to the higher data rates and the need for more channel estimates.

Clearly the increased system parameters will affect the power consumption of multiple components in the transceiver, but in this study the analysis is limited to the receiver. Figure 5.1 illustrates the commonly used, [16], direct conversion receiver architecture, where the received signal is converted to BB in one step. This is a popular design because the power consumption is lower than e.g. the superheterodyne receiver which relies on an intermediate frequency and thus consists of many more components.

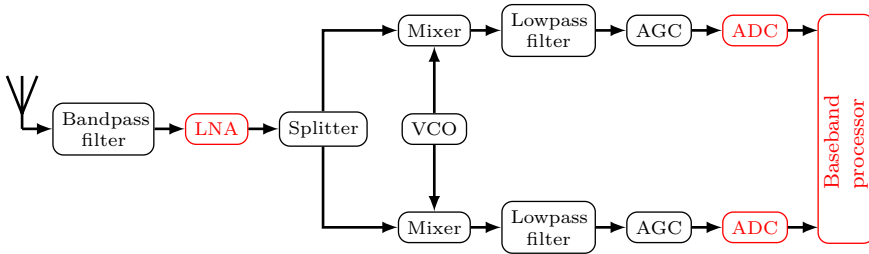


Figure 5.1: General block diagram of a direct conversion architecture receiver. Components marked with red are examined in detail in this chapter.

The task of the analog RF is to filter, amplify, and down-convert the low-power, wideband, and high carrier frequency signal from the antenna, such that the ADC can digitize the signal. These operations are handled by use of filters, one or more Low Noise Amplifiers (LNAs) and one or more mixers depending on the number of intermediate frequencies if any. The filters are passive components while the LNA and the mixer are active, power consuming devices whose performance can be modified by adjusting the supply power. In addition to the aforementioned components antenna tuners and switches are also needed to support the many frequency bands. In this study the LNA and the ADC, marked with red in figure 5.1 are examined in detail together with the baseband processor.

In the following sections the performance evolution of the analog RF, the ADC, and the digital BB is examined to determine if the hardware is able to handle the increased 5G requirements in 2020. After the analysis of the individual components an estimate of the total expected power consumption in a 5G compliant mobile terminal is provided in section 5.4. Note that the focus of this evolution study is on the receiver, but a discussion on transmitter challenges is also provided, because this component comprises a significant amount of the total power consumption as discussed in section 2.5.

5.1 Analog RF Evolution

The analog RF will be affected by increasing bandwidth, carrier frequency, dynamic range, and number of chains. The scope of this section is thus to examine how the performance of the RF, with regards to these parameters, has evolved over time to predict it in 2020, with special focus on the related change in power consumption.

In general the chipset manufacturers strive to implement the RF transceiver, the digital BB and additional features such as the Power Management Unit (PMU) in a

single chip solution to achieve low area and cost, by use of the same low Complementary Metal–Oxide–Semiconductor (CMOS) technology node. This is complicated due to the use of many frequency bands and CA to obtain sufficient spectrum [16], and table 2.6 also reports that the Long Term Evolution (LTE) User Equipments (UEs) are often composed of multiple chips with different CMOS technology nodes. The RF transceiver is however composed of one single chip and therefore it is assumed that the individual performance of the LNA and mixer is fairly comparable because they move to a lower technology node concurrently.

Since the evolution is expected to be quite similar for both the mixer and the LNA the latter was selected for detailed examination. Unfortunately such performance evolution estimates or even just a detailed literature survey is not available in open literature. One of the few examples is the paper [113] by Szczepkowski and Farrell where they examine about 30 LNAs published from year 2004 to 2013, but with just a single paper from the years 2004, 2012, and 2013. This entails the trend is only observable over 7 years, which is a short time frame considering the target of predicting another 6 years ahead to 2020. Another example is the LNA roadmap from 2001 [114], which predicts performance for CMOS technology nodes from 130 nm to 22 nm, but without any specific details except the calculation of a Figure of Merit (FoM). Therefore a new literature study was performed including 115 papers from year 1991 until 2014. The complete details and references are given in appendix C. The distribution of the papers is illustrated in figure 5.2 where it can be noted that from 1995 an onwards at least 4 papers have been considered per year.

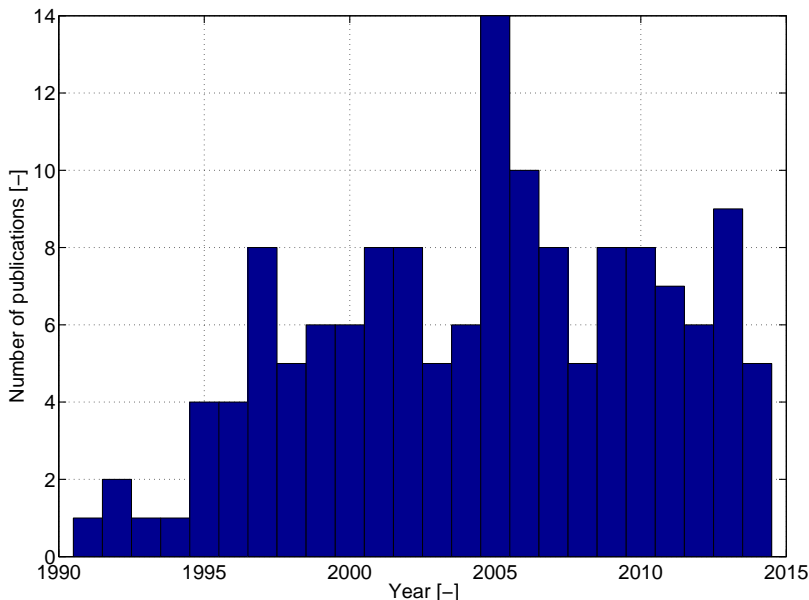


Figure 5.2: Number of examined LNA publications per year, used for performance survey.

The first observation considers the CMOS technology node and the values are illustrated in figure 5.3 together with a trend line. The node has evolved a bit slower

than expected by for example [114, 115], but one reason may be that it is rather costly to fabricate the chips and that most papers are made by academia. Note that not all LNAs are based on the CMOS technology and that some do not report the node.

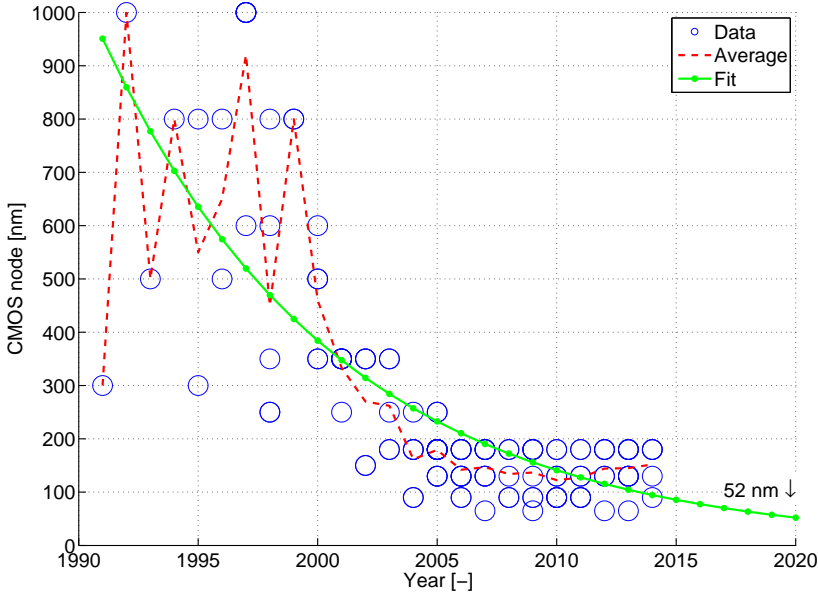


Figure 5.3: LNA CMOS technology node evolution.

The supply voltage is strongly correlated with the CMOS node and one of the main reasons why the power consumption decreases when moving to a lower node. The reported supply voltage for the surveyed LNAs is given in figure 5.4 and again an improvement is observed, but as with the technology node it lacks behind the few available predictions [114, 115]. Lowering the supply voltage does however also complicate the transistor design, and it may increase the leakage current as will be discussed in section 5.3.

In general there are five key parameters describing the performance of an LNA (or mixer); the Noise Figure (NF), the power gain, the intermodulation points, the bandwidth, and the maximum carrier frequency. In this survey the best parameters have been chosen i.e. the minimum NF, the maximum power gain, and the lowest Input Third-Order Intercept Point (IP3) (or Output IP3 minus the power gain). Since some LNAs are narrowband they only report the carrier frequency, while wideband LNAs also report the bandwidth. Therefore not all surveyed papers contribute to the bandwidth observation presented later.

Amplifiers do not only amplify the input signal, consisting of the signal and the noise i.e. having a specific Signal to Noise Ratio (SNR), but also add some noise for example thermal noise, due to moving electrons depending on the temperature, and shot noise generated in transistors. Thus the output will have a degraded SNR even though the signal is amplified. The degradation is known as the NF and it is defined as

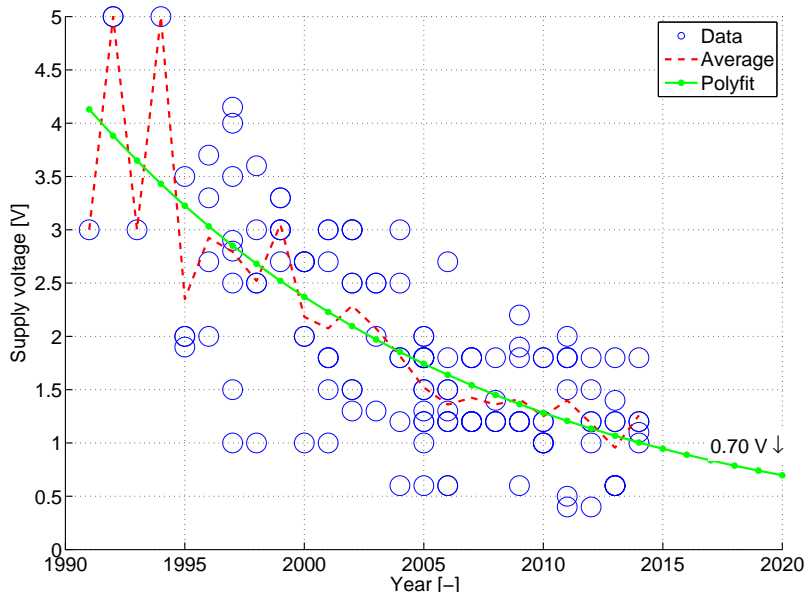


Figure 5.4: LNA voltage evolution.

the relationship between the input SNR and the output SNR

$$\begin{aligned}
 NF &= \frac{S_i/N_i}{S_o/N_o} = \frac{S_i/N_i}{G_{LNA} \cdot S_i / (G_{LNA} \cdot N_i + N_{LNA})} \\
 &= \frac{G_{LNA} \cdot N_i + N_{LNA}}{G_{LNA} \cdot N_i} = 1 + \frac{N_{LNA}}{G_{LNA} \cdot N_i} \quad [-] \quad (5.1)
 \end{aligned}$$

where: NF is the noise figure of the LNA [-]
 S_i is the input signal [W]
 N_i is the input noise [W]
 S_o is the output signal [W]
 N_o is the output noise [W]
 G_{LNA} is the power gain of the LNA [-]
 N_{LNA} is the noise of the LNA [W]

thus the NF does not depend on the input signal level, but only the input noise level and the LNA performance in terms of gain and noise level.

When multiple active devices are connected in a cascade i.e. one after another Friis' formula can be used to calculate the total NF of the system as [116, Eq. 8.29]:

$$NF = NF_1 + \frac{NF_2 - 1}{G_1} + \frac{NF_3 - 1}{G_1 \cdot G_2} + \frac{NF_4 - 1}{G_1 \cdot G_2 \cdot G_3} + \dots \quad [-] \quad (5.2)$$

where: NF is the noise figure of the complete chain [-]
 NF_1 is the noise figure of the first component [-]
 G_1 is the power gain of the first component [-]

Clearly the chain will experience the lowest NF if the first component has a low NF and a high power gain, and this is the reason why the LNA is usually the first active component as illustrated in figure 5.1. When examining the performance of the LNAs it is thus important to note how these parameters evolve. Figure 5.5 shows that the NF performance has decreased 1 dB over 20 years. There are multiple reasons for this; it is power consuming to improve the NF, the NF also depends on the bandwidth, which has increased as will be shown later in this section, and finally the system requirements have decreased. The NF requirements were reported, [117], to have decreased from < 2 dB for Global System for Mobile Communications (GSM) to < 3 dB for Wideband Code Division Multiple Access (WCDMA), and be < 4.5 dB for WiFi. In [118] the NF requirement for LTE was estimated to be 5 dB and thus this explains why the NF performance has decreased. In the 5G Radio Access Technology (RAT) a low NF is important due to the use of advanced receivers and higher order modulation, but requirements have not been defined yet.

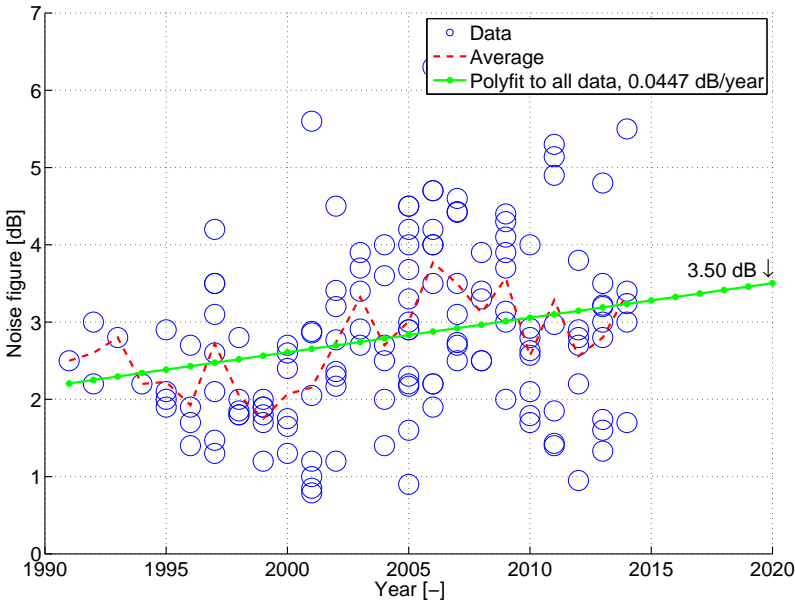


Figure 5.5: LNA Noise Figure evolution.

Friis formula in eq. (5.2) showed how the LNA, if it is the first device in the receive chain, will also benefit from high gain. However the LNA gain cannot be too high because if a blocker, i.e. an interfering signal, is present it will desensitise the following components. The surveyed papers however show that the LNA power gain has remained approximately constant as illustrated in figure 5.6, and based on equation (5.1) this is

another reason why the NF has not improved. In general it is not trivial to improve both gain and NF unless another performance parameter such as power consumption is sacrificed [119]. In addition the gain may not have changed much due to linearity considerations in the components following the LNA in the chain.

In the 5G RAT the gain requirements are not expected to change a lot compared to existing generations because the received power is expected to be similar or possibly a bit higher due to the lower path loss of the Ultra-Dense Small Cell (UDSC) scenario.

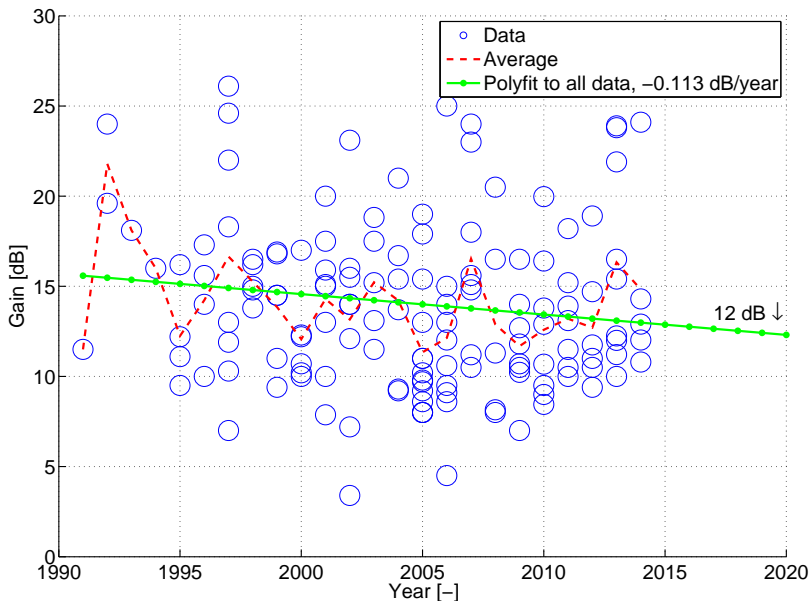


Figure 5.6: LNA Power Gain evolution.

The third important parameter for an LNA is the intermodulation performance. The IP3 is often of particular interest because it affects how powerful an interferer may become, but increasing the IP3 leads to higher power consumption, [119]. Most of the observed LNAs have an input IP3 in the range -10 - 0 dBm, with a slightly decreasing trend as illustrated in figure 5.7. This means lower power consumption, and this is expected to be the case in the 5G RAT as well because the use of Time Division Duplexing (TDD) entails transmission and reception will not occur simultaneously i.e. leading to less strict IP3 requirements.

Bandwidth and carrier frequency are two other important parameters for LNAs, and the devices can be divided into two distinct subgroups: narrowband and wideband. The narrowband LNA is designed to support one or a few frequency bands at a specific carrier frequency, for example for cellular or WiFi applications, while the wideband LNA is a more general device. Examining the upper frequency of the studied LNAs, illustrated in figure 5.8 it is clear that specific cellular bands at 900 MHz and 1.8 GHz together with WiFi bands at 2.4 GHz and 5 GHz have received a lot of attention. In 2002 the Federal Communications Commission defined the Ultra-Wideband frequency range to be 3.1-10.6 GHz [120], and this is also reflected in the figure. Thus the improvement

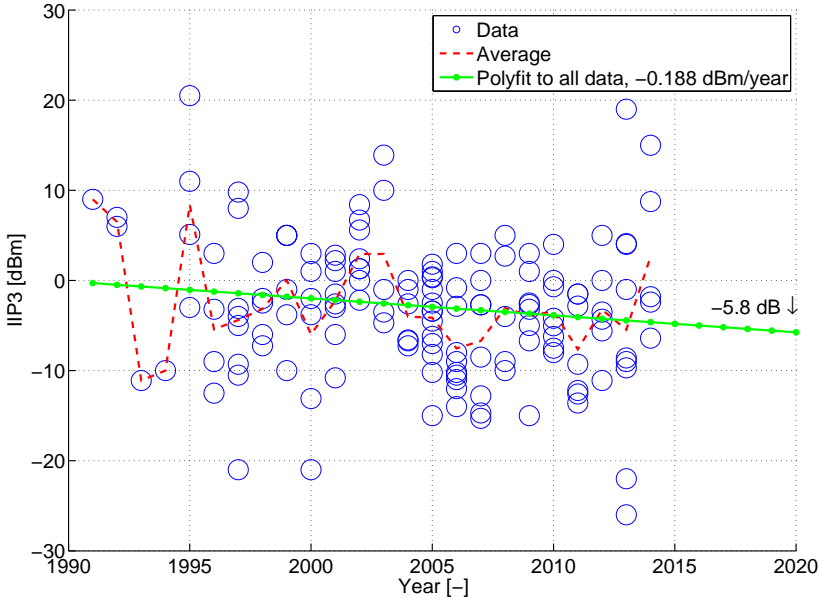


Figure 5.7: LNA Input IP3 evolution.

in upper maximum frequency depends primarily on application demand. Since the 5G concept includes all Centimeter Waves (cmW) there will be a need for LNAs supporting up to 30 GHz and this will definitely pose new challenges to the LNA designer, but as can be seen in figure 5.8 some designs are already available above 20 GHz.

About 80 of the surveyed LNAs report the bandwidth in which the gain, NF and IP3 are relatively constant, but as illustrated in figure 5.9 the bandwidth spread is 3 decades. Similar to the maximum frequency the bandwidth improvement primarily depends on application demand and because the 5G RAT has a bandwidth of up to 400 MHz it will not push the boundaries, except if the LNA has to support bands at both ends of the cmW.

The survey has showed that the NF, gain, and IP3 have not improved the last 20-25 years while there are some distinctive steps in bandwidth and carrier frequency support due to new applications. The hypothesis is therefore that the designers have focused on reducing the power consumption and this is supported by figure 5.10, which shows the power consumption of the LNAs. In 20 years the power consumption has been halved, but since the CMOS technology node and the supply voltage has also decreased, the latter also by half, a larger reduction was expected [121]. Using the trend line the average power consumption in 2020 and 2030 is expected to be 7.5 mW and 1.2 mW respectively.

One reason for the less significant power consumption improvement is that designers have also strived to reduce the area as illustrated in figure 5.11. Examining the papers it is clear that it is an important factor, because the area is often mentioned before the electrical performance parameters (gain, NF, and IP3) in the abstracts and because some designers choose to only report the area of the LNA core without the connection

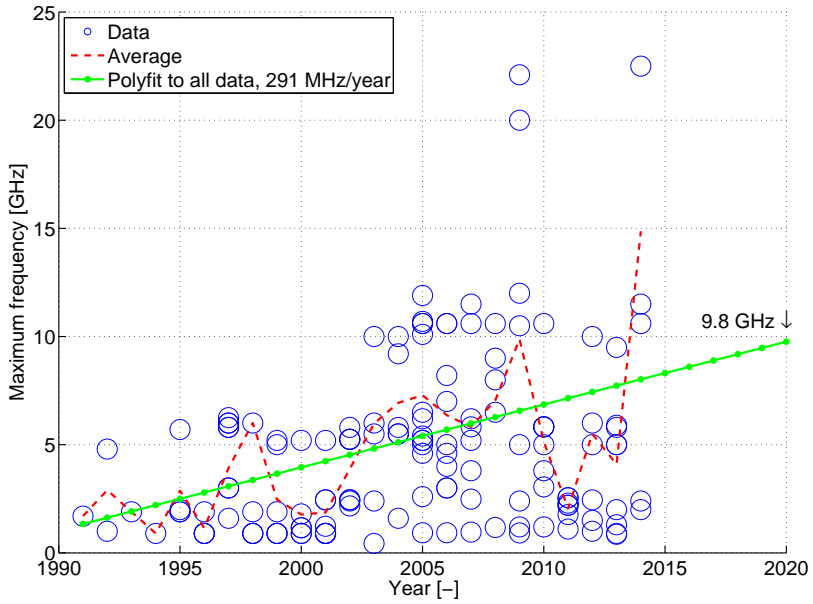


Figure 5.8: LNA maximum frequency evolution.

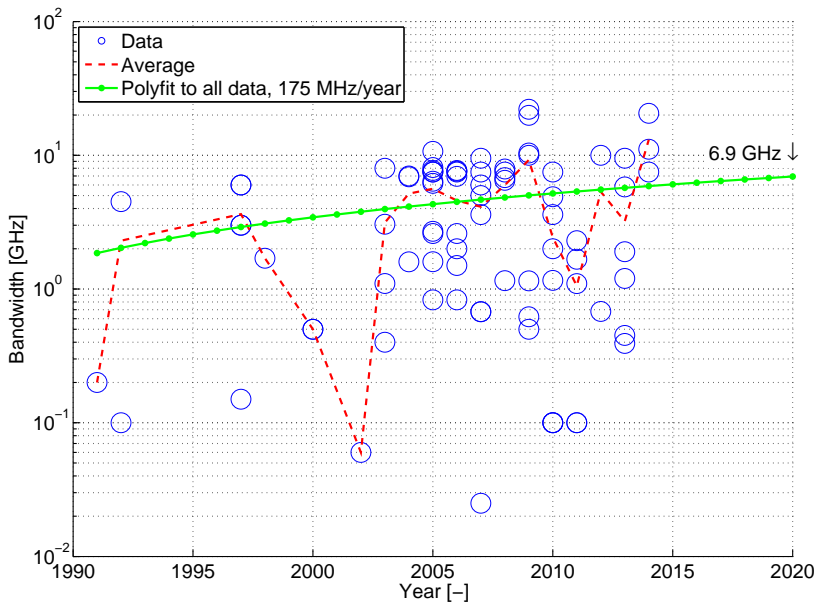


Figure 5.9: LNA bandwidth evolution (not reported for all LNAs).

pads to decrease the reported area of their design.

Due to the many performance parameters it is commonly used to calculate a FoM

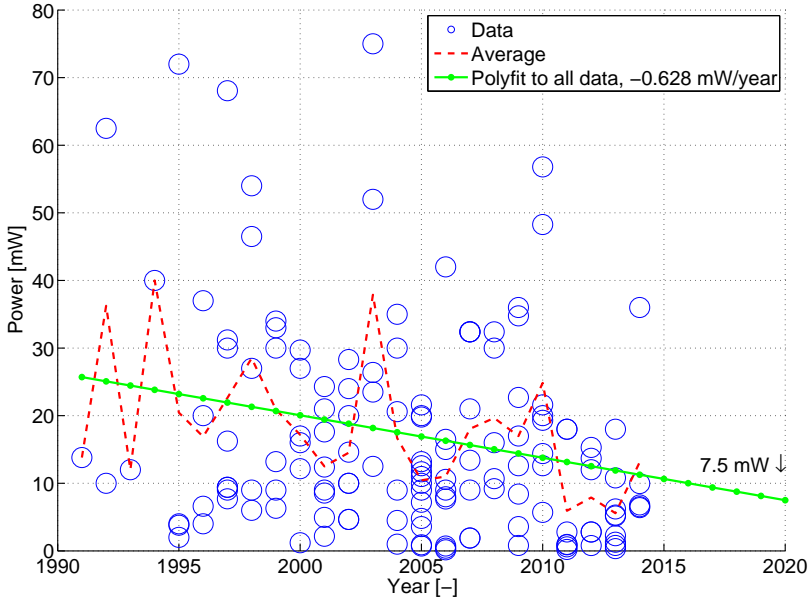


Figure 5.10: LNA power consumption evolution.

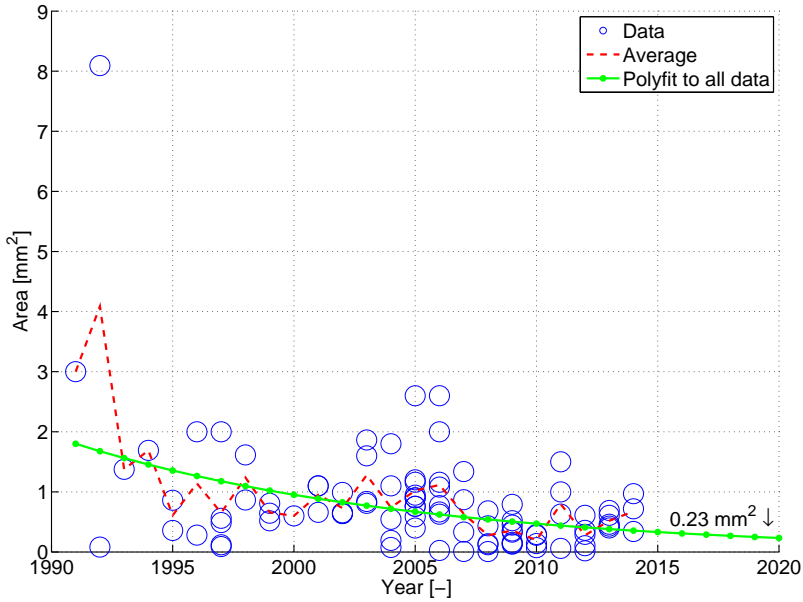


Figure 5.11: LNA area evolution. Not reported for all LNAs, and some only report core area without connection pads.

for the proposed LNA design, but as pointed out in [122] there exists a multitude of

FoMs depending on the device type (multiband, narrowband, or wideband) and the parameters in focus. One FoM targeted towards LTE LNAs is defined as [113, Eq. 17]:

$$\text{FoM} = G + IIP3 + 10 \cdot \log_{10} \left(100 \cdot \frac{BW}{f_c} \right) - NF \quad [\text{dBm}] \quad (5.3)$$

where: $IIP3$ is the input IP3 [dB]
 f_c is the carrier frequency [MHz]

The FoM is plotted versus the power consumption in figure 5.12 and as expected the FoM can be increased by increasing the power consumption. The 1st order fit to the

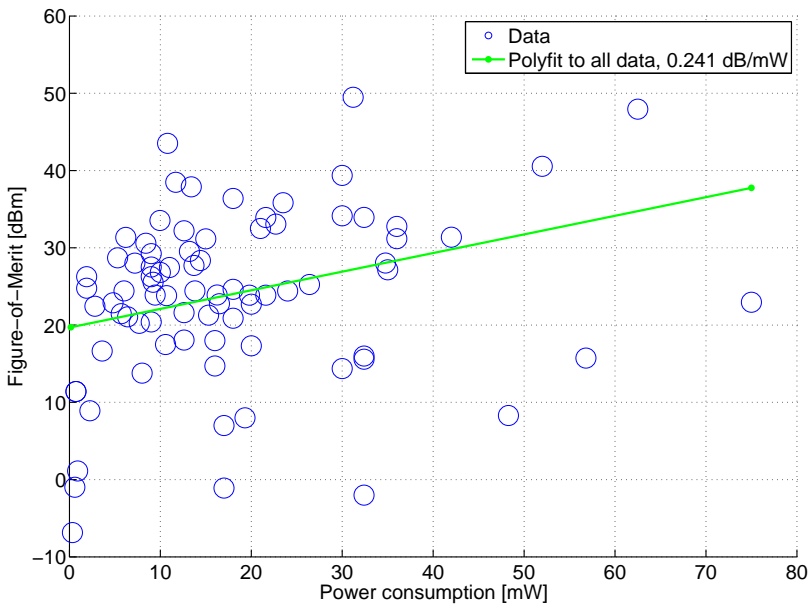


Figure 5.12: Figure-of-merit as a function of power consumption.

data shows the FoM can be increased 0.24 dB if the power consumption is increased 1 mW, e.g. a 3 dB power gain improvement will increase the power consumption about 12 mW, which is approximately the double of the average power of a modern LNA. In [113] the trend line was approximated to be 0.19 dB/mW, but the FoM spread was also smaller.

The conclusion on the survey is that designers have focused on minimizing the power consumption and the physical chip area, which in 2020 will approach 7.5 mW and be halved as compared to the area of 2010, respectively. To achieve this the other performance parameters such as gain, IP3, and NF are either maintained or slightly reduced. In 5G the area and power will continue to be Key Performance Indicators (KPIs), while gain and NF also are important due to the higher order modulation and

advanced receivers. The IP3 will be less important due to the use of TDD and this has a positive effect on power consumption because improving IP3 entails increased power consumption [119]. The survey also showed that the LNAs have evolved to support the demanded carrier frequency and bandwidth improvements, and based on the current performance the bandwidth target of 100 MHz per 5G receive chain is feasible, and even also using a single 400 MHz chain. It is however an open issue to provide support for the higher carrier frequencies in the cmW concept, but the emergence of business in this area is expected to push technology development.

5.2 ADC Evolution

After the received signal has been down-converted and amplified to BB the ADC will perform the conversion to the digital domain. The challenges of the 5G concept are that the bandwidth and the dynamic range are increased, and in addition the increased number of RF chains entails the number of ADCs will increase proportionally. In this section the ADC performance evolution is examined with focus on dynamic range, bandwidth, and power consumption. Parts of the work were previously presented in the contribution [34].

In LTE the maximum bandwidth of a channel is 20 MHz, but in an intra-band contiguous CA configuration the bandwidth may be up to $5 \cdot 20 \text{ MHz} = 100 \text{ MHz}$. Current commercial UEs support up to 40 MHz. The dynamic range depends on the Effective Number of Bits (ENOB), which is estimated to be 12 bits, and this is also estimated to be sufficient for the 5G RAT. In the UDSC scenario the receiver may even become Signal to Interference + Noise Ratio (SINR) limited before the dynamic range becomes an issue, [123].

As opposed to the RF front end components discussed in the previous section there are multiple comprehensive ADC performance surveys available. They include the public Excel sheet by Murmann, which covers about 400 conference papers from 1997 to 2014 [124], and the comprehensive report by Jonsson which includes more than 1700 publications from 1974 to 2012 [125]. The first observation about ADC evolution is however purely based on RAT evolution because in approximately 20 years the bandwidth has changed from 200 kHz in GSM to LTE's 20 MHz i.e.

$$\frac{20 \text{ MHz}}{200 \text{ kHz}} = 100 = x^{20 \text{ years}} \quad \rightarrow \quad x = 10^{\frac{\log_{10}(100)}{20 \text{ years}}} = 26 \%/ \text{year} \quad (5.4)$$

In previous work Manganaro [126] has examined the ADC performance evolution using Murmann's data [124] and estimated that the energy efficiency for high speed ADCs with a bandwidth greater than or equal to 100 MHz improves 1.82 db/year. Furthermore he estimated that the progress is 0.8 dB/year for high resolution ADCs i.e. having an Signal to Noise and Distortion Ratio (SNDR) greater than or equal to 75 dB where SNDR is related to ENOB as follows [126, Eq. 2.1]

$$\text{ENOB} = \frac{\text{SNDR} - 1.76 \text{ dB}}{6.02 \text{ dB}} \quad [\text{bits}] \quad (5.5)$$

Jonsson has published several estimates of the evolution based on his data and in 2010 he conservatively estimated that the sampling rate of ADCs would increase less

than 5 times until 2020 [127] i.e.

$$5 = x^{10 \text{ years}} \quad \rightarrow \quad x = 10^{\frac{\log_{10}(5)}{10 \text{ years}}} = 17 \%/\text{year} \quad (5.6)$$

However in his most recent report [125] from 2013 he estimates the thermal FoM, defined as [125, Eq. 11.1]

$$\text{FoM}_{\text{thermal}} = \frac{P}{2^{2 \cdot \text{ENOB}} \cdot f_s} \quad [\text{J}] \quad (5.7)$$

where: $\text{FoM}_{\text{thermal}}$ is the thermal FoM [J]
 P is the power consumption [W]
 ENOB is the effective number of bits [bits]
 f_s is the sampling frequency [Hz]

to improve 2 times every 2 years i.e.

$$2 = x^{2 \text{ years}} \quad \rightarrow \quad x = 10^{\frac{\log_{10}(2)}{2 \text{ years}}} = 41 \%/\text{year} \quad (5.8)$$

Finally Ho of Mediatek has predicted [128] the Schreier FoM, defined as

$$\text{FOM}_S = \text{SNDR} + 10 \log_{10} (\text{BW}/P) \quad (5.9)$$

to improve 10 dB from 2014 to 2020 i.e.

$$10 = x^{6 \text{ years}} \quad \rightarrow \quad x = 10^{\frac{\log_{10}(10)}{6 \text{ years}}} = 47 \%/\text{year} \quad (5.10)$$

This yields an average estimated annual improvement of 34% and assuming that the power consumption and the ENOB are kept constant, the bandwidth can be improved as illustrated in figure 5.13. The 100 MHz bandwidth is feasible in 2020 independent of the selected estimate, while the average improvement also entails 200 MHz bandwidth ADCs should be possible. Note that the improvements correspond well with the general 19-37% improvement for Information and Communications Technology (ICT) [18] discussed in the introduction of the previous chapter 4.

The next step is to examine the power consumption and it can be estimated using the Schreier FoM in eq. (5.9). The FoM is plotted in figure 5.14 using Murmann's data collection. The performance edge of the current data is then extrapolated using the average improvement of 34% which corresponds to $1.34^{(2020-2014)} = 7.6$ dB higher FoM in 2020.

The current FoM is approximately 167 dB for an ADC with 100 MHz bandwidth and maintaining the assumption of 12 ENOB the power consumption is estimated by re-arranging eq. (5.5) and (5.9):

$$\begin{aligned} P_{2014}(\text{BW}) &= \frac{\text{BW}}{10^{(\text{FOM}_S - \text{SNDR})/10}} \\ P_{2014}(100 \text{ MHz}) &= \frac{100 \text{ MHz}}{10^{(167 \text{ dB} - (12 \cdot 6.02 \text{ dB} + 1.76 \text{ dB}))/10}} \approx 50 \text{ mW} \end{aligned} \quad (5.11)$$

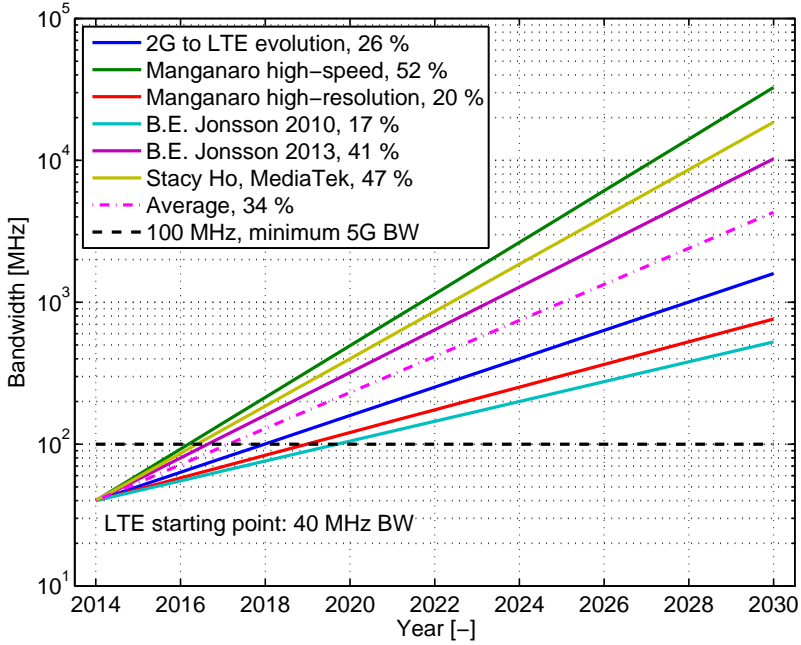


Figure 5.13: Predicted ADC bandwidth assuming constant power consumption and ENOB. [34, Fig. 11]

Examining figure 5.14 two distinct fronts on the performance edge can be observed. The horizontal section is called the “architecture front”, [126] because the performance depends mainly on the energy efficiency of the selected architecture. The sloping section is known as the “technology front” because the ADCs depend on exploiting the improvement in technology to maintain their performance. Using the Schreier FoM of 2020, estimated to be 174.7 dB in figure 5.14, the power consumption in 2020 will be $P_{2020}(100 \text{ MHz}) \approx 8.5 \text{ mW}$. Based on a constant FOM_S a doubling of the BW will entail the double power, but since Murmann has also assumed the FOM_S slope of the “technology front” to be -10 dB/decade, the power consumption in 2020 as a function of bandwidth is estimated to be (relative to 100 MHz):

$$P_{2020}(\text{BW}) = \frac{\text{BW}}{10^{(\text{FOM}_S@100 \text{ MHz} - \text{SNDR} - 10 \log_{10}(\frac{\text{BW}}{100 \text{ MHz}}))}/10}} \quad (5.12)$$

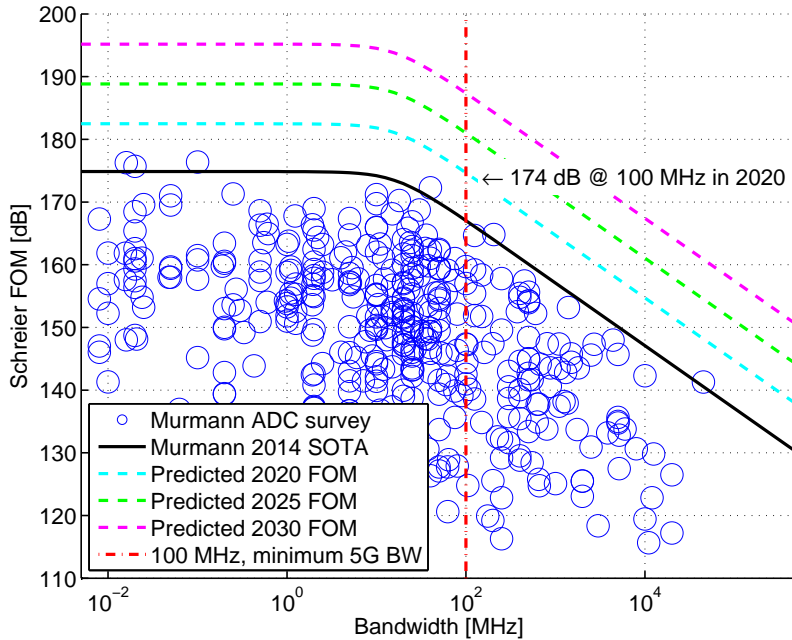


Figure 5.14: Murmann state-of-the-art ADC survey [124] combined with predicted Schreier FOM improvement from figure 5.13. [34, Fig. 12]

Using 100 MHz as the baseline the power consumption as a function of BW is

$$\begin{aligned}
 \frac{P_{2020}(100 \text{ MHz})}{10^{(\text{FOM}_{\text{S@100 MHz}} - \text{SNDR})/10}} &= \frac{P_{2020}(\text{BW})}{10^{(\text{FOM}_{\text{S@100 MHz}} - \text{SNDR} - 10 \log_{10}(\frac{\text{BW}}{100 \text{ MHz}}))}/10}} & (5.13) \\
 &\Downarrow \\
 P_{2020}(\text{BW}) &= \frac{P_{2020}(100 \text{ MHz}) \cdot \frac{\text{BW}}{10^{(-10 \log_{10}(\frac{\text{BW}}{100 \text{ MHz}}))}}}{100 \text{ MHz}} \\
 &= \frac{P_{2020}(100 \text{ MHz}) \cdot \frac{\text{BW}}{10^{(\log_{10}(\frac{100 \text{ MHz}}{\text{BW}}))}}}{100 \text{ MHz}} \\
 &= P_{2020}(100 \text{ MHz}) \cdot \left(\frac{\text{BW}}{100 \text{ MHz}}\right)^2 \quad [\text{W}] & (5.14)
 \end{aligned}$$

thus doubling the bandwidth will quadruple the power consumption due to the FOM_{S} slope. Note that not all combinations of power, bandwidth and ENOB, resulting in a realistic FOM_{S} , are feasible due to technical limitations.

Equation (5.14) demonstrates how a narrowband ADC consumes less power than a wideband ADC with the same dynamic range, but if multiple ADCs are needed to obtain the required total bandwidth the situation may change. The reason is that besides consuming more physical space and possibly increasing the component cost, the use of multiple narrowband channels will require an equal number of RF front ends further

increasing the power consumption, physical space, and cost. In addition the number of ADCs and Front Ends will increase linearly with the number of spatial streams. It may however be possible to achieve some power savings by combining multiple ADCs in one Integrated Circuit (IC) and share the voltage reference source, digital control, bus connections etc..

In equation (4.1) the target bandwidth was estimated to be 400 MHz and the number of spatial streams to be 4. This total bandwidth can be achieved by the use of CA, e.g. 4 CCs each 100 MHz wide. This will lower the ADC performance requirements and reduce the power consumption per ADC. Table 5.1 contains the estimated ADC power consumption and an overview of the number of required converters. Since the power consumption has a quadratic dependence on the bandwidth, see equation (5.14), the use of 4 CCs each 100 MHz wide results in the lowest total ADC power consumption, but it will entail a significant increase in chip area.

Table 5.1: ADC power consumption in 2020 as a function of CC BW, number of spatial layers, and number of CCs. The example is for a total bandwidth of 400 MHz, 4 spatial streams, and 2 ADCs per stream for I and Q branches

Single ADC BW [MHz]	100	200	400
Single ADC power [mW]	8.51	34.0	135.5
Number of CCs [-]	4	2	1
Number of chains [-]	16	8	4
Number of ADCs [-]	32	16	8
Total ADC power [mW]	272	543	1084

The conclusion is that ADCs in 2020 are expected to be able to fulfil the 5G requirements in terms of increased dynamic range and bandwidth, at least for CCs of 100 MHz and 200 MHz. The current predictions does however show that supporting 400 MHz bandwidth in a single CC will lead to a significant increase in power consumption, but it may also be difficult to obtain such a large continuous spectrum anyway. The use of many narrowband CCs is beneficial from the ADC power consumption perspective, but the related increase in number of components and area in the RF front end may be a limiting factor, and in addition the study showed that there is little power consumption difference in using 100 MHz and 200 MHz where the latter option only requires half the number of chains.

5.3 Digital Processing Evolution

The processing requirements to a 5G receiver will be significantly higher than the current requirements to an LTE receiver. The two main reasons are the 100 times increase in data rate and the use of advanced, complex receivers, [129], for interference cancellation.

In section 2.5 the power consumption as a function of downlink data rate was examined, and as illustrated in figure 2.7 the power consumption decreases with each new chipset generation. The chipset manufacturers improve their BB processor designs and thereby lowers the power consumption, but decreasing the CMOS technology node also

helps. The evolution in transistor technology was predicted by Moore in 1965 [130] where he stated that the number of transistors on a chip will double approximately every two years, one reason being the lower technology node. A related observation by Moore's colleague House was that the combination of more and faster transistors would entail the performance would double every 18 months [131], and this is also reflected in Gene's law, [132] stating that the power consumption per Million Instructions Per Second (MIPS) is halved every 18 months. This is useful in the area of mobile processors, because the computational complexity increases with the channel bandwidth, the data rate, and the more advanced receivers. In LTE the Fast Fourier Transform (FFT), channel estimation, and equalization all depend linearly on the channel bandwidth [59, Figure 11.31] and the number of antennas, while the Turbo decoding complexity depends on the data rate [59, Eq. 11.13]

$$C_{\text{Turbodecoder}} = 200 \cdot N_{\text{it}} \cdot r \quad \text{[MIPS]} \quad (5.15)$$

where: $C_{\text{Turbodecoder}}$ is the Turbo decoding complexity [MIPS]
 N_{it} is the number of iterations (8 according to [59]) [-]
 r is the data rate [Mb/s]

Due to the 5G RAT using Orthogonal Frequency Division Multiplexing (OFDM) as in LTE, and the linear relationship between complexity and channel bandwidth the 5G receiver must be able to handle a complexity which is at least 20 times higher (from 20 MHz to 400 MHz), while the Turbo decoder complexity may increase up to 100 times due to the increased data rate. Furthermore the requirements for larger dynamic range, both due to the advanced receiver algorithms and the higher order modulation, entail the baseband processor must utilize more bits i.e. a higher precision leading to higher power consumption. Another factor which affects baseband processing power is the mobility of the receiver because a fast moving mobile terminal entails the channel changes faster and therefore the channel estimate and equalization operations need to be updated more frequently. The UDSC scenario may however have lower mobility as compared to previous RATs.

Moore's law has been predicted to come to an end multiple times, but the International Technology Roadmap for Semiconductors, which sets targets (called requirements in their terminology) for the future, still envision an improvement in transistor technology and thus improved processing performance according to House [131] and Gene [132]. Figure 5.15 illustrates the evolution in physical transistor gate length, not to be confused with the technology node which usually is larger, and the related evolution of the dynamic power consumption i.e. the power consumed when the transistor is ON. The figure contains two sets of data based on the targets set in 2003 [121], which last until 2018, and the newest targets from 2013 [115], which last until 2028. As the physical gate length, illustrated with blue lines, decreases so does the dynamic power consumption, which entails the processor can be composed of more transistors while maintaining or even lowering its power consumption. The rate of improvement in the physical gate length, for the 2003 prediction, is approximately 0.7 every 2 years and since the gate length is scaled with 0.7 on both sides the area will be approximately

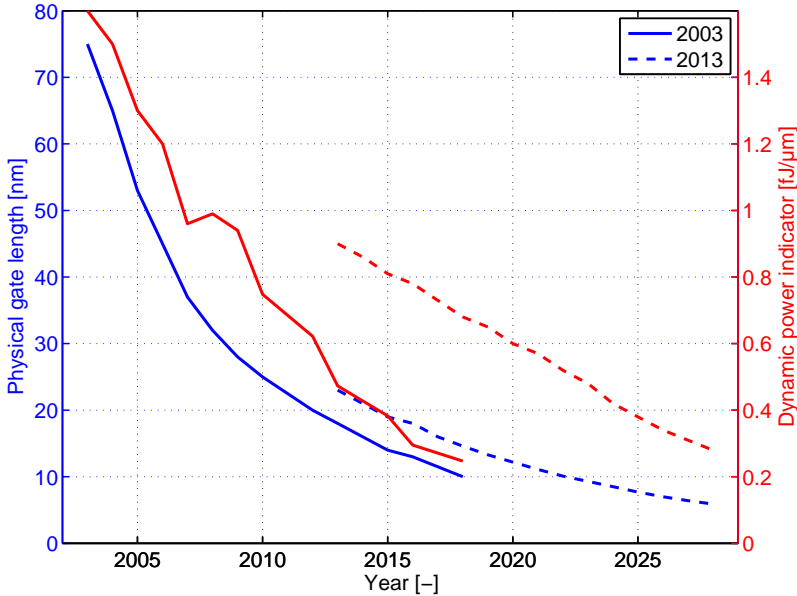


Figure 5.15: Physical gate length and dynamic power indicator as a function of year. 2003 data is based on [121, Table 48c and 48d] using Low Standby Power Technology requirements, and 2013 data is based on [115, Table 2013PIDS3a-LP] Low Power Technology requirements. Note the physical gate length is smaller than the technology node, which is not reported by ITRS.

$0.7 \cdot 0.7 \approx 0.50$ after 2 years, and this doubling in density corresponds well with Moore's law. The 2013 curve shows a slower improvement, about $0.7/4$ years, because scaling and tuning of the transistors becomes more and more difficult as discussed in the section on challenges in [115]. Furthermore issues with lithography (the process of printing the transistors on wafers) and use of new materials is complicating the process [115]. The mismatch between the 2003 and 2013 predictions is attributed to the long prediction range of 15 years, and in [115] the accuracy is stated to be $\pm 20\%$.

Examining the evolution from 2013 to 2020 in further detail it is noted that the physical gate length will approximately be halved from 2013 (23 nm) to 2020 (12.2 nm) according to [115]. This results in the dynamic power being reduced 33% from 0.9 fJ/ μm in 2013 to 0.6 fJ/ μm in 2020. Furthermore the intrinsic delay of each transistor, which is proportional to the clock frequency, is expected to improve 8% from 2013 to 2020, [115]. This entails each transistor will have slightly improved performance at 33% less dynamic power consumption, which is significantly less than the prediction by Gene [132]. As noted earlier in this section the complexity will increase 20 and 100 times, for channel bandwidth and data rate related components respectively, thus there is a need for higher clock frequencies to perform the calculations in due time, and given the small improvement in transistor performance it is necessary to implement more transistors in the BB processor. A key challenge will therefore be to support the higher complexity in 5G provided the estimated improvements in transistor speed and power consumption become reality.

The dynamic power is proportional to the total gate capacitance per device multiplied with the supply voltage squared, [115], and this explains why it improves, as illustrated with red lines in figure 5.15, because the smaller gate length leads to lower capacitance and lower supply voltage. However there is a gap between the 2003 and 2013 estimates because the capacitance has not decreased as much as predicted in 2003.

The lower supply voltage is accompanied by lower threshold voltage, because the transistor must maintain a certain difference between the threshold voltage and the gate-source voltage, which has to be lower than the supply voltage, in order to conduct current [133]. However when the gate-source voltage is smaller than but close to the threshold voltage subthreshold leakage current flows. Previously the threshold voltage was significantly higher than the gate-source voltage, when the transistor was OFF, but as the threshold voltage is lowered the leakage current increases exponentially, because the voltage difference becomes smaller, and thus harming the battery life [134, Equation 2.1]

$$I_{\text{off}} = \frac{\alpha}{L_{\text{GL}}} \exp\left(\frac{V_{\text{GS}} - V_{\text{t}}}{V_{\text{thermal}}}\right) \quad [\text{A}] \quad (5.16)$$

where: I_{off} is the subthreshold leakage current [A]
 α is a constant [Am]
 L_{GL} is the effective gate length [m]
 V_{GS} is the gate-source voltage [V]
 V_{t} is the threshold voltage [V]
 V_{thermal} is the thermal voltage [V]

This is also evident in figure 5.16 which shows how the supply voltage is decreasing, having a positive effect on the dynamic power, while the subthreshold leakage current increases over time as the gate length is decreasing (illustrated in figure 5.15). The estimated supply voltage for the 2003 and 2013 predictions follow the same trend, while the subthreshold leakage current has a significantly better starting point in the 2013 estimates as compared to what was expected in 2013 using the 2003 estimates. The reason is expected to be that low subthreshold leakage current is the main goal when scaling the transistors, [121] and it seems the designers have exceeded their expectations. Finally it is worth noting that it has even been predicted [135] that the leakage current, which consists of the subthreshold leakage and other minor contributors such as reverse biased current, will exceed the dynamic power consumption when moving towards lower CMOS technology nodes, posing a new challenge. Examining figure 5.16 the designers currently seem to have the leakage current under control.

To conclude this section it would be beneficial to estimate the power consumption in a 5G BB processor, but as illustrated in the above discussion there are so many variables that affect the transistor design that it is even difficult for the International Technology Roadmap for Semiconductors to provide good long term estimates. Given the current predictions [115] it is expected that the BB processing power consumption will be a significant challenge in a 5G mobile terminal, but if the laws of Moore and his colleagues continue to be valid it will be feasible. As mentioned in the introduction

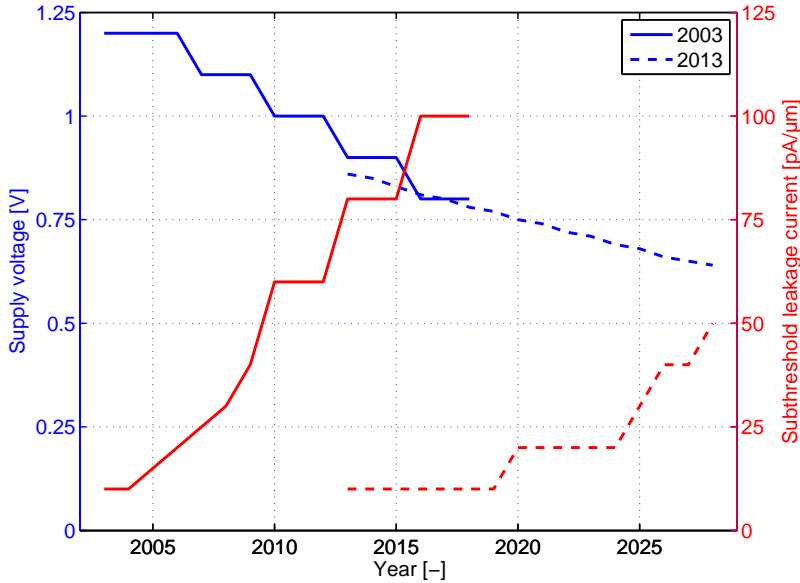


Figure 5.16: Supply voltage and subthreshold current leakage as a function of year. 2003 data is based on [121, Table 48c and 48d] Low Standby Power Technology requirements, and 2013 data is based on [115, Table 2013PIDS3a-LP] Low Power Technology requirements.

Gene [132] estimated the power consumption per MIPS to be halved every 18 months i.e.

$$0.5 = x^{18 \text{ months}} \rightarrow x = 10^{\frac{\log_1 0(0.5)}{1.5 \text{ years}}} = 0.63/\text{year} \quad (5.17)$$

That is the receiver can perform the same number of MIPSs at 0.63 times less power. Therefore the processing power consumption will be $0.63^{2020-2010} \approx 0.01$ i.e. 1% of what it was in 2010 for the same number of MIPSs. Because the data rate increases 100 times a crude estimate of the processing power is therefore expected to be about the same as in 2010.

In addition to the processing power consumption it is important to note the cost and the power consumption of the memory the processor uses for buffering. The high data rate entails more data needs to be stored in the buffers as compared to LTE, but on the other hand the efficient Hybrid Automatic Repeat Request (HARQ) design, discussed in section 4.7 lowers the need for buffer space.

5.4 Estimation of Receiver Power Consumption

In the previous sections selected receiver components were examined with a performance evolution and power consumption perspective. In this section the obtained knowledge is used to provide a crude estimate of the total receiver power consumption in 2020 and 2030. The estimates are based on equation (4.1) where a 400 MHz

bandwidth and 4 spatial streams were estimated to fulfil the 10 Gb/s requirement of 5G.

The starting point is an LTE receiver in 2014 using 2x2 MIMO in a single 20 MHz carrier to achieve a data rate of 100 Mb/s. Assuming the direct conversion architecture of figure 5.1 is used a receive chain will apply one common LNA, a mixer per I and Q branch, and a Voltage Controlled Oscillator (VCO) per CC of which there is only one in single carrier LTE. In figure 5.10 the average LNA power consumption was estimated to be 11.3 mW in 2014 and 7.5 mW in 2020 and based on [136] it is assumed that each mixer and VCO will consume about the same power. The filters of figure 5.1 are assumed to be passive devices and therefore they do not consume power while the Automatic Gain Controls (AGCs) are assumed to have a negligible consumption.

The power consumption of the ADCs, of which there are 4 in total; 2 MIMO chains each with an ADC per I and Q sampling branch, can be estimated using the FoM illustrated in figure 5.14. For example the FoM at 20 MHz bandwidth is determined to be 172.9 dB in 2014 and using equation (5.11) the power consumption is estimated to be:

$$P_{2014}(20\text{ MHz}) = \frac{20\text{ MHz}}{10^{(172.9\text{ dB} - (12 \cdot 6.02\text{ dB} + 1.76\text{ dB}))/10}} \approx 2.58\text{ mW} \quad (5.18)$$

The final step is to estimate the power consumption of the BB processor, which will perform channel estimation, equalization, and decoding among other tasks. Unfortunately the estimate cannot be based on the measurements presented in chapter 2 because the contribution of the BB processor cannot be separated from the total power consumption. Instead the estimate is based on the three recent publications presented in table 5.2. The power consumption values are not given for the same data rate, but based on the observations in section 2.5 about the minor power consumption dependence on data rate this is not expected to be an issue. Due to [139] being published in 2013 the

Table 5.2: LTE baseband processors from literature.

References	[137]	[138]	[139]	Average
Year	2014	2014	2013	2014
Data rate [Mb/s]	60	≤150	54	100
Power consumption [mW]	480	576	651	489

power consumption is scaled with 0.63 as defined in equation (5.17). The average BB processor power consumption is thus estimated to be 489 mW.

Combining the observations about RF, ADC, and BB processor power consumption the total power consumption of an LTE receiver in year 2014 can be estimated. The result is given in the second column of table 5.3 and the estimate of 578 mW is not too far from the ≈ 800 mW measurements in figure 2.9. One reason for the difference is that the estimate only includes the cellular subsystem receiver, while it cannot be separated from the whole smartphone in the empirical values.

Using the LNA power prediction of figure 5.10, the ADC FoM prediction of figure 5.14, and Gene's law of equation 5.17 for scaling the BB processor the power consumption is also estimated for LTE in year 2020. The power consumption is reduced to 1/7

due to the aggressive scaling of the ADC and BB processor and thus if the estimate is accurate within a factor of 3-5 a significant improvement in battery life can be expected.

Table 5.3: Estimated receiver power consumption. The example is for 2x2 MIMO, 20 MHz LTE and 4x4 MIMO, 400 MHz 5G.

RAT	LTE			5G					
Year	2014	2020		2020			2030		
Data rate [Mb/s]	100			10.000			10.000		
Baseband power [mW]	489	30.6		3060			30.1		
Single CC BW [MHz]	20	20	100	200	400	100	200	400	
Number of CCs [-]	1	1	4	2	1	4	2	1	
Number of chains [-]	2	2	16	8	4	16	8	4	
ADC FoM [dB]	172.9	180.6	174.7	171.7	168.7	187.4	184.4	181.4	
Single ADC power [mW]	2.58	0.44	8.51	34.0	135.5	0.46	1.82	7.28	
Number of ADCs [-]	4	4	32	16	8	32	16	8	
Single LNA power [mW]	11.3	7.50		7.50			1.20		
Number of LNAs [-]	2	2	16	8	4	16	8	4	
Number of mixers [-]	4	4	32	16	8	32	16	8	
Number of VCOs [-]	1	1	4	2	1	4	2	1	
Total power [mW]	578	84.8	3720	3790	4240	107	90.5	104	

Table 5.3 contains similar estimates for a 5G receiver, which is also expected to be based on the direct conversion architecture of figure 5.1. Note that the data rate is increased to 10 Gb/s, as required, and thus the complexity is also expected to increase 100 times. In addition the use of 100, 200, and 400 MHz bandwidth CCs entails there are multiple versions of the receiver with varying number of ADCs and RF components.

Increasing the bandwidth to at least 100 MHz in 2020 increases the power consumption significantly, but the main power consumer is the BB processor, which due to the factor 100 increase in complexity is expected to consume about 3 W. This is not a feasible number because it would severely harm the battery life, but also entail thermal issues in the chip [140]. However Gene's law entails that moving from 2020 to 2022 the BB power consumption will be reduced to about 1.2 W and the total receiver power consumption will be below 2 W, which is on par with the first LTE USB dongles, [25]. The receiver power consumption evolution is illustrated in figure 5.17. The figure shows that the 5G receiver's power consumption will not be comparable with the current LTE version before 2025. If the BB processor designers can keep up with the expectations of Gene's law or even propose a leap in technology it will thus be possible to obtain an acceptable power consumption level in the 5G receiver. Assuming that the scaling continues to be valid until year 2030 the BB processor will contribute with only one third of the overall power consumption, which at that time is estimated to be just 100 mW.

The estimates of ADC and LNA power consumption are based on averages of multiple

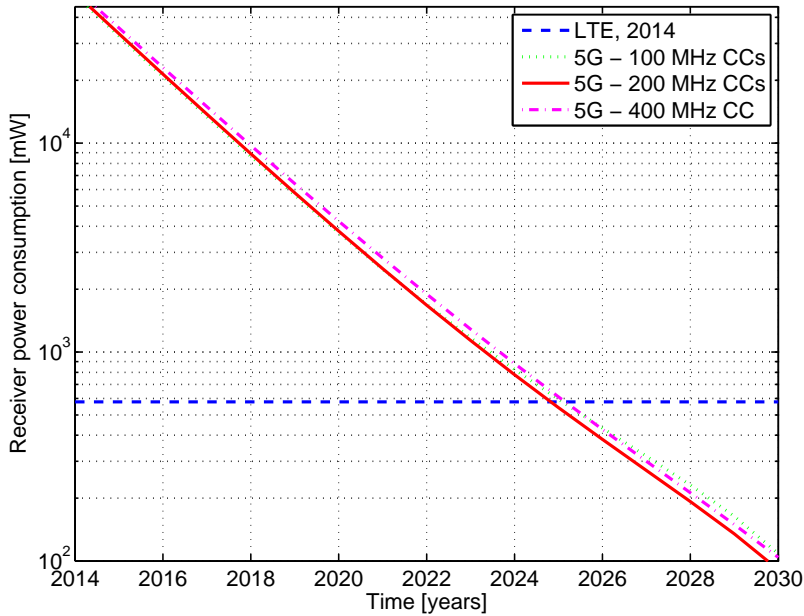


Figure 5.17: Receiver power consumption evolution when using 100, 200, and 400 MHz CCs for 5G.

sources, while the BB scaling is only based on Gene’s law. By applying a sensitivity to the 0.63/year scaling the power consumption is varied as calculated in table 5.4. Using a $\pm 5\%$ scaling of Gene’s law entails the power consumption in 2020 is either 25% lower or more than 30% higher than the estimate of table 5.3 and thus it is clear that the exact estimate of Gene’s law must be considered a rough estimate.

Table 5.4: Estimated BB power consumption when Gene’s law is scaled. The starting point is the 489 mW consumed in 2014, table 5.2.

Scaling [%]	-10	-5	0	5	10
Power reduction factor [-]	0.5670	0.5985	0.6300	0.6615	0.6930
Consumption in 2020 [mW]	1620	2250	3060	4090	5410
Consumption in 2030 [mW]	5.58	13.2	30.1	65.7	138

Due to the ADCs’s power consumption’s quadruple dependence on bandwidth the 200 MHz seems to be a good trade-off between number of CCs and power consumption per chain. One major issue is however to implement the many CCs and spatial stream chains in the mobile terminal and handle the coexistence issues of the bands creating in-band blockers. On the other hand the use of multiple narrowband CCs allows the receiver to discard a single CC if it experiencing significant interference. This is not possible when a single wideband CC is used. In addition to implementation of multiple CCs the need for support of various frequency bands will complicate and increase the area of the design. Finally the varying number of CCs will also affect the number of

required channel estimates and thus the processing complexity.

5.5 Notes on Transmission

This chapter has focused on the power consumption challenges of the 5G receiver, but in this section a few remarks on the transmitter are provided.

The main power consumer in the transmitter is the transmit Power Amplifier (PA). In the most recent LTE UEs efficient supply techniques such as Envelope Tracking (ET) have been applied to improve the Energy Efficiency (EE) as discussed in section 2.5. The supported bandwidth of ET has increased from the 5 MHz of WCDMA to 20 MHz in LTE according to Nujira and Qualcomm [141, 142], but it is a challenge to increase the support to 200 MHz or more, because the ET supply voltage, the analogue envelope detector, and the ADC tracking the input RF signal need to be changed and measured according to the bandwidth, [143]. Yet ETA Devices recently claimed they support 100 MHz [144] and therefore it is expected that the support for 200 MHz is feasible in 2020. The power consumption of the circuit controlling the supply voltage may however become an issue, which can limit the feasibility, but because the ET modulator can be implemented in CMOS, thus providing the possibility of a fully integrated CMOS PA, the CMOS evolution may entail that the ET technique becomes the best option [16]. The alternative is the Average Power Tracking (APT) technique, which adjusts the supply voltage and/or the bias voltage with a lower frequency, e.g. Transmission Time Interval (TTI) level, but the issue of this technique is that its efficiency is low for high Peak-to-Average-Power Ratio (PAPR) schemes where ET excels. The reason is that APT needs to adjust the supply voltage to support the highest peak over the current TTI while ET can adjust it in almost real time.

One main challenge for the transmitter, besides the increased bandwidth, is the increased Error Vector Magnitude (EVM) requirements, due to use of higher order modulation. The 3GPP defines EVM as [145, Annex F.2]

$$\text{EVM} = \sqrt{\frac{\sum_{v \in T_m} |z(v) - i(v)|^2}{|T_m| \cdot P_0}} \quad [-] \quad (5.19)$$

where: T_m is a set of the considered modulation symbols [s]
 z are the samples of the modulated signal [V]
 i are the samples of the ideal signal [V]
 P_0 is the average power of i [W]

i.e. EVM represents the impairment of the transmitted signal, and it is limited to 17.5% for Quadrature Phase-Shift Keying (QPSK) and 12.5% for 16 Quadrature Amplitude Modulation (16QAM) in LTE, [145]. There are multiple reasons for these impairments such as phase noise in the VCO, amplitude ripple in filters and non-linearities in the PA [59]. As the modulation order increases it is necessary to limit the EVM such that the receiver can distinguish and decode the individual symbols. Therefore the EVM requirements will increase for 5G due to the use of 256QAM. This may entail that

the PA has to increase the Output Back-Off (OBO), see figure 4.5 to improve linearity. However the 256QAM is only likely to be used in high SINR situations where the mobile terminal is close to the Access Point (AP) thus the transmit power will already be low and have sufficient high linearity.

Another main challenge for PA designers is the increased carrier frequency. One estimate, [146], says that the PA efficiency drops 3 percentage points when the carrier frequency is increased from 900 MHz to 1.8 GHz, but another 30 percent at 2.7 GHz. The issue of decreasing efficiency as a function of increasing carrier frequency is illustrated in figure 5.18, which is based on data from [147, 148, 149, 150]. The figure shows how the efficiency drops 40-50 percentage points when the carrier frequency exceeds 5-6 GHz. In [148, 149, 150] most of the work is based on CMOS implementations while [147] relies on a different transistor technology because it targets output powers of multiple Watts. However figure 1 of [148] illustrates that CMOS can achieve similar efficiency levels at the 0.5-3 GHz range. It is therefore estimated that the drop in efficiency is due to lack of interest in the 5-30 GHz spectrum because there have been limited business possibilities to drive the technology improvement. This is opposed to the Milimeter Waves (mmW) spectrum where a lot of work has already been done as illustrated in figure 5.18.

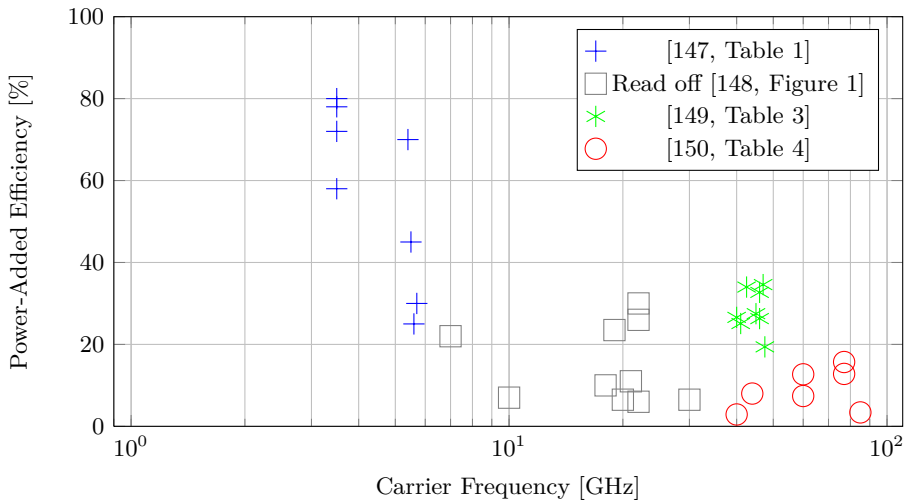


Figure 5.18: Power-Added Efficiency for selected PAs as a function of carrier frequency.

The Power-Added Efficiency, used in figure 5.18, is defined as

$$\eta_{PAE} = \frac{P_{RFout} - P_{RFin}}{P_{DC}} \quad [-] \quad (5.20)$$

where: η_{PAE} is the Power-Added Efficiency [-]
 P_{RFout} is the RF output power [W]
 P_{RFin} is the RF input power [W]
 P_{DC} is the supply power [W]

and assuming an input power of 10 dBm and an output power of 20 dBm the power consumption for efficiencies of 70 % and 20 % is

$$\eta_{\text{PAE}} = 0.7 = \frac{100 \text{ mW} - 10 \text{ mW}}{P_{\text{DC}}} \rightarrow P_{\text{DC}} = \frac{90 \text{ mW}}{0.7} \approx 130 \text{ mW} \quad (5.21)$$

$$\eta_{\text{PAE}} = 0.2 \rightarrow P_{\text{DC}} = \frac{90 \text{ mW}}{0.2} \approx 450 \text{ mW} \quad (5.22)$$

thus the overall battery life will be significantly harmed if the efficiency is not improved at the upper part of the cmW band and the mmW band in general. It is however expected that the 5G standardization will lead to profitable business in the area and therefore drive the development of new PA technology.

Due to the UDSC scenario the mobile terminal may be able to reduce its transmission power and still achieve sufficient receive power at the AP. Usually the PA is optimized to achieve peak efficiency at maximum transmit power, and thus if the PA is not re-configured the efficiency will be lower at the reduced transmit power. For example a single 23 dBm PA will consume less power than four 17 dBm PAs, also having a combined output power of 23 dBm, but by optimizing for 17 dBm transmission power the power consumption will in principle be the same. The main cost will then be the increased chip area and the power consumption overhead of the supporting circuits such as the control logic.

As mentioned in section 4.4 the guard period of the 5G frame is $0.87 \mu\text{s}$. This entails the mobile terminal must be able to switch from the transmitter branch to the receiver branch within this time, but according to [146] this is not an issue. The reason is that the switching time can easily be supported today for a 24 dBm transmit power signal with an insertion loss much smaller than 1 dB. Furthermore the switching time has a linear relation with the transmit power thus the lower transmit power of the UDSC will help reduce the switching time. A more severe issue related to the use of TDD and CA is that the many antenna switches and filters entail a high insertion loss. The filter loss is small when the band of interest and the interfering band are well separated in frequency, which e.g. is the case for a 900 MHz and a 2.5 GHz signal, but this will not be the case for e.g. a 28 GHz and 30 GHz signal. Thus it is important to analyse how coexistence of the many bands can be ensured without introducing severe insertion loss penalties between the PA and the antenna.

5.6 Summary

In this chapter the performance and power consumption evolution was examined for key components in the cellular subsystem. The 5G concept leads to significant challenges because the components must support an increased bandwidth of up to 400 MHz, increased data rate of up to 10 Gb/s, and increased number of CCs and MIMO streams.

The effect of these challenges on the LNA was examined by performing a literature survey of the evolution from 1990 to 2014. The survey showed that the LNA improves in terms of occupying half the physical area and consuming 7.5 mW in 2020, while other parameters such as gain, IP3, and NF are not improved. However it was concluded that LNAs can comply with the 5G requirements.

Next the evolution of ADCs was examined using an estimation of the Schreier FoM. The conclusion is that an ADC bandwidth of 100 or 200 MHz is possible with a minor increase in power consumption, but using a single 400 MHz ADC will entail a power consumption of ≈ 1.1 W. However to fulfil the 10 Gb/s data rate requirement it is estimated that 400 MHz bandwidth is needed and thus CA must be applied. This entails the number of receive chains increase and therefore also the number of ADCs. The use of a 200 MHz CCs is a good tradeoff between number of components and single ADC power consumption.

The evolution of CMOS transistor technology for low-power BB processing was also studied using the International Technology Roadmap for Semiconductors. The complexity of the processing will increase about 100 times as compared to LTE because the data rate increases from 100 Mb/s to 10 Gb/s, but if the laws proposed by Moore and Gene continue to be valid the complexity can be handled with about the same power consumption 10 years from now, but not as early as 2020.

Using the estimates described above the power consumption of a 5G receiver was estimated for 2020 and 2030. In 2020 the receiver will be dominated by the BB processing complexity, and to a smaller extent by the ADCs, and is estimated to consume more than 3.5 W. This poses a significant challenge for the chipset designers which must be addressed in the coming years. In 2025 the power consumption is however estimated to be on par with current LTE implementations. The long term estimate for 2030 show that the receiver at this time may consume as little as 100 mW. In addition to the challenges with power consumption the use of 4x4 MIMO and CA will entail the chip area and cost increases significantly, and it may give rise to coexistence issues when using multiple frequency bands.

To conclude the chapter the evolution of the key power consumer in current LTE implementations: the transmit PA was examined. In recent LTE UEs the use of efficient supply techniques such as ET has emerged and they are expected to be applied in 5G as well. This is especially important for the proposed concept because the use of OFDM entails larger PAPR and thus high power consumption, but this can be mitigated by the use of techniques such as ET. Another issue for current PAs is that the carrier frequency will be increased to above 5 GHz in the cmW concept. This is an area where little effort has been made to improve the efficiency, which was observed to be 30% or less as compared to being above 70% for many PAs employed below 3 GHz today. It is however expected that the emergence of a new market and a profitable business case will lead to the development of new PA technologies that support the high carrier frequencies with sufficient efficiency.

The overall conclusion is thus that the 5G concept results in some significant challenges for the hardware manufacturers including the increased processing complexity, chip area, ADC power consumption, coexistence when using multiple CCs, and support for high carrier frequencies.

Changing and new user scenarios with different traffic profiles impose further challenges to securing the desired long battery life. In the next chapter video streaming and Machine Type Communication (MTC) scenarios are presented to discuss how 5G may include methods for both period and aperiodic low-power sleep. The chapter presents

an evaluation of the battery life in the 5G concept when using Discontinuous Reception (DRX), which is a key method for fulfilling the always ON requirement, an a new concept for event based pre-paging which can handle aperiodic traffic.

Chapter 6

DRX and Aperiodic Sleep Modes in 5G

In 2020 there will be new and changed user scenarios which require a new Radio Access Technology (RAT) generation. In this section video streaming and Machine Type Communication (MTC) user scenarios are analysed with focus on how they are affected by and will affect the design of Fifth Generation (5G) sleep modes, and how they will impact mobile terminal battery life.

These two scenarios are selected because they are expected to be dominant in 2020 either in terms of traffic volume or number of connected mobile terminals. Video streaming results in a periodic traffic pattern, which is well suited for combination with Discontinuous Reception (DRX) sleep mode as implemented in the previous RAT generations, but besides the brief analysis in our contribution [35], it has not been examined how DRX can be applied in 5G. In this chapter simulations are therefore performed for DRX, and also Discontinuous Transmission (DTX), and compared with Time Division Duplexing (TDD) Long Term Evolution (LTE) using a battery model.

The MTC traffic is very diverse, and while some applications may have periodic traffic patterns that fit DRX others may be aperiodic. Therefore a concept is proposed to target the short comings of DRX when the traffic is aperiodic. The concept is not complete and ready for implementation and does not contain exact evaluations of the potential energy savings, but it is included here to provide input to an area where 5G needs to be optimized to separate itself from the previous RATs, especially LTE. Note that another new 5G concept targeting MTC and Device-to-Device (D2D) is described in appendix D.

6.1 Examples of 5G User Scenarios

In this section the video streaming and MTC user scenarios are examined with focus on how they evolve towards 2020 and whether they can be supported in 5G.

For further information on expected 5G user scenarios the Metis project [93] has made an extensive study in Work Package 1 and presented them in [151].

6.1.1 Video Streaming

The video streaming user scenario cannot be neglected because since 2012 it has accounted for more than half of the total mobile data consumption according to Cisco, [7], and for example the International Wireless Industry Consortium identified it as the key driving force for 5G [92].

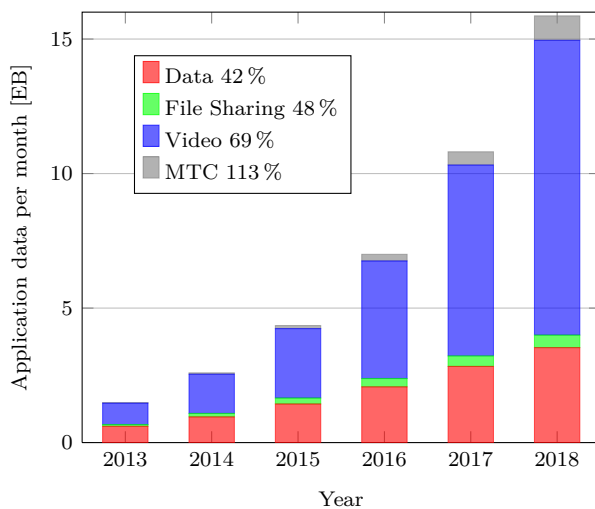
Given a year-over-year growth rate of 69% between 2013 and 2018 it will constitute 69% of the traffic in 2018 [7]. This is only surpassed by the MTC traffic which will increase with 113% as discussed later in this chapter. The mobile data traffic distribution is illustrated in figure 6.1a as a function of application type and it shows that even though the growth rate of MTC is higher than video the total amount of data is much smaller. On a side-note figure 6.1b shows the same data forecast but divided by device type instead and it underlines the necessity for improving the smartphone Energy Efficiency (EE) which constitute two thirds of the data usage.

One reason for video's large share is the emergence of social video sharing sites such as YouTube and the popularity of video-on-demand services like Netflix and HBO. The major reason is however video's high data rate, which is shifting from Standard Definition (2 Mbps) accounting for 43% of all IP traffic in 2013 and only 7% in 2018 via High Definition (7.2 Mbps) towards Ultra High Definition (18 Mbps) which will increase from 0.2% towards 22% in 2018 [152]. Given the low number of expected mobile terminals per Access Point (AP) and the videos' relative low data rate, even if it increases to 8K definition, it is not an issue for the 5G concept's capacity. Another new technology, which may add to the video streamed data is the trend of moving processing capabilities to the cloud such that local devices act as windows towards the processed data in the cloud [92].

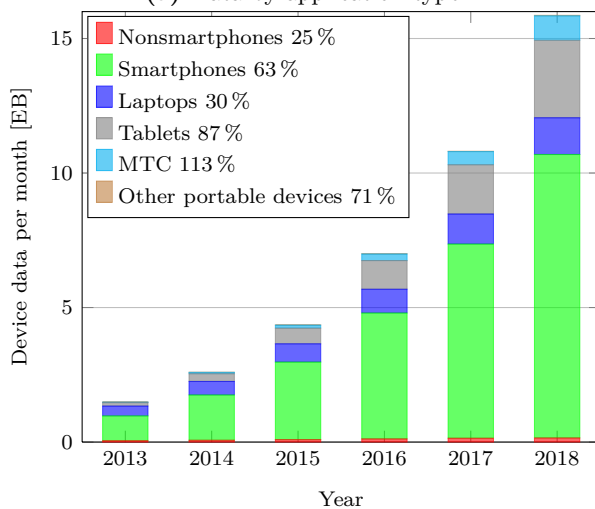
Usually video is streamed from the internet using the Transmission Control Protocol (TCP) where various techniques can be applied that have a major influence on the RAT design and mobile terminal EE. In [153] the authors examined streaming traces from YouTube and Netflix and identified 3 distinct techniques illustrated in figure 6.2. In the simplest case the receiver will download the entire video as fast as possible i.e. utilizing the full bandwidth of the current TCP window as if a normal file transfer was ongoing. This entails the mobile terminal needs to have large buffer memory and if the user decides to quit watching the video before it is finished data has been wasted. Furthermore it may prevent the streaming server from providing parallel streams to the connected users.

The two other techniques will also utilize the maximum bandwidth in the beginning, known as the buffering phase, but when sufficient video data has been downloaded and the playback can commence a periodic behaviour is observed consisting of ON periods, where data is downloaded at maximum rate, and OFF periods where the data connection is inactive. The target of this steady state phase is to have an average download rate, which is a little larger than the video rate. By doing this the need for mobile terminal buffer memory is smaller and the streaming server can handle more users.

From RAT design perspective the bulk transfer is simple to handle because the mobile terminal will be connected for a certain amount of time after which it can enter sleep mode or disconnect. One issue is that the streaming mobile terminal will consume a large amount of channel capacity during the video download. However with



(a) Data by application type.



(b) Data by device type.

Figure 6.1: Mobile data traffic forecast in Exabytes ($=10^9$ GB), based on [7, Table 6]. The values in percent indicate the year-by-year growth rate.

the 5G concept where there are few mobile terminals per AP in the Ultra-Dense Small Cell (UDSC) scenario and large available bandwidth this may not be problematic. Furthermore larger TCP packets are expected in the 5G concept and therefore larger data chunks can be transferred with the same overhead.

The use of the ON-OFF techniques will require less bandwidth on average but occupy the system for longer, possibly consuming limited control channel space for the many downlink grants. If the Long ON-OFF method is used the mobile terminal may apply

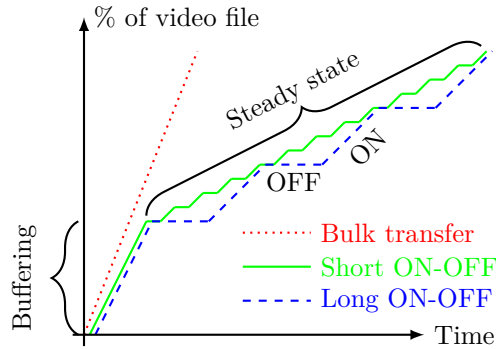


Figure 6.2: Video stream phases, based on [153, Figure 1].

DRX to save power and therefore not occupy system bandwidth. But DRX makes the scheduling decisions more complicated because the AP will need to allocate data for the mobile terminal, using DRX, in specific time instants and thereby limit the degrees of freedom in the scheduler. The TCP usually applies timed Acknowledgements (ACKs) to determine the available bandwidth and if no ACK is received within a certain time window the packet size may be reduced. If the OFF window is long this could be expected to happen, causing the next ON period to start with a low data rate, but [153] observed that the timed ACK was not used on YouTube. That may cause problems for the 5G concept's fast varying channel conditions because a smaller packet may be needed in certain interference limited situations. The clocked ACK was however used for Netflix streams to Android devices proving that the video streaming services do not agree how to configure the TCP stream, and thus 5G must be flexible.

From a power consumption perspective the bulk transfer is the most energy efficient given that a 5G mobile terminal's performance is similar to 4G. The reason is that the transfer can be completed fast after which the mobile terminal can enter an energy saving sleep mode. In section 2.5 it was also shown that the EE increases with data rate and this further improves the advantage of bulk transfer. In principle the ON-OFF techniques will have the same active time as the bulk transfer if they can achieve the maximum data rate instantaneously at the beginning of each ON period, but the many OFF periods, which are either used in connected mode, but unscheduled, consuming high power listening for grants or DRX mode where a lot of power-up and -down phases (see section 2.3) will occur, causes excessive power consumption. However the ON-OFF techniques are the preferred choice, because the waste of channel capacity and energy is a big issue for the bulk transfer when a user quits watching video prematurely. The study in [153] was based on both desktop browser streaming and using iOS and Android devices, and it was noted that the mobile devices never used the bulk transfer method probably due to the aforementioned issues and the need for more buffer memory.

To summarize the proposed 5G concept can handle the increase in video streaming traffic both in terms of system capacity and data rate, but it is important to ensure 5G provides an energy efficient DRX scheme.

6.1.2 Machine Type Communications

According to Cisco the Machine Type Communication (MTC) segment have the fastest growing number of connections of all consumer mobile devices from 2013 to 2018 increasing from 211 million to 1.5 billion [154] with a year-by-year growth of 49%. The market share will be 17.3% only surpassed by non-smartphones at 36.0% and smartphones at 39.1%. The Groupe Speciale Mobile Association has published a similar estimate and expects the number of cellular MTC devices to be 2.3 billion by 2020 [155]. Therefore the MTC, also known as Machine-to-Machine, must be included in the 5G concept.

Another reason is that current RATs were initially not designed to handle the diverse type of mobile terminals and traffic, which constitute MTC where the size of each data package typically is quite small but the expected number of devices is much larger. This is also evident in the Third Generation Partnership Project (3GPP) study item [156] where it is discussed how LTE may be changed to allow for low-cost and low-power MTC devices for example by reducing the bandwidth and lowering transmit power and data rate. Besides 3GPP's effort on MTC standardization the oneM2M partnership project has been launched [157] and released a set of initial MTC specifications in August 2014. oneM2M consist of the standardization organizations ARIB, ATIS, CCSA, ETSI, TTA, and TTC and industrial partners which in total amounts to 220 members.

An example of where MTC is already being applied is in the European Union. The European Commission has proposed that "eCall", which is a service that automatically calls the emergency line in case of accidents, is to be installed in new cars from end 2017 [158]. The emergency vehicle response time is estimated to be reduced by 40-50% and several hundred less deaths are expected in the EU per year.

A general definition of MTC is that it is autonomous communication between mobile terminals which is neither user controlled nor user initiated. The list of possible MTC devices is already long, but it may be even longer and more diverse when 5G is launched. The following is a non-exhaustive list of possible MTC devices:

- Electric power meters and other household meters sending data to the smart grid and service providers
- Satellite navigation devices for in-car usage receiving traffic updates
- Devices for home, office, and industry security and automation i.e. controlling lights, temperature, contents of the fridge/storage and who has entered/excited the premises
- Automated machinery in industry, for example robots and conveyor belts
- Remote monitoring of patients not staying at the hospital/health care unit
- Wearables such as smart watches, fitness trackers and personal navigation units
- Device-to-Device (D2D) communication such as Vehicle-to-Vehicle (V2V) for traffic safety e.g. by use of autonomous driving and carpooling
- Monitoring of chipped farm animals and pets

In total these devices will constitute what is known as the Internet of Everything (or Things) and also support the new business area, which is known as Big Data. Here the target is to collect large amounts of data about users and their actions and analyze it by data mining and machine learning to support marketing and sales of products [159].

Examining the list it is clear that the requirements the devices impose on the RAT is very diverse. For example the electric power meters require long range transmissions to send the meter reading to the provider while the wearable devices communicate over a much shorter range. In addition the wearable device must be low power to support small physical dimensions and therefore also low complexity, while the power meter may be connected to the power outlet. Besides the diversity in terms of coverage and power consumption the robustness and data rate of the transmission is also very different between automated machinery in the industry and vehicle-to-vehicle communication, which both require reliable and fast connections, and home appliances and wearables, which do not impose strong requirements in this area. The challenge is therefore to support these diverse requirements, but also to avoid congestion, and ensure security and privacy is protected [159]. In addition the requirement for high reliability and low latency will require significant investments in network infrastructure, and thus the 5G concept must provide not only a technical solution, but also be commercially feasible to be successful.

One common parameter is that the data is expected to come in small and possibly periodic bursts. Due to the periodic nature, for example caused by request for updates from central servers towards sensors, the MTC devices are expected to use low-power DRX sleep modes in between transmissions. If a large number of devices are utilizing periodic sleep it complicates the scheduling procedure because the freedom to allocate resources is limited by the predetermined ON time of the sleeping devices. Another implication of the periodic sleep method is that the delay in contacting such a device increases with the length of the sleep period because the device will not be listening for downlink transmissions. The limited scheduling opportunities and the delay issue is illustrated in figure 6.3. Note that this is only an issue for paging in downlink whereas the

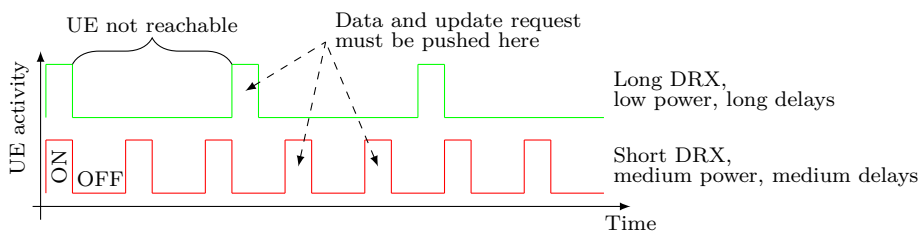


Figure 6.3: Limited scheduling opportunities and delays due to DRX.

mobile terminal can always rely on the uplink Random Access to initiate a data transfer.

To summarize this section the future user scenarios of 5G will rely on an efficient DRX sleep mode. The target is to reduce the energy consumption by allowing the mobile terminal to sleep most of the time while periodically listening for paging messages. Using this principle the mobile terminal is periodically available to the network, but it

is also able to achieve lower energy consumption as compared to continuously listening for paging messages each Transmission Time Interval (TTI). In the following section a simulation based comparison of DRX in 5G and TDD LTE is presented to determine if the new RAT design provides battery life improvements.

As described above some types of MTC traffic may not be paged periodically, but only when certain events are triggered by a user or the network. If the periodic DRX mode is applied to this type of traffic it will lead to either long delays or increased energy consumption due to too long or short DRX periods respectively. Therefore a new event based pre-paging concept, which accommodates aperiodic traffic, is presented in section 6.3 to avoid some of the DRX drawbacks.

6.2 DRX in 5G

The efficiency and applicability of DRX, and also DTX, depend on how fast the mobile terminal can change mode and the level of low-power sleep it can achieve as discussed in section 4.6. Another important parameter is the time it takes the mobile terminal to request resources, upload the data, and await the ACK, in case of an uplink transmission, or to decode the scheduling information and downlink data and then transmit the ACK in case of downlink. Because of the shorter frame structure and the fewer Hybrid Automatic Repeat Request (HARQ) periods this can be completed significantly faster in the 5G concept as compared to LTE.

In this section the battery life is calculated and compared for a mobile terminal using DRX and DTX in the proposed 5G concept and TDD LTE. A key assumption is that the amount of data is small such that the mobile terminal only requires one subframe to transfer the data, and that the transfer and the ACK are always successful received. It is furthermore assumed that the power consumption and the time it takes to power ON/OFF is the same for both devices, similar to [35]. The power consumption model parameters are given in table 6.1. The model is based on the predictions in [160] which cover a MTC device in 2020, and modified as in [35]. The battery capacity is set accordingly to [35].

Table 6.1: Power consumption parameters for MTC mobile terminal in 2020, based on [35, 160]

Description	Parameter	Value
Transmit power consumption	P_{tx}	550 mW
Receive power consumption	P_{rx}	100 mW
Clock power consumption	P_{clk}	10 mW
Sleep power consumption	P_{sleep}	0.015 mW
Time to power ON/OFF	t_{trx}	20 μ s
Battery capacity (3 V and 3 Ah)	E_{bat}	32.4 kJ

The clock is assumed to be ON during the entire active period, while the t_{trx} parameter describes the additional time it takes to power ON the receiver and the transmitter. This value is much lower than what was measured in LTE, see section 2.5.1, but due to

the lower power consumption and the optimized MTC hardware design the authors of [160] estimate it to be feasible.

To simplify the simulations the transition energy consumption is calculated as:

$$E_{\text{clk-Tx}} = (P_{\text{tx}} - P_{\text{clk}}) \cdot t_{\text{trx}}/2 = 5.4 \mu\text{J} \quad (6.1)$$

$$E_{\text{clk-Rx}} = (P_{\text{rx}} - P_{\text{clk}}) \cdot t_{\text{trx}}/2 = 0.9 \mu\text{J} \quad (6.2)$$

where: $E_{\text{clk-Tx}}$ is the energy consumed when powering on the transmitter [J]
 $E_{\text{clk-Rx}}$ is the energy consumed when powering on the receiver [J]

The procedures for transmitting and receiving data in 5G were presented in section 4.4, and they are repeated here to determine the total ON time, and the individual ON time of the transmitter and the receiver. The procedure for transmitting data is illustrated in figure 6.4, and the starting point is that the mobile terminal powers ON its receiver to synchronize with the AP and also to estimate the current level of interference. In the next frame it sends a scheduling request and then awaits the grant. In the following frame it will receive a grant for the requested amount of resources, provided they are available. It will then proceed to prepare the data for transmission, perform the actual data transmission and finally receive the ACK from the AP. The

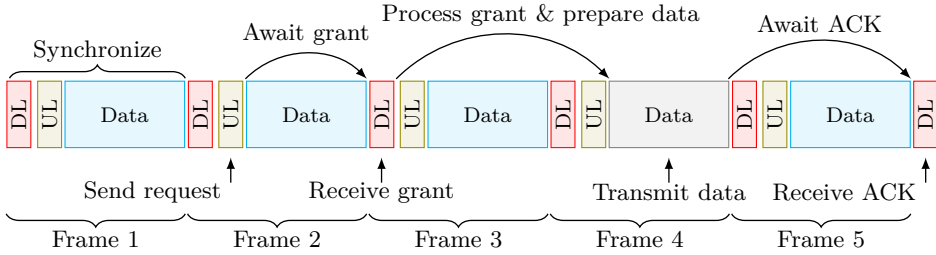


Figure 6.4: Procedure for transmitting data in uplink including synchronization.

total ON time is thus:

$$\begin{aligned} t_{\text{tx5G}} &= t_{\text{sync5G}} + 4 \cdot t_{\text{frame5G}} + t_{\text{symp}} + 2 \cdot t_{\text{trx}} \quad [\text{s}] \\ &= 0.25 \text{ ms} + 4 \cdot 0.25 \text{ ms} + 17.67 \mu\text{s} + 2 \cdot 20 \mu\text{s} = 1.30767 \text{ ms} \quad (6.3) \end{aligned}$$

where: t_{tx5G} is total ON time for a 5G transmission [s]
 t_{sync5G} is the time to synchronize, equal to one frame [s]
 t_{frame5G} is the frame duration [s]
 t_{symp5G} is the symbol duration [s]

The energy consumption for a transmission in 5G, where the data is fitted into one

frame and successfully received and acknowledged is thus:

$$\begin{aligned}
 E_{tx5G} &= t_{sync5G} \cdot P_{rx} + t_{syimb5G} \cdot P_{tx} + 2 \cdot t_{syimb5G} \cdot P_{rx} + t_{data5G} \cdot P_{tx} + \\
 &\quad 4 \cdot E_{clk-Tx} + 6 \cdot E_{clk-Tx} + t_{tx5G} \cdot P_{clk} \quad [J] \\
 &= 0.25 \text{ ms} \cdot 100 \text{ mW} + 17.67 \mu\text{s} \cdot 550 \text{ mW} + 2 \cdot 17.67 \mu\text{s} \cdot 100 \text{ mW} + \\
 &\quad 0.25 \text{ ms} \cdot 550 \text{ mW} + 4 \cdot 5.4 \mu\text{J} + 6 \cdot 0.9 \mu\text{J} + 1.30767 \text{ ms} \cdot 10 \text{ mW} \\
 &= 195.0 \mu\text{J} \quad (6.4)
 \end{aligned}$$

Similar calculations can be made for receiving data in the downlink, which follows the procedure illustrated in figure 6.5. First the mobile terminal will synchronize and estimate the channel and interference after which it will receive a grant in the downlink control channel. According to system design the data will follow in the next frame and then the mobile terminal has one frame duration to decode and generate the ACK. The

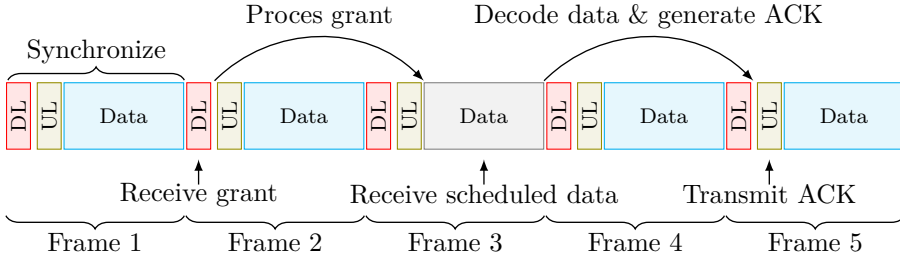


Figure 6.5: Procedure for receiving data in downlink including synchronization.

total ON time t_{rx5G} for a 5G reception is:

$$\begin{aligned}
 t_{rx5G} &= t_{sync5G} + 3 \cdot t_{frame5G} + 2 \cdot t_{syimb5G} + 2 \cdot t_{trx} \quad [s] \\
 &= 0.25 \text{ ms} + 3 \cdot 0.25 \text{ ms} + 2 \cdot 17.67 \mu\text{s} + 2 \cdot 20 \mu\text{s} = 1.07534 \text{ ms} \quad (6.5)
 \end{aligned}$$

and the energy consumption is:

$$\begin{aligned}
 E_{rx5G} &= t_{sync5G} \cdot P_{rx} + t_{syimb5G} \cdot P_{rx} + t_{data5G} \cdot P_{rx} + t_{syimb5G} \cdot P_{tx} + \\
 &\quad 2 \cdot E_{clk-Tx} + 4 \cdot E_{clk-Tx} + t_{rx5G} \cdot P_{clk} \quad [J] \\
 &= 0.25 \text{ ms} \cdot 100 \text{ mW} + 17.67 \mu\text{s} \cdot 100 \text{ mW} + 0.25 \text{ ms} \cdot 100 \text{ mW} + \\
 &\quad 17.67 \mu\text{s} \cdot 550 \text{ mW} + 2 \cdot 5.4 \mu\text{J} + 4 \cdot 0.9 \mu\text{J} + 1.07534 \text{ ms} \cdot 10 \text{ mW} \\
 &= 82.8 \mu\text{J} \quad (6.6)
 \end{aligned}$$

As mentioned in the introduction to this section 5G is to be compared with TDD LTE. This version of LTE differs significantly from the Frequency Division Duplexing (FDD) version because it has multiple different frame structures, which can be adapted to current traffic needs. The overall structure of a 10 ms subframe, composed of 10 subframes each 1 ms long, is still employed, but the link direction of each subframe can be varied according to the 7 configurations listed in table 6.2.

The downlink and uplink subframes contain the same channels as in FDD LTE, thus they can be used for requests and to transfer data. Because the same frequency resources

Table 6.2: Frame configuration for TDD LTE, [71, Table 4.2-2]. A downlink subframe is denoted by D, an uplink subframe by U, and the special subframe by S.

Configuration	Switching periodicity	Subframe number									
		0	1	2	3	4	5	6	7	8	9
0	5 ms	D	S	U	U	U	D	S	U	U	U
1	5 ms	D	S	U	U	D	D	S	U	U	D
2	5 ms	D	S	U	D	D	D	S	U	D	D
3	10 ms	D	S	U	U	U	D	D	D	D	D
4	10 ms	D	S	U	U	D	D	D	D	D	D
5	10 ms	D	S	U	D	D	D	D	D	D	D
6	5 ms	D	S	U	U	U	D	S	U	U	D

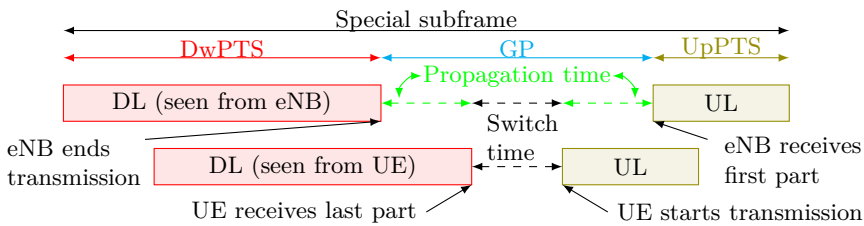


Figure 6.6: The special subframe of TDD LTE, [71].

are used for both downlink and uplink data the special subframe is introduced. The structure of this frame is illustrated in figure 6.6. The first part of the special subframe is called Downlink Pilot Timeslot (DwPTS), and it is similar to a normal subframe i.e. it has reference and control signals followed by data. The next part is the Guard Period (GP), which is implemented to ensure the propagation time of the radio channel can be handled without selfinterference in the User Equipment (UE). The GP also includes a pre-defined amount of time the UE can use to switch link direction i.e. power OFF the receiver and power ON the transmitter. The final part of the special subframe is the Uplink Pilot Timeslot (UpPTS). This part has no Physical Uplink Control Channel (PUCCH), but it includes the Sounding Reference Signals, which the Evolved Node B (eNB) can use to perform channel estimation, and the Random Access Channel, which is used by the UE to request resources in uplink for data transmission. To cope with the traffic load and propagation times the length of each of the 3 parts can be varied. Because the DwPTS contains both normal control and data channels the minimum length is 3 symbols, while the maximum is 12. The GP can be varied between 1 and 10 symbols while the UpPTS can be 1 or 2 symbols [71, 161].

The procedure for performing a transmission or a reception in TDD LTE is similar to the one in 5G, but due to the 7 frame configurations, listed in table 6.2 and the special subframe’s ability to carry downlink scheduling and data, but only uplink requests, there are many possible combinations in which the UE can perform the transfer. This

also affects the delay of a transfer and thus it has to be included when calculating the DTX and DRX performance.

Figure 6.7 illustrates frame configuration 0, which has a switching periodicity of 5 ms due to the special subframe located in subframe 1 and 6. There are multiple ways

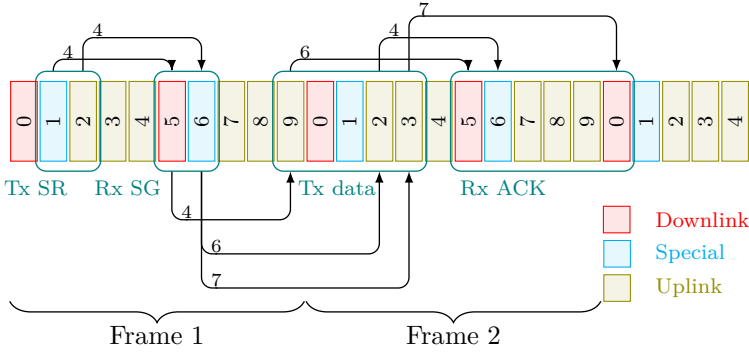


Figure 6.7: Procedure for uplink transmission in TDD LTE using frame configuration 0.

the UE can perform an uplink transmission using this frame configuration, and the starting point is that it has to transmit a scheduling request, denoted SR in figure 6.7, to obtain resources from the eNB. This is done using either the Random Access Channel of the UpPTS or the PUCCH of a normal uplink subframe, thus the first possibilities are subframes 1 and 2. If the UE decides to use subframe 3 or 4 instead the delays will increase. The maximum allowed processing time for both the eNB and UE is defined to be 3 ms i.e. 3 subframes, and therefore the UE can expect a scheduling grant, denoted SG in figure 6.7, in the first downlink or special subframe 3 ms after the transmission has occurred. This will thus be subframe 5 and 6 depending on whether the UE used subframe 1 or 2 as illustrated in figure 6.7. Assuming resources were granted the UE has another 3 ms for processing the data to be transmitted, hence it can commence transmission in subframe 9 or in subframe 2 of the following frame. The use of subframe 3 in frame 2 is also illustrated to indicate how delays in an individual procedure may increase the overall delay significantly. As mentioned earlier it is assumed that the data transfer is completed within one subframe and successfully received and decoded and thus the UE can receive an ACK in subframe 5 or 6 of frame 2 or even in subframe 0 of frame 3. The total number of subframes expired from the transmission of the scheduling request and until the reception of the ACK is $1 + 4 + 4 + 6 = 15$ to $1 + 4 + 7 + 7 = 19$, counted using the numbers on the process arrows of figure 6.7. This analysis has also been performed for the other frame configurations and the results are given in table 6.3. The minimum number of subframes required to perform an uplink transmission is 13 while the maximum is 19. In addition it is assumed that the UE has to power ON the receiver 5 subframes in advance to achieve proper synchronization and channel estimates.

Table 6.3: Total number of subframes required to perform uplink transmission in TDD LTE.

Configuration	Starting subframe number										Minimum	Maximum
	0	1	2	3	4	5	6	7	8	9		
0	-	15	15	18	18	-	15	15	18	18	15	18
1	-	16	15	17	-	-	16	15	17	-	15	17
2	-	16	15	-	-	-	16	15	-	-	15	16
3	-	16	15	14	13	-	-	-	-	-	13	16
4	-	16	15	14	-	-	-	-	-	-	14	16
5	-	16	15	-	-	-	-	-	-	-	15	16
6	-	16	15	17	16	-	-	15	19	-	15	19

The total ON time for a TDD LTE transmission is:

$$\begin{aligned}
 t_{\text{txLTE}} &= t_{\text{syncLTE}} + [13; 19] \cdot t_{\text{frameLTE}} + 2 \cdot t_{\text{trx}} & [\text{s}] \\
 &= 5 \text{ ms} + [13; 19] \cdot 1 \text{ ms} + 2 \cdot 20 \mu\text{s} = [18.04 \text{ ms}; 24.04 \text{ ms}] & (6.7)
 \end{aligned}$$

where: t_{txLTE} is total ON time for a TDD LTE transmission [s]
 t_{syncLTE} is the time to synchronize, equal to 5 frames [s]
 t_{frameLTE} is the frame duration [s]

As illustrated in figure 6.7 the UE will power ON its transmitter twice, to transmit the scheduling request and the data, and its receiver three times, to receive the synchronization and channel estimate signals, the scheduling grant and the ACK. Therefore the total energy consumption for a TDD LTE transmission is:

$$\begin{aligned}
 E_{\text{txLTE}} &= t_{\text{syncLTE}} \cdot P_{\text{rx}} + 2 \cdot t_{\text{frameLTE}} \cdot P_{\text{tx}} + 2 \cdot t_{\text{frameLTE}} \cdot P_{\text{rx}} + \\
 &\quad 4 \cdot E_{\text{clk-Tx}} + 6 \cdot E_{\text{clk-Rx}} + t_{\text{txLTE}} \cdot P_{\text{clk}} & [\text{J}] \\
 &= 5 \text{ ms} \cdot 100 \text{ mW} + 2 \cdot 1 \text{ ms} \cdot 550 \text{ mW} + 2 \cdot 1 \text{ ms} \cdot 100 \text{ mW} + \\
 &\quad 4 \cdot 5.4 \mu\text{J} + 6 \cdot 0.9 \mu\text{J} + [18.04 \text{ ms}; 24.04 \text{ ms}] \cdot 10 \text{ mW} \\
 &= [2007.4 \mu\text{J}; 2067.4 \mu\text{J}] & (6.8)
 \end{aligned}$$

The estimated energy consumption of TDD LTE is approximately 10 times higher than the energy consumption estimated in equation (6.4) for 5G. The reasons are the shorter and optimized frames of 5G.

The procedure for a downlink transmission in frame configuration 0 is illustrated in figure 6.8. Because the Physical Downlink Control Channel (PDCCH) is followed immediately by data in the Physical Downlink Shared Channel (PDSCH) the UE will receive the scheduling information and data in either subframe 0 or 1. After a successful decoding it can then transmit the ACK in subframe 4 or 7 thus the total number of subframes is either 5 or 7 for this frame configuration.

Performing the same analysis for the other frame configurations yields the results given in table 6.4 for performing a downlink reception. The minimum 5 subframes is

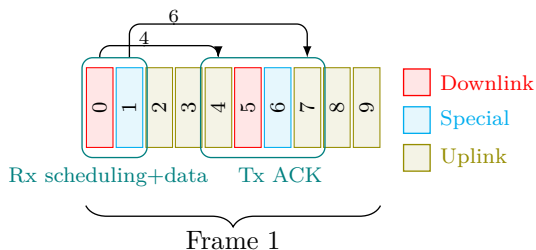


Figure 6.8: Procedure for downlink reception in TDD LTE using frame configuration 0. The number at each of the process arrows indicate the number of subframes between the two events.

possible with all frame configurations, while the maximum 14 subframes is observed for configuration 5, which only has one uplink subframe, see table 6.2.

Table 6.4: Total number of subframes required to perform downlink reception in TDD LTE.

Configuration	Starting subframe number									Minimum	Maximum	
	0	1	2	3	4	5	6	7	8			9
0	5	7	-	-	-	5	7	-	-	-	5	7
1	8	7	-	-	5	8	7	-	-	5	5	8
2	8	7	-	5	9	8	7	-	5	9	5	9
3	5	12	-	-	-	8	7	6	5	5	5	12
4	13	12	-	-	9	8	7	6	5	5	5	13
5	13	12	-	10	9	8	7	6	5	14	5	14
6	5	7	-	-	-	8	7	-	-	5	5	8

Using the estimated number of subframes of table 6.4 the total ON time for a TDD LTE reception is:

$$\begin{aligned}
 t_{rxLTE} &= t_{syncLTE} + [5; 14] \cdot t_{frameLTE} + 2 \cdot t_{trx} & [s] \\
 &= 5 \text{ ms} + [5; 14] \cdot 1 \text{ ms} + 2 \cdot 20 \mu\text{s} = [10.04 \text{ ms}; 19.04 \text{ ms}] & (6.9)
 \end{aligned}$$

where: t_{rxLTE} is total ON time for a TDD LTE reception [s]

During a reception the UE will power ON its transmitter once to send the ACK and its receiver twice to receive the synchronization and channel estimate signals, and the data. Since the data is expected to be scheduled periodically the UE will know when to power ON and thus it can receive the synchronization and channel estimate signals just before the data to reduce the number of receiver power ON sequences to one. Therefore

the total energy consumption is:

$$\begin{aligned}
 E_{\text{rxLTE}} &= t_{\text{syncLTE}} \cdot P_{\text{rx}} + t_{\text{frameLTE}} \cdot P_{\text{tx}} + t_{\text{frameLTE}} \cdot P_{\text{rx}} + \\
 &\quad 2 \cdot E_{\text{clk-Tx}} + 2 \cdot E_{\text{clk-Rx}} + t_{\text{rxLTE}} \cdot P_{\text{clk}} \quad [\text{J}] \\
 &= 5 \text{ ms} \cdot 100 \text{ mW} + 1 \text{ ms} \cdot 550 \text{ mW} + 1 \text{ ms} \cdot 100 \text{ mW} + \\
 &\quad 2 \cdot 5.4 \mu\text{J} + 2 \cdot 0.9 \mu\text{J} + [10.04 \text{ ms}; 19.04 \text{ ms}] \cdot 10 \text{ mW} \\
 &= [1263.0 \mu\text{J}; 1353.0 \mu\text{J}] \quad (6.10)
 \end{aligned}$$

This result shows that the receiving part of TDD LTE consumes approximately 15 times the energy of 5G, and similar to the transmission the reasons are the shorter and more optimized frame structure of 5G.

Now that the time and energy consumption has been defined for TDD LTE and 5G the battery life can be calculated for various combinations of receive and transmit activity factors. For low activity factors the battery life of the 32.4 kJ battery, table 6.1 and [35], may become very long i.e. $\gg 10$ years and thus it is necessary to model the self discharge of the battery. According to [162] a Lithium Ion battery will self discharge 5% the first 24 hours after it has been fully charged and then about 2% per month. The remaining energy level of the battery as a function of time is illustrated with a blue line in figure 6.9. The red dashed line illustrates the consumed energy for a scenario where

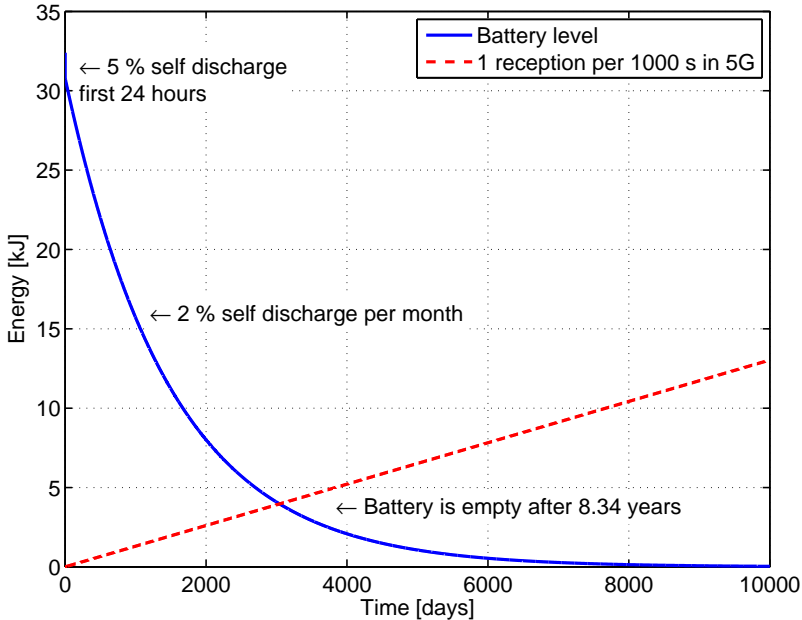


Figure 6.9: Battery model.

the 5G mobile terminal has 1 reception per 1000 s. This entails an energy consumption

per 1000 s of:

$$\begin{aligned} E_{\text{rx5G}}(t_p) &= E_{\text{rx5G}} + (t_p - t_{\text{rx5G}}) \cdot P_{\text{sleep}} & [\text{J}] \\ &= 82.8 \mu\text{J} + (1000 \text{ s} - 1.075 \text{ ms}) \cdot 15 \mu\text{W} = 15.08 \text{ mJ} & (6.11) \end{aligned}$$

where: $E_{\text{rx5G}}(t_p)$ is the receive energy consumption as a function of time period [J]
 t_p is the time period [s]

The battery life can be determined by finding the intersection of the remaining battery energy, due to self discharge defined as:

$$E_{\text{batLevel}}(t) = E_{\text{bat}} \cdot \alpha^t \quad [\text{J}] \quad (6.12)$$

where: $E_{\text{batLevel}}(t)$ is the remaining battery energy [J]
 t is the time expired [s]
 α is the discharge factor [-]

and the consumed energy:

$$E_{\text{cons}}(t) = E_{\text{rx5G}}(t_p) \cdot \frac{t}{t_p} \quad [\text{J}] \quad (6.13)$$

where: $E_{\text{cons}}(t)$ is the consumed energy [J]

Thus the battery will be empty when:

$$\begin{aligned} E_{\text{batLevel}}(t) &= E_{\text{cons}}(t) & [\text{J}] \\ E_{\text{bat}} \cdot \alpha^t &= E_{\text{rx5G}}(t_p) \cdot \frac{t}{t_p} & [\text{J}] \end{aligned} \quad (6.14)$$

It is not trivial to find the intersection between an exponential and a linear function i.e. $\alpha^t = \beta \cdot t$ by hand, and therefore the iterative bisection method is applied [163]. The method requires the function is rewritten and that it is continuous:

$$f(t) = \alpha^t - \beta \cdot t = 0 \quad [-] \quad (6.15)$$

First two starting points a, b are selected such that $f(a) \cdot f(b) < 0$. A midpoint $m = (a + b) / 2$ is then calculated and it is evaluated whether $f(a) \cdot f(m) \leq 0$. If this is the case the next iteration will use $m = b$ and otherwise $m = a$. The iterations continue until m is below a certain threshold, which was set to half an hour in the battery model. Using the bisection method the battery life was calculated to be 8.34 years as illustrated in figure 6.9. This is a very long battery life, which is close to the 5G requirement of 10 years, and the reason is the long period t_p that entails the mobile terminal is sleeping most of the time.

Figure 6.10 shows the battery life as a function of the number of receptions per second for 5G and LTE. The aforementioned calculation with one reception per 1000 s,

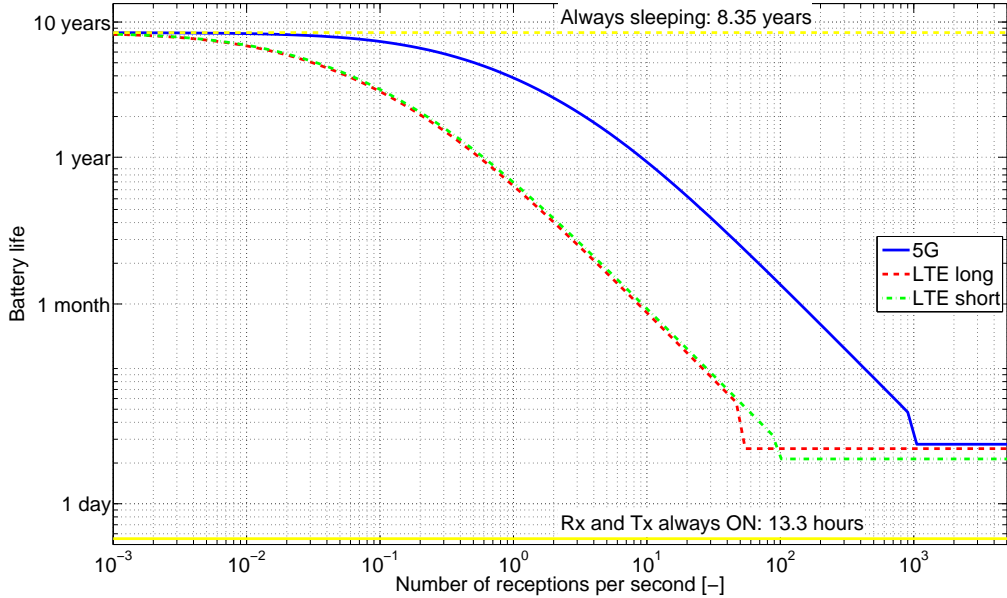


Figure 6.10: Battery life as a function of number of receptions per second for LTE and 5G.

i.e. 0.001 reception per second, is close to the point where the mobile terminal is always sleeping resulting in about 8.35 years of battery life, but as the number of receptions increases the battery life drops as expected. When the number of receptions approach 50 and 100 receptions per second the mobile terminal using LTE transitions to an always ON state, because the time to receive one data packet is about 20 and 10 ms as calculated in equation (6.9). The green line, called *LTE short* consumes the most energy in this region because it has more frequent transmissions of ACKs. Comparing with the 5G simulation results the benefit of the shorter frame is clear, because the mobile terminal enters the always ON state much later due to the receive time of about 1.08 ms, as calculated in equation (6.5). For very frequent receptions the overall battery life is dominated by the energy consumed while receiving (right part of figure 6.10), but as the number of receptions is reduced the sleep energy consumption becomes dominating and the simulation results approach the same value (left part of figure 6.10). For example the battery life of the LTE UE is approximately 250 days, when there is 1 reception per second, but almost 6 times better (1440 days) for 5G. If the number of receptions is increased to 10 per second the numbers are about 1 month and almost a full year (340 days) i.e. 12 times better, thus 5G provides huge improvements for frequent receptions. This will be very beneficial for keep-alive messages, video streaming, and MTC.

The mobile terminal can not rely solely on receptions and therefore figure 6.11 illustrates the simulation results for selected combinations of receive and transmit periods. The left hand side of the figure, where the number of transmissions per second is very low resembles the values obtained in figure 6.10. When the number of transmissions is increased the transmit energy consumption starts to dominate indicated by the sloping

parts on the right hand side of the figure. Due to the transmission energy being approximately 5 times higher than the receive energy, see table 6.1, the number of transmissions will start to dominate when they are about one fifth of the number of receptions. In addition the longer active periods of LTE entails the active energy consumption dominates the sleep mode energy consumption earlier as compared to 5G.

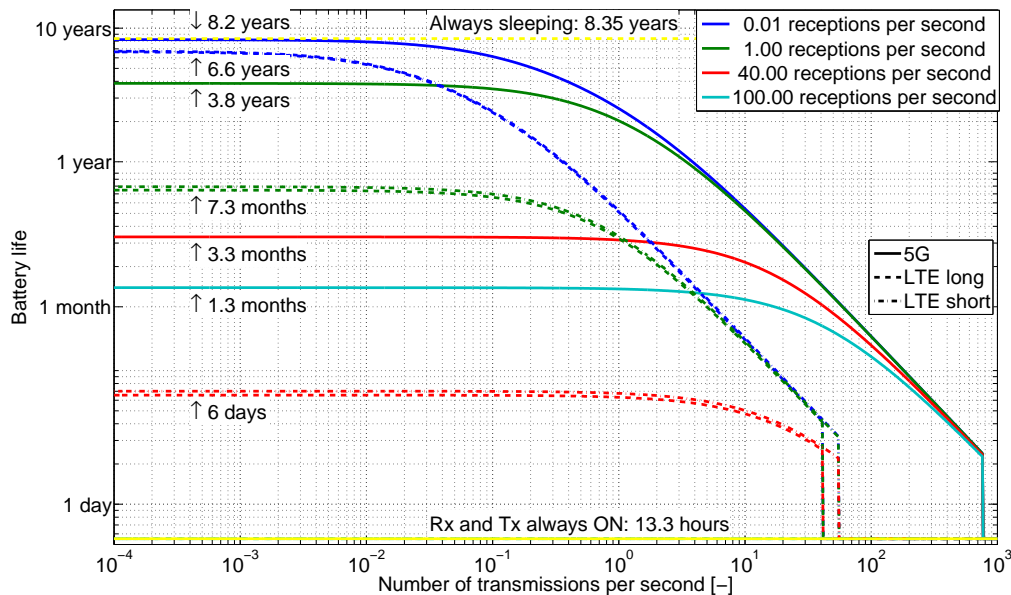


Figure 6.11: Battery life as a function of number of receptions and transmissions per second for LTE and 5G.

Note that the transceiver is set to be always ON when either the number of transmissions or receptions exceed the transmit and receive times calculated in equations (6.3), (6.5), (6.7), and (6.9).

Figure 6.11 clearly indicates the advantage of the shorter and optimized frame structure in 5G, and the relative improvement compared to *LTE long* is visualised in figure 6.12. For a low number of receptions and transmissions the battery life is dominated by the sleep mode power and therefore there is only a minor gain as illustrated with the blue bars in the left-most columns. If the number of receptions is high, as illustrated with the red bars, the 5G concept provides approximately 12-15 times better battery life. As the number of transmissions increase the improvement is closer to 10 times, because this is the ratio between transmission energy consumption in LTE and 5G, see calculations in equation (6.4) and (6.8).

The conclusion is that over a broad combination of receptions and transmissions per second the 5G concept provides 5-15 times better battery life. Furthermore the short and optimized frame structure entails the mobile terminal can handle very frequent transmissions and receptions without having the receiver and transmitter always ON. For very low activity the battery life is however dominated by the sleep mode energy consumption, which is assumed to be the same for both RATs.

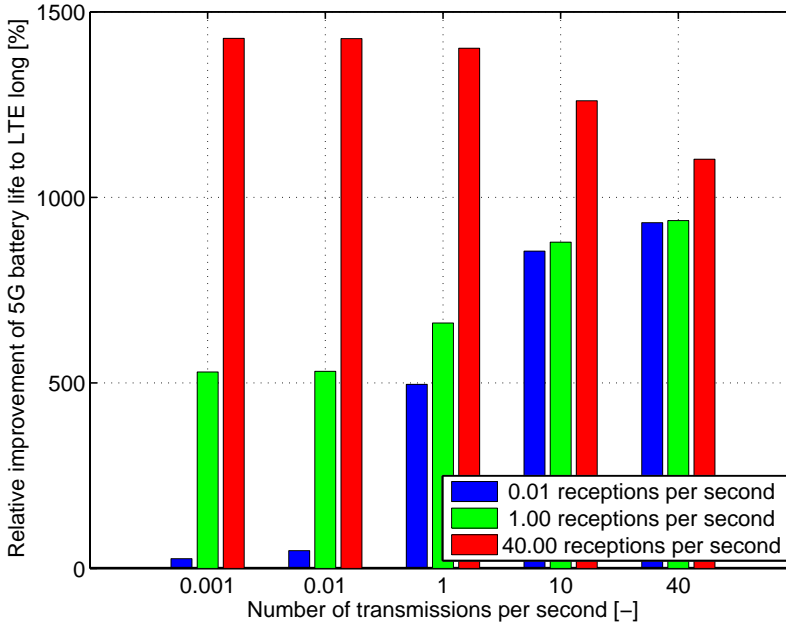


Figure 6.12: Relative improvement in battery life for 5G as compared to LTE.

This improvement in DRX and DTX energy consumption will significantly improve the overall user experience because the combination of short transfers and long sleep mode is one of the key enablers for long battery life.

6.3 Event Based Pre-Paging Concept

There are significant issues related to the use of periodic paging i.e. DRX and therefore a concept is proposed in this section to mitigate the issues. Specific components of the concept has been filed in multiple patent applications, but references cannot be provided due to confidentiality requirements.

Using DRX affects the delay and energy consumption of the individual mobile terminal if the traffic is not periodic. If the DRX Long Period (DRX LP) is too long multiple events may occur before the next paging instant and thus lead to increase delays or loss of data as illustrated in figure 6.13. On the other hand if the DRX LP is too short it will decrease the delay and avoid lost data, but increase the energy consumption of the mobile terminal because it will wake up multiple times before being paged. In addition the short DRX LP precludes the use of the deep sleep mode as indicated by the LTE DRX measurements in section 2.5.1. Furthermore the scheduling complexity will be increased if a large number of devices apply DRX.

The third option illustrated in figure 6.13 is known as the WuRx. The concept of WuRx has been proposed for use in contention-based, unlicensed spectrum mainly for sensor networks, because they generate the low data rate, infrequent traffic that may

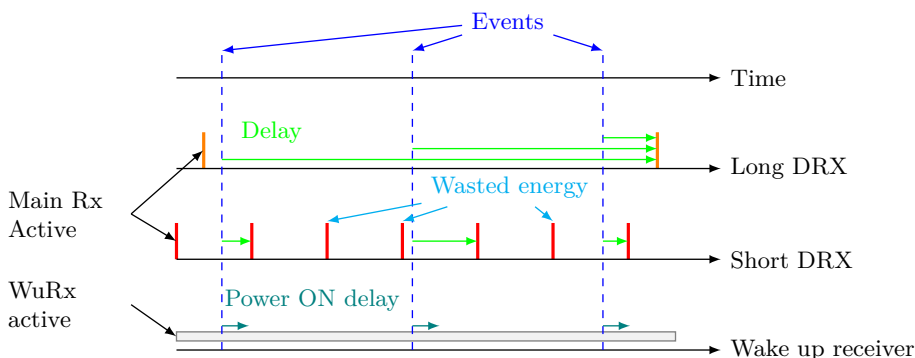


Figure 6.13: Use of DRX with short and long periodicity and a Wake up Receiver (WuRx) in event-driven traffic, which may not be periodic.

not be suitable for DRX while requiring very low power consumption.

The WuRx concept is based on the use of a secondary receiver, which is designed to have significantly lower power consumption than the main transceiver. The idea is that the secondary receiver is able to receive a specific wake up signal from the AP, while the main transceiver is powered OFF. Upon detection of the wake up signal the secondary receiver will send an interrupt signal to main transceiver, which then can power ON and receive the normal paging signal as illustrated in figure 6.14. Therefore the concept is generally known as WuRx, but a more complete name is event based pre-paging because the AP will send a pre-paging message to wake up the mobile terminal whenever a data transfer event occurs.

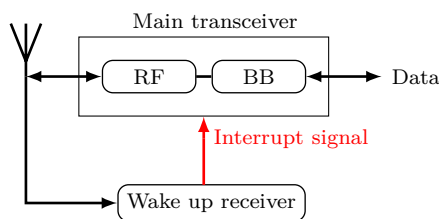


Figure 6.14: WuRx principle.

As illustrated in figure 6.13 the WuRx is always ON and listening for the pre-paging signal. Therefore the power consumption must be lower than the DRX sleep mode power consumption to result in improved battery life. Provided that the signal is received reliably and correct the overall system delay will be almost constant even for aperiodic events as compared to DRX where the delay may vary. This is useful for the 5G concept because of the requirement that the mobile terminal must be able transfer from being inactive to active within 10 ms as noted in the introduction to chapter 4. In principle this limits the applicability of DRX, but if the WuRx concept is not applied the 10 ms requirement must be relaxed to ensure sufficient battery life. Note that for uplink there is no significant delay, besides the time to connect via Random Access and receive

the ACK as discussed in section 6.2, because the mobile terminal can connect to and request resources from the network whenever it needs to.

In previous work the main focus has been on implementing the receiver in an unlicensed band and to reduce the power consumption, because the sensors are deployed in unlicensed bands e.g. using WiFi and because they require very long battery life. Table 6.5 contains a list of some of the WuRx implementations in current literature. Most of the work is targeting WiFi nodes and sensor networks, while [171] is a medical

Table 6.5: Examples of WuRx implementations, and comparison with the low power standards for Bluetooth (BT) and ZigBee.

Ref.	Power	Rate	Wake up Signal	Sensitivity	Frequency
[164]	2.4 μ W	10 kb/s	7 ms	-71 dBm	868 MHz
[165]	3 μ W	1 kb/s	32 ms	-60 dBm	868 MHz
[166]	19 μ W	50 kb/s	-	-53 dBm	2.4 GHz
[167]	25.4 μ W	2.73 kb/s	12.5 ms	-53 dBm	868 MHz
[168]	52 μ W	100 kb/s	-	-72 dBm	2 GHz
[169]	1 mW	100 kb/s	1.4 ms	-82 dBm	2.4 GHz
[170]	1.8 mW	25 kb/s	-	-105 dBm	433 & 868 MHz
[171]	5.4 mW	36.5 kb/s	-	-75 dBm	2.45 GHz
[172]	7 mW	19.2 kb/s	3.07 ms	-95 dBm	915 MHz
[173]	31.5 mW	370 b/s	-	-122 dBm	916 MHz
BT 4.0 LE [174]	53.7 mW	1 Mb/s	-	-88 dBm	2.4 GHz
ZigBee [41]	103 mW	250 kb/s	-	-92 dBm	2.4 GHz

device specifically developed for implantation in humans. The power consumption is in the range a few μ W to a few mW for the examined receivers. Some of the designs even apply a DRX-like concept to the wake up signal to reduce the power consumption further, and for example [171] uses a period of 1 s with an ON duration of 200 μ s thus leading to an average power consumption of 2 μ W. The lowest LTE DRX sleep mode power consumption was measured to about 10 mW in section 2.5.1 and thus the WuRx can improve the battery life with the cost of implementing additional hardware.

The power consumption of the WuRx depends on the data rate of the wake up signal just as normal receivers were noted to in section 2.5. A high data rate allows the receiver to decode a longer bit sequence within the allotted time. This entails the receiver can either achieve a larger processing gain or that the transmitter is able to separately address nodes using separate bit sequences. The processing gain is a key component for the proposed WuRx techniques to increase the receive sensitivity because most of them rely on use of few active components in the receive chain, but it is clear that the receivers with high power consumption also achieve the best sensitivity. Referring to the Low Noise Amplifier (LNA) survey of section 5.1 the average power consumption of an LNA was noted to be about 10 mW and thus the use of these active components must be limited in the WuRx. Therefore the receive sensitivity for several of the proposed designs is also significantly lower than the sensitivity of LTE which was measured to be better than -100 dBm in [27]. The low sensitivity is a problem if the WuRx is deployed in a macro cell, but since the 5G concept is targeting UDSC the sensitivity requirements

can be reduced.

The time duration of the wake up signal is of key importance, because if it is too long the responsiveness of the system is harmed and if it too short the processing gain is limited. Only a few of the examined WuRx techniques report the duration and it varies between 1.4 ms and 32 ms and therefore some of the designs fulfil the 10 ms 5G requirement provided the main transceiver can power ON fast.

A transceiver using the Low Energy edition of BT [174] and a ZigBee transceiver [41] are included for comparison in table 6.5. These transceivers are made for a fully functional two-way communication RAT and therefore they also consume more power, but they clearly indicate that a dedicated receiver is needed to achieve the event based pre-paging functionality.

Finally it must be noted that the proposed WuRx techniques are mainly designed to operate in the Industrial, Scientific and Medical (ISM) radio band where short range and low power communication is allowed [175].

The contribution of this section is to examine how the event based pre-paging concept can be adopted to and implemented in a scheduled wireless system with licensed frequency bands where the resources are already used for the standardized RATs. This entails new challenges because the wake up functionality must have limited impact on system capacity and also be able to handle the interference caused by the general 5G nodes.

Assuming that the wake up signal must be implemented in-band it has to fit into the proposed 5G frame structure in section 4.4. The downlink control channel only occupies one symbol hence resources are already scarce and therefore it is proposed to allocated the wake up signal within a downlink data frame. Due to the flexible link direction technique of 5G this may increase the delay because the transmitter has to wait for a downlink frame. The signal can for example be implemented using super position of a wideband wake up signal on the entire data frame as illustrated in figure 6.15a. Another option is to allocate a narrowband wake up signal as illustrated in figure 6.15b, where only a few subcarriers are affected by the wake up signal, while the third option is to implement the wake up signal periodically either narrow- or wideband as illustrated in figure 6.15c.

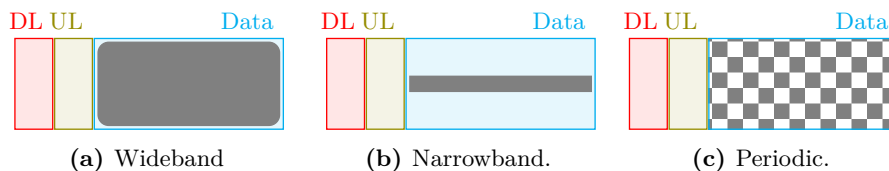


Figure 6.15: Allocation of the wake up signal (gray color) in the data part of a frame.

The narrowband option has been favoured in the examined literature, but a fourth option has also been observed. It relies on adjusting the frame length of a WiFi signal and let each predefined length correspond to a bit sequence, [176]. Due to WiFi's contention based design other devices may however transmit in the silent period of the wake-up signal, and therefore the authors introduced a state machine which waits for

the expected frame after detection of the previous frame in a wake up signal. This method is however not applicable in 5G because the frame length is fixed.

If the wideband solution were to be implemented one option would be to use a spreading scheme, i.e. Code Division Multiple Access (CDMA), similar to 3G [78]. In this way the transmitter is able to spread a low data rate signal across a large bandwidth, and since the codes are orthogonal multiple users can be addressed simultaneously if needed. Assuming the signal is spread across the entire cell channel bandwidth the WuRx can re-use parts of the analog Radio Frequency (RF) front end, but configured to low performance to save power. After the signal has been mixed to Base Band (BB) the mobile terminal can apply its assigned scrambling code and decide whether it is supposed to wake up. Figure 6.16 shows a simplified block diagram of how the WuRx is implemented together with the main receiver.

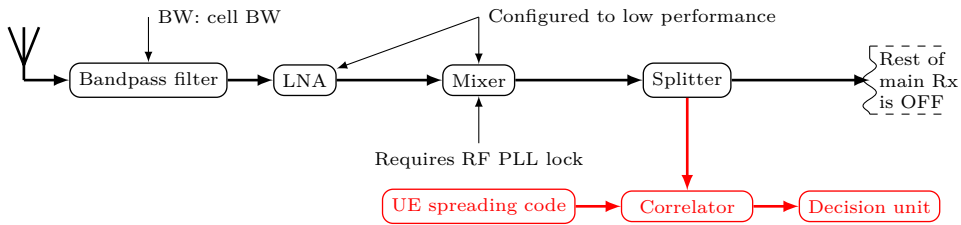


Figure 6.16: Simplified block diagram for a wideband WuRx, in red, connected with the main receiver.

The main 5G signals are transmitted using Orthogonal Frequency Division Multiplexing (OFDM) and thus the CDMA would be perceived as noise by the main receivers of the mobile terminals that are not applying the wake up scheme in the current frame. This will limit the Signal to Interference + Noise Ratio (SINR), but due to the processing gain of CDMA the wake up signal may be transmitted with significantly lower power to reduce the impact. Another issue of the CDMA scheme is the need for time synchronization, but this may be handled using multiple correlators each time shifted a bit as in a RAKE receiver, [78].

If the narrowband option were to be implemented the AP could allocate a few subcarriers of a single Physical Resource Block (PRB) to the wake up signal, which may not happen often depending on the number of sleeping users. Each subcarrier is 60 kHz wide in 5G, see equation (4.4) and thus if three are used the loss in frequency capacity is only $3 \cdot 60 \text{ kHz} / 100 \text{ MHz} = 0.18\%$. Another option is to use the Direct Current subcarrier of the OFDM signal, which is not used in most implementations due to the risk of imbalance in the RF front end. If the WuRx used this subcarrier it could rely on mixing with a slightly offset frequency and thus still receive the signal, which would be less affected by interference. This would however require a better Direct Current filter in the main receiver and in addition the wake up signal cannot be reallocated in case of a deep fade.

Due to the limited bandwidth the spreading codes applied in the wideband model cannot be reused. Instead the WuRx must rely on coding gain in the time domain only. For good detection performance this entails the selected sequence must have high auto-

correlation and low cross-correlation. This is not trivial to achieve and especially not if the receiver is not time synchronized to the transmitter. Furthermore the code selection depends on the number of codes needed. In the simplest case only one code is available i.e. all sleeping users wake up and scans for a paging signal. For a low number of users this is a feasible solution, but due the massive number of expected MTC connections it is necessary to at least define some user groups or in the extreme case individual wake up signals.

Provided that useful codes exist the transmitter can rely on On-Off-Keying (OOK), which turns the carrier wave ON and OFF according to the selected code, which therefore must be binary. This is a widely used concept in literature [171, 165, 164, 173] because it can be combined with an Envelope Detector, which transforms the received RF signal into a signal that is a slow moving average of the RF envelope. If the envelope detector is tuned to the applied carrier frequency it will produce a simple binary sequence due to the OOK. The next step is then to correlate the sequence with the mobile terminal's pre-assigned sequence and decide whether to wake up. In [164] time synchronization is avoided in BB by applying $2^N - 1$ correlators where N is the number of bits in the sequence. Figure 6.17 provides a simplified block diagram for the narrowband WuRx.

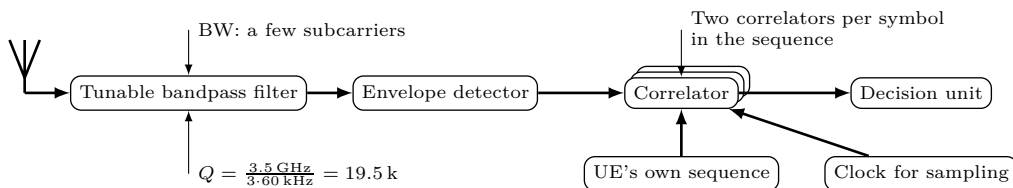


Figure 6.17: Simplified block diagram for a narrowband WuRx.

As compared to the implementations in literature, all relying on narrowband frequencies in the Industrial, Scientific and Medical (ISM) radio band, this proposal is targeted to fit the wide bandwidth of the 5G concept. This entails the RF bandpass filter must be tunable, in order to select the assigned subcarrier(s), and this dramatically affects the complexity of the filter design as indicated by [177, Page 82]

$$Q = \frac{f_c}{B} \quad [-] \quad (6.16)$$

where: Q is the filter quality factor [-]
 f_c is the center frequency [MHz]
 B is the filter bandwidth [MHz]

As illustrated in the drawing the bandpass filter of the direct conversion architecture will have a quality factor of almost 20.000. This is not achievable in current filter architectures, and thus the block diagram is changed to re-use the first part of the main receiver's RF front end similar to the wideband WuRx. The simplified block diagram is

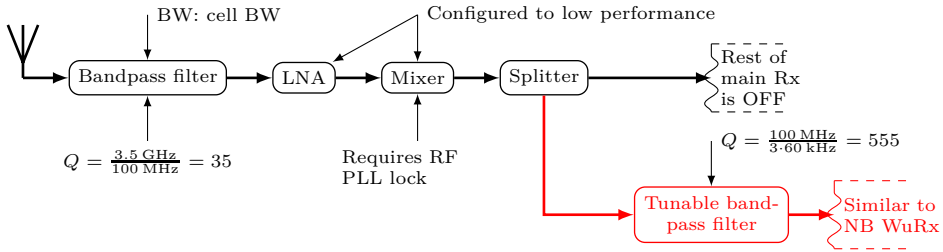


Figure 6.18: Simplified block diagram for a narrowband WuRx, in red, partly reusing the main receiver’s front end.

illustrated in figure 6.18. The quality factor of the first bandpass filter is now reduced to 35, while the newly introduced second filter will have a quality factor of about 550. This is still difficult to achieve, but in [168] quality factors between 500 and a few thousand are described, though not for tunable filters. Besides that the introduction of the LNA and mixer will increase the energy consumption of the WuRx.

Assuming the narrowband design is feasible in 2020 it is also important to consider how the AP can transmit the wake up signal. Figure 6.19 illustrates the logical implementation of how the AP may be composed of two individual transmitters; a main transmitter which allocates the normal data and control channels according to the 5G concept, but also has the functionality to mute subcarriers, and a wake up transmitter which generates the narrowband wake up signal and informs the main transmitter about it as illustrated in figure 6.19b. The main transmitter must also be able to inform the

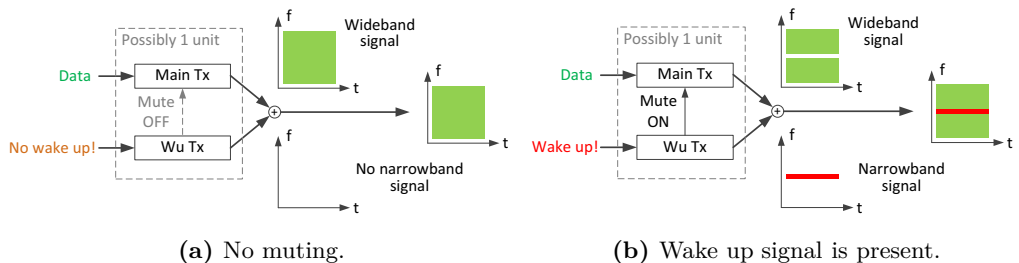


Figure 6.19: Logical implementation of a secondary wake up transmitter, denoted Wu Tx, in the AP and use of muting.

mobile terminal, equipped with a WuRx about the selected subcarriers and the wake up identification sequence before the WuRx is powered ON and the main transceiver OFF.

Besides the AP’s wake up signals other APs and mobile terminals may use the dedicated subcarriers for transmissions in neighbor cells and thus create interference. This may prevent proper decoding in the WuRx and lead to a false positive detection if the interference mimics the wake up identification sequence. This will lead to increased mobile terminal power consumption due to unnecessary power ON sequences after which the mobile terminal will detect it is not scheduled and power OFF again. In the pro-

posed concept this is handled by letting the mobile terminal monitor the number of false positives during a certain predefined period. If the number is too high, and not interrupted by an actual wake up signal, the mobile terminal must request to use other subcarriers for the wake up channel as illustrated in figure 6.20. When the AP receives

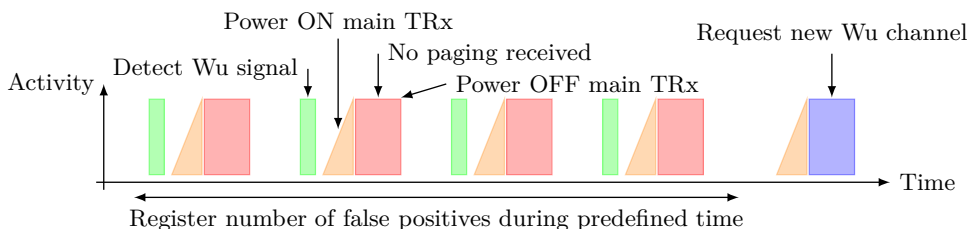


Figure 6.20: False positive detection.

such a request from a mobile terminal, for example by use of the normal Channel State Information (CSI) procedures, it has to consider the input and weigh the information according to input from other WuRx equipped mobile terminals if they use the same channel. Before the AP can change the wake up channel it will thus have to wake up the other mobile terminals to inform them about incoming information updates or use multiple wake up channels for a period of time until all relevant mobile terminals have received the information. The latter option will waste channel capacity while the first option will cause increased mobile terminal energy consumption.

In addition to the false positive the mobile terminal may also experience a false negative due to a deep fade. This entails the WuRx cannot determine whether it is not being pre-paged or the signal is faded. In the concept it is thus proposed that the WuRx after a long silent period must make a receive power level comparison with the wideband channel signal as illustrated in figure 6.21. The idea is that a measurement is made in the main receiver, e.g. at the point where the splitter is inserted in figure 6.18, and compare it with the received power in the WuRx. If the difference between the two measured powers exceeds a certain threshold the mobile terminal must initiate the previously described procedure to request a new wake up channel.

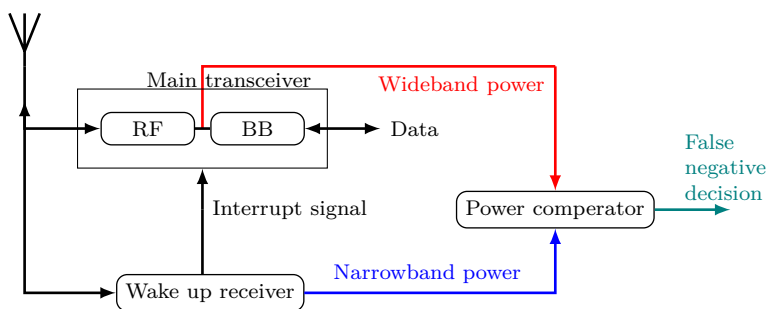


Figure 6.21: False negative detection.

To summarize this section a new method was proposed to circumvent the limitations of DRX, which in case of infrequent traffic will lead to either unnecessary energy consumption or long delays. The idea is to use a secondary low-power receiver, which continuously scans for pre-paging messages while the main receiver is OFF. In case of a pre-paging the secondary receiver, called WuRx, will interrupt the main receiver which then proceeds to receive the standardized paging message and act as a normal 5G mobile terminal. The WuRx concept has previously only been applied in sensor and WiFi networks i.e. contention-based bands as opposed to the scheduled 5G scenario. Allocating a wake up channel in-band in 5G has been analyzed for both a narrow- and a wideband receiver to limit the effect on system capacity. Challenges were identified in terms of filter quality factor, the ability to tune filters, selection of wake up signal codes, and synchronization. In addition it was proposed how the WuRx can handle false negatives, due to deep fades, and false positives, due to interference.

The existing WuRx literature has showed that it is possible to develop devices that consume 100-1000 times less power than DRX deep sleep mode and thus it is important to develop the concept further for 5G.

6.4 Summary

In this chapter the capabilities of the 5G concept were compared with the video streaming and MTC scenarios. The 5G concept is expected to have a positive effect on mobile terminal battery life, as discussed in section 4.8 due to the application of OFDM, larger bandwidth, Carrier Aggregation (CA), Multiple Input Multiple Output (MIMO), TDD and the optimized frame structure. However, it was not clear how periodic and aperiodic traffic will fit the sleep modes in 5G.

It is concluded that video streaming, which will be the main traffic type in the coming years, can be successfully delivered to the user, because the data rates increase to provide for higher video quality and because DRX for 5G provides 5-15 times better battery life as compared to LTE due to the short and optimized frame structure.

The fast growing MTC user scenario was identified to be challenging to accommodate in the 5G concept because the requirements shift from high data rates, mobility, and low latency perceivable by humans towards high reliability and ultra-low latency, only perceivable by machines, and in addition year-long battery life is also important. In addition the coverage requirement may both be close proximity, e.g. wearables and machines in industry, and wide areas, e.g. reading of power meters and sensors from a distant location. For mobile terminals, which are paged by the AP aperiodically and required to be always ON, it was discussed how the periodic nature of DRX is difficult to adapt and thus leading to either unnecessary energy consumption or long delays. Therefore the use of a secondary, event based pre-paging receiver with very low power consumption was proposed to wake up the main receiver, when the AP is requesting updates. Implementing this concept in-band in a scheduled system however poses new challenges both with regards to mitigating the impact on system capacity and designing a reliable wake up signal and a low-power receiver. The concept is not ready to be implemented but it provides input to the direction the future work and standardization can take to ensure the long battery life users demand.

Chapter 7

Conclusion

This study has dealt with prolonging smartphone battery life, which is limited due to the use of large, high resolution displays, the increasing data rates of each new Radio Access Technology (RAT), and the emergence of diverse traffic types and applications. In addition, recent surveys have reported that battery life is the feature receiving the largest amount of improvement requests, and furthermore that the smartphone has the largest and increasing market share.

The battery life of a smartphone, and mobile terminals in general, can be improved by optimizing the hardware and software, by using a bigger or more efficient battery, by adjusting relevant network settings, and by carefully selecting the technology features of the RAT that the mobile terminal connects to. In this study the focus has been on the cellular subsystem of a mobile terminal, both in terms of hardware and network optimization. In the following subsections the outcome of the study is summarized based on the previous chapters, after which a main conclusion is given.

7.1 System Level Analysis of Power Consumption in LTE User Equipment

In order to examine potential power consumption improvements, a power model was needed for system level simulations, but that was not available for the recently launched Third Generation Partnership Project Long Term Evolution (LTE) when this study was initiated in 2010.

The first contribution is therefore the development of a cellular subsystem power model. It is based on a measurement methodology, where the commercial LTE smartphone is connected to a base station emulator, and the battery is replaced with a measurement power supply as opposed to many other measurements in literature, which rely on connecting to a commercial network and logging the power consumption via an application installed on the smartphone. The latter results in less control and lower accuracy. The measurement methodology is designed so that a single parameter, e.g. downlink data rate, is varied while the contribution of other parameters is kept at a constant minimum. This entails that the power consumption as a function of only the data

rate can be examined. The model covers receive and transmit power and data rates, which are parameters that can be varied independently, and in addition it has been updated with measurements on Discontinuous Reception (DRX) and Carrier Aggregation (CA).

The main findings are that the cellular subsystem being ON and transmit powers above 10 dBm contribute the most to high power consumption, while DRX periods longer than 40 ms provide a sleep mode that consumes less than 1/50 of the ON power. In addition, high data rates are 10 times more energy efficient than low data rates, and this is also reflected in CA where bulk traffic relying on high data rates can be transferred at a lower energy consumption than by use of a single carrier. The proposed model has been updated with measurements on 6 smartphones to study the chipset power consumption evolution, which has been halved in 2.5 years.

7.2 Energy Saving in LTE User Equipment

The model has already been employed for several studies in academia, and using the knowledge obtained while developing the model, additional contributions for LTE include the proposal of a new uplink resource allocation scheme and the micro sleep concept. The first exploits the fact that the transmit Power Amplifier efficiency increases with increasing transmit power, and this was not a metric that had been included in previous literature on LTE scheduling. Therefore a Time Division Multiple Access like scheduling scheme was proposed, and by allocating up to 48 resources to a single mobile terminal at least 24% energy was saved as compared to a terminal with 8 resources. The micro sleep concept aims at decoding scheduling information faster, because LTE's control-data structure can lead to unnecessary receive and buffer operations for unscheduled users. If the mobile terminal can decode the scheduling information within the time frame of a few symbols, it can save 5-25% energy by applying low-power micro sleep. The cost is that less reference signals for channel estimation are received, and this leads to a throughput degradation of 1-4%.

7.3 Fifth Generation Radio Access Technology

It is time to initiate the development of a new Fifth Generation (5G) RAT due to increased traffic volume and technology improvements. The targets of 5G include 10 Gb/s peak data rate, 1 ms latency, and 10 ms idle to active mode transfer. This study has contributed to a 5G concept by proposing and examining features that can improve the battery life and thus the user experience. The concept is based on flexible uplink/downlink transfers using Time Division Duplexing (TDD), and advanced interference cancellation Multiple Input Multiple Output (MIMO) receivers in an Ultra-Dense Small Cell, Centimeter Waves network with large channel bandwidth. For example the frame structure has been reorganized and shortened, as compared to LTE, to allow for pipelined processing and fast synchronization, both reducing the energy consumption and the latency. The use of TDD is another example of how energy efficient features are used, because it allows for discarding the duplexer, and thus avoid up to 3 dB loss between the antenna and the Radio Frequency (RF) front end, relaxed

Third-Order Intercept Point requirements, because the transmitter will not be active while receiving, and less channel feedback due to reciprocity.

7.4 Power Consumption Challenges in 5G

The 5G RAT is expected to be deployed around 2020, and it will utilize 400 MHz of bandwidth combined with advanced 4x4 MIMO receivers to achieve the 10 Gb/s data rate requirement. This entails increased requirements to the analog Radio Frequency including the Power Amplifier (PA), the converters, and the baseband processor. Another contribution is thus the analysis of how the performance and power consumption of selected cellular subsystem hardware components evolve. The study showed that due to Complementary Metal–Oxide–Semiconductor evolution and improved designs, the examined Low Noise Amplifier and Analog-to-Digital Converter can handle the requirements, but channel bandwidths above 200 MHz are not recommended for implementation in 2020. However, the 100 times increase in complexity, caused by increasing the data rate from LTE’s 100 Mb/s to 5G’s 10 Gb/s, leads to an estimated baseband processor power consumption of about 3 W in 2020, which will severely harm the battery life. The estimates show that by 2025 the power consumption will be on par with current LTE implementations consuming about 0.6 W. In addition to the high baseband power consumption, the use of multiple MIMO streams and possibly CA will increase the cost and chip area, and may cause coexistence issues due to the mixing of multiple frequency bands, which are used to obtain sufficient spectrum,. Furthermore the PA efficiency decreases about 50 percentage points for carrier frequencies above 5 GHz, and thus this component needs specific attention despite the fact that the Ultra-Dense Small Cell scenario will lead to lower transmit powers.

7.5 DRX and Aperiodic Sleep Modes in 5G

The DRX mechanism was measured to be a key component for long battery life in LTE and another contribution of this study was to perform a similar evaluation for 5G, because user scenarios such as video streaming and Machine Type Communication will benefit from DRX. Simulations show that 5G, using the same power consumption model, leads to 5-15 times longer battery life due to the shorter and optimized frame. However it was also observed that DRX will result in either increased energy consumption or long delays for aperiodic traffic, and thus an event based pre-paging concept was proposed. The idea is to apply a secondary low-power receiver which continuously scans for pre-paging messages, and upon detection can power ON the main transceiver. The applicability of the concept in a scheduled, in-band network was studied and suggestions for hardware implementations and error detection protocols were presented.

7.6 Main Conclusion

To conclude and answer the research questions of chapter 1 this PhD study showed, by use of a proposed system level LTE cellular subsystem power model that transmit powers

above 10 dBm and the subsystem being ON are the main power consumers. Therefore the battery life of the mobile terminal can be improved by scheduling mechanisms that increase the DRX sleep time, by use of micro sleep, and by exploiting the peaking energy efficiency of high data rates in both link directions.

The obtained cellular subsystem power consumption knowledge has been applied in the development of a 5G RAT concept. The future 5G can result in improved mobile terminal battery life by utilizing Orthogonal Frequency Division Multiplexing to support MIMO, TDD to obtain sufficient spectrum but also lower insertion loss and Third-Order Intercept Point requirements, and a 0.25 ms frame with an optimized control-data structure. In addition the event based pre-paging concept was proposed to complement DRX and improve the battery life by extended low-power sleep.

The main 10 Gb/s target of 5G cannot be achieved in 2020 due to high baseband processing power consumption in the mobile terminal, but in 2025 the users should be able to experience reasonable battery life combined with wireless 5G performance.

7.7 Future Work

To achieve long battery life in a commercial 5G smartphone, there are some areas that need further work.

The 5G concept relies on a short and optimized frame to achieve low latency and energy consumption, but for this to be as effective as possible, it is important to study how the power ON/OFF procedure and time can be optimized and reduced, respectively. This is important both for use in connection with DRX and general mode transfers.

Furthermore, the 5G concept is dependent on several hundred megahertz of bandwidth to achieve the peak data rates, and this large spectrum is not available in one continuous frequency band and thus many bands and Carrier Aggregation must be applied. However, it is already a major challenge in current LTE mobile terminals to accommodate many frequency bands and carriers, because they create interference and blockers in the Radio Frequency components. In addition, the use of MIMO on each carrier increases the component count and chip layout complexity.

The performance evolution estimate also showed that the increased baseband processing complexity of about 100 times will result in a power consumption level, which will significantly degrade the battery life, and may create thermal issues if not addressed.

A final proposal for future work is the further study and development of the event based pre-paging concept. It is especially important to identify which type of hardware implementations can be combined with useful codes and protocols to provide low power consumption, proper sensitivity, and reliable paging messages, while not harming the general 5G communication in terms of interference and occupation of resources. Specifically the codes must have low complexity, but also significant coding gain, and provide possibility to individually address users.

Bibliography

- [1] Gartner Inc. *Gartner Estimates ICT Industry Accounts for 2 Percent of Global CO2 Emissions*. Press Release. 2007. URL: <http://www.gartner.com/newsroom/id/503867>.
- [2] ITU-T Study Group 5 - Environment and climate change. *List of Questions (Study Period 2009-2012)*. 2009. URL: <http://www.itu.int/net/ITU-T/lists/questions.aspx?Group=5%5C&Period=14>.
- [3] Centre for Energy-Efficient Telecommunications. *CEET Annual Report 2013*. 2013.
- [4] GreenTouch. *Official website*. 2014. URL: <http://www.greentouch.org/>.
- [5] European Commission. *ICT footprint - Pilot testing on methodologies for energy consumption and carbon footprint of the ICT-sector*. 2013.
- [6] R. Kumar and L. Mieritz. “Conceptualizing Green IT and data center power and cooling issues”. In: *Gartner Research* (2007).
- [7] Cisco. *Visual Networking Index: Global Mobile Data Traffic Forecast Update, 2013–2018*. White paper. 2014.
- [8] Ericsson. *Energy and Carbon Report*. 2013.
- [9] Gilbert Micallef. “Energy Efficient Evolution of Mobile Broadband Networks”. PhD thesis. Aalborg University, June 2013.
- [10] Gartner Inc. *Market Share Analysis: Mobile Phones, Worldwide, 2Q13*. Press release. Aug. 2013. URL: <http://www.gartner.com/newsroom/id/2573415>.
- [11] Gartner Inc. *Market Share Analysis: Mobile Phones, Worldwide, 3Q13*. Press release. Nov. 2013. URL: <http://www.gartner.com/newsroom/id/2623415>.
- [12] Qualcomm Technologies. *Designing Mobile Devices for Low Power and Thermal Efficiency*. Oct. 2013.
- [13] J.D. Power and Associates. *J.D. Power Insights: Battery Life: Is That All There Is?* 2012. URL: <http://tinyurl.com/19mft9n>.
- [14] H. Holma, A. Toskala, and P. Tapia. *HSPA+ Evolution to Release 12: Performance and Optimization*. John Wiley & Sons, Ltd., 2014. ISBN: 978-1-118-50321-8.
- [15] A.D. Joseph. “Energy harvesting projects”. In: *IEEE journal on Pervasive Computing* 4.1 (2005), pp. 69–71.

- [16] J.M Lemenager, L.D. Capua, V. Wilkerson, M. Guenais, T. Meslet, and L. Noël. “Multimode Multiband Terminal Design Challenges”. In: *HSPA+ Evolution to Release 12: Performance and Optimization*. Ed. by H. Holma, A. Toskala, and P. Tapia. John Wiley & Sons, Ltd., 2014. ISBN: 978-1-118-50321-8.
- [17] Adam Kerin, Qualcomm. *The Thermal Efficiency Behind Smartphone Trends*. Oct. 2013. URL: <http://www.qualcomm.com/media/blog/2013/10/09/thermal-efficiency-snapdragon-processors-under-screen-and-behind-trends>.
- [18] Heebyung Koh and Christopher L. Magee. “A functional approach for studying technological progress: Extension to energy technology”. In: *Technological Forecasting and Social Change* 75.6 (2008), pp. 735–758. ISSN: 0040-1625.
- [19] Chen-Xi Zu and Hong Li. “Thermodynamic analysis on energy densities of batteries”. In: *Energy Environ. Sci.* 4 (8 2011), pp. 2614–2624. DOI: 10.1039/C0EE00777C.
- [20] James F. Rohan, Maksudul Hasan, Sanjay Patil, Declan P. Casey, and Tomas Clancy. “Energy Storage: Battery Materials and Architectures at the Nanoscale”. In: *ICT - Energy - Concepts Towards Zero-Power Information and Communication Technology*. Ed. by Douglas Paul Giorgos Fagas Luca Gammaitoni and Gabriel Abadal Berini. InTech, 2014. ISBN: 978-953-51-1218-1.
- [21] James Miller. *Energy Storage: Current Status and Future Trends*. Presented at Building a Scientific Bridge on Trans-Atlantic Eco-Industries. European Commission - Joint Research Centre - Brussels - Belgium, Sept. 2013.
- [22] Andrew S. Tanenbaum. *Computer Networks*. 4th ed. Pearson Education International, 2003. ISBN: 0130384887.
- [23] Ekhiotz Jon Vergara, Simon Andersson, and Simin Nadjm-Tehrani. “When Mice Consume Like Elephants: Instant Messaging Applications”. In: *Proceedings of the 5th International Conference on Future Energy Systems*. Cambridge, United Kingdom: ACM, 2014, pp. 97–107. ISBN: 978-1-4503-2819-7. URL: <http://doi.acm.org/10.1145/2602044.2602054>.
- [24] Christian Piguet. *Low-power electronics design*. CRC Press LLC, 2004. ISBN: 0849319412.
- [25] A. Jensen, M. Lauridsen, P. Mogensen, T. Sørensen, and P. Jensen. “LTE UE Power Consumption Model - for System Level Energy and Performance Optimization”. In: *VTC Fall, IEEE 76th* (Sept. 2012).
- [26] M. Lauridsen, P. Mogensen, and L. Noël. “Empirical LTE Smartphone Power Model with DRX Operation for System Level Simulations”. In: *VTC Fall, IEEE 78th* (Sept. 2013).
- [27] M. Lauridsen, L Noël, T. Sørensen, and P. Mogensen. “An Empirical LTE Smartphone Power Model with a view to Energy Efficiency Evolution”. In: *Intel Technology Journal* 18 (1 Jan. 2014).
- [28] M. Lauridsen, A. Jensen, and P. Mogensen. “Fast Control Channel Decoding for LTE UE Power Saving”. In: *VTC Spring, 75th* (May 2012).

- [29] M. Lauridsen, A.R. Jensen, and P. Mogensen. “Reducing LTE Uplink Transmission Energy by Allocating Resources”. In: *VTC Fall, IEEE 74th*. Sept. 2011.
- [30] M. Lauridsen, H. Wang, and P. Mogensen. “LTE UE Energy Saving by Applying Carrier Aggregation in a HetNet Scenario”. In: *VTC Spring, IEEE 77th*. 2013.
- [31] R. Sanchez-Mejias, Y. Guo, L.A.M.R.D Temino, M. Lauridsen, and P. Mogensen. “Current Consumption Measurements with a Carrier Aggregation Smartphone”. In: *VTC Fall, IEEE 80th* (2014).
- [32] M. Lauridsen, G. Berardinelli, T. Sørensen, and P. Mogensen. “Ensuring Energy Efficient 5G User Equipment by Technology Evolution and Reuse”. In: *VTC Spring, IEEE 79th*. 2014.
- [33] P. Mogensen, K. Pajukoski, E. Tirola, J. Vihriälä, E. Lähetkangas, G. Berardinelli, FML. Tavares, NH. Mahmood, M. Lauridsen, D. Catania, and AF. Cattoni. “Centimeter-wave concept for 5G ultra-dense small cells”. In: *VTC Spring, IEEE 79th* (May 2014).
- [34] B. Panzner, W. Zirwas, S. Dierksy, M. Lauridsen, P. Mogensen, K. Pajukoski, and D. Miao. “Deployment and Implementation Strategies for Massive MIMO in 5G”. In: *Globecom Workshops, IEEE*. Accepted. 2014.
- [35] E. Lähetkangas, K. Pajukoski, J. Vihriälä, G. Berardinelli, M. Lauridsen, E. Tirola, and P. Mogensen. “Achieving low latency and energy consumption by 5G TDD mode optimization”. In: *IEEE International Conference on Communications* (2014).
- [36] Keysight Technologies. *Power-Consumption Measurements for LTE User Equipment. Application Note*. Ed. by Mads Lauridsen. 2014.
- [37] NH. Mahmood, G. Berardinelli, FML. Tavares, M. Lauridsen, P. Mogensen, and K. Pajukoski. “An Efficient Rank Adaptation Algorithm for Cellular MIMO Systems with IRC Receivers”. In: *VTC Spring, IEEE 79th* (May 2014).
- [38] AR. Jensen, KI. Pedersen, J. Faaborg, M. Lauridsen, and P. Mogensen. “LTE HetNet Mobility Performance Through Emulation with Commercial Smartphones”. In: *VTC Spring, IEEE 79th* (May 2014).
- [39] Lide Zhang, Birjodh Tiwana, Zhiyun Qian, Zhaoguang Wang, Robert P. Dick, Zhuoqing Morley Mao, and Lei Yang. “Accurate Online Power Estimation and Automatic Battery Behavior Based Power Model Generation for Smartphones”. In: *Proceedings of the Eighth IEEE/ACM/IFIP International Conference on Hardware/Software Codesign and System Synthesis. CODES/ISSS '10*. ACM, 2010, pp. 105–114. ISBN: 978-1-60558-905-3.
- [40] Aaron Carroll and Gernot Heiser. “An analysis of power consumption in a smartphone”. In: *Proceedings of the 2010 USENIX conference*. 2010.
- [41] E. Casilari, J.M. Cano-García, and G. Campos-Garrido. “Modeling of Current Consumption in 802.15.4/ZigBee Sensor Motes”. In: *Sensors* 10.6 (2010), pp. 5443–5468.
- [42] G. P. Perrucci, F. H P Fitzek, and J. Widmer. “Survey on Energy Consumption Entities on the Smartphone Platform”. In: *Vehicular Technology Conference (VTC Spring), 2011 IEEE 73rd*. May 2011, pp. 1–6.

- [43] M. Gupta, A.T. Koc, and R. Vannithamby. “Analyzing mobile applications and power consumption on smartphone over LTE network”. In: *Energy Aware Computing (ICEAC), 2011 International Conference on*. Nov. 2011, pp. 1–4.
- [44] Martin Kennedy, Hrishikesh Venkataraman, and Gabriel-Miro Muntean. “Energy Consumption Analysis and Adaptive Energy Saving Solutions for Mobile Device Applications”. In: *Green IT: Technologies and Applications*. Ed. by JaeH. Kim and MyungJ. Lee. Springer Berlin Heidelberg, 2011, pp. 173–189. ISBN: 978-3-642-22178-1.
- [45] Junxian Huang, Feng Qian, Alexandre Gerber, Z. Morley Mao, Subhabrata Sen, and Oliver Spatscheck. “A close examination of performance and power characteristics of 4G LTE networks”. In: *10th MobiSys*. 2012, pp. 225–238.
- [46] E. Harjula, O. Kassinen, and M. Ylianttila. “Energy consumption model for mobile devices in 3G and WLAN networks”. In: *Consumer Communications and Networking Conference (CCNC), 2012 IEEE*. Jan. 2012.
- [47] N. Warty, R. Sheshadri, W. Zheng, and D. Koutsonikolas. “A first look at 802.11n power consumption in smartphones”. In: *ACM PINGEN*. 2012.
- [48] Rahul Murmura, Jeffrey Medsger, Angelos Stavrou, and Jeffrey M. Voas. “Mobile Application and Device Power Usage Measurements”. In: *Software Security and Reliability, IEEE 6th conference on*. June 2012, pp. 147–156.
- [49] J. Bornholt, T. Mytkowicz, and K.S. McKinley. “The Model Is Not Enough: Understanding Energy Consumption in Mobile Devices”. In: *Hot Chips*. 2012.
- [50] MikkelBaun Kjaergaard and Henrik Blunck. “Unsupervised Power Profiling for Mobile Devices”. In: *Mobile and Ubiquitous Systems: Computing, Networking, and Services*. Ed. by Alessandro Puiatti and Tao Gu. Vol. 104. Lecture Notes of the Institute for Computer Sciences, Social Informatics and Telecommunications Engineering. Springer Berlin Heidelberg, 2012, pp. 138–149. ISBN: 978-3-642-30972-4.
- [51] D. Musiige, L. Vincent, F. Anton, and D. Mioc. “LTE handset RF power consumption emulation”. In: *Society of Digital Information and Wireless Communications*. 2013.
- [52] Muhammad Yasir Malik. “Power Consumption Analysis of a Modern Smartphone”. In: *CoRR* abs/1212.1896 (2012).
- [53] Ning Ding, Daniel Wagner, Xiaomeng Chen, Abhinav Pathak, Y. Charlie Hu, and Andrew Rice. “Characterizing and Modeling the Impact of Wireless Signal Strength on Smartphone Battery Drain”. In: *SIGMETRICS Perform. Eval. Rev.* 41.1 (May 2013), pp. 29–40. ISSN: 0163-5999.
- [54] A. A. Nacci, F. Trovò, F. Maggi, M. Ferroni, A. Cazzola, D. Sciuto, and M. D. Santambrogio. “Adaptive and Flexible Smartphone Power Modeling”. In: *Mob. Netw. Appl.* 18.5 (Oct. 2013), pp. 600–609. ISSN: 1383-469X.
- [55] A.E. Kouche, A. M. Rashwan, and H. Hassanein. “Energy Consumption Measurements and Reduction of Zigbee based Wireless Sensor Networks”. In: *Globecom, 2013 IEEE*. 2013, pp. 579–584.

- [56] Chengke Wang, Fengrun Yan, Yao Guo, and Xiangqun Chen. “Power estimation for mobile applications with profile-driven battery traces”. In: *Low Power Electronics and Design (ISLPED), 2013 IEEE International Symposium on*. Sept. 2013, pp. 120–125.
- [57] B. Dusza, C. Ide, L. Cheng, and C. Wietfeld. “An Accurate Measurement-Based Power Consumption Model for LTE Uplink Transmissions”. In: *IEEE INFOCOM*. 2013.
- [58] Takeshi Kamiyama, Hiroshi Inamura, and Ken Ohta. “A model-based energy profiler using online logging for Android applications”. In: *Mobile Computing and Ubiquitous Networking (ICMU), 2014 Seventh International Conference on*. Jan. 2014, pp. 7–13.
- [59] H. Holma and A. Toskala. *LTE for UMTS, OFDMA and SC-FDMA Based Radio Access*. John Wiley & Sons, Ltd., 2009.
- [60] 3GPP. *RRC protocol specification*. TS 36.331 V8.14.0. 2011.
- [61] Nokia. *DRX parameters in LTE*. 3GPP R2-071285. 2007.
- [62] C. Bontu and E. Illidge. “DRX mechanism for power saving in LTE”. In: *Communications Magazine, IEEE* 47.6 (May 2009), pp. 48–55. ISSN: 0163-6804.
- [63] Lei Zhou, Haibo Xu, Hui Tian, Youjun Gao, Lei Du, and Lan Chen. “Performance Analysis of Power Saving Mechanism with Adjustable DRX Cycles in 3GPP LTE”. In: *Vehicular Technology Conference, 2008. VTC 2008-Fall. IEEE 68th*. Sept. 2008, pp. 1–5. DOI: 10.1109/VETECF.2008.312.
- [64] J. Wigard, T. Kolding, L. Dalsgaard, and C. Coletti. “On the User Performance of LTE UE Power Savings Schemes with Discontinuous Reception in LTE”. In: *Communications Workshops, IEEE International Conference on*. 2009, pp. 1–5.
- [65] Gye Su Kim, Yeong Ho Je, and Suki Kim. “An adjustable power management for optimal power saving in LTE terminal baseband modem”. In: *Consumer Electronics, IEEE Transactions on* 55.4 (Nov. 2009), pp. 1847–1853. ISSN: 0098-3063. DOI: 10.1109/TCE.2009.5373741.
- [66] M. Hassan, Myoungbo Kwak, V.W. Leung, Chin Hsia, J.J. Yan, D.F. Kimball, L.E. Larson, and P.M. Asbeck. “High efficiency envelope tracking power amplifier with very low quiescent power for 20 MHz LTE”. In: *Radio Frequency Integrated Circuits Symposium (RFIC), 2011 IEEE*. May 2011, pp. 1–4. DOI: 10.1109/RFIC.2011.5940618.
- [67] C. Studer, C. Benkeser, S. Belfanti, and Quiting Huang. “Design and Implementation of a Parallel Turbo-Decoder ASIC for 3GPP-LTE”. In: *Solid-State Circuits, IEEE Journal of* 46.1 (Jan. 2011), pp. 8–17. ISSN: 0018-9200. DOI: 10.1109/JSSC.2010.2075390.
- [68] C.U. Castellanos, D.L. Villa, C. Rosa, K.I. Pedersen, F.D. Calabrese, P.-H. Michaelsen, and J. Michel. “Performance of Uplink Fractional Power Control in UTRAN LTE”. In: *Vehicular Technology Conference Spring, IEEE*. 2008, pp. 2517–2521.

- [69] Zhenwei Li, Changchuan Yin, and Guangxin Yue. “Delay-Bounded Power-Efficient Packet Scheduling for Uplink Systems of LTE”. In: *Wireless Communications, Networking and Mobile Computing, 2009. WiCom '09. 5th International Conference on*. Sept. 2009, pp. 1–4. DOI: 10.1109/WICOM.2009.5303491.
- [70] International Telecommunication Union - Radiocommunication Sector. *Requirements related to technical performance for IMT-Advanced radio interface(s)*. Report M.2134. 2008.
- [71] 3GPP. *Physical channels and modulation*. TS 36.211 V8.9.0. 2010.
- [72] 3GPP. *E-UTRA, Physical layer procedures*. TS 36.213 V8.8.0. 2009.
- [73] Kuo-Chang Ting, Hwang-Cheng Wang, Chih-Cheng Tseng, and Fang-Chang Kuo. “Energy-Efficient DRX Scheduling for QoS Traffic in LTE Networks”. In: *Parallel and Distributed Processing with Applications, IEEE International Symposium on*. 2011.
- [74] R. Love, R. Kuchibhotla, A. Ghosh, R. Ratasuk, B. Classon, and Y. Blankenship. “Downlink Control Channel Design for 3GPP LTE”. In: *IEEE Wireless Communications and Networking Conference WCNC*. 2008.
- [75] Ericsson. *UE specific reference signal pattern*. 3GPP R1-080506. 2008.
- [76] M. Boussif, N. Quintero, F.D. Calabrese, C. Rosa, and J. Wigard. “Interference Based Power Control Performance in LTE Uplink”. In: *Wireless Communication Systems. IEEE Int. Symp. on*. 2008, pp. 698–702.
- [77] R. Müllner, C. F. Ball, M. Boussif, J. Lienhart, P. Hric, H. Winkler, K. Kremnitzer, and R. Kronlachner. “Enhancing uplink performance in UTRAN LTE networks by load adaptive power control”. In: *European Transactions on Telecommunications* 21.5 (2010), pp. 458–468. ISSN: 1541-8251.
- [78] H. Holma and A. Toskala. *WCDMA for UMTS - HSPA Evolution and LTE*. 5th. John Wiley & Sons, Ltd., 2010. ISBN: 978-0-470-68646-1.
- [79] F.D. Calabrese, C. Rosa, M. Anas, P.H. Michaelsen, K.I. Pedersen, and P.E. Mogensen. “Adaptive Transmission Bandwidth Based Packet Scheduling for LTE Uplink”. In: *Vehicular Technology Conference Fall, IEEE 68th*. 2008, pp. 1–5.
- [80] K.I. Pedersen, F. Frederiksen, C. Rosa, H. Nguyen, L.G.U. Garcia, and Yuanye Wang. “Carrier Aggregation for LTE-Advanced: Functionality and Performance Aspects”. In: *Communications Magazine, IEEE* 49.6 (June 2011), pp. 89–95. ISSN: 0163-6804.
- [81] 3GPP. *Feasibility Study for Further Advancements for E-UTRA (LTE-Advanced)*. TS 36.912 V9.3.0. 2010.
- [82] Zukang Shen, A. Papasakellariou, J. Montojo, D. Gerstenberger, and Fangli Xu. “Overview of 3GPP LTE-Advanced Carrier Aggregation for 4G Wireless Communications”. In: *Communications Magazine, IEEE* 50.2 (Feb. 2012), pp. 122–130.
- [83] Samsung Mobile. *Samsung LTE Leadership and Future-Focused Innovation Produces World’s First LTE-Advanced Smartphone*. Press Release. May 2013.

- [84] 4G Americas. *4G Americas' Summary of Global 5G Initiatives*. White paper. 2014.
- [85] Qualcomm. *The Evolution of Mobile Technologies: 1G to 2G to 3G to 4G LTE*. 2014. URL: <http://www.qualcomm.com/media/documents/evolution-mobile-technologies-1g-2g-3g-4g-lte>.
- [86] H. Holma and A. Toskala. *LTE-advanced: 3GPP Solution for IMT-advanced*. John Wiley & Sons, Ltd., 2012. ISBN: 9781119974055.
- [87] P. Mogensen, K. Pajukoski, B. Raaf, E. Tiirola, E. Lähetkangas, I.Z. Kovacs, G. Berardinelli, L.G.U. Garcia, Liang Hu, and A.F. Cattoni. "B4G local area: High level requirements and system design". In: *Globecom Workshops, 2012 IEEE*. 2012, pp. 613–617.
- [88] Nokia Networks. *Working document towards a preliminary draft new report ITU-R on IMT traffic estimates beyond the year 2020*. Document 5D/TEMP/435-E. Oct. 2014.
- [89] Yi Wang, Jian Li, Lei Huang, Yao Jing, A Georgakopoulos, and P. Demestichas. "5G Mobile: Spectrum Broadening to Higher-Frequency Bands to Support High Data Rates". In: *Vehicular Technology Magazine, IEEE* 9.3 (Sept. 2014), pp. 39–46. ISSN: 1556-6072. DOI: 10.1109/MVT.2014.2333694.
- [90] P. Demestichas, A. Georgakopoulos, D. Karvounas, K. Tsagkaris, V. Stavroulaki, Jianmin Lu, Chunshan Xiong, and Jing Yao. "5G on the Horizon: Key Challenges for the Radio-Access Network". In: *Vehicular Technology Magazine, IEEE* 8.3 (2013), pp. 47–53.
- [91] P. Mogensen, K. Pajukoski, E. Tiirola, E. Lähetkangas, J. Vihriälä, S. Vesterinen, M. Laitila, G. Berardinelli, GWOD. Costa, LGU. Garcia, FML. Tavares, and AF. Cattoni. "5G small cell optimized radio design". In: *GlobeCom* (Dec. 2013).
- [92] International Wireless Industry Consortium. *Evolutionary & Disruptive Visions Towards Ultra High Capacity Networks*. White paper. 2014.
- [93] Metis. *Mobile and wireless communications Enablers for the Twenty-twenty Information Society*. 2014. URL: www.metis2020.com.
- [94] E. Dahlman, G. Mildh, S. Parkvall, J. Peisa, J. Sachs, and Y. Selen. "5G Radio Access". In: *Ericsson Review* 91.6 (June 2014). ISSN: 0014-0171.
- [95] 3GPP. *3GPP Technologies*. 2013. URL: www.3gpp.org/Technologies.
- [96] 5GNOW. *5th Generation Non-Orthogonal Waveforms for Asynchronous Signalling*. 2013. URL: www.5gnow.eu.
- [97] 5G-PPP. *5G Infrastructure Public Private Partnership*. 2014. URL: <http://5g-ppp.eu/>.
- [98] T.S. Rappaport. *Wireless Communications Principles and Practice*. 2nd. Prentice Hall, 2002. ISBN: 0130422320.
- [99] I. Rodriguez, H.C. Nguyen, T.B. Sørensen, J. Elling, J.A. Holm, P. Mogensen, and B. Vejlggaard. "Analysis of 38 GHz mmWave Propagation Characteristics of Urban Scenarios". In: *Submitted for IEEE ICC*. 2015.

- [100] D. Gesbert. “Multipath: curse or blessing? A system performance analysis of MIMO wireless systems”. In: *Communications, 2004 International Zurich Seminar on*. 2004, pp. 14–17.
- [101] F. Bohagen, P. Orten, and G.E. Oien. “Design of Optimal High-Rank Line-of-Sight MIMO Channels”. In: *Wireless Communications, IEEE Transactions on* 6.4 (Apr. 2007), pp. 1420–1425. ISSN: 1536-1276.
- [102] David Tse and Pramod Viswanath. *Fundamentals of Wireless Communication*. Cambridge University Press, 2005. ISBN: 0521845270.
- [103] E. McCune. *Practical Digital Wireless Signals*. The Cambridge RF and Microwave Engineering Series. Cambridge University Press, 2010. ISBN: 978-0-521-51630-3.
- [104] MB. Pautet M. Mouly. *The GSM System for Mobile Communications*. 1992. ISBN: 2950719007.
- [105] B. E. Priyanto, H. Codina, S. Rene, T. B. Sørensen, and P. Mogensen. “Initial Performance Evaluation of DFT-Spread OFDM Based SC-FDMA for UTRA LTE Uplink”. In: *IEEE 65th VTC Spring* (Apr. 2007). ISSN: 1550-2252.
- [106] Y. Saito, Y. Kishiyama, A. Benjebbour, T. Nakamura, A. Li, and K. Higuchi. “Non-Orthogonal Multiple Access (NOMA) for Cellular Future Radio Access”. In: *VTC Spring, IEEE 77th* (2013).
- [107] Gilberto Berardinelli, Fernando M.L. Tavares, Troels B. Sørensen, Preben Mogensen, and Kari Pajukoski. “Zero-tail DFT-spread-OFDM signals”. In: *Globecom Workshops, IEEE*. Dec. 2013, pp. 229–234.
- [108] F.M.L. Tavares, G. Berardinelli, N.H. Mahmood, T.B. Sørensen, and P. Mogensen. “On the Potential of Interference Rejection Combining in B4G Networks”. In: *Vehicular Technology Conference (VTC Fall), 2013 IEEE 78th*. Sept. 2013, pp. 1–5.
- [109] S. Dengo and H. Balakrishnan. “Traffic-aware techniques to reduce 3G/LTE wireless energy consumption”. In: *8th CoNEXT*. 2012.
- [110] M. Gupta, S.C. Jha, AT. Koc, and R. Vannithamby. “Energy impact of emerging mobile internet applications on LTE networks: issues and solutions”. In: *Communications Magazine, IEEE* 51.2 (Feb. 2013), pp. 90–97. ISSN: 0163-6804. DOI: 10.1109/MCOM.2013.6461191.
- [111] Marta Gatnau Sarret, Davide Catania, Frank Frederiksen, Andrea F. Cattoni, Gilberto Berardinelli, and Preben Mogensen. “Improving link robustness in 5G ultra-dense small cells by hybrid ARQ”. In: *Wireless Communications Systems (ISWCS), 2014 11th International Symposium on*. Aug. 2014, pp. 491–495. DOI: 10.1109/ISWCS.2014.6933403.
- [112] D. Catania, M. Gatnau, A.F. Cattoni, F. Frederiksen, G. Berardinelli, and P. Mogensen. “The Potential of Flexible UL/DL Slot Assignment in 5G Systems”. In: *VTC Fall, IEEE 80th* (2014).
- [113] G. Szczepkowski and R. Farrell. “Linearity vs. power consumption of CMOS LNAs in LTE systems”. In: *Signals and Systems Conference (ISSC 2013), 24th IET Irish*. June 2013, pp. 1–8. DOI: 10.1049/ic.2013.0044.

- [114] R. Brederlow, W. Weber, J. Sauerer, S. Donnay, P. Wambacq, and M. Vertregt. “A mixed-signal design roadmap”. In: *Design Test of Computers, IEEE* 18.6 (Nov. 2001), pp. 34–46. ISSN: 0740-7475. DOI: 10.1109/54.970422.
- [115] International Technology Roadmap for Semiconductors. *Process Integration, Devices, and Structures*. 2013.
- [116] S. Haykin. *Communication Systems*. John Wiley and Sons, Inc., 2001. ISBN: 0471178691.
- [117] José M. de la Rosa, Rafael Castro-López, Alonso Morgado, Edwin C. Becerra-Alvarez, Rocio del Río, Francisco V. Fernández, and Belén Pérez-Verdú. “Adaptive CMOS analog circuits for 4G mobile terminals - Review and state-of-the-art survey”. In: *Microelectronics Journal* 40.1 (2009), pp. 156–176. ISSN: 0026-2692. DOI: <http://dx.doi.org/10.1016/j.mejo.2008.07.001>.
- [118] R. Szczepkowski G. Farrell. “Study of Linearity and Power Consumption Requirements of CMOS Low Noise Amplifiers in Context of LTE Systems and Beyond”. In: *International Scholarly Research Notices - Electronics*. Mar. 2014. DOI: doi:10.1155/2014/391240.
- [119] T. Baker. *Successful LNA design involves performance trade-offs*. Nov. 2006. URL: www.rfdesign.com.
- [120] Federal Communications Commission. *FCC 02-48: Revision of Part 15 of the Commission’s Rules Regarding Ultra-Wideband Transmission Systems*. Apr. 2002.
- [121] International Technology Roadmap for Semiconductors. *Process Integration, Devices, and Structures*. 2003.
- [122] R. Ramzan, F. Zafar, S. Arshad, and Q. Wahab. “Figure of merit for narrowband, wideband and multiband LNAs”. In: *International Journal of Electronics* 99.11 (2012), pp. 1603–1610. DOI: 10.1080/00207217.2012.692635.
- [123] D. Catania and F. Frederiksen. *Dynamic Range Needs in 5G Deployments*. Internal Nokia presentation. Sept. 2014.
- [124] B. Murmann. *ADC Performance Survey 1997-2014*. 2014. URL: <http://www.stanford.edu/m%CC%83urmann/adcsurvey.html>.
- [125] B.E. Jonsson. *A/D-converter performance evolution v.1.1*. 2013. URL: www.admsdesign.com.
- [126] Gabriele Manganaro. “Advanced Data Converters”. In: *Cambridge University Press*. 2012.
- [127] B.E. Jonsson. “A survey of A/D-Converter performance evolution”. In: *17th IEEE conference on Electronics, Circuits, and Systems*. 2010.
- [128] Stacy Ho. *Email discussion*. MediaTek USA Inc. 2014.
- [129] J. Ketonen, M. Juntti, and J.R. Cavallaro. “Performance-Complexity Comparison of Receivers for a LTE MIMO-OFDM System”. In: *Signal Processing, IEEE Transactions on* 58.6 (June 2010), pp. 3360–3372. ISSN: 1053-587X. DOI: 10.1109/TSP.2010.2044290.

- [130] G.E. Moore. “Cramming More Components Onto Integrated Circuits”. In: *Proceedings of the IEEE* 86.1 (Jan. 1998), pp. 82–85. ISSN: 0018-9219. DOI: 10.1109/JPROC.1998.658762.
- [131] P.J. Bentley. *Digitized: The science of computers and how it shapes our world*. OUP Oxford, 2012. ISBN: 9780191633683.
- [132] G. Frantz. “Digital signal processor trends”. In: *Micro, IEEE* 20.6 (2000), pp. 52–59. ISSN: 0272-1732.
- [133] A.S. Sedra and K.C. Smith. *Microelectronic Circuits*. 5th ed. Oxford University Press, 2004. ISBN: 0195142527.
- [134] M. Belleville and O. Faynot. “Evolution of Deep Submicron Bulk and SOI Technologies”. In: *Low-power Electronics Design*. Ed. by C. Piguet. CRC Press LLC, 2005. ISBN: 0849319412.
- [135] W. Nebel and D. Helms. “High-Level Power Estimation and Analysis”. In: *Low-power Electronics Design*. Ed. by C. Piguet. CRC Press LLC, 2005. ISBN: 0849319412.
- [136] A. Didioui, C. Bernier, D. Morche, and O. Sentieys. “Power reconfigurable receiver model for energy-aware applications”. In: *IEEE 56th International MWS-CAS*. 2013.
- [137] B. Noethen, O. Arnold, E. Perez Adeva, T. Seifert, E. Fischer, S. Kunze, E. Matius, G. Fettweis, H. Eisenreich, G. Ellguth, S. Hartmann, S. Hoppner, S. Schiefer, J.-U. Schlusler, S. Scholze, D. Walter, and R. Schuffny. “10.7 A 105GOPS 36mm² heterogeneous SDR MPSoC with energy-aware dynamic scheduling and iterative detection-decoding for 4G in 65nm CMOS”. In: *Solid-State Circuits Conference Digest of Technical Papers (ISSCC), 2014 IEEE International*. Feb. 2014, pp. 188–189. DOI: 10.1109/ISSCC.2014.6757394.
- [138] Shan Huang, Ziyuan Zhu, Yongtao Su, and Jinglin Shi. “A system-level design approach for SDR-based MPSoC in LTE baseband processing”. In: *Circuits and Systems (MWSCAS), 2014 IEEE 57th International Midwest Symposium on*. Aug. 2014, pp. 623–626. DOI: 10.1109/MWSCAS.2014.6908492.
- [139] Zhu Ziyuan, Tang Shan, Su Yongtao, Han Juan, Sun Gang, and Shi Jinglin. “A 100 GOPS ASP based baseband processor for wireless communication”. In: *Design, Automation Test in Europe Conference Exhibition (DATE), 2013*. Mar. 2013, pp. 121–124. DOI: 10.7873/DATE.2013.038.
- [140] P. Jensen, J.L. Faaborg, and M. Rumney. “Temperature impact on drive test throughput measurements”. In: *COST IC1004 TD(11)02069* (2011).
- [141] Nujira. *High Accuracy Envelope Tracking for LTE’ Smartphones and Modems*. 2013. URL: www.nujira.com/pages/files/Coolteq.L%5C_Feb%5C_2013.pdf.
- [142] Qualcomm. *QFE1100: The World’s First Envelope Tracking Technology for 3G/4G LTE Devices*. 2013. URL: http://www.qualcomm.com/sites/default/files/uploads/gobi_et_infographic_rd3.pdf.
- [143] Wang Zhancang. “Modern High Efficiency Amplifier Design: Envelope Tracking, Doherty and Outphasing.” In: *Microwave Journal* 57.4 (2014), pp. 20–32. ISSN: 01926225.

- [144] ETA Devices. *Eta Devices Launches ETAdvanced - Next Generation Envelope Tracking for Smartphones*. Press Release. 2014.
- [145] 3GPP. *UE radio transmission and reception*. TS 36.101 V8.20.0. 2013.
- [146] Anonymous RF company. *Presentations and discussions*. Confidential. 2014.
- [147] P. Saad, H.M. Nemati, K. Andersson, and C. Fager. “Highly efficient GaN-HEMT power amplifiers at 3.5 GHz and 5.5 GHz”. In: *Wireless and Microwave Technology Conference (WAMICON), 2011 IEEE 12th Annual*. Apr. 2011, pp. 1–4. DOI: 10.1109/WAMICON.2011.5872865.
- [148] A.M. Niknejad, D. Chowdhury, and Jiashu Chen. “Design of CMOS Power Amplifiers”. In: *Microwave Theory and Techniques, IEEE Transactions on* 60.6 (June 2012), pp. 1784–1796. ISSN: 0018-9480. DOI: 10.1109/TMTT.2012.2193898.
- [149] H. Dabag, B. Hanafi, F. Golcuk, A. Agah, J.F. Buckwalter, and P.M. Asbeck. “Analysis and Design of Stacked-FET Millimeter-Wave Power Amplifiers”. In: *Microwave Theory and Techniques, IEEE Transactions on* 61.4 (Apr. 2013), pp. 1543–1556. ISSN: 0018-9480. DOI: 10.1109/TMTT.2013.2247698.
- [150] A. Cathelin, B. Martineau, N. Seller, S. Douyere, J. Gorisse, S. Pruvost, C. Raynaud, F. Giancesello, S. Montusclat, S.P. Voinigescu, A.M. Niknejad, D. Belot, and J- P. Schoellkopf. “Design for millimeter-wave applications in silicon technologies”. In: *Solid State Circuits Conference, 2007. ESSCIRC 2007. 33rd European*. Sept. 2007, pp. 464–471. DOI: 10.1109/ESSCIRC.2007.4430343.
- [151] A. Osseiran, F. Boccardi, V. Braun, K. Kusume, P. Marsch, M. Maternia, O. Queseth, M. Schellmann, H. Schotten, H. Taoka, H. Tullberg, M.A. Uusitalo, B. Timus, and M. Fallgren. “Scenarios for 5G mobile and wireless communications: the vision of the METIS project”. In: *Communications Magazine, IEEE* 52.5 (May 2014), pp. 26–35. ISSN: 0163-6804.
- [152] Cisco. *The Zettabyte Era: Trends and Analysis*. White paper. 2014.
- [153] Ashwin Rao, Arnaud Legout, Yeon-sup Lim, Don Towsley, Chadi Barakat, and Walid Dabbous. “Network Characteristics of Video Streaming Traffic”. In: *Proceedings of the Seventh Conference on Emerging Networking EXperiments and Technologies*. CoNEXT ’11. ACM, 2011, 25:1–25:12. ISBN: 978-1-4503-1041-3.
- [154] Cisco. *Cisco VNI Service Adoption Forecast, 2013–2018*. White paper. 2014.
- [155] Groupe Speciale Mobile Association. *Connected Living Latin America Summit*. June 2012. URL: <http://www.gsma.com/connectedliving/wp-content/uploads/2012/05/GSMA-Ana-Tavares-Lattibeaudiere-Tues-26th-10.00am-Presentation.pdf>.
- [156] 3GPP. *Study on provision of low-cost Machine-Type Communications (MTC) User Equipments (UEs) based on LTE*. TR 36.888 v.12.0.0. 2013.
- [157] oneM2M. 2014. URL: <http://www.onem2m.org>.
- [158] European Commission. *eCall: Time saved = lives saved*. Oct. 2014. URL: <http://ec.europa.eu/digital-agenda/ecall-time-saved-lives-saved>.

- [159] Woon Hau Chin, Zhong Fan, and Russell J. Haines. “Emerging technologies and research challenges for 5G wireless networks”. In: *IEEE Wireless Commun.* 21.2 (2014), pp. 106–112.
- [160] Tuomas Tirronen, Anna Larmo, Joachim Sachs, Bengt Lindoff, and Niclas Wiberg. “Machine-to-machine communication with long-term evolution with reduced device energy consumption”. In: *Transactions on Emerging Telecommunications Technologies* 24.4 (2013), pp. 413–426. ISSN: 2161-3915. DOI: 10.1002/ett.2643. URL: <http://dx.doi.org/10.1002/ett.2643>.
- [161] Motorola. *TD-LTE, Exciting Alternative, Global Momentum*. White paper. 2010.
- [162] Cadex Electronics Inc. *BU-802b: Elevating Self-discharge*. Accessed on October 9th 2014. Oct. 2014. URL: http://batteryuniversity.com/learn/article/elevating_self_discharge.
- [163] P.R. Turner. *Guide to Scientific Computing*. 2nd ed. Macmillan Press LTD, 2000. ISBN: 0333794508.
- [164] Christian Hambeck, Stefan Mahlknecht, and Thomas Herndl. “A 2.4 uW Wake-up Receiver for wireless sensor nodes with -71dBm sensitivity”. In: *ISCAS’11*. 2011, pp. 534–537.
- [165] Fraunhofer Institute for Integrated Circuits IIS. *Ultra low-current wakeup receiver*. Datasheet. 2010.
- [166] Philippe Le-Huy and Sébastien Roy. “Low-Power Wake-Up Radio for Wireless Sensor Networks”. In: *Mob. Netw. Appl.* 15.2 (Apr. 2010), pp. 226–236. ISSN: 1383-469X. DOI: 10.1007/s11036-009-0184-3. URL: <http://dx.doi.org/10.1007/s11036-009-0184-3>.
- [167] Joaquim Oller, Ilker Demirkol, Jordi Casademont, Josep Paradells, Gerd Ulrich Gamm, and Leonhard Reindl. “Performance Evaluation and Comparative Analysis of SubCarrier Modulation Wake-up Radio Systems for Energy-Efficient Wireless Sensor Networks”. In: *Sensors* 14.1 (2013), pp. 22–51. ISSN: 1424-8220. DOI: 10.3390/s140100022.
- [168] N.M. Pletcher, S. Gambini, and J. Rabaey. “A 52 uW Wake-Up Receiver With -72 dBm Sensitivity Using an Uncertain-IF Architecture”. In: *Solid-State Circuits, IEEE Journal of* 44.1 (Jan. 2009), pp. 269–280. ISSN: 0018-9200. DOI: 10.1109/JSSC.2008.2007438.
- [169] Suhua Tang, H. Yomo, Y. Kondo, and S. Obana. “Wakeup Receiver for Radio-On-Demand Wireless LANs”. In: *Global Telecommunications Conference (GLOBECOM 2011), 2011 IEEE*. Dec. 2011, pp. 1–6. DOI: 10.1109/GLOCOM.2011.6133533.
- [170] C.C. Enz, A. El-Hoiydi, J.-D. Decotignie, and V. Peiris. “WiseNET: an ultralow-power wireless sensor network solution”. In: *Computer* 37.8 (Aug. 2004), pp. 62–70. ISSN: 0018-9162. DOI: 10.1109/MC.2004.109.
- [171] Microsemi. *ZL70103 Medical Implantable RF Transceiver, rev.1*. Datasheet. 2014.

- [172] Eugene Shih, Paramvir Bahl, and Michael J. Sinclair. “Wake on Wireless: An Event Driven Energy Saving Strategy for Battery Operated Devices”. In: *Proceedings of the 8th Annual International Conference on Mobile Computing and Networking*. MobiCom '02. ACM, 2002, pp. 160–171. ISBN: 1-58113-486-X. DOI: 10.1145/570645.570666. URL: <http://doi.acm.org/10.1145/570645.570666>.
- [173] Wen-Chan Shih, Raja Jurdak, Bih-Hwang Lee, and David Abbott. “High sensitivity wake-up radio using spreading codes: design, evaluation, and applications”. In: *EURASIP Journal on Wireless Communications and Networking* 2011.1, 26 (2011). DOI: 10.1186/1687-1499-2011-26. URL: <http://dx.doi.org/10.1186/1687-1499-2011-26>.
- [174] Texas Instruments. *CC2541, 2.4-GHz Bluetooth low energy and Proprietary System-on-Chip*. Datasheet. 2012.
- [175] Texas Instruments. *ISM-Band and Short Range Device Regulatory Compliance Overview*. Application Report SWRA048. 2005.
- [176] Y. Kondo, H. Yomo, Suhua Tang, M. Iwai, T. Tanaka, H. Tsutsui, and S. Obana. “Wake-up radio using IEEE 802.11 frame length modulation for Radio-On-Demand wireless LAN”. In: *Personal Indoor and Mobile Radio Communications (PIMRC), 2011 IEEE 22nd International Symposium on*. Sept. 2011, pp. 869–873. DOI: 10.1109/PIMRC.2011.6140091.
- [177] Kendall Su. *Analog Filters*. 2nd ed. Kluwer Academic Publishers, 2002.
- [178] 3GPP. *Study on LTE Device to Device Proximity Services; Radio Aspects*. TR 36.843 v.12.0.1. 2014.
- [179] M.N. Tehrani, M. Uysal, and H. Yanikomeroglu. “Device-to-device communication in 5G cellular networks: challenges, solutions, and future directions”. In: *Communications Magazine, IEEE* 52.5 (May 2014), pp. 86–92. ISSN: 0163-6804.
- [180] S. Mumtaz and j. Rodriguez. *Smart Device to Smart Device Communication*. Springer, 2014. ISBN: 9783319049625.
- [181] P. Pahlevani, M. Hundebøll, M.V. Pedersen, D. Lucani, H. Charaf, F.H.P. Fitzek, H. Bagheri, and M. Katz. “Novel concepts for device-to-device communication using network coding”. In: *Communications Magazine, IEEE* 52.4 (Apr. 2014), pp. 32–39. ISSN: 0163-6804. DOI: 10.1109/MCOM.2014.6807944.
- [182] G. Fodor, A. Pradini, and A. Gattami. “Device-to-Device Communications and Network Coding: Friends or Foes?” In: *IEEE Comsoc MMTC E-Letter* 9.1 (Jan. 2014), pp. 33–35.
- [183] 3GPP. *Evolved Universal Terrestrial Radio Access and Evolved Universal Terrestrial Radio Access Network - Overall description - Stage 2*. TS 36.300 V8.12.0. 2010.
- [184] 3GPP. *MAC protocol specification*. TS 36.321 V8.9.0. 2010.
- [185] 3GPP. *Non-Access-Stratum protocol for Evolved Packet System Stage 3*. TS 24.301 V8.10.0. 2011.
- [186] 3GPP. *Evolved Universal Terrestrial Radio Access Network - Architecture description*. TS 36.401 V8.8.0. 2010.

- [187] IMS Research. *Handset Power Requirements Dramatically Outpacing Capacity*. 2009.
- [188] Ye Li, B. Bakkaloglu, and C. Chakrabarti. “A System Level Energy Model and Energy-Quality Evaluation for Integrated Transceiver Front-Ends”. In: *Very Large Scale Integration (VLSI) Systems, IEEE Transactions on* 15.1 (Jan. 2007), pp. 90–103.
- [189] John C. McCullough, Yuvraj Agarwal, Jaideep Chandrashekar, Sathyanarayan Kuppuswamy, Alex C. Snoeren, and Rajesh K. Gupta. “Evaluating the effectiveness of model-based power characterization”. In: *Proceedings of USENIX conference*. 2011.
- [190] 3GPP. *Multiplexing and channel coding*. TS 36.212 V8.8.0. 2010.
- [191] Bobae Kim, Cholho Kwak, and Jongsoo Lee. “A Dual-Mode Power Amplifier With On-Chip Switch Bias Control Circuits for LTE Handsets”. In: *Circuits and Systems II, IEEE Transactions on* 58 (2011), pp. 857–861.
- [192] Yan Li, J. Lopez, Po-Hsing Wu, Weibo Hu, Ruili Wu, and D.Y.C. Lie. “A SiGe Envelope-Tracking Power Amplifier With an Integrated CMOS Envelope Modulator for Mobile WiMAX/3GPP LTE Transmitters”. In: *Microwave Theory and Techniques, IEEE Transactions on* 59 (2011), pp. 2525–2536.
- [193] J. Borremans, G. Mandal, V. Giannini, B. Debaillie, M. Ingels, T. Sano, B. Verbruggen, and J. Craninckx. “A 40 nm CMOS 0.4-6 GHz Receiver Resilient to Out-of-Band Blockers”. In: *Solid-State Circuits, IEEE Journal of* 46.7 (July 2011), pp. 1659–1671.
- [194] C. Studer, C. Benkeser, S. Belfanti, and Quiting Huang. “Design and Implementation of a Parallel Turbo-Decoder ASIC for 3GPP-LTE”. In: *Solid-State Circuits, IEEE Journal of* 46.1 (Jan. 2011), pp. 8–17. ISSN: 0018-9200.
- [195] Lajos L. Hanzo, T. H. Liew, B. L. Yeap, R. Y. S. Tee, and Soon Xin Ng. *Turbo Coding, Turbo Equalisation and Space-Time Coding: EXIT-Chart-Aided Near-Capacity Designs for Wireless Channels*. Wiley-IEEE Press, 2011.
- [196] M. Kennedy, H. Venkataraman, and G. Muntean. “Energy Consumption Analysis and Adaptive Energy Saving Solutions for Mobile Device Applications”. In: *Springer* (2011).
- [197] 3GPP. *Long Term Evolution*. 2012. URL: <http://www.3gpp.org/article/lte>.
- [198] H. Holma and A. Toskala. *LTE for UMTS - Evolution to LTE-Advanced*. 2nd. John Wiley & Sons, Ltd., 2011. ISBN: 978-0-470-60000-3.
- [199] Haolu Xie, O. Oliaei, P. Rakers, R. Fernandez, J. Xiang, J. Parkes, J. Riches, R. Verellen, M. Rahman, V. Bhan, and D.B. Schwartz. “Single-Chip Multiband EGPRS and SAW-Less LTE WCDMA CMOS Receiver With Diversity”. In: *Microwave Theory and Techniques* 60.5 (2012). ISSN: 0018-9480.
- [200] Samsung. *2GHz+ processing power aimed at high-performance mobile applications*. 2013. URL: <http://www.samsung.com/us/business/oem-solutions/pdfs/28nmLPH-DS-Final-0212.pdf>.

- [201] Stephane Cordova. “Harvesting the Future of Mobile”. In: *IQ Magazine*. Vol. 9. 3. 2010, pp. 26–29.
- [202] J. Öfversten. *Mobile Internet Battery Life*. Forum Nokia Webinar. 2009.
- [203] T. Kolding, J. Wigard, and L. Dalsgaard. “Balancing power saving and single user experience with discontinuous reception in LTE”. In: *Wireless Communication Systems. IEEE Int. Symp. on*. 2008, pp. 713–717.
- [204] Abdelnaser Adas. “Traffic Models in Broadband Networks”. In: *IEEE Communications Magazine* 35 (1997), pp. 82–89.
- [205] Alberto Leon-Garcia. *Probability and Random Processes for Electrical Engineering*. 2nd. Addison Wesley, 1994.
- [206] T. Wirth, L. Thiele, T. Haustein, J. Brandenburg, and B. Stabernack. “Scalable video broadcasting trials in 4G cellular deployments”. In: *Future Network and Mobile Summit, 2010*. May 2010, pp. 1–7.
- [207] 3GPP. *UE radio transmission and reception*. TS 36.101 V8.10.0. 2010.
- [208] M. Boussif, C. Rosa, J. Wigard, and R. Müllner. “Load adaptive power control in LTE Uplink”. In: *Wireless Conference, European*. 2010, pp. 288–293.
- [209] B. Muhammad and A. Mohammed. “Performance Evaluation of Uplink Closed Loop Power Control for LTE System”. In: *Vehicular Technology Conference Fall, IEEE 70th*. 2009, pp. 1–5.
- [210] A. Simonsson and A. Furuskar. “Uplink Power Control in LTE - Overview and Performance”. In: *Vehicular Technology Conference, VTC 2008-Fall. IEEE 68th*. Sept. 2008, pp. 1–5.
- [211] Robert Müllner, Carsten F. Ball, Kolio Ivanov, Johann Lienhart, and Peter Hric. “Contrasting open-loop and closed-loop power control performance in UTRAN LTE uplink by UE trace analysis”. In: *Proceedings of the IEEE international conference on Communications*. 2009, pp. 4031–4036. ISBN: 978-1-4244-3434-3.
- [212] F. Capozzi, D. Laselva, F. Frederiksen, J. Wigard, I.Z. Kovacs, and P.E. Mogenssen. “UTRAN LTE Downlink System Performance under Realistic Control Channel Constraints”. In: *Vehicular Technology Conference Fall, IEEE 70th*. 2009, pp. 1–5.
- [213] Phillipa Gill, Martin Arlitt, Zongpeng Li, and Anirban Mahanti. “Youtube traffic characterization: a view from the edge”. In: *Proceedings of the 7th ACM SIGCOMM conference on Internet measurement*. 2007, pp. 15–28. ISBN: 978-1-59593-908-1.
- [214] Xu Cheng, C. Dale, and Jiangchuan Liu. “Statistics and Social Network of YouTube Videos”. In: *Quality of Service. 16th International Workshop on*. 2008, pp. 229–238.
- [215] Dongwoon Bai, Cheolhee Park, Jungwon Lee, Hoang Nguyen, J. Singh, A. Gupta, Zhouyue Pi, Taeyoon Kim, Chaiman Lim, Min-Goo Kim, and Inyup Kang. “LTE-Advanced Modem Design: Challenges and Perspectives”. In: *Communications Magazine, IEEE* 50.2 (Feb. 2012), pp. 178–186. ISSN: 0163-6804.

- [216] Yaojun Wang, Dengkun Xiao, and Wenjie Wang. “A Research on Power Consumption of Receiver in CA Scenarios”. In: *Information Engineering (ICIE), 2010 WASE International Conference on*. Vol. 1. Aug. 2010, pp. 247–250.
- [217] Motorola. *Spectrum Aggregation Operations - UE Impact Considerations*. 3GPP R1-084405. 2008.
- [218] NTT Docomo. *Views on Downlink Reception Bandwidth Considering Power Saving Effect in LTE-Advanced*. 3GPP R1-090310. 2009.
- [219] Qualcomm. *Qualcomm Third Generation LTE Chipsets are first to Support HSPA+ Release 10, LTE-Advanced with LTE Carrier Aggregation*. 2012. URL: <http://www.qualcomm.com>.
- [220] K. Pedersen, Y. Wang, B. Soret, and F. Frederiksen. “eICIC Functionality and Performance for LTE HetNet Co-Channel Deployments”. In: *VTC Fall 2012* (Sept. 2012).
- [221] Yuanye Wang, Klaus Pedersen, Preben Mogensen, and Troels Sørensen. “Carrier Load Balancing and Packet Scheduling for Multi-carrier Systems”. In: *Wireless Communications, IEEE Transactions on* 9 (2010), pp. 1780–1789.
- [222] C.S. Park, L. Sundström, A. Wallén, and A. Khayrallah. “Carrier Aggregation for LTE-Advanced: Design Challenges of Terminals”. In: *Communications Magazine, IEEE* 51.12 (Dec. 2013), pp. 76–84.
- [223] J.D. Power & Associates. *U.S. Wireless Smartphone Satisfaction Studies - Volume 1*. 2012.
- [224] B. Dusza, P. Marwedel, O. Spinczyk, and C. Wietfeld. “A Context-Aware Battery Lifetime Model for Carrier Aggregation Enabled LTE-A Systems”. In: *IEEE CCNC*. Jan. 2014.
- [225] 3GPP. *E-UTRA: User Equipment radio transmission and reception*. TS 36.101 V11.7.0. Jan. 2014.
- [226] 3GPP. *E-UTRA: Medium Access Control protocol specification*. TS 36.321 V11.4.0. Jan. 2014.
- [227] Daquan Feng, Chenzi Jiang, Gubong Lim, Jr. Cimini L.J., Gang Feng, and G.Y. Li. “A survey of energy-efficient wireless communications”. In: *Communications Surveys Tutorials, IEEE* 15.1 (2013), pp. 167–178. ISSN: 1553-877X.
- [228] Yan Chen, Shunqing Zhang, Shugong Xu, and G.Y. Li. “Fundamental trade-offs on green wireless networks”. In: *ComMag, IEEE* 49.6 (2011). ISSN: 0163-6804.
- [229] Le Wang and J. Manner. “Energy Consumption Analysis of WLAN, 2G and 3G interfaces”. In: *IEEE/ACM GreenCom*. 2010, pp. 300–307.
- [230] Mike Mayberry. *Enabling Breakthroughs in Technology*. Intel. 2011.
- [231] R. Steele, CC. Lee, and P. Gould. *GSM, cdmaOne and 3G Systems*. John Wiley and Sons, 2001. ISBN: 0471491853.
- [232] Motorola. *Comparison of PAR and Cubic Metric for Power De-rating*. 3GPP TSG RAN WG1 #37 R1-040522. 2004.
- [233] 3GPP. *UE radio transmission and reception*. TS 25.101 v.8.16.0. 2012.

- [234] ETSI. *Feasibility study on SAIC for GSM networks*. TR145.903 v7.0.1. 2007.
- [235] B. Farhang-Boroujeny. “OFDM versus Filter Bank Multicarrier”. In: *Signal Processing Magazine, IEEE* 28.3 (2011), pp. 92–112. ISSN: 1053-5888.

Appendix A

Smartphone Details

The details of the smartphones discussed in chapter 1 are given in table A.1.

Table A.1: Data collected from manufacturer websites (Nokia and Samsung) and Wikipedia (Apple and Google).

Model	Launch year	Battery capacity	Screen size	$\frac{\text{Battery capacity}}{\text{Screen area}}$
Apple iPhone 1	2007	1400 mAh	3.5 in	248 $\frac{\text{mAh}}{\text{in}^2}$
Apple iPhone 3G	2008	1150 mAh	3.5 in	203 $\frac{\text{mAh}}{\text{in}^2}$
Apple iPhone 3GS	2009	1220 mAh	3.5 in	216 $\frac{\text{mAh}}{\text{in}^2}$
Apple iPhone 4	2010	1420 mAh	3.5 in	251 $\frac{\text{mAh}}{\text{in}^2}$
Apple iPhone 4s	2011	1430 mAh	3.5 in	253 $\frac{\text{mAh}}{\text{in}^2}$
Apple iPhone 5	2012	1440 mAh	4 in	210 $\frac{\text{mAh}}{\text{in}^2}$
Apple iPhone 5s	2013	1560 mAh	4 in	228 $\frac{\text{mAh}}{\text{in}^2}$
Google Nexus One	2010	1400 mAh	3.7 in	232 $\frac{\text{mAh}}{\text{in}^2}$
Google Nexus S	2010	1500 mAh	4 in	213 $\frac{\text{mAh}}{\text{in}^2}$
Google Galaxy Nexus	2011	1750 mAh	4.65 in	189 $\frac{\text{mAh}}{\text{in}^2}$
Google Nexus 4	2012	2100 mAh	4.7 in	215 $\frac{\text{mAh}}{\text{in}^2}$
Google Nexus 5	2013	2300 mAh	4.95 in	220 $\frac{\text{mAh}}{\text{in}^2}$
Nokia Lumia 800	2011	1450 mAh	3.7 in	240 $\frac{\text{mAh}}{\text{in}^2}$
Nokia Lumia 820	2012	1650 mAh	4.3 in	202 $\frac{\text{mAh}}{\text{in}^2}$
Nokia Lumia 925	2013	2000 mAh	4.5 in	224 $\frac{\text{mAh}}{\text{in}^2}$
Nokia Lumia 930	2014	2420 mAh	5 in	227 $\frac{\text{mAh}}{\text{in}^2}$
Samsung Galaxy S	2010	1500 mAh	4 in	213 $\frac{\text{mAh}}{\text{in}^2}$
Samsung Galaxy S2	2011	1650 mAh	4.3 in	202 $\frac{\text{mAh}}{\text{in}^2}$
Samsung Galaxy S3	2012	2100 mAh	4.8 in	213 $\frac{\text{mAh}}{\text{in}^2}$
Samsung Galaxy S4	2013	2600 mAh	5 in	243 $\frac{\text{mAh}}{\text{in}^2}$
Samsung Galaxy S5	2014	2800 mAh	5.1 in	252 $\frac{\text{mAh}}{\text{in}^2}$

Appendix B

Power-Consumption Measurements for LTE User Equipment

Mads Lauridsen

The application has been published by Keysight Technologies, 2014
<http://literature.cdn.keysight.com/litweb/pdf/5991-4594EN.pdf>

© 2014 Keysight Technologies
The layout has been revised.

Keysight Technologies

Power-Consumption Measurements for LTE User Equipment

Application Note

If you are designing smartphone chipsets or operating a mobile network, you need to determine how certain parameters affect a specific smartphone's power consumption and figure out how to adjust the parameters to improve battery life. In this application note we show how to use the Keysight Technologies, Inc. E6621A PXT wireless communications test set and the Keysight N6705B DC power analyzer to establish a power consumption model for LTE user equipment (UE). The model is useful when you need to examine the UE battery life in system-level simulations.

We will explain how the Keysight equipment can be used in manual tests, but we do not discuss how to make automated tests (for example, using VEE software).

In this application note, we analyze smartphones adhering to the 3GPP LTE standard [1].

Introduction

Modern smartphones have limited battery life, and this affects user satisfaction. Chipset manufacturers and mobile network operators will want to evaluate a smartphones' power consumption in a realistic setup and establish a power consumption model based on the evaluation. The model helps you determine how certain parameters affect a specific smartphone's power consumption and how you can adjust the parameters to improve battery life.

The key parameters are uplink (UL) and downlink (DL) data rates (R), transmit (Tx) and receive (Rx) power levels (S), cell bandwidth (BW), and discontinuous reception (DRX). The parameters affect the smartphone's modem, and more specifically, the Rx and Tx base band (BB) and Rx and Tx radio frequency (RF) components. A power consumption model that includes these components has been proposed in an article entitled Empirical LTE Smartphone Power Model with DRX Operation for System Level Simulations [2]. It covers the contribution from each parameter on the related component, as illustrated in Figure 1.

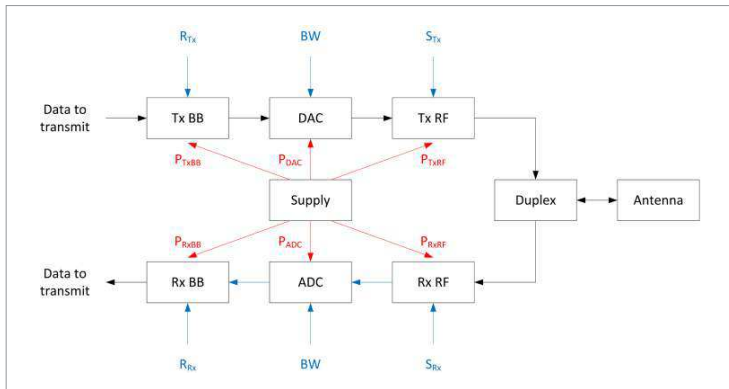


Figure 1. UE power consumption model, based on Figure 1 in [2]

The model is made by measuring how each parameter affects the power consumption, but the model does so by capturing major trends and not implementation-specific peculiarities.

Procedure

In this section, we outline the procedure for performing a UE power consumption measurement. You can make the measurement manually using the control/button interface of the PXT and N6705B or automatically using Keysight VEE programming and a PC connected to the equipment via LAN.

The steps for a manual measurement are:

1. Set up the N6705B mainframe and N6781A SMU module
2. Set up the PXT according to the test case in Table 1
3. Initiate the measurement
4. Run the data logging tool in the N6705B and note important PXT values (data rate, power level, and so forth)

Step 1: Setting up the N6705B mainframe and N6781A SMU module

First, you must determine the appropriate battery voltage level (typically 3.7 to 3.8 V) and set the voltage and maximum current in the N6705B. Next, configure the data logger properties – Duration, Sample Period and File Name – as illustrated in Figure 4. Start the log by pressing **Run/stop** in the **Data logger** menu.

Note that the N6781A option offers multiple ways to connect the UE, even including the battery [5].

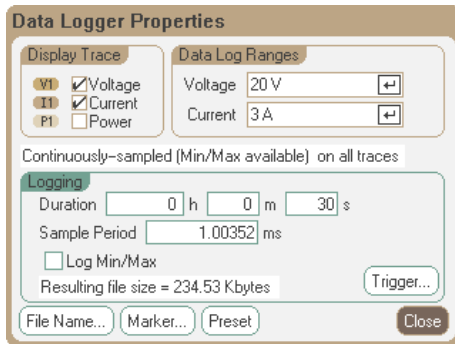


Figure 4. Data logger properties on the N6705B

Step 2: Setting up the PXT

The PXT setup involves adjusting many parameters, so after you have set the initial parameters (such as cell bandwidth, carrier frequency and so forth), it can be beneficial to save the setup to a scenario file.

After loading the scenario file, adjust the physical (PHY) layer settings. The **PHY Settings** menu has submenus for adjusting downlink and uplink settings. In each submenu, you can set the modulation and coding scheme (MCS) and the number of physical resource blocks (PRBs). As shown in Table 1, these two parameters are varied when you examine BB power consumption. The parameters have a direct effect on data rate, which affects the BB processing and power consumption.

In the same submenu, you will see an option for **Resource Allocation Mode**. This mode lets you schedule DL and UL data on the PDSCH and PUSCH. In **Auto** mode, the PXT will schedule data if another entity within the PXT is generating it. This could be, for example, the dedicated traffic channel (DTCH) throughput test found in the **Func** menu. The other option is **Fixed MAC padding**, as illustrated in Figure 5. This option will pad transport blocks with random data unless real data is available, and therefore fully load the PRBs specified. The receiving MAC layer is able to determine what is real and what is padded data, and it discards the padded data (this could be the entire PRB). If no other data-generating entities are running, the UE will discard all the received data and send only acknowledgements (ACKs) from the layers below the Medium Access Control MAC layer. This is a nice feature because it reduces power consumption from transmitting ACKs on the reverse link.

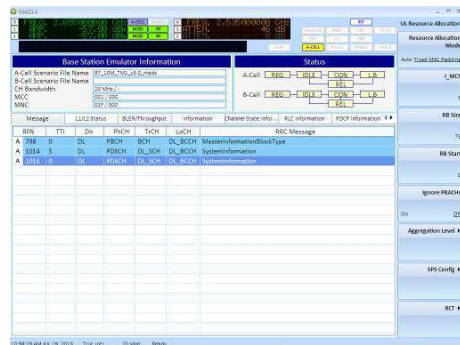


Figure 5. UL resource allocation menu

When you have finished adjusting the PHY-layer settings, the next task is to adjust the Radio Resource Control (RRC) settings. The **RRC Settings** menu include maximum transmit power level (p-Max) and default paging cycle, as illustrated in Figure 6. Furthermore the **RRC Settings** menu has a **DRX Settings** submenu that lets you adjust the aforementioned DRX parameters including period length and inactivity and on duration timers.



Figure 6. RRC settings menu

Keep the maximum transmit power as low as possible in all test cases except number 6 because the power amplifier has a major impact on power consumption. Because the UE transmits a low-power signal, be sure to set the RF1 attenuation accordingly using the **Atten** button.

The final settings you need to adjust are the RF1 and RF2 amplitude settings. In this menu, you can set the UE receive power in dBm, which is specified to a fairly high level in all test cases, except for number 3. To minimize the power consumption impact, the UE RF should use gain settings as low as possible.

Step 3: Initiating the measurement

After the phone is powered on, close programs, make sure other radios such as WiFi and **Bluetooth**® radios are off, and finally, turn the screen off or use a specified brightness level. Then set the PXT **Emulator Mode** to **Run**. You will notice that some parts of the **PHY** and **RRC Settings** menus become grayed out, so these parameters cannot be changed during run time. The status window of the PXT should change to "con" (connected), as illustrated in Figure 8. Now you can start the test. In all the test cases in Table 1, the tests are initiated by applying the MAC padding, to ensure the UE is active, and then running the N6705B data logger as explained in the next section.

Step 4: Run the N6705B data logger and note important PXT values

When the UE e.g. has started receiving data as specified in test case 1, begin logging the power consumption using the N6705B by pressing the **Run/stop** button. When you are finished logging data, the N6705B screen should look similar to Figure 7.

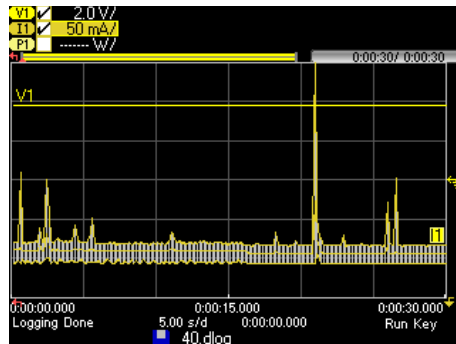


Figure 7. Screen shot of data log window. Notice the 30 s duration in the upper right corner and the file name in the lower middle

Next, export the logged data from the N6705B to a USB stick. To export data, select **File > Export**. To store a comma-separated file on the USB stick, select **Export logged data (.csv)**.

At this time it is also important to note the relevant PXT parameters according to the given test case. If data rate is of interest, you can run the DTCH throughput test, because it reports the achieved data rate, as illustrated in Figure 8.

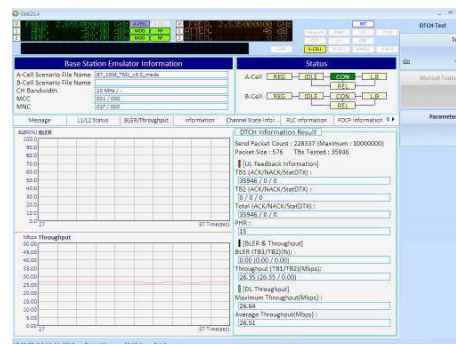


Figure 8. DTCH throughput test

If the transmit power level is important, you can check the power level received by the PXT. This value is available in several PXT submenus, including the **LTE UL demodulation** menu, as illustrated in Figure 9.

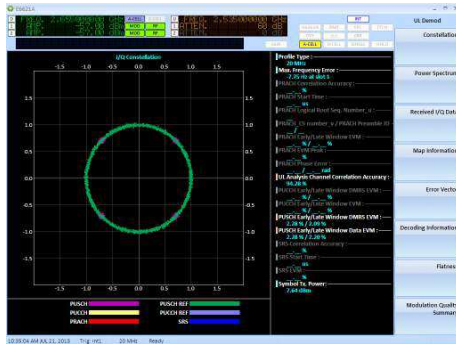


Figure 9. Demodulation of uplink signal. Notice the symbol transmit power is reported in the lower right corner.

Results/measurement data

When you have collected the relevant parameters from the PXT and N6705B, you can post-process them to generate the model illustrated in Figure 1. Each test case provides input for one UE component, and an example of such a combination is given in Figure 10, where the downlink data rate, which was controlled and measured using the PXT, has been combined with the supply power consumption measured by the N6705B.

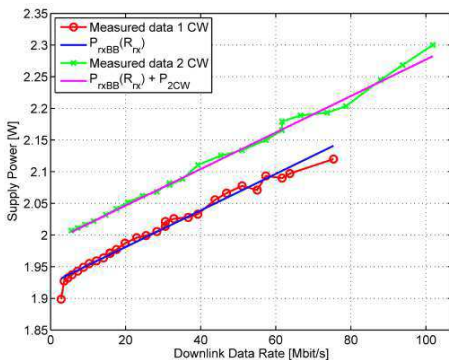


Figure 10. Supply power consumption as a function of downlink data rate. Figure 3 in [7]

Next, calculate a polynomial fit to the data, as shown in the $P_{rxBB}(R_x)$ line in Figure 10. Then insert the polynomial function in the appropriate part of the power consumption model.

Two articles discuss using the PXT and N6705B setup. In *LTE UE Power Consumption Model - For System Level Energy and Performance Optimization* [7], the authors discuss the basis for the model in Figure 1 and report power consumption for commercial LTE dongles. The article mentioned earlier [2] is an updated version of this paper [7], and it includes measurements on first-generation LTE smartphones and examines screen and DRX power consumption. Refer to the papers for further details on measurement setup and results.

Number of test points per test case

The number of test points required to reproduce the results was discussed in the article [2]. The discussion is repeated here because the number of test points has a huge effect on overall test time and that influences the possibility of keeping the model up to date by making measurements on new UEs.

Test case 1 includes 29 points, but when you examine Figure 10 it is clear that the power consumption is almost a linear function of downlink data rate. Therefore, three test points should be sufficient. The same goes for test case 2, which could be omitted completely.

Test case 3 is designed to study Rx RF power consumption as a function of receive power level. The results reported in the articles [2, 7] show two to three power steps, which are caused by adjustments in the low-noise amplifiers. Therefore, five to six points are required.

Power consumption as a function of transmit data rate is studied using test case 4. You can see that the power is almost independent of the encoding rate and changes only when the modulation scheme is changed from QPSK to 16QAM. Because the standard specifies when the modulation changes, the test case could be performed using four points, where two of them are located around the modulation change.

The final test case is used to examine the Tx RF, which is the most power-consuming component. The behavior is UE specific, especially for transmit powers above 0 dBm, and therefore a very complete set of test points (for example, with 1 dB steps) is needed. It is important to note that different power amplifiers are used for different frequency bands, as pointed out in the article *LTE Power Model* [8].

Uncertainties

The measurement setup includes uncertainties, some of which are listed below:

- Because supply power is measured, it is not possible to separate the contributions from each of the components in the model. If you carefully design the test cases, however, you can minimize the undesired contributions. Furthermore, other UE peripherals such as the screen and the CPU also contribute.
- The measurements are not conducted over the air, as would be the case in real life. Because real antennas are lossy, the power consumption in real life will probably be a bit higher. It may, however, only have a very minor effect on the relative accuracy between the model's components.
- The temperature of the UE has an impact on power consumption. The optimal method would be to ensure the same UE test temperature at each measurement, but this would require either time-consuming cool-down periods or some type of warm-up procedure.
- Some UEs have sophisticated power management chips that continuously adjust specific components. These continuous changes and the temperature issue make repeatability difficult to achieve.
- A careful calibration of the PXT-UE cables is required.

Conclusion

In this application note we showed you how to measure smartphone power consumption as a function of relevant network parameters with the Keysight PXT and the Keysight N6705B with the N6781A SMU module installed.

The measurements are useful to both chipset manufacturers and mobile network operators, because they can help estimate the smartphone's battery life, which is a key performance indicator for the user.

We offered a list of relevant test cases for developing a smartphone power model and discussed how many measurements point are needed to repeat and update the model. We also explored some measurement uncertainties.

Thank you to Mads Lauridsen, Aalborg University for writing this application note.

Thanks to Janus Faaborg, Keysight Technologies Denmark for supporting this work.

This project was partly funded by the 4GMCT project.

References

- [1] *Third Generation Partnership Project (3GPP)*. 2013. Long Term Evolution <http://3gpp.org/lte>
- [2] Lauridsen, Mads et al. *Empirical LTE Smartphone Power Model with DRX Operation for System Level Simulations*. VTC Fall 2013.
- [3] Keysight Technologies. May 2013. *Keysight PXT Wireless Communications Test Set (E6621A) User's Guide v.6.5*
- [4] Keysight Technologies. June 2012. *Keysight N6700 Modular Power System Family*
- [5] Keysight Technologies. March 2011. *Evaluating Battery Run-Down with the N6781A 2-Quadrant Source/Measure Unit and the 14585A Control and Analysis Software*
- [6] 3GPP. 2010. *MAC protocol specification*, TS 36.321 V8.9.0.
- [7] Jensen, Anders R. et al. *LTE UE Power Consumption Model - For System Level Energy and Performance Optimization*. VTC Fall 2012
- [8] Dusza, Björn et al. 2013. *LTE Power Model*. <http://www.kn.e-technik.tu-dortmund.de/en/forschung/lte-ue-power-model.html>

myKeysight**myKeysight**www.keysight.com/find/mykeysight

A personalized view into the information most relevant to you.

**Three-Year Warranty**www.keysight.com/find/ThreeYearWarranty

Keysight's commitment to superior product quality and lower total cost of ownership. The only test and measurement company with three-year warranty standard on all instruments, worldwide.

Keysight Channel Partnerswww.keysight.com/find/channelpartners

Get the best of both worlds: Keysight's measurement expertise and product breadth, combined with channel partner convenience.

Bluetooth and the Bluetooth logos are trademarks owned by Bluetooth SIG, Inc., U.S.A. and licensed to Keysight Technologies, Inc.

www.keysight.com/find/N6705B

For more information on Keysight

Technologies' products, applications or services, please contact your local Keysight office. The complete list is available at: www.keysight.com/find/contactus

Americas

Canada	(877) 894 4414
Brazil	55 11 3351 7010
Mexico	001 800 254 2440
United States	(800) 829 4444

Asia Pacific

Australia	1 800 629 485
China	800 810 0189
Hong Kong	800 938 693
India	1 800 112 929
Japan	0120 (421) 345
Korea	080 769 0800
Malaysia	1 800 888 848
Singapore	1 800 375 8100
Taiwan	0800 047 866
Other AP Countries	(65) 6375 8100

Europe & Middle East

Austria	0800 001122
Belgium	0800 58580
Finland	0800 523252
France	0805 980333
Germany	0800 6270999
Ireland	1800 832700
Israel	1 809 343051
Italy	800 599100
Luxembourg	+32 800 58580
Netherlands	0800 0233200
Russia	8800 5009286
Spain	0800 000154
Sweden	0200 882255
Switzerland	0800 805353
	Opt. 1 (DE)
	Opt. 2 (FR)
	Opt. 3 (IT)
United Kingdom	0800 0260637

For other unlisted countries:

www.keysight.com/find/contactus
(BP-07-10-14)

Appendix C

LNA Survey Details

This appendix contains the details on the surveyed Low Noise Amplifiers (LNAs). The data is provided in tables C.1, C.2, C.3, C.4, and C.5 while the references are available at the end of the appendix. As mentioned in section 5.1 the best parameters have been chosen from each reference. That is the minimum Noise Figure (NF), the maximum power gain, and the lowest Input Third-Order Intercept Point (IP3). Some LNAs are narrowband and therefore only report the carrier frequency, while wideband LNAs also report the bandwidth.

Table C.1: Details of surveyed LNAs, part 1.

Ref.	Year	Type	Node [nm]	Gain [dB]	NF [dB]	IIP3 [dBm]	Power [mW]	Supply [V]	Area [mm ²]	f _{min} [f _{max} GHz	f _c GHz	BW]
[1]	1991	GaAs	300	11.5	2.5	9	13.8	3	3	1.5	1.7	1.6	0.2
[2]	1992	MESFET	1000	19.6	2.2	6	10	5	8.093	0.9	1	0.95	0.1
[3]	1992	GaAs HBT		24	3	7	62.5	5	0.081	0.3	4.8	2.55	4.5
[4]	1993	GaAs JFET	500	18.1	2.8	-11.1	12	3	1.375			1.9	
[5]	1994	CMOS	800	16	2.2	-10	40	5	1.69			0.9	
[6]	1995	GaAs HBT		11.1	1.9	11	4	2	0.861			2	
[6]	1995	GaAs HBT		16.2	2.9	20.5	72	3.5				5.7	
[7]	1995	GaAs	300	12.2	2	5.1	2	2				1.9	
[8]	1995	CMOS	800	9.5	2.1	-3	3.8	1.9	0.358			1.9	
[9]	1996	CMOS	500	15.6	1.9	-3.2	20	2.7	0.28			0.9	
[10]	1996	CMOS	800	10	2.7	-12.5	4	2	2			1.9	
[11]	1996			14	1.4	-9	6.6	3.3				0.9	
[11]	1996			17.3	1.7	3	37	3.7				0.9	
[12]	1997	CMOS	600	22	3.5	-9.3	30	1.5	0.12	1.45	1.6	1.525	0.15
[13]	1997	SiGe HBT		18.3	3.5	-21	9.4	2.5	0.49			6.25	
[14]	1997	SiGe HBT		13	2.1	-10.5	9	1	0.56			5.8	
[15]	1997			7	4.2	-4	7.7	3.5	2			5.8	
[16]	1997	GaAs HBT	1000	24.6	1.3	8	31.2	4	0.09	0	3	1.5	3
[16]	1997	GaAs HBT	1000	11.9	3.1	-3.1	9.425	2.9		0	3	1.5	3
[16]	1997	GaAs HBT	1000	26.1	1.47	9.8	68.06	4.15		0	6	3	6
[16]	1997	GaAs HBT	1000	10.3	2.6	-5	16.24	2.8		0	6	3	6
[17]	1998	GaAs MESFET	600	16.5	1.8	-6	6	1	1.615	4.3	6	5.15	1.7
[18]	1998	CMOS	800	15	2.8	2	54	3.6	0.865			1.9	
[19]	1998	CMOS	350	14.8	1.8	-2.5	9	3				0.9	
[20]	1998	CMOS	250	13.8	2	-2	46.5	2.5				0.9	
[20]	1998	CMOS	250	16.2	1.85	-7.25	27	2.5				0.9	
[21]	1999	GaAs MESFET	600	11	1.9	5	13.2	3	0.645			5	
[22]	1999	FET	400	14.5	1.7	-10	9	3	0.81			5.2	
[23]	1999	CMOS	800	14.5	1.2	-1	30	3	0.518			0.9	
[23]	1999	CMOS	800	9.4	2	-3.8	6.3	2.7				0.9	
[24]	1999			16.8	1.9	5	33.99	3.3				1.9	
[24]	1999			16.9	1.8	5	33	3.3				0.9	

Table C.2: Details of surveyed LNAs, part 2.

Ref.	Year	Type	Node [nm]	Gain [dB]	NF [dB]	IIP3 [dBm]	Power [mW]	Supply [V]	Area [mm ²]	f _{min} [f _{max} GHz	f _c GHz	BW]
[25]	2000	MESFET	600	12.3	2.4	-13.1	1.2	1	0.6			5.2	
[26]	2000	CMOS		17	1.3	-2	12.15	2.7				1.8	
[27]	2000	CMOS	350	10.2	1.65	1	29.7	2.7				0.9	
[27]	2000	CMOS	350	10	1.75	3	27	2.7				0.9	
[28]	2000	CMOS	500	12.2	2.7	-21	17	2		0.66	1.16	0.91	0.5
[28]	2000	CMOS	500	10.7	2.6	-3.8	16	2		0.66	1.16	0.91	0.5
[29]	2001	CMOS	350	17.5	2.05	-6	2.16	2.7				0.9	
[30]	2001	CMOS	350	10	1.2	-3	4.95	1.8	0.66			0.9	
[30]	2001	CMOS	350	13	1	-1.5	8.55	1.8				0.9	
[30]	2001	CMOS	350	15	0.85	1	17.6	1.8				0.9	
[31]	2001	CMOS		20	0.79	-10.8	9	1.5				1.23	
[32]	2001	CMOS	250	15.1	2.88	2.2	24.3	3	1.1			2.45	
[32]	2001	SiGe		15.9	2.86	-2.6	21	3	1.1			2.45	
[33]	2001	CMOS	350	7.87	5.6	2.8	12.4	1				5.2	
[34]	2002	CMOS	150	12.1	2.77	2.4	4.65	1.5	0.64			2.4	
[34]	2002	CMOS	150	14	2.36	-2.2	4.65	1.5				2.46	
[35]	2002	SiGe HBT	180	16	1.2	8.415	24	3		2.11	2.17	2.14	0.06
[36]	2002	CMOS	350	7.2	3.2	6.7	20	1.3	0.651			5.8	
[37]	2002	InGaP HBT		23.1	2.17	1.3	28.3	3	0.99			5.25	
[37]	2002	InGaP HBT		3.4	3.41	1.3	14.6	3				5.25	
[38]	2002	CMOS	350	14	2.3	0	10	2.5	0.64			2.45	
[38]	2002	CMOS	350	15.5	4.5	5.6	10	2.5				5.25	
[39]	2003	CMOS	180	13.1	3.7	-4.7	75			2.45	5.5	3.975	3.05
[40]	2003	CMOS	350	17.5	2.91	-1	12.5	2.5	0.84			0.435	
[41]	2003	CMOS	180	11.5	3.4	10	52	1.3	1.6	2	10	6	8
[42]	2003	CMOS	350	18.82	3.9	-3.5	26.4	2	1.865	4.9	6	5.45	1.1
[43]	2003	CMOS	250	15.2	2.7	13.9	23.5	2.5	0.81	2	2.4	2.2	0.4
[44]	2004	CMOS	180	9.3	4	-6.7	9	1.8	1.1	2.3	9.2	5.75	6.9
[45]	2004	CMOS	250	13.7	2	0	35	2.5	0.075	0.02	1.6	0.801	1.598
[46]	2004	CMOS	180	16.7	1.4	-2.6	4.5	1.8	0.192			5.8	
[47]	2004	CMOS	90	15.4	2.7	-6.6	20.6	1.2	0.543			5.5	
[47]	2004	CMOS	90	9.2	3.6	-7.25	1	0.6				5.5	
[48]	2004	CMOS	180	21	2.5	-1	30	3	1.8	3	10	6.5	7

Table C.3: Details of surveyed LNAs, part 3.

Ref.	Year	Type	Node [nm]	Gain [dB]	NF [dB]	IIP3 [dBm]	Power [mW]	Supply [V]	Area [mm ²]	f _{min} [f _{max}]	f _c GHz	BW]
[49]	2005	CMOS	180	9.2	4.5	-15	0.9	0.6	0.946			5	
[50]	2005	CMOS	180	8.6	4.2	1.8	9	1.3	1.16	0.03	6.2	3.115	6.17
[51]	2005	CMOS	130	19	3	1	11.7	1.8		0.1	6.5	3.3	6.4
[52]	2005	CMOS	180	9.8	2.3	-7	12.6	1.8	0.9	2	4.6	3.3	2.6
[53]	2005	CMOS	130	11	2.2	-8.2	4.8	1.2	0.9	3	10.7	6.85	7.7
[54]	2005	CMOS	180	15.4	0.9	-2.5	11	1.5		1	2.6	1.8	1.6
[54]	2005	CMOS	180	17.9	1.6	-4.5	13.2	1.5		2.7	5.4	4.05	2.7
[55]	2005	CMOS	130	13	4	-10.2	0.72	1.2	2.6	0.1	0.93	0.515	0.83
[56]	2005	CMOS	250	8	3.3	0.4	3.6	2	0.398			5.2	
[56]	2005	CMOS	250	11	2.17	0.3	10	2				5.2	
[57]	2005	CMOS	180	10.2	3.68	-1	7.2	1	1.2	2	10.1	6.05	8.1
[58]	2005	CMOS	180	8	2.9	-3.4	21.6	1.8	0.760	3.1	10.6	6.85	7.5
[59]	2005	CMOS	180	9.7	4.5	-6.2	20	1.8	0.585	1.2	11.9	6.55	10.7
[60]	2005	CMOS	180	8	2.9	-3.4	19.8	1.8	0.760	3.1	10.6	6.85	7.5
[61]	2006	CMOS	130	4.5	6.3	-10.5	0.16	0.6	2			3	
[61]	2006	CMOS	130	9.1	4.7	-11	0.4	0.6				3	
[62]	2006	CMOS	180	14	2.2	-2.87	15	1.8		3	10.6	6.8	7.6
[63]	2006	CMOS	180	8.6	4.2	3	9	1.3	1.16	0.040	7	3.52	6.96
[64]	2006	CMOS	130	13	4	-10.2	0.72	1.2	2.6	0.1	0.930	0.515	0.830
[65]	2006	CMOS	180	15	2.2	-9	7.68	1.2	0.629	3	5	4	2
[66]	2006	CMOS	180	12.02	4.7	-12	10.57	1.5	0.665	3.1	10.6	6.85	7.5
[67]	2006	CMOS	130	9.5	3.5	-0.8	16.5	1.5	1.08	2	4.6	3.3	2.6
[68]	2006	CMOS	90	10.6	4	-8	8	1.2	0.77	2.5	4	3.25	1.5
[69]	2006	CMOS	90	25	1.9	-14	42	2.7	0.025	0.5	8.2	4.35	7.7
[70]	2007	CMOS	130	11.2	2.7	-2.7	1.9	1.2		0.2	3.8	2	3.6
[70]	2007	CMOS	130	10.5	2.735	-2.7	1.9	1.2		0.2	6.2	3.2	6
[71]	2007	CMOS	180	18	4.6	-12.8	32.4	1.8	1.338	0.935	0.96	0.9475	0.025
[71]	2007	CMOS	180	24	4.43	-15.3	32.4	1.8		1.805	2.483	2.144	0.678
[71]	2007	CMOS	180	23	4.42	-14.7	32.4	1.8		5.15	5.825	0.5488	0.675
[72]	2007	CMOS	180	14.8	3.1	3	13.4	1.2	0.331	2	11.5	6.75	9.5
[73]	2007	CMOS	65	15.6	3.5	0	21	1.2	0.009	0.2	5.2	2.7	5
[74]	2007	CMOS	130	15.1	2.5	-8.5	9	1.2	0.87	3.1	10.6	6.85	7.5
[75]	2008	CMOS	90	16.5	2.5	-10	9.2	1.2	0.007	0	6.5	3.25	6.5
[76]	2008	CMOS	180	11.3	3.9	5	30	1.2	0.684	2.2	9	5.6	6.8
[77]	2008	CMOS	130	8.15	2.5	-4	10.68	1.2	0.435	3.1	10.6	6.85	7.5
[78]	2008	CMOS	90	8	3.4	-9	16	1.4	0.137	0.1	8	4.05	7.9
[79]	2008	CMOS	180	20.5	3.3	2.7	32.4	1.8	0.12	0.02	1.175	0.5975	1.155

Table C.4: Details of surveyed LNAs, part 4.

Ref.	Year	Type	Node [nm]	Gain [dB]	NF [dB]	IIP3 [dBm]	Power [mW]	Supply [V]	Area [mm ²]	f_{\min} [f_{\max} GHz	f_c GHz	BW]
[80]	2009	CMOS	180	10.23	4.1	-15	0.8	0.6	0.792			5	
[81]	2009	CMOS	90	12.7	4.4	-2.5	12.6	1.2	0.35	0.1	20	10.05	19.9
[82]	2009	CMOS	90	10.7	4.3	-2.67	8.4	1.2	0.131	0	22.1	11.05	22.1
[83]	2009	CMOS	180	11.8	3.14	1	22.7	1.9	0.447	2	12	7	10
[84]	2009	CMOS	65	16.5	3.9	-5	36	1.2	0.137	0.1	10.5	5.3	10.4
[85]	2009	CMOS	180	14	3	3	34.76	2.2	0.16	0.048	1.2	0.624	1.152
[86]	2009	CMOS	130	7	3.7	-6.7	17	1.2	0.52	1.9	2.4	2.15	0.5
[87]	2009	CMOS	180	10.5	2	-3.2	3.6	1.8	0.33	0.3	0.92	0.61	0.62
[88]	2010	CMOS	90	13.80	1.7	-7.51	19.31	1		5.725	5.825	5.775	0.1
[88]	2010	CMOS	90	12.89	1.79	-6.22	48.28	1		5.725	5.825	5.775	0.1
[88]	2010	CMOS	90	19.97	2.63	-5.03	56.8	1		5.725	5.825	5.775	0.1
[89]	2010	CMOS	180	16.4	2.1	0	14.4	1.8	0.277	0.04	1.2	0.62	1.16
[90]	2010	CMOS	90	10.68	2.92	4	21.6	1.2	0.139	3.1	10.6	0.685	7.5
[91]	2010	CMOS	130	9.5	2.8	-4.2	5.7	1	0.291	0.2	3.8	2	3.6
[92]	2010	CMOS	180	8.45	2.57	-0.7	12.6	1.8	0.073	1.05	3.05	2.05	2
[93]	2010	CMOS	130	9	4	-8	20	1.2		0.1	5	2.55	4.9
[94]	2011	CMOS	130	13.1	5.3	-12.2	0.6	0.4	0.63	2.45	2.55	2.5	0.1
[94]	2011	CMOS	130	15.2	4.9	-12.6	0.9	0.5		2.45	2.55	2.5	0.1
[95]	2011	CMOS	180	18.2	2.97	-13.6	0.954	1.8	1.5			2.2	
[95]	2011	CMOS	180	13.9	5.14	-9.3	0.21	1.5				2.2	
[96]	2011	CMOS	90	10	1.43	-1.5	18	1.8	0.06	0.02	1.1	0.551	1.098
[96]	2011	CMOS	90	10.5	1.4	-1.5	18	1.8		0.02	2.3	1.151	2.298
[97]	2011	CMOS	90	11.5	1.85	-2.85	2.8	2	1	0.1	1.77	0.935	1.67
[98]	2012	CMOS	180	14.7	2.9	-11.1	0.79	0.4				1.5	
[99]	2012	CMOS	180	11	0.95	5	12	1.5	0.293			5	
[100]	2012	CMOS	65	10.5	2.7	-3.5	13.7	1	0.02	0	10	5	10
[101]	2012	CMOS	130	9.4	2.8	-4.3	2.79	1.2	0.61			2.45	
[101]	2012	CMOS	130	18.9	3.8	-5.6	2.79	1.2	0.36			6	
[102]	2012	CMOS	180	11.75	2.2	0	15.3	1.8	0.105	0.32	1	0.66	0.68

Table C.5: Details of surveyed LNAs, part 5.

Ref.	Year	Type	Node [nm]	Gain [dB]	NF [dB]	IIP3 [dBm]	Power [mW]	Supply [V]	Area [mm ²]	f_{\min} [f_{\max}]	f_c GHz	BW]
[103]	2013	CMOS	130	15.4	1.74	4.09	5.16	0.6	0.691			0.9	
[104]	2013	CMOS	180	11.21	3.22	-9	0.798	0.6	0.461			5.8	
[105]	2013	CMOS	65	12	2.8	4	18	1.4	0.4	0	9.5	4.75	9.5
[106]	2013	CMOS	180	16.5	1.33	19	10.8	1.8	0.43	0.047	0.862	0.666	0.392
[107]	2013	CMOS	180	10	4.8	-22	0.336	0.6	0.61	4.55	5	4.775	0.45
[108]	2013	CMOS	180	12.25	3.5	-1	1.28	0.6				5	
[109]	2013	CMOS	130	23.8	1.6	-9.7	5.3	1.2		0.1	2	1.05	1.9
[110]	2013	CMOS	130	21.9	3	-8.6	6.2	1.2		0.1	5.9	3	5.8
[110]	2013	CMOS	130	23.9	3.2	-26	2.25	0.6		0.1	1.3	0.7	1.2
[111]	2014	CMOS	90	12.02	3.24	-1.8	9.96	1.2	0.718	1.9	22.5	12.2	20.6
[112]	2014	CMOS	180	24.1	1.7	8.75	6.53	1				2.4	
[113]	2014	CMOS	130	14.3	3	-2.4	36	1.2		0.4	11.5	5.95	11.1
[114]	2014	CMOS	180	12.9	3.4	15	6.8	1.8	0.341			2	
[115]	2014	CMOS	180	10.8	5.5	-6.4	6.4	1.1	0.97	3.1	10.6	6.85	7.5

LNA References

- [1] Y. Imai, M. Tokumitsu, and A. Minakawa. “Design and performance of low-current GaAs MMICs for L-band front-end applications”. In: *Microwave Theory and Techniques, IEEE Transactions on* 39.2 (Feb. 1991), pp. 209–215. ISSN: 0018-9480. DOI: 10.1109/22.102962.
- [2] K.R. Cioffi. “Monolithic L-band amplifiers operating at milliwatt and sub-milliwatt DC power consumptions”. In: *Microwave and Millimeter-Wave Monolithic Circuits Symposium, 1992. Digest of Papers, IEEE 1992*. June 1992, pp. 9–12. DOI: 10.1109/MCS.1992.185984.
- [3] K.W. Kobayashi and A.K. Oki. “Sub-2.5 dB noise figure GaAs HBT direct-coupled LNAs for high volume commercial applications to 6 GHz”. In: *Gallium Arsenide Integrated Circuit (GaAs IC) Symposium, 1994. Technical Digest 1994., 16th Annual*. Oct. 1994, pp. 303–306. DOI: 10.1109/GAAS.1994.636989.
- [4] T. Ohgihara, S. Kusunoki, M. Wada, and Y. Murakami. “GaAs JFET front-end MMICs for L-band personal communications”. In: *Microwave and Millimeter-Wave Monolithic Circuits Symposium, 1993. Digest of Papers., IEEE 1993*. June 1993, pp. 9–12. DOI: 10.1109/MCS.1993.247488.
- [5] R.G. Meyer and W.D. Mack. “A 1-GHz BiCMOS RF front-end IC”. In: *Solid-State Circuits, IEEE Journal of* 29.3 (Mar. 1994), pp. 350–355. ISSN: 0018-9200. DOI: 10.1109/4.278360.
- [6] K.W. Kobayashi, A.K. Oki, L.T. Tran, and D.C. Streit. “Ultra-low dc power GaAs HBT S- and C-band low noise amplifiers for portable wireless applications”. In: *Microwave Theory and Techniques, IEEE Transactions on* 43.12 (Dec. 1995), pp. 3055–3061. ISSN: 0018-9480. DOI: 10.1109/22.475674.
- [7] M. Nakatsugawa, Y. Yamaguchi, and M. Muraguchi. “An L-band ultra-low-power-consumption monolithic low-noise amplifier”. In: *Microwave Theory and Techniques, IEEE Transactions on* 43.7 (July 1995), pp. 1745–1750. ISSN: 0018-9480. DOI: 10.1109/22.392948.
- [8] J.R. Long and M.A. Copeland. “A 1.9 GHz low-voltage silicon bipolar receiver front-end for wireless personal communications systems”. In: *Solid-State Circuits, IEEE Journal of* 30.12 (Dec. 1995), pp. 1438–1448. ISSN: 0018-9200. DOI: 10.1109/4.482191.
- [9] A.N. Karanicolas. “A 2.7-V 900-MHz CMOS LNA and mixer”. In: *Solid-State Circuits, IEEE Journal of* 31.12 (Dec. 1996), pp. 1939–1944. ISSN: 0018-9200. DOI: 10.1109/4.545816.
- [10] N. Suematsu, M. Ono, S. Kubo, H. Sato, Y. Iyama, and O. Ishida. “L-band internally matched Si-MMIC low noise amplifier”. In: *Microwave Symposium Digest, 1996., IEEE MTT-S International*. Vol. 3. June 1996, 1225–1228 vol.3. DOI: 10.1109/MWSYM.1996.512157.
- [11] K. Vennema. *Ultra Low Noise Amplifiers for 900 and 2000 MHz with High IP3*. Philips Semiconductors. Dec. 1996.

- [12] D.K. Shaeffer and T.H. Lee. “A 1.5-V, 1.5-GHz CMOS low noise amplifier”. In: *Solid-State Circuits, IEEE Journal of* 32.5 (May 1997), pp. 745–759. ISSN: 0018-9200. DOI: 10.1109/4.568846.
- [13] H. Ainspan, M. Soyuer, J.-O. Plouchart, and J. Burghartz. “A 6.25-GHz low DC power low-noise amplifier in SiGe”. In: *Custom Integrated Circuits Conference, 1997., Proceedings of the IEEE 1997*. May 1997, pp. 177–180. DOI: 10.1109/CICC.1997.606608.
- [14] M. Soyuer, J.-O. Plouchart, H. Ainspan, and J. Burghartz. “A 5.8-GHz 1-V low-noise amplifier in SiGe bipolar technology”. In: *Radio Frequency Integrated Circuits (RFIC) Symposium, 1997., IEEE*. June 1997, pp. 19–22. DOI: 10.1109/RFIC.1997.598733.
- [15] S.P. Voinigescu and M.C. Maliepaard. “5.8 GHz and 12.6 GHz Si bipolar MMICs”. In: *Solid-State Circuits Conference, 1997. Digest of Technical Papers. 43rd ISSCC., 1997 IEEE International*. Feb. 1997, pp. 372–373.
- [16] K.W. Kobayashi, L.T. Tran, M.D. Lammert, T.R. Block, P.C. Grossman, A.K. Oki, and D.C. Streit. “Sub-1.3 dB noise figure direct-coupled MMIC LNAs using a high current-gain 1 um GaAs HBT technology”. In: *Gallium Arsenide Integrated Circuit (GaAs IC) Symposium, 1997. Technical Digest 1997., 19th Annual*. Oct. 1997, pp. 240–243. DOI: 10.1109/GAAS.1997.628278.
- [17] J.J. Kucera and U. Lott. “A 1.8 dB noise figure low DC power MMIC LNA for C-band”. In: *Gallium Arsenide Integrated Circuit (GaAs IC) Symposium, 1998. Technical Digest 1998., 20th Annual*. Nov. 1998, pp. 221–224. DOI: 10.1109/GAAS.1998.722675.
- [18] Cheon-Soo Kim, Min Park, Chung-Hwan Kim, Yeong Cheol Hyeon, Hyun-Kyu Yu, Kwyyro Lee, and Kee-Soo Nam. “A fully integrated 1.9-GHz CMOS low-noise amplifier”. In: *Microwave and Guided Wave Letters, IEEE* 8.8 (Aug. 1998), pp. 293–295. ISSN: 1051-8207. DOI: 10.1109/75.704599.
- [19] G. Hayashi, H. Kimura, H. Simomura, and A Matsuzawa. “A 9 mW 900 MHz CMOS LNA with mesh arrayed MOSFETs”. In: *VLSI Circuits, 1998. Digest of Technical Papers. 1998 Symposium on*. June 1998, pp. 84–85. DOI: 10.1109/VLSIC.1998.688010.
- [20] Qiuting Huang, P. Orsatti, and F. Piazza. “Broadband, 0.25 um CMOS LNAs with sub-2dB NF for GSM applications”. In: *Custom Integrated Circuits Conference, 1998. Proceedings of the IEEE 1998*. May 1998, pp. 67–70. DOI: 10.1109/CICC.1998.694908.
- [21] Seungyup Yoo, D. Heo, J. Laskar, and S.S. Taylor. “A C-band low power high dynamic range GaAs MESFET low noise amplifier”. In: *Radio and Wireless Conference, 1999. RAWCON 99. 1999 IEEE*. 1999, pp. 191–194. DOI: 10.1109/RAWCON.1999.810962.
- [22] F. Ellinger, U. Lott, and W. Bachtold. “A 5.2 GHz variable gain LNA MMIC for adaptive antenna combining”. In: *Radio Frequency Integrated Circuits (RFIC) Symposium, 1999 IEEE*. 1999, pp. 197–200. DOI: 10.1109/RFIC.1999.805270.

- [23] B.A Floyd, J. Mehta, C. Gamero, and K. O. Kenneth. "A 900-MHz, 0.8 μm CMOS low noise amplifier with 1.2-dB noise figure". In: *Custom Integrated Circuits, 1999. Proceedings of the IEEE 1999*. 1999, pp. 661–664. DOI: 10.1109/CICC.1999.777367.
- [24] J. Lucek and R. Damen. *Designing an LNA for a CDMA front end*. Feb. 1999. URL: www.rfdesign.com.
- [25] F. Ellinger, U. Lott, and W. Bachtold. "Ultra low power GaAs MMIC low noise amplifier for smart antenna combining at 5.2 GHz". In: *Radio Frequency Integrated Circuits (RFIC) Symposium, 2000. Digest of Papers. 2000 IEEE*. June 2000, pp. 157–159. DOI: 10.1109/RFIC.2000.854438.
- [26] O. Shana'A, I Linscott, and L. Tyler. "Frequency-scalable SiGe bipolar RFIC front-end design". In: *Custom Integrated Circuits Conference, 2000. CICC. Proceedings of the IEEE 2000*. 2000, pp. 183–186. DOI: 10.1109/CICC.2000.852645.
- [27] G. Gramegna, A Magazzu, C. Sclafani, and M. Paparo. "Ultra-wide dynamic range 1.75 dB noise-figure, 900 MHz CMOS LNA". In: *Solid-State Circuits Conference, 2000. Digest of Technical Papers. ISSCC. 2000 IEEE International*. Feb. 2000, pp. 380–381. DOI: 10.1109/ISSCC.2000.839824.
- [28] K. Sharaf. "2-V, 1-GHz CMOS inductorless LNAs with 2-3dB NF". In: *Circuits and Systems, 2000. Proceedings of the 43rd IEEE Midwest Symposium on*. Vol. 2. 2000, 714–717 vol.2. DOI: 10.1109/MWSCAS.2000.952856.
- [29] F. Gatta, E. Sacchi, F. Svelto, P. Vilmercati, and R. Castello. "A 2-dB noise figure 900-MHz differential CMOS LNA". In: *Solid-State Circuits, IEEE Journal of* 36.10 (Oct. 2001), pp. 1444–1452. ISSN: 0018-9200. DOI: 10.1109/4.953472.
- [30] Giuseppe Gramegna, M. Paparo, P.G. Erratico, and P. De Vita. "A sub-1-dB NF 2.3-kV ESD-protected 900-MHz CMOS LNA". In: *Solid-State Circuits, IEEE Journal of* 36.7 (July 2001), pp. 1010–1017. ISSN: 0018-9200.
- [31] P. Leroux, J. Janssens, and M. Steyaert. "A 0.8 dB NF ESD-protected 9 mW CMOS LNA". In: *Solid-State Circuits Conference, 2001. Digest of Technical Papers. ISSCC. 2001 IEEE International*. Feb. 2001, pp. 410–411. DOI: 10.1109/ISSCC.2001.912696.
- [32] X. Li, T. Brogan, M. Esposito, B. Myers, and K.K. O. "A comparison of CMOS and SiGe LNA's and mixers for wireless LAN application". In: *Custom Integrated Circuits, 2001, IEEE Conference on*. 2001, pp. 531–534. DOI: 10.1109/CICC.2001.929836.
- [33] Chih-Chun Tang and Shen-Iuan Liu. "Low-voltage CMOS low-noise amplifier using planar-interleaved transformer". In: *Electronics Letters* 37.8 (Apr. 2001), pp. 497–498. ISSN: 0013-5194. DOI: 10.1049/e1:20010366.
- [34] V. Chandrasekhar, C. -M Hung, Y.C. Ho, and K. Mayaram. "A packaged 2.4 GHz LNA in a 0.15 μm CMOS process with 2kV HBM ESD protection". In: *Solid-State Circuits Conference, 2002. ESSCIRC 2002. Proceedings of the 28th European*. Sept. 2002, pp. 347–350.

- [35] Jeyiyoung Lee, Geunho Lee, Guofu Niu, J.D. Cressler, J.H. Kim, J.C. Lee, B. Lee, and N.Y. Kim. "The design of SiGe HBT LNA for IMT-2000 mobile application". In: *Microwave Symposium Digest, 2002 IEEE MTT-S International*. Vol. 2. June 2002, 1261–1264 vol.2. DOI: 10.1109/MWSYM.2002.1011891.
- [36] Ren-Chieh Liu, Chung-Rung Lee, Huei Wang, and Chorng-Kuang Wang. "A 5.8-GHz two-stage high-linearity low-voltage low noise amplifier in a 0.35 um CMOS technology". In: *Radio Frequency Integrated Circuits (RFIC) Symposium, 2002 IEEE*. June 2002, pp. 221–224. DOI: 10.1109/RFIC.2002.1012036.
- [37] Y. Aoki, N. Hayama, M. Fujii, and H. Hida. "A 23-3-dB dual-gain low-noise amplifier for 5-GHz-band wireless applications". In: *Gallium Arsenide Integrated Circuit (GaAs IC) Symposium, 2002. 24th Annual Technical Digest*. Oct. 2002, pp. 197–200. DOI: 10.1109/GAAS.2002.1049059.
- [38] H. Hashemi and A Hajimiri. "Concurrent multiband low-noise amplifiers-theory, design, and applications". In: *Microwave Theory and Techniques, IEEE Transactions on* 50.1 (Jan. 2002), pp. 288–301. ISSN: 0018-9480. DOI: 10.1109/22.981282.
- [39] S. Andersson, C. Svenson, and O. Drugge. "Wideband LNA for a multistandard wireless receiver in 0.18 um CMOS". In: *Solid-State Circuits Conference, 2003. ESSCIRC '03. Proceedings of the 29th European*. Sept. 2003, pp. 655–658. DOI: 10.1109/ESSCIRC.2003.1257220.
- [40] E. Zencir, N.S. Dogan, and E. Arvas. "A low-power 435-MHz SOI CMOS LNA and mixer". In: *Microwave Symposium Digest, 2003 IEEE MTT-S International*. Vol. 1. June 2003, 555–558 vol.1. DOI: 10.1109/MWSYM.2003.1210999.
- [41] Ren-Chieh Liu, Chin-Shen Lin, Kuo-Liang Deng, and Huei Wang. "A 0.5-14-GHz 10.6-dB CMOS cascode distributed amplifier". In: *VLSI Circuits, 2003. Digest of Technical Papers. 2003 Symposium on*. June 2003, pp. 139–140. DOI: 10.1109/VLSIC.2003.1221183.
- [42] E. Imbs, I Telliez, S. Detout, and Y. Imbs. "A low-cost-packaged 4.9-6 GHz LNA for WLAN applications". In: *Microwave Symposium Digest, 2003 IEEE MTT-S International*. Vol. 3. June 2003, 1569–1572 vol.3. DOI: 10.1109/MWSYM.2003.1210436.
- [43] Yong-Sik Youn, Jae-Hong Chang, Kwang-Jin Koh, Young-Jae Lee, and Hyun-Kyu Yu. "A 2GHz 16dBm IIP3 low noise amplifier in 0.25 um CMOS technology". In: *Solid-State Circuits Conference, 2003. Digest of Technical Papers. ISSCC. 2003 IEEE International*. Feb. 2003, 452–507 vol.1. DOI: 10.1109/ISSC C.2003.1234383.
- [44] A Bevilacqua and AM. Niknejad. "An ultrawideband CMOS low-noise amplifier for 3.1-10.6-GHz wireless receivers". In: *Solid-State Circuits, IEEE Journal of* 39.12 (Dec. 2004), pp. 2259–2268. ISSN: 0018-9200. DOI: 10.1109/JSSC.2004.836338.
- [45] F. Bruccoleri, E.AM. Klumperink, and B. Nauta. "Wide-band CMOS low-noise amplifier exploiting thermal noise canceling". In: *Solid-State Circuits, IEEE Journal of* 39.2 (Feb. 2004), pp. 275–282. ISSN: 0018-9200. DOI: 10.1109/JSSC.2003.821786.

- [46] B. Mohammadi and C.AT. Salama. "A 5.8 GHz CMOS LNA for WLAN applications". In: *Radio Frequency Integrated Circuits (RFIC) Symposium, 2004. Digest of Papers. 2004 IEEE*. June 2004, pp. 113–116. DOI: 10.1109/RFIC.2004.1320542.
- [47] D. Linten, L. Aspemyr, W. Jeamsaksiri, J. Ramos, A Mercha, S. Jenei, S. Thijs, R. Garcia, H. Jacobsson, P. Wambacq, S. Donnay, and S. Decoutere. "Low-power 5 GHz LNA and VCO in 90 nm RF CMOS". In: *VLSI Circuits, 2004. Digest of Technical Papers. 2004 Symposium on*. June 2004, pp. 372–375. DOI: 10.1109/VLSIC.2004.1346619.
- [48] A Ismail and AA Abidi. "A 3-10-GHz low-noise amplifier with wideband LC-ladder matching network". In: *Solid-State Circuits, IEEE Journal of* 39.12 (Dec. 2004), pp. 2269–2277. ISSN: 0018-9200. DOI: 10.1109/JSSC.2004.836344.
- [49] Hsieh-Hung Hsieh and Liang-Hung Lu. "A CMOS 5-GHz micro-power LNA". In: *Radio Frequency integrated Circuits (RFIC) Symposium, 2005. Digest of Papers. 2005 IEEE*. June 2005, pp. 31–34. DOI: 10.1109/RFIC.2005.1489202.
- [50] F. Zhang and P. Kinget. "Low power programmable-gain CMOS distributed LNA for ultra-wideband applications". In: *VLSI Circuits, 2005. Digest of Technical Papers. 2005 Symposium on*. June 2005, pp. 78–81. DOI: 10.1109/VLSIC.2005.1469338.
- [51] S. Chehrazi, A Mirzaei, R. Bagheri, and AA Abidi. "A 6.5 GHz wideband CMOS low noise amplifier for multi-band use". In: *Custom Integrated Circuits Conference, 2005. Proceedings of the IEEE 2005*. Sept. 2005, pp. 801–804. DOI: 10.1109/CICC.2005.1568790.
- [52] Chang-Wan Kim, Min-Suk Kang, Phan Tuan Anh, Hoon-Tae Kim, and Sang-Gug Lee. "An ultra-wideband CMOS low noise amplifier for 3-5-GHz UWB system". In: *Solid-State Circuits, IEEE Journal of* 40.2 (Feb. 2005), pp. 544–547. ISSN: 0018-9200. DOI: 10.1109/JSSC.2004.840951.
- [53] Yanxin Wang, J.S. Duster, and K.T. Kornegay. "Design of an ultra-wideband low noise amplifier in 0.13 μm CMOS". In: *Circuits and Systems, 2005. IS-CAS 2005. IEEE International Symposium on*. May 2005, 5067–5070 Vol. 5. DOI: 10.1109/ISCAS.2005.1465773.
- [54] R. Molavi, S. Mirabbasi, and M. Hashemi. "A wideband CMOS LNA design approach". In: *Circuits and Systems, 2005. ISCAS 2005. IEEE International Symposium on*. May 2005, 5107–5110 Vol. 5. DOI: 10.1109/ISCAS.2005.1465783.
- [55] S.B.-T. Wang, AM. Niknejad, and R.W. Brodersen. "A sub-mW 960-MHz ultra-wideband CMOS LNA". In: *Radio Frequency integrated Circuits (RFIC) Symposium, 2005. Digest of Papers. 2005 IEEE*. June 2005, pp. 35–38. DOI: 10.1109/RFIC.2005.1489203.
- [56] Hung-Wei Chiu, Shey-Shi Lu, and Yo-Sheng Lin. "A 2.17-dB NF 5-GHz-band monolithic CMOS LNA with 10-mW DC power consumption". In: *Microwave Theory and Techniques, IEEE Transactions on* 53.3 (Mar. 2005), pp. 813–824. ISSN: 0018-9480. DOI: 10.1109/TMTT.2004.842510.

- [57] Bo-Yang Chang and C.F. Jou. "Design of a 3.1-10.6GHz low-voltage, low-power CMOS low-noise amplifier for ultra-wideband receivers". In: *Microwave Conference Proceedings, 2005. APMC 2005. Asia-Pacific Conference Proceedings*. Vol. 2. Dec. 2005. DOI: 10.1109/APMC.2005.1606458.
- [58] P. Heydari and D. Lin. "A performance optimized CMOS distributed LNA for UWB receivers". In: *Custom Integrated Circuits Conference, 2005. Proceedings of the IEEE 2005*. Sept. 2005, pp. 337–340. DOI: 10.1109/CICC.2005.1568674.
- [59] Chih-Fan Liao and Shen-Iuan Liu. "A broadband noise-canceling CMOS LNA for 3.1-10.6-GHz UWB receiver". In: *Custom Integrated Circuits Conference, 2005. Proceedings of the IEEE 2005*. Sept. 2005, pp. 161–164. DOI: 10.1109/CICC.2005.1568632.
- [60] P. Heydari, D. Lin, A. Shamel, and A. Yazdi. "Design of CMOS distributed circuits for multiband UWB wireless receivers [LNA and mixer]". In: *Radio Frequency Integrated Circuits (RFIC) Symposium, 2005. Digest of Papers. 2005 IEEE*. June 2005, pp. 695–698. DOI: 10.1109/RFIC.2005.1489909.
- [61] Hanil Lee and S. Mohammadi. "A 3GHz subthreshold CMOS low noise amplifier". In: *Radio Frequency Integrated Circuits (RFIC) Symposium, 2006 IEEE*. June 2006. DOI: 10.1109/RFIC.2006.1651199.
- [62] T. Ragheb, A. Nieuwoudt, and Y. Massoud. "Modeling of 3.1-10.6 GHz CMOS Filter-Based Low Noise Amplifier for Ultra-Wideband Receivers". In: *Wireless and Microwave Technology Conference, 2006. WAMICON '06. IEEE Annual*. Dec. 2006, pp. 1–5. DOI: 10.1109/WAMICON.2006.351903.
- [63] F. Zhang and P.R. Kinget. "Low-power programmable gain CMOS distributed LNA". In: *Solid-State Circuits, IEEE Journal of* 41.6 (June 2006), pp. 1333–1343. ISSN: 0018-9200. DOI: 10.1109/JSSC.2006.874283.
- [64] S.B.-T. Wang, A.M. Niknejad, and R.W. Brodersen. "Design of a Sub-mW 960-MHz UWB CMOS LNA". In: *Solid-State Circuits, IEEE Journal of* 41.11 (Nov. 2006), pp. 2449–2456. ISSN: 0018-9200. DOI: 10.1109/JSSC.2006.883321.
- [65] H.-J. Lee, D.S. Ha, and S.S. Choi. "A 3 to 5GHz CMOS UWB LNA with input matching using miller effect". In: *Solid-State Circuits Conference, 2006. ISSCC 2006. Digest of Technical Papers. IEEE International*. Feb. 2006, pp. 731–740. DOI: 10.1109/ISSCC.2006.1696112.
- [66] Chang-tsung Fu and Chien-Nan Kuo. "3-11 GHz CMOS UWB LNA using dual feedback for broadband matching". In: *Radio Frequency Integrated Circuits (RFIC) Symposium, 2006 IEEE*. June 2006. DOI: 10.1109/RFIC.2006.1651089.
- [67] A. Bevilacqua, C. Sandner, A. Gerosa, and A. Neviani. "A fully integrated differential CMOS LNA for 3-5-GHz ultrawideband wireless receivers". In: *Microwave and Wireless Components Letters, IEEE* 16.3 (Mar. 2006), pp. 134–136. ISSN: 1531-1309. DOI: 10.1109/LMWC.2006.869855.
- [68] S.C. Blaakmeer, E.A.M. Klumperink, D.M.W. Leenaerts, and B. Nauta. "A wideband noise-canceling CMOS LNA exploiting a transformer". In: *Radio Frequency Integrated Circuits (RFIC) Symposium, 2006 IEEE*. June 2006. DOI: 10.1109/RFIC.2006.1651110.

- [69] J.-H.C. Zhan and S.S. Taylor. "A 5GHz resistive-feedback CMOS LNA for low-cost multi-standard applications". In: *Solid-State Circuits Conference, 2006. ISSCC 2006. Digest of Technical Papers. IEEE International*. Feb. 2006, pp. 721–730. DOI: 10.1109/ISSCC.2006.1696111.
- [70] A Amer, E. Hegazi, and H. Ragai. "A Low-Power Wideband CMOS LNA for WiMAX". In: *Circuits and Systems II: Express Briefs, IEEE Transactions on* 54.1 (Jan. 2007), pp. 4–8. ISSN: 1549-7747. DOI: 10.1109/TCSII.2006.884113.
- [71] Chyuen-Wei Ang, Yuanjin Zheng, and Chun-Huat Heng. "A Multi-band CMOS Low Noise Amplifier for Multi-standard Wireless Receivers". In: *Circuits and Systems, 2007. ISCAS 2007. IEEE International Symposium on*. May 2007, pp. 2802–2805. DOI: 10.1109/ISCAS.2007.378635.
- [72] Hsien-Ku Chen, Da-Chiang Chang, Y. -Z Juang, and Shey-Shi Lu. "A Compact Wideband CMOS Low-Noise Amplifier Using Shunt Resistive-Feedback and Series Inductive-Peaking Techniques". In: *Microwave and Wireless Components Letters, IEEE* 17.8 (Aug. 2007), pp. 616–618. ISSN: 1531-1309. DOI: 10.1109/LMWC.2007.901797.
- [73] S.C. Blaakmeer, E.A.M. Klumperink, B. Nauta, and D.M.W. Leenaerts. "An inductorless wideband balun-LNA in 65nm CMOS with balanced output". In: *Solid State Circuits Conference, 2007. ESSCIRC 2007. 33rd European*. Sept. 2007, pp. 364–367. DOI: 10.1109/ESSCIRC.2007.4430319.
- [74] M.T. Reiha and J.R. Long. "A 1.2 V Reactive-Feedback 3.1-10.6 GHz Low-Noise Amplifier in 0.13 μm CMOS". In: *Solid-State Circuits, IEEE Journal of* 42.5 (May 2007), pp. 1023–1033. ISSN: 0018-9200. DOI: 10.1109/JSSC.2007.894329.
- [75] J. Borremans, P. Wambacq, C. Soens, Y. Rolain, and M. Kuijk. "Low-Area Active-Feedback Low-Noise Amplifier Design in Scaled Digital CMOS". In: *Solid-State Circuits, IEEE Journal of* 43.11 (Nov. 2008), pp. 2422–2433. ISSN: 0018-9200. DOI: 10.1109/JSSC.2008.2005434.
- [76] G.D. Nguyen, K. Cimino, and Milton Feng. "A RF CMOS amplifier with optimized gain, noise, linearity and return losses for UWB applications". In: *Radio Frequency Integrated Circuits Symposium, 2008. RFIC 2008. IEEE*. June 2008, pp. 505–508. DOI: 10.1109/RFIC.2008.4561487.
- [77] H.-Y. Yang, Y.-S. Lin, and C.-C. Chen. "2.5 dB NF 3.1-10.6 GHz CMOS UWB LNA with small group-delay variation". In: *Electronics Letters* 44.8 (Apr. 2008), pp. 528–529. ISSN: 0013-5194. DOI: 10.1049/e1:20083425.
- [78] Tienyu Chang, Jinghong Chen, L. Rigge, and Jenshan Lin. "A Packaged and ESD-Protected Inductorless 0.1-8 GHz Wideband CMOS LNA". In: *Microwave and Wireless Components Letters, IEEE* 18.6 (June 2008), pp. 416–418. ISSN: 1531-1309. DOI: 10.1109/LMWC.2008.922677.
- [79] Seong-Sik Song, Dong-Gu Im, Hong-Teuk Kim, and Kwyro Lee. "A Highly Linear Wideband CMOS Low-Noise Amplifier Based on Current Amplification for Digital TV Tuner Applications". In: *Microwave and Wireless Components Letters, IEEE* 18.2 (Feb. 2008), pp. 118–120. ISSN: 1531-1309. DOI: 10.1109/LMWC.2007.915101.

- [80] Chieh-Pin Chang, Ja-Hao Chen, and Yeong-Her Wang. “A Fully Integrated 5 GHz Low-Voltage LNA Using Forward Body Bias Technology”. In: *Microwave and Wireless Components Letters, IEEE* 19.3 (Mar. 2009), pp. 176–178. ISSN: 1531-1309. DOI: 10.1109/LMWC.2009.2013745.
- [81] Mingqi Chen and Jenshan Lin. “A 0.1-20 GHz Low-Power Self-Biased Resistive-Feedback LNA in 90 nm Digital CMOS”. In: *Microwave and Wireless Components Letters, IEEE* 19.5 (May 2009), pp. 323–325. ISSN: 1531-1309. DOI: 10.1109/LMWC.2009.2017608.
- [82] M. Okushima, J. Borremans, D. Linten, and G. Groeseneken. “A DC-to-22 GHz 8.4mW compact dual-feedback wideband LNA in 90 nm digital CMOS”. In: *Radio Frequency Integrated Circuits Symposium, 2009. RFIC 2009. IEEE*. June 2009, pp. 295–298. DOI: 10.1109/RFIC.2009.5135543.
- [83] Chi-Chen Chen, Jen-How Lee, Yo-Sheng Lin, Chang-Zhi Chen, Guo-Wei Huang, and Shey-Shi Lu. “Low Noise-Figure PAA Mesh Inductors for CMOS UWB RFIC Applications”. In: *Electron Devices, IEEE Transactions on* 55.12 (Dec. 2008), pp. 3542–3548. ISSN: 0018-9383. DOI: 10.1109/TED.2008.2006537.
- [84] S.K. Hampel, O. Schmitz, M. Tiebout, and I Rolfes. “Inductorless 1-10.5 GHz wideband LNA for multistandard applications”. In: *Solid-State Circuits Conference, 2009. A-SSCC 2009. IEEE Asian*. Nov. 2009, pp. 269–272. DOI: 10.1109/ASSCC.2009.5357261.
- [85] Donggu Im, Ilku Nam, Hong-Teuk Kim, and Kwyro Lee. “A Wideband CMOS Low Noise Amplifier Employing Noise and IM2 Distortion Cancellation for a Digital TV Tuner”. In: *Solid-State Circuits, IEEE Journal of* 44.3 (Mar. 2009), pp. 686–698. ISSN: 0018-9200. DOI: 10.1109/JSSC.2008.2010804.
- [86] M. El-Nozahi, E. Sanchez-Sinencio, and K. Entesari. “A CMOS Low-Noise Amplifier With Reconfigurable Input Matching Network”. In: *Microwave Theory and Techniques, IEEE Transactions on* 57.5 (May 2009), pp. 1054–1062. ISSN: 0018-9480. DOI: 10.1109/TMTT.2009.2017249.
- [87] Sanghyun Woo, Woonyun Kim, Chang-Ho Lee, Kyutae Lim, and J. Laskar. “A 3.6mW differential common-gate CMOS LNA with positive-negative feedback”. In: *Solid-State Circuits Conference - Digest of Technical Papers, 2009. ISSCC 2009. IEEE International*. Feb. 2009, 218–219, 219a. DOI: 10.1109/ISSCC.2009.4977386.
- [88] M.A.G. Lorenzo and M.T.G. de Leon. “Comparison of LNA Topologies for WiMAX Applications in a Standard 90-nm CMOS Process”. In: *Computer Modelling and Simulation (UKSim), 2010 12th International Conference on*. Mar. 2010, pp. 642–647. DOI: 10.1109/UKSIM.2010.122.
- [89] Yueh-Hua Yu, Yong-Sian Yang, and Yi-Jan Chen. “A Compact Wideband CMOS Low Noise Amplifier With Gain Flatness Enhancement”. In: *Solid-State Circuits, IEEE Journal of* 45.3 (Mar. 2010), pp. 502–509. ISSN: 0018-9200. DOI: 10.1109/JSSC.2010.2040111.

- [90] Hsien-Ku Chen, Yo-Sheng Lin, and Shey-Shi Lu. "Analysis and Design of a 1.6-28 GHz Compact Wideband LNA in 90-nm CMOS Using a pi-Match Input Network". In: *Microwave Theory and Techniques, IEEE Transactions on* 58.8 (Aug. 2010), pp. 2092–2104. ISSN: 0018-9480. DOI: 10.1109/TMTT.2010.2052406.
- [91] Hongrui Wang, Li Zhang, and Zhiping Yu. "A Wideband Inductorless LNA With Local Feedback and Noise Cancelling for Low-Power Low-Voltage Applications". In: *Circuits and Systems I: Regular Papers, IEEE Transactions on* 57.8 (Aug. 2010), pp. 1993–2005. ISSN: 1549-8328. DOI: 10.1109/TCSI.2010.2042997.
- [92] Jusung Kim, S. Hoyos, and J. Silva-Martinez. "Wideband Common-Gate CMOS LNA Employing Dual Negative Feedback With Simultaneous Noise, Gain, and Bandwidth Optimization". In: *Microwave Theory and Techniques, IEEE Transactions on* 58.9 (Sept. 2010), pp. 2340–2351. ISSN: 0018-9480. DOI: 10.1109/TMTT.2010.2057790.
- [93] Donggu Im, Ilku Nam, Jae-Young Choi, Bum-Kyum Kim, and Kwyro Lee. "A CMOS active feedback wideband single-to-differential LNA using inductive shunt-peaking for saw-less SDR receivers". In: *Solid State Circuits Conference (ASSCC), 2010 IEEE Asian*. Nov. 2010, pp. 1–4. DOI: 10.1109/ASSCC.2010.5716578.
- [94] T. Taris, J. Begueret, and Y. Deval. "A 60 uW LNA for 2.4 GHz wireless sensors network applications". In: *Radio Frequency Integrated Circuits Symposium (RFIC), 2011 IEEE*. June 2011, pp. 1–4. DOI: 10.1109/RFIC.2011.5940633.
- [95] C.J. Jeong, W. Qu, Y. Sun, D.Y. Yoon, S.K. Han, and S-G Lee. "A 1.5V, 140 A CMOS ultra-low power common-gate LNA". In: *Radio Frequency Integrated Circuits Symposium (RFIC), 2011 IEEE*. June 2011, pp. 1–4. DOI: 10.1109/RFIC.2011.5940634.
- [96] M. El-Nozahi, AA Helmy, E. Sanchez-Sinencio, and K. Entesari. "An Inductor-Less Noise-Cancelling Broadband Low Noise Amplifier With Composite Transistor Pair in 90 nm CMOS Technology". In: *Solid-State Circuits, IEEE Journal of* 46.5 (May 2011), pp. 1111–1122. ISSN: 0018-9200. DOI: 10.1109/JSSC.2011.2118310.
- [97] E.A Sobhy, AA Helmy, Sebastian Hoyos, K. Entesari, and E. Sanchez-Sinencio. "A 2.8-mW Sub-2-dB Noise-Figure Inductorless Wideband CMOS LNA Employing Multiple Feedback". In: *Microwave Theory and Techniques, IEEE Transactions on* 59.12 (Dec. 2011), pp. 3154–3161. ISSN: 0018-9480. DOI: 10.1109/TMTT.2011.2169081.
- [98] A Zafarian, I Kalali Fard, A Golmakani, and J. Shirazi. "A 0.4V 790 uw CMOS low noise amplifier in sub-threshold region at 1.5GHz". In: *Design and Test Symposium (IDT), 2013 8th International*. Dec. 2013, pp. 1–6. DOI: 10.1109/IDT.2013.6727104.
- [99] A Madan, M.J. McPartlin, C. Masse, W. Vaillancourt, and J.D. Cressler. "A 5 GHz 0.95 dB NF Highly Linear Cascode Floating-Body LNA in 180 nm SOI CMOS Technology". In: *Microwave and Wireless Components Letters, IEEE* 22.4 (Apr. 2012), pp. 200–202. ISSN: 1531-1309. DOI: 10.1109/LMWC.2012.2187882.

- [100] Ke-Hou Chen and Shen-Iuan Liu. “Inductorless Wideband CMOS Low-Noise Amplifiers Using Noise-Canceling Technique”. In: *Circuits and Systems I: Regular Papers, IEEE Transactions on* 59.2 (Feb. 2012), pp. 305–314. ISSN: 1549-8328. DOI: 10.1109/TCSI.2011.2162461.
- [101] N.M. Neihart, J. Brown, and Xiaohua Yu. “A Dual-Band 2.45-6 GHz CMOS LNA Utilizing a Dual-Resonant Transformer-Based Matching Network”. In: *Circuits and Systems I: Regular Papers, IEEE Transactions on* 59.8 (Aug. 2012), pp. 1743–1751. ISSN: 1549-8328. DOI: 10.1109/TCSI.2011.2180436.
- [102] M. Moezzi and M.S. Bakhtiar. “Wideband LNA Using Active Inductor With Multiple Feed-Forward Noise Reduction Paths”. In: *Microwave Theory and Techniques, IEEE Transactions on* 60.4 (Apr. 2012), pp. 1069–1078. ISSN: 0018-9480. DOI: 10.1109/TMTT.2012.2185947.
- [103] Yeo Myung Kim, Honggul Han, and Tae Wook Kim. “A 0.6-V +4 dBm IIP3 LC Folded Cascode CMOS LNA With gm Linearization”. In: *Circuits and Systems II: Express Briefs, IEEE Transactions on* 60.3 (Mar. 2013), pp. 122–126. ISSN: 1549-7747. DOI: 10.1109/TCSII.2013.2240811.
- [104] Mu-Tsung Lai and Hen-Wai Tsao. “Ultra-Low-Power Cascaded CMOS LNA With Positive Feedback and Bias Optimization”. In: *Microwave Theory and Techniques, IEEE Transactions on* 61.5 (May 2013), pp. 1934–1945. ISSN: 0018-9480. DOI: 10.1109/TMTT.2013.2256144.
- [105] Jianxun Zhu, H. Krishnaswamy, and P.R. Kinget. “A DC-9.5GHz noise-canceling distributed LNA in 65nm CMOS”. In: *Radio Frequency Integrated Circuits Symposium (RFIC), 2013 IEEE*. June 2013, pp. 177–180.
- [106] Jaeyoung Lee, Jeyoung Lee, Bonkee Kim, Bo-Eun Kim, and C. Nguyen. “A highly linear low-noise amplifier using a wideband linearization technique with tunable multiple gated transistors”. In: *Radio Frequency Integrated Circuits Symposium (RFIC), 2013 IEEE*. June 2013, pp. 181–184.
- [107] Chia-Lin Hsieh, Ming-Hang Wu, Jen-Hao Cheng, Jeng-Han Tsai, and Tian-Wei Huang. “A 0.6-V 336 uW 5-GHz LNA using a low-voltage and gain-enhancement architecture”. In: *Microwave Symposium Digest (IMS), 2013 IEEE MTT-S International*. June 2013, pp. 1–3. DOI: 10.1109/MWSYM.2013.6697468.
- [108] Ehsan Kargaran, Negar Zoka, Abbas Z. Kouzani, Khalil Mafinezhad, and Hooman Nabovati. “Highly linear low voltage low power CMOS LNA”. In: *IEICE Electronics Express* 10.21 (2013), pp. 20130557–20130557.
- [109] Ivan Bastos, F. Querido, D. Amoêdo, LuisB. Oliveira, J.P. Oliveira, João Goes, and ManuelM. Silva. “A 1.2 V Low-Noise-Amplifier with Double Feedback for High Gain and Low Noise Figure”. English. In: *Technological Innovation for the Internet of Things*. Ed. by LuisM. Camarinha-Matos, Slavisa Tomic, and Paula Graça. Vol. 394. IFIP Advances in Information and Communication Technology. Springer Berlin Heidelberg, 2013, pp. 573–581. ISBN: 978-3-642-37290-2. DOI: 10.1007/978-3-642-37291-9_62.

- [110] Ivan Bastos, L.B. Oliveira, J.P. Oliveira, J. Goes, and M.M Silva. “Ultra-low-voltage LNA with High Gain and Low Noise Figure”. In: *International Journal of Microelectronics and Computer Science* 4.3 (2013), pp. 124–128.
- [111] Yo-Sheng Lin, Chien-Chin Wang, and Jen-How Lee. “A 9.96 mW 3.24 +0.5 dB NF 1.9-22.5 GHz wideband low-noise amplifier using 90 nm CMOS technology”. In: *Radio and Wireless Symposium (RWS), 2014 IEEE*. Jan. 2014, pp. 208–210. DOI: 10.1109/RWS.2014.6830072.
- [112] Ruofan Dai, Yunlong Zheng, Hongwei Zhu, Weiran Kong, and Shichang Zou. “A high gain and high linearity current-reused CMOS LNA using modified derivative superposition technique with bulk-bias control”. In: *Microwave and Optical Technology Letters* 56.10 (2014), pp. 2444–2446. ISSN: 1098-2760. DOI: 10.1002/mop.28608. URL: <http://dx.doi.org/10.1002/mop.28608>.
- [113] CheeHan Cheong, Norlaili Mohd. Noh, and Harakrishnan Ramiah. “A Wideband LNA for Cognitive Radios”. English. In: *The 8th International Conference on Robotic, Vision, Signal Processing & Power Applications*. Ed. by Harsa Amylia Mat Sakim and Mohd Tafir Mustaffa. Vol. 291. Lecture Notes in Electrical Engineering. Springer Singapore, 2014, pp. 427–433. ISBN: 978-981-4585-41-5. DOI: 10.1007/978-981-4585-42-2_49.
- [114] Benqing Guo, Guangjun Wen, and Shiquan An. “6.8 mW 15 dBm IIP3 CMOS common-gate LNA employing post-linearisation technique”. In: *Electronics Letters* 50.3 (Jan. 2014), pp. 149–151. ISSN: 0013-5194. DOI: 10.1049/el.2013.3442.
- [115] Meng Ting Hsu, Yu Chang Hsieh, and Wei Lun Huang. “Design of Low Power UWB CMOS LNA Based on Common Source Inductor”. In: *Computer, Consumer and Control (IS3C), 2014 International Symposium on*. June 2014, pp. 1026–1029. DOI: 10.1109/IS3C.2014.268.

Appendix D

Limited Functionality Mode Concept

In this appendix the Limited Functionality Mode concept is described. It is applicable to both Device-to-Device (D2D) and Machine Type Communication (MTC), and since the latter was described in section 6.1.2 this section provides a brief overview of D2D before the concept is presented.

D2D is becoming a hot topic in wireless communications and actually Third Generation Partnership Project (3GPP) has already initiated a study item for Long Term Evolution (LTE) release 12 [178]. Due to backwards compatibility issues it is thus expected that the full potential will not be released before Fifth Generation (5G) is launched [179].

The main principle of D2D is that devices i.e. mobile terminals communicate directly in the sense that the data path is not routed via the serving Access Point (AP). This is very useful for proximity based services such as gaming, local advertising and social services and therefore it is also closely related to MTC. One common area for these techniques is Vehicle-to-Vehicle (V2V) communication, which can be used to improved traffic safety by letting the vehicles distribute warnings about queues, accidents etc. The D2D concept is also useful if the normal cellular infrastructure is damaged, e.g. by an earthquake, and this is what 3GPP has focused on [178]. In this scenario mobile terminals can distribute safety advice to users who are out of coverage of the functioning APs. It may also be beneficial for reducing signalling overhead if for example a group of mobile terminals in a bus or train all are to perform a handover to the same AP, [180]. In this scenario one mobile terminal may receive the required AP parameters and relay them to the mobile terminals within its proximity. The D2D concept may also apply Network Coding, [181] if for example multiple mobile terminals are to receive the same data. This could be the case if they are attending a sports event and all wish to receive up-to-date statistics and watch replays. The combination of D2D and Network Coding entail the mobile terminals can form a cooperation and each receive a part of the data after which they can share and combine to receive the full transmission, and this has also been shown to reduce the average power consumption [182].

The D2D communication can be either inband or outband, [180]. The inband communication can be underlaid, using the same spectrum resources as regular data transfers, or overlaid using dedicated resources, and all devices should therefore be able to apply it. The underlaid inband can obviously improve the spectral efficiency because it may reuse the spectrum resources, but it also poses challenging interference problems if the AP is not in control of transmit power control and scheduling.

According to [179] there are four main types of D2D; the first is relaying data from one mobile terminal via another to the AP if coverage is bad for the first mobile terminal. The D2D link can either be established via the AP or the mobile terminals as illustrated in figures D.1a and D.1b respectively. The third and fourth types are direct D2D where the mobile terminals exchange data while the link is either established via the AP or directly between the mobile terminals as illustrated in figures D.1c and D.1d respectively.

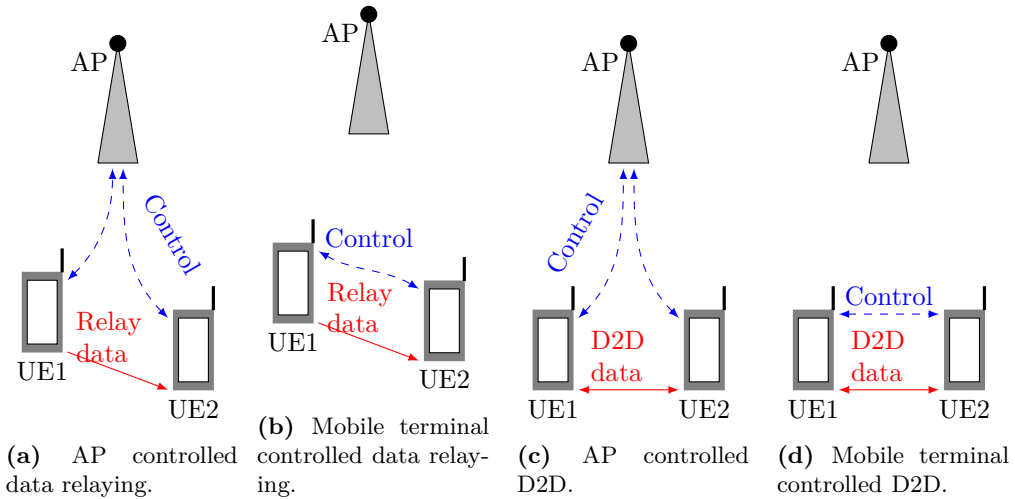


Figure D.1: D2D methods for relayed and direct data transfer, based on [179].

Given the 5G concept's frame structure with variable link direction it is easy to accommodate the AP established links, but since the uplink is contention based mobile terminals (see figure 4.9) will also have to rely on requesting permissions to transmit via the AP. Allowing the mobile terminals to control it would cause collisions i.e. uncontrolled interference in uplink. Another issue is the security because the AP and the core network may not be involved in the transfer, but this can also be seen as an advantage since the data will no longer be routed via the Internet. Other issues are handling mobility of the mobile terminals and pricing the D2D when the AP is only facilitating the transfer but not performing it as illustrated in figures D.1a and D.1c, [179]. The main advantage of D2D is the capacity gain which can be achieved if the regular cellular users and the D2D users can share the licensed spectrum.

Since D2D is expected to be proximity driven it entails the mobile terminals may use a lower transmit power, to save energy, and achieve higher data rates, because the path loss is smaller. Finally the latency may also be lower because the two ends are

closer to each other avoiding long Internet routing lines. This is especially important for low-latency applications such as V2V and gaming, but the short 5G frame should be able to handle such a requirement.

Note that currently WiFi and Bluetooth (BT) can be used for D2D but in unlicensed bands where there is limited management of interference and no guarantee of Quality of Service (QoS), [179].

One key issue that has not been addressed is the time it takes to set up secure connections between devices in LTE. Security is important, but in some cases the data may have less strict requirements or the environment may provide security due to close proximity and therefore it may be possible to reduce the security to reduce latency and save energy. In the next section a concept is proposed to allow for these trade-offs.

D.0.1 The Concept

In this section a new mobile terminal mode, which is positioned between LTE's Radio Resource Control (RRC) connected and idle mode, is proposed. The target is to reduce the ON time of the mobile terminal by reducing the time spent on authentication with the core network. In principle it can be applied in both LTE and 5G, but it is especially important for the latter because it has been defined to be always ON and thus efficient methods to mimic this behaviour are needed. The concept has been filed for patenting, but a reference cannot be provided due to confidentiality requirements.

Due to the expected increase in MTC traffic the data transfers will often consist of short and infrequent messages. This does not fit LTE's Discontinuous Reception (DRX) functionality well, when the time between messages is longer than 2.56 s which is the maximum DRX Long Period (DRX LP) in LTE. Note the maximum length for 5G DRX is still undefined. The User Equipment (UE), with infrequent traffic, may therefore be pushed to RRC idle mode, but this will cause the Evolved Node B (eNB) and the UE to discard the keys used for secure communication, [183]. The next time the UE has a message to transfer it needs to establish a new secure connection with the eNB, and possibly also with the core network using the Mobility Management Entity (MME), which manages the control plane connection and the radio bearers between the user and the core network. The user plane data bypasses the MME and is managed by the System Architecture Evolution Gateway, but this can only occur after the security has been set up with the MME. The gateway is connected to the external networks e.g. the Internet via the Packet Data Network Gateway [59].

The procedure for establishing a secure connection the first time the UE connects to an LTE eNB is illustrated in figure D.2 and the following description is based on [60, 184, 185, 186]. *Step 1* for the UE is to select a Random Access Preamble and send it on the Random Access Channel to the eNB. The preamble is connected with a Random Access Radio Network Temporary Identifier (RNTI), which is used by the UE to identify the response sent by the eNB on the Physical Downlink Control Channel (PDCCH). Provided the UE detects the message in the PDCCH it will know where to receive the Random Access Response, *step 2*, in the time-frequency slots of the Physical Downlink Shared Channel (PDSCH). The response includes timing alignment for subsequent uplink transmissions, uplink resource grants for the next messages, and the Cell RNTI, which is a unique identifier for the UE in the specific cell.

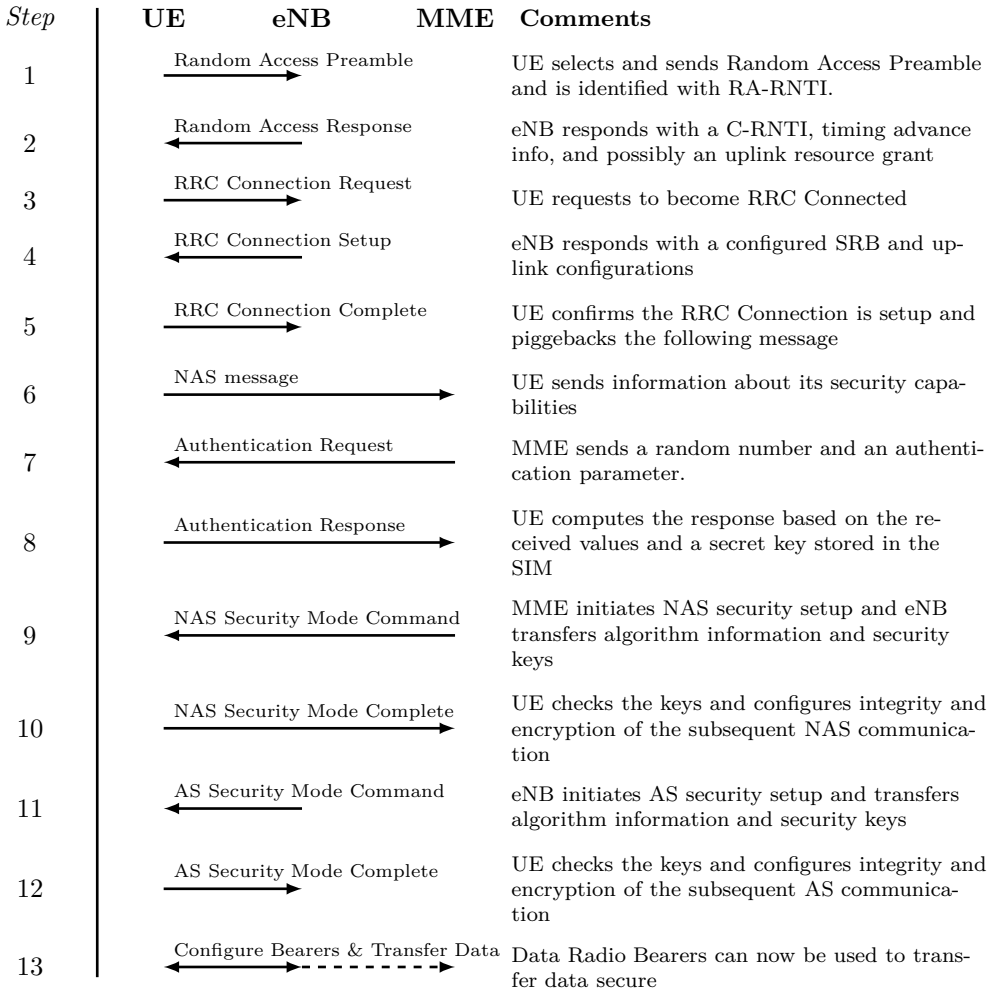


Figure D.2: Flow for establishment of connection and security in LTE. Based on [184, 60, 185].

In *step 3* the UE will request to become RRC connected using the allocated uplink resource. The UE will also detail why it wants to connect e.g. to perform a voice call. In *step 4* the eNB confirms the RRC connection setup by creating the Signalling Radio Bearer, which is used to transfer subsequent RRC messages. The response also contains uplink configuration information such as details on the applied Transmit Power Control. The RRC connection setup is complete when the UE confirms it in *step 5*. This message will also contain a Non-Access Stratum (NAS) message in which the UE informs the MME about its security capabilities, marked as *step 6* in figure D.2. The NAS is a collection of functions and protocols used for communication between the UE and the core network, which are not targeted a specific Radio Access Technology (RAT), as

opposed to the Access Stratum (AS) which are for a specific RAT. The MME will then contact the Home Environment, which stores a secret key that is also programmed in the UE's Subscriber Identity Module (SIM) card. Using the secret key K several other keys, refer to [183, Chapter 14] for the full list, are derived and forwarded to the MME. In addition to the keys an authentication token, a random number, and an expected response is also generated. In *step 7* the eNB receives the authentication token and the random number and forwards them to the UE, which by using the same secret key K of the SIM card can compute a result which is used in the response in *step 8*.

Provided that the UE's computed response matches the expected response the MME considers the UE to be authenticated. Therefore the MME will proceed with the NAS security setup in *step 9* by transferring the identifier for the Access Security Management Entity key, derived from key K , to the UE and information about the encryption and integrity algorithms. By using the identifier the UE can lookup the correct key and derive the required keys for the encryption and integrity algorithms and finally respond with an encrypted and integrity protected message in *step 10*. The encryption entails only the receiver is able to decode the message using a secret key, while the integrity entails the receiver can verify that the received message is the same as the transmitted message.

Because NAS security is now installed the MME provides the eNB with keys used to secure the RRC and user plane signalling between eNB and the UE i.e. the AS. Therefore the eNB forwards the key identifier and information about the encryption and integrity algorithms to the UE in *step 11*. The UE will then apply a similar procedure as in *step 10* and respond with an encrypted and integrity protected message in *step 12*. Now that the UE is able to communicate securely with the MME using NAS and the eNB using AS it is possible to configure radio bearers for data transmission as indicated in *step 13*.

When the UE at some point releases the RRC connection and enters idle mode the UE and the eNB must delete all the keys that are related to the user plane and RRC signalling while the NAS related keys may be kept in the MME and the UE, [183]. This entails that the UE, which performs infrequent transmissions has to perform many of the steps of figure D.2 whenever it has to transfer data after returning from idle mode. Furthermore re-authentication with the MME is estimated to occur approximately every 30 minutes thus the UE is forced to perform all steps again. This is similar to 3G where the UE must also be authenticated and have the Cell RNTI before it can transfer data. Thus for the existing RATs a single data transfer, after being idle, will entail the activities illustrated in figure D.3.

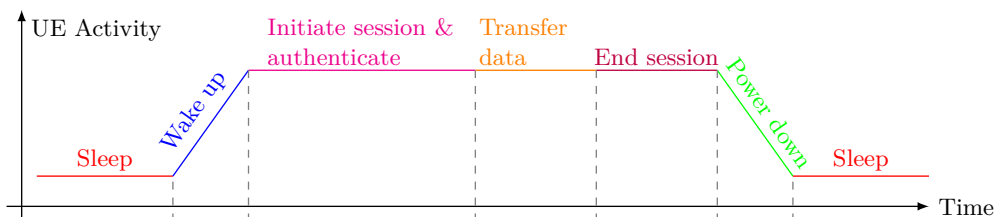


Figure D.3: Activity for a data transfer in LTE when the UE has been RRC idle.

Because the amount of traffic may be small the overhead of the authentication and security setup can become significant and thus lead to higher power consumption. Therefore a new RRC mode, called Limited Functionality, is proposed for 5G where the target is to outsource the authentication and security setup such that the mobile terminal can quickly transfer the data to the AP and return to the low-power sleep mode. Figure D.4 illustrates one possible implementation where the mobile terminal and AP follows the normal procedure for random access in *steps 1 & 2* and in addition requests Limited Functionality mode. The following *step 3* is then to perform a pre-authentication procedure where the mobile terminal requests the AP to authenticate it towards the MME and the core network later. Assuming that the mobile terminal previously has been connected with the MME it can rely on the keys associated to that connection, but otherwise it may derive a new key using the secret key of the SIM card. Assuming the AP accepts to authenticate the mobile terminal in *step 4*, and informs about allocated uplink resources, the mobile terminal may transfer the data in *step 5* after which it can return to a low-power sleep mode. When the AP has received the data it can initiate a secure session with the MME on behalf of the mobile terminal in *step 6*. In *steps 7 & 8* the AP and MME may then perform the security setup, which was performed in LTE in step 7-12 of figure D.2. After the authentication and security is in place the AP may finally forward the data onwards to the destination, unless it was intended for the AP itself, in *step 9*.

The proposed Limited Functionality mode may not be as secure as in LTE, depending on how the keys are derived, but in some cases the mobile terminal may not need to forward the data further than the AP and thus less secure transfers may be acceptable. This is also the reason why the mode is called Limited Functionality, because it does not allow for high security transfers to be completed nor does it allow the mobile terminal to wait for responses to the transferred data. Table D.1 contains an overview of the three proposed mobile terminal modes for 5G; the full functionality mode, which corresponds to the RRC connected mode of LTE, the limited functionality mode as described in this section, and the minimum functionality, which corresponds to RRC idle. The mobile terminal energy consumption increases with increasing functionality because the ON time increases. The latency, defined as the time it takes for a data transfer to complete, is long for the idle mobile terminal because the time to set up security is long. The full functionality mode has the lowest latency, because it is always ON, while the limited functionality mode has medium latency due to the less secure transfers. Thus the cost to achieve the trade-off between latency and energy consumption is the lower security, but this may be acceptable in a spatially limited Ultra-Dense Small Cell (UDSC) scenario, such as a hospital or a private home. Furthermore some data transfers may also accept lower security.

One example of data transfers with lower security requirements is the updates the mobile terminal sends to the AP about its current capabilities, which may have changed due to a low battery level or the connection with a power plug. Other examples are the measurement reports the mobile terminal sends with information about the receive power strength from other APs and mobile terminals, and when the mobile terminal requests a different sleep/paging pattern. It may also be possible for the mobile terminal to send a less secure Tracking Area Update, when it has moved into a new coverage area. For simplicity the mobile terminal may just inform the new AP about which AP

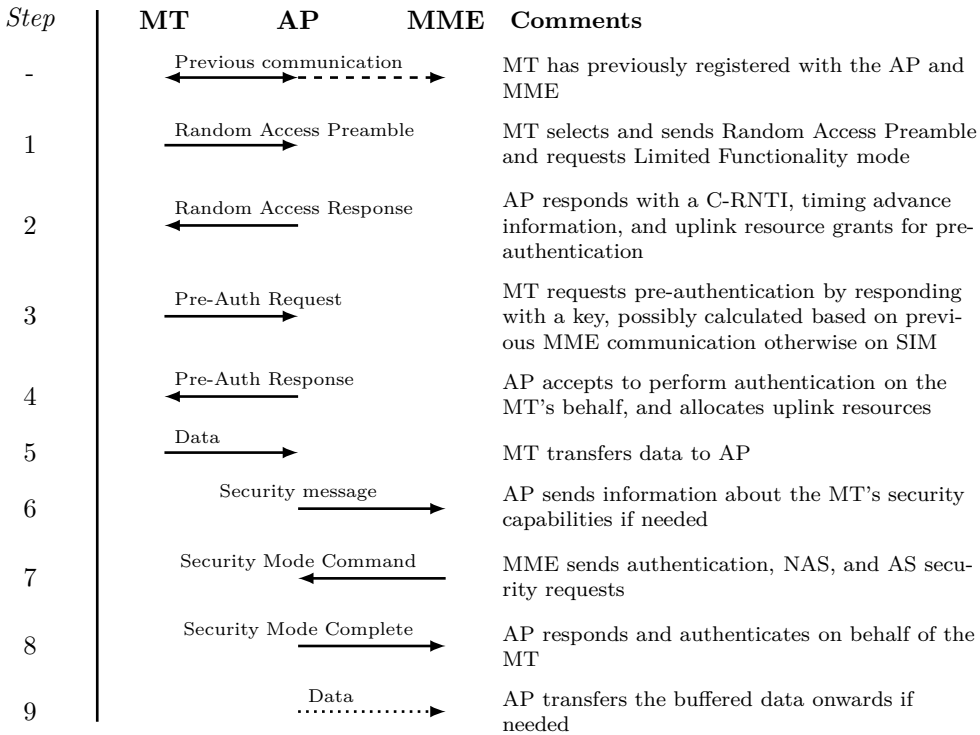


Figure D.4: Proposed flow for establishment of connection and security in 5G. Mobile terminal is denoted MT.

it was previously connected to, after which the new AP can obtain relevant information about the mobile terminal from the previous AP.

Assuming the Limited Functionality mode is implemented in 5G the activity for a data transfer, after exiting idle mode, will be as illustrated in figure D.5. The activity drawing assumes the mobile terminal has already registered with the MME and thus it just performs pre-authentication and transfers data to the AP after which it returns to a low-power sleep mode. Next the AP will authenticate on behalf of the mobile terminal and forward the data to the right entity, and because these operations take place using a backhaul they may be performed faster e.g. if the connection is fiber based. If the mobile terminal is not registered with the MME it has to follow a procedure similar to figure D.2.

As mentioned earlier the MME of LTE requires re-authentication approximately every 30 minutes, but this limit has not yet been defined for 5G. It is assumed that after the mobile terminal has completed the pre-authentication the subsequent data transfers can occur immediately after the mobile terminal exits idle mode as illustrated in figure D.6 and thus reduce latency and power consumption further. This behaviour resembles the use of DRX in RRC connected mode, but allows for much longer sleep

Table D.1: Proposed mobile terminal modes in 5G.

Mode	Connection	Functionality	Latency	Energy Consumption
Full (RRC connected in LTE)	Terminal is connected to MME and core network via the AP	Data transfer and exchange of network and terminal settings	Low, due to always ON	High, due to long ON time and limited DRX
Limited	Terminal is connected to AP	Less secure data transfer and exchange of network and terminal settings	Medium, due to fast data dump	Medium, due to the short ON period
Minimum (RRC idle in LTE)	Terminal periodically wakes up and scans the network	Reception of paging messages and measurements on other network entities	High, due to the set up of security	Low, due to extended use of sleep

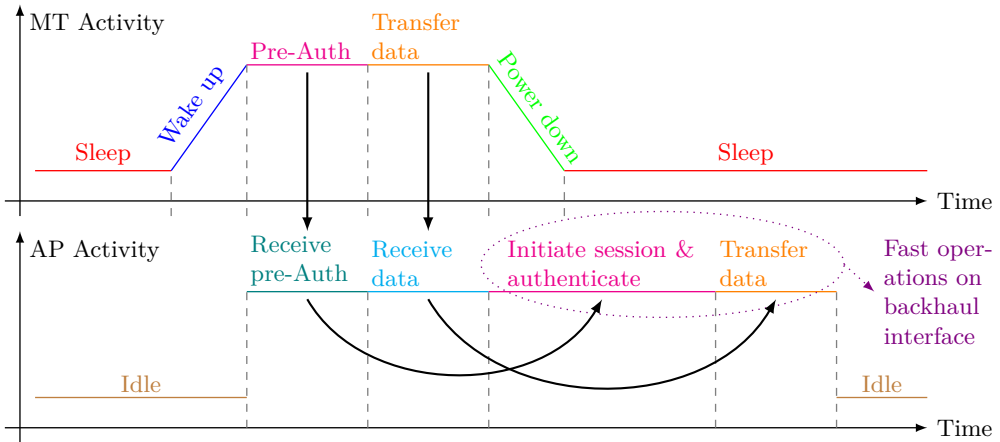


Figure D.5: Activity for a data transfer in 5G assuming the mobile terminal has been in idle (minimum functionality) mode, and that the initial registration with the MME has occurred previously.

periods than what is currently standardized for DRX.

The Limited Functionality mode is expected to provide some improvement in energy consumption because less handshaking procedures are required as compared to the current modes of LTE. As illustrated in figure D.2 13 steps are needed in LTE to make the initial registration with both MME and eNB, while this number is reduced to 8 steps if the mobile terminal has previously communicated with the MME. Figure D.4 illustrates that this number, after MME registration, is reduced to 5 and 3 steps depending on whether pre-authentication is needed. Thus the ON time is approximately reduced by half for short data transmissions. Referring to the discussion on battery life as a function

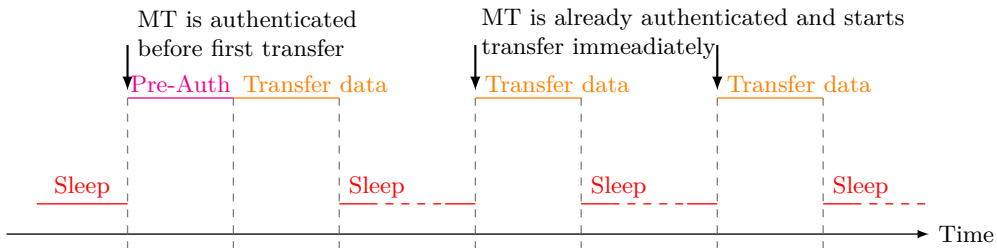


Figure D.6: Data transfer procedure in 5G after initial pre-authentication.

of number of receptions and transmissions in section 6.2 it was shown in figure 6.11 that the number of transmissions dominates the battery life even when there is less than one transmission per 10th second when the number of receptions is comparable. Therefore the halved ON time related to transmissions using Limited Functionality mode will have a positive effect on battery life.

Besides the direct communication between mobile terminal and AP the proposed concept also provides power consumption benefits for D2D, where a trusted man-in-the-middle can be used as an authentication assistant to forward data from mobile terminals to the AP. One example is illustrated in figure D.7 where a patient's health is being monitored using multiple sensors. Assuming that the sensors are in limited functionality mode they may let a data collector device, carried e.g. by a nurse on ward round, perform authentication and forwarding of the collected data in one package to the main AP. This scenario is expected to be a secure environment where the low power consumption of the sensors, which e.g. can be based on patches, is of importance. In

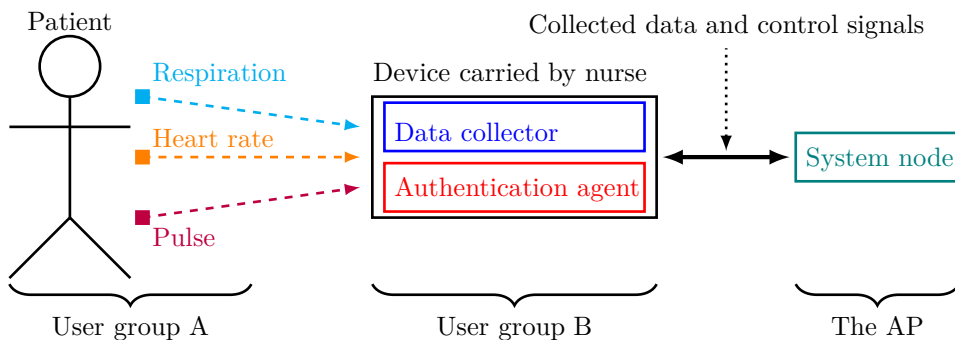


Figure D.7: Use of an authentication assistant and data collector in a D2D scenario with limited functionality mode.

general the concept allows nodes in one user group; A in figure D.7, which is in close proximity to another group of nodes; B in the figure, to forward the data to these nodes and let them authenticate the first group's nodes towards the AP.

To conclude this section a new mobile terminal mode has been presented, which is positioned between LTE's RRC connected and idle mode. The idea is to allow certain

less secure data transfers to occur without the mobile terminal performing the full security and authentication procedure after it exits RRC idle. This can help reduce both the latency and the power consumption of the transfer because the ON time will be reduced to half. The concept is especially useful when the data is only concerning the AP and the mobile terminal, and when applied in secure, close proximity D2D environments.

Appendix E

LTE UE Power Consumption Model - For System Level Energy and Performance Optimization

Anders R. Jensen, Mads Lauridsen, Preben Mogensen, Troels B. Sørensen,
and Per Jensen

The paper has been published in the
VTC Fall 2012

© 2012 IEEE

The layout has been revised.

Abstract

In this work a novel LTE user equipment (UE) power consumption model is presented. It was developed for LTE system level optimization, because it is important to understand how network settings like scheduling of resources and transmit power control affect the UE's battery life.

The proposed model is based on a review of the major power consuming parts in an LTE UE radio modem. The model includes functions of UL and DL power and data rate. Measurements on a commercial LTE USB dongle were used to assign realistic power consumption values to each model parameter. Verification measurements on the dongle show that the model results in an average error of 2.6 %.

The measurements show that UL transmit power and DL data rate determines the overall power consumption, while UL data rate and DL receive power have smaller impact.

E.1 Introduction

The gap between available and required energy in battery supplied wireless user equipment (UE) is increasing year by year [187]. The 3GPP LTE standard therefore includes energy saving methods like discontinuous reception. Unfortunately the available methods cannot fill the gap, and therefore new methods are investigated to further reduce the energy consumption. They focus on both optimizing network settings [29] and improving the UE [28], but one critical problem is that valid and comprehensive UE power consumption models are not publicly available. A model is much needed to evaluate the potential of new energy saving methods on system level.

For 3GPP, Nokia has presented a power model [61], but it only depends on the Radio Resource Configuration (RRC) mode, and not data rate and power levels. Another model was presented in [78], and it describes the Power Amplifier (PA) in details, but uses a static power for the receiver and is based on WCDMA UEs. Carroll et al. analysed the consumption of a smartphone in [40], but the level of detail is not sufficient for optimization on system level. In [188] Li et al. presented a detailed model, but it only covers the Radio Frequency (RF) parts, and e.g. the PA-model is out-dated. The chip manufacturers have detailed models based on development platforms [189], but they are confidential. The recent launch of LTE networks has made first generation LTE UEs publicly available, hence an empirical model can be established.

In this work a literature survey was performed to develop a UE power consumption model. It was fitted to measurements made on a commercial LTE USB dongle using linear regression. The target was a sparse model, which is robust and transferable as suggested in [189]. The model can be applied in system level optimization, e.g. to examine how network settings affect the UEs as in [29], but the model is not intended for optimization on UE component level. The reason is that the model reflects the power consumption trends and not implementation specific behaviour. The model is novel because it describes an LTE UE radio modem and is dynamic in the sense that it depends on power levels and data rates.

First we present a survey of power consumption in the LTE physical layer and define

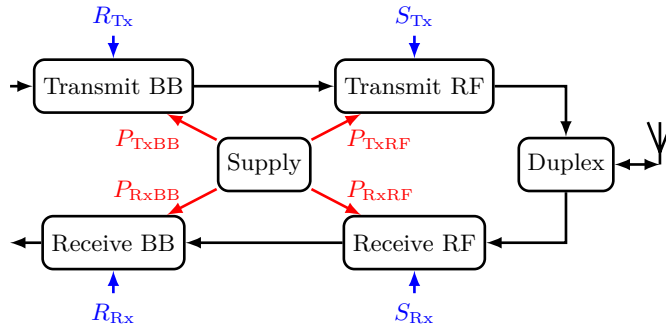


Figure E.1: LTE UE physical layer

a model in section E.2. Then we present measurement results in section E.3, fit the suggested model to the measurements in section E.4, and finally we verify and discuss the model in sections E.5 and E.6.

E.2 UE Model Design

In this section the UE's power consuming physical layer components are examined one by one. The purpose is to determine how the components affect the total power consumption. Figure E.1 shows the LTE physical layer components and the UE model parameters. The envisioned UE model shall depend on receive (Rx) and transmit (Tx) power levels, uplink (UL) and downlink (DL) data rate, and RRC mode. In the following sections the parts in figure E.1 are examined to determine if and how they depend on the aforementioned parameters.

E.2.1 Transmit Baseband

In the LTE Tx baseband (BB) the main task is to turbo encode user data with Forward Error Correction codes. Turbo encoding relies on convolutional encoding and generates a bitstream with code rate 1/3. The Turbo encoding complexity scales linearly with the amount of data to encode which is set by the Transport Block Size (TBS) i.e. the UL data rate, but is independent of the UL Tx power [190].

E.2.2 Transmit RF

In general the RF will not depend on the UL data rate, but when the modulation format is changed the Peak-to-Average Power Ratio (PAPR) is affected. This entails the PA will adjust its performance to comply with the Tx emission requirements in [145], such as the Adjacent Channel Leakage Ratio (ACLR), and this may affect the power consumption. The Tx RF will obviously depend on the UL Tx power. A single PA only has one output power level where it achieves its maximum energy efficiency, and therefore researchers develop methods to increase the efficiency at other output power levels. These include the use of multiple PAs [191], supply voltage and bias switching [78], and the envelope

tracking concept [192]. The Power Added Efficiency is expected to be stepwise increasing with output power as each of the methods are utilized.

E.2.3 Receive RF

The Rx RF power consumption is expected to be independent of the DL data rate, but it will depend on the DL Rx power level. The reason is that the RF contains Gain Controls and Low Noise Amplifiers, which are used to obtain a certain signal level at the ADC. If the DL Rx power level is high the gain in the aforementioned circuits can be reduced, and they may be powered off, to reduce the power consumption [193].

E.2.4 Receive Baseband

The majority of the BB processing tasks' complexity, e.g. channel estimation and equalization, is independent of the DL data rate. To decode the received user data the UE applies turbo decoding, which is an iterative algorithm and the most computational complex task in the digital BB. To support the high data rates of LTE a highly parallelized turbo decoder architecture is required, [194]. The complexity and thus the power consumption scale linearly with DL data rate [195].

E.2.5 UE Power Consumption Model

Based on the review of the four physical layer parts, the model is defined as follows:

$$\begin{aligned}
 P_{\text{tot}} = & m_{\text{idle}} \cdot P_{\text{idle}} + \overline{m_{\text{idle}}} \cdot \{ P_{\text{con}} + m_{\text{Tx}} \cdot m_{\text{Rx}} \cdot P_{\text{Rx+tx}} + \\
 & m_{\text{Rx}} \cdot [P_{\text{Rx}} + P_{\text{RxRF}}(S_{\text{Rx}}) + P_{\text{RxBB}}(R_{\text{Rx}}) + m_{2\text{CW}} \cdot P_{2\text{CW}}] \\
 & m_{\text{Tx}} \cdot [P_{\text{Tx}} + P_{\text{TxRF}}(S_{\text{Tx}}) + P_{\text{TxBB}}(R_{\text{Tx}})] \} \quad [\text{W}]
 \end{aligned} \tag{E.1}$$

where P is the power consumption. The subscript *tot* defines the total consumption, *idle* and *con* the consumption in RRC idle and connected mode, *rxRF* and *txRF* the consumption of the RF part in the Rx and Tx chains respectively, *rxBB* and *txBB* the consumption of the BB parts, and *2CW* is related to increased consumption when using two code words (CW) in DL. The parameters P_{Rx} , P_{Tx} , and $P_{\text{Rx+Tx}}$ are included to model the base power the Rx and Tx chains consume when active. The logical variable m is the mode, which can be RRC idle, transmitting, receiving, and indicate the use of 2 CW. The Rx and Tx power levels are designated by S , and R is the Rx and Tx data rate.

E.3 LTE UE Measurements

In order to assign meaningful values to the proposed power consumption model the authors performed measurements on a commercial LTE USB dongle. The reason for measuring on a dongle is that it do not include peripherals such as display, general purpose processor, and other radios (wifi, fm, bluetooth). This is a benefit since the focus is on the LTE UE radio itself. The downside is that the measurements include the power the USB driver consumes.

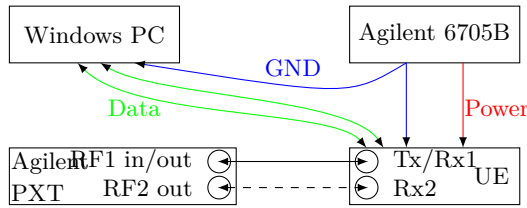


Figure E.2: Measurement setup.

Table E.1: Measurement parameters. The channel bandwidth was 20 MHz, and the link was loaded using Fixed MAC test. P is in dBm.

Measurement	DL MCS	DL PRB	P_{Rx}	UL MCS	UL PRB	P_{Tx}
Rx BB	<i>[0, 28]</i>	100	-60	3	75	-20
Rx RF	0	100	<i>[-80, -20]</i>	3	75	-20
Tx BB	5	100	-57	<i>[0, 28]</i>	50	5
Tx RF	5	100	-57	3	100	<i>[-30, 23]</i>

The UE was supplied using the Agilent 6705B DC Measurement Power Supply, which was set up to comply with the USB standard (5 V, 1 A). The supply sampled the current consumption every 1 ms for 30 s. The measurements were performed as conducted interference free tests using the Agilent PXT E6621A Wireless Communication Tester, which emulated a band 7 LTE base station. Measurements were made for SISO and DL 2x2 MIMO as shown in figure E.2.

Based on the setup, current consumption measurements were performed and related to the proposed model in equation (E.1) by varying one variable at a time. This is illustrated in table E.1 where italic fonts indicate the varied parameter in each measurement. The current consumption as a function of DL data rate was examined by keeping the DL Rx power level constant and adjusting the Modulation and Coding Scheme (MCS) index, and the results are shown in figure E.3. The MCS index was mapped to TBS using [72]. The mapping also depends on the number of allocated PRBs and the link direction. Next the MCS was fixed and the DL Rx power varied to examine current as a function of the DL Rx power, see figure E.4. Similar measurements were made in UL and the results are given in figure E.5 and E.6. The measurement parameters are given in table E.1. Note that the measurements in DL were repeated for a 2x2 MIMO setup using 2 CW. The connected mode current, P_{con} , was measured in RRC_connected mode without scheduled traffic and the idle mode current, P_{idle} , was measured in RRC_idle mode with paging messages monitored every 320 ms. Finally a DL Rx sensitivity test was made, and it showed the UE always utilizes both receive antennas.

The PXT's Fixed MAC padding test was used to generate data on either PUSCH or PDSCH. The test exploits that the MAC layer has to multiplex the logical channels to a MAC Protocol Data Unit (one unit per transport block) [184]. In order to fill the transport block the MAC layer pads the multiplexed data with random data, and when a padded transport block is received the padding will be discarded and the remaining

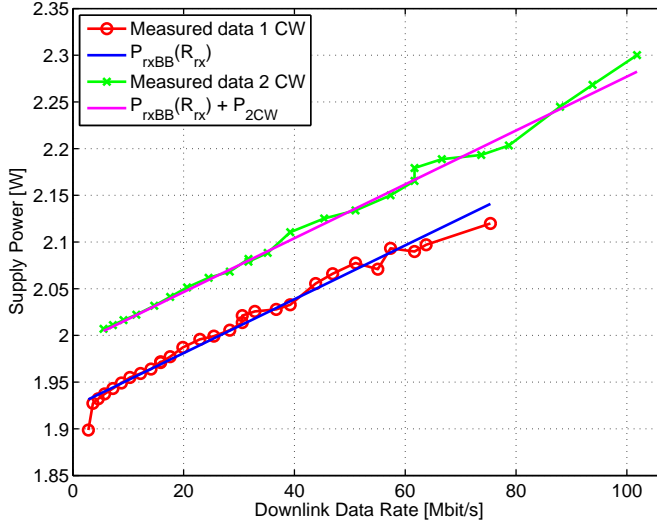


Figure E.3: Receive BB.

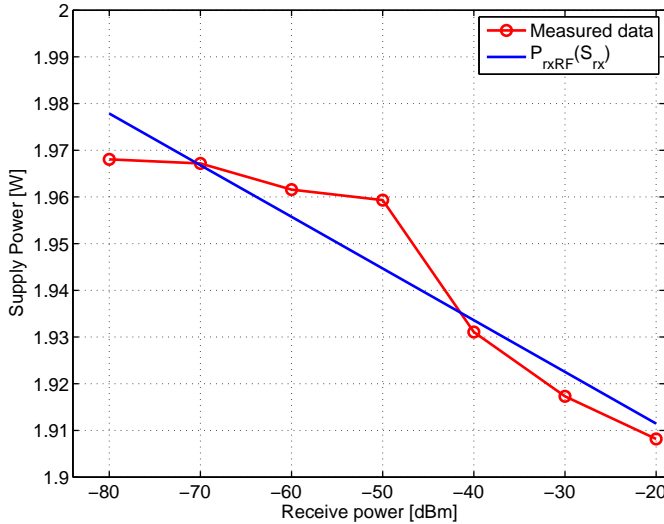


Figure E.4: Receive RF.

data if any, forwarded to the logical channels. When the Fixed MAC padding test is initiated by the PXT it will pad the DL stream, fully loading the assigned PRBs. If there is no other applications running the only payload on the DL channel is padded data, hence the UE will only send ACK/NACKs from layers below the MAC.

As mentioned in section E.2 the varying PAPR were expected to affect the current consumption. To examine this a measurement was made where the UE was transmitting QPSK signals (MCS10) and 16QAM (MCS11), and the current consumption as a function of UL Tx power was measured. Figure E.7 show that the modulation format

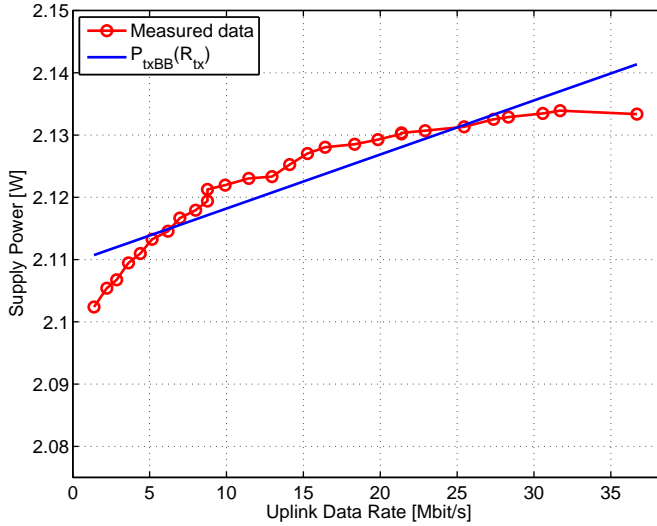


Figure E.5: Transmit BB.

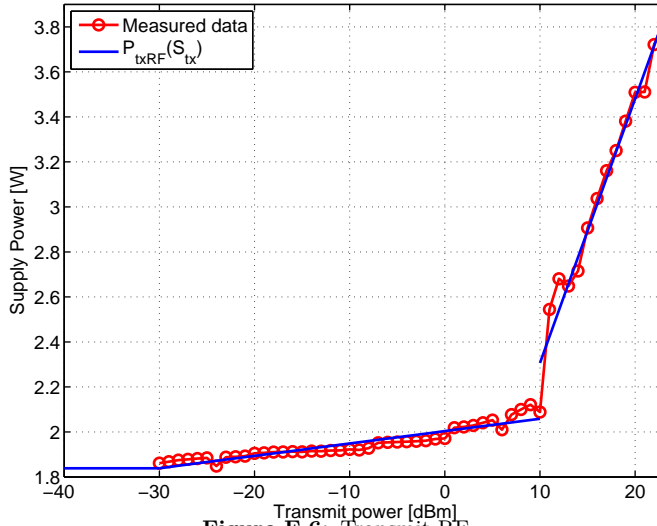


Figure E.6: Transmit RF.

do not affect the current consumption except for UL Tx powers 0 and 10 dBm, where the 16QAM signal forces the UE to adjust a little earlier than the QPSK signal. This adjustment is implementation specific and therefore not modelled.

E.4 Model Fitting

The model for each power function in equation (E.1), is derived either as a constant or a polynomial fit. It is desired that each function reflects the general power consumption

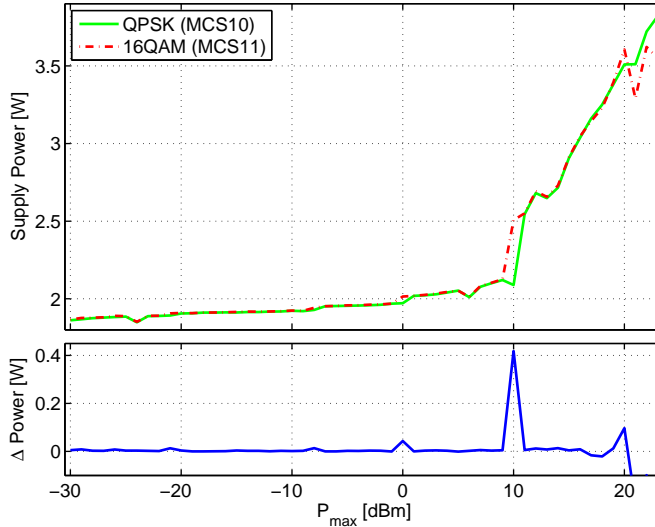


Figure E.7: UL Tx power measurement for UL QPSK & 16QAM. The lower plot shows the current difference between the two lines in the upper plot.

Table E.2: Constant Model Parameters in Watt.

Part	P_{idle}	P_{con}	P_{Rx}	P_{Tx}	$P_{\text{Rx+Tx}}$	$P_{2\text{CW}}$
Mode	m_{idle}	$\overline{m_{\text{idle}}}$	m_{Rx}	m_{Tx}	$m_{\text{Tx}} \cdot m_{\text{Rx}}$	$m_{2\text{CW}}$
Value	0.50	1.53	0.42	0.55	0.16	0.07

trend and not unique implementation specific solutions.

The idle, P_{idle} , and connected mode, P_{con} , are the average powers in each RRC mode and given in table E.2. The connected mode power is measured without user data in UL and DL.

The complexity, hence the power consumption, of BB processing in UL and DL are highly linear dependent on data rate, and therefore they are modeled as first order polynomials.

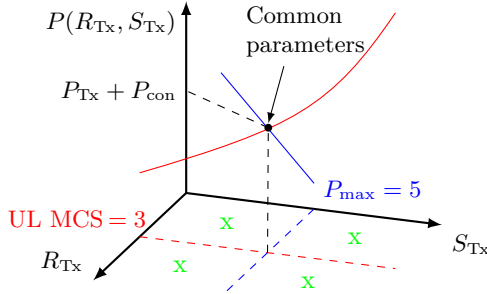
The receiver and transmitter RF architecture can be based on several different techniques as described in section E.2. This makes it difficult to predict a suitable model and therefore the model selection for transmitter RF and receiver RF rely on curve-fitting. The polynomial values of the models are found by minimizing the least square error given as

$$e = \frac{1}{N} \sum_{n=0}^N (p_0 + p_1 x_n - Y_n)^2 \quad [\text{W}^2] \quad (\text{E.2})$$

where e is the residual error, Y_n is the measured power, N is the number of measurements, p are polynomial values and x is the input variable. The polynomials and the corresponding residuals are given in table E.3. Note that Tx RF is composed of two

Table E.3: Polynomial Model Parameters in Milliwatt.

Part	Variable	p_0	$p_{0\text{-mod}}$	p_1	Residual e
Rx BB	R_{Rx} [Mbit/s]	1923	-26.6	2.89	0.08
Tx BB	R_{Tx} [Mbit/s]	2110	34.5	0.87	0.01
Rx RF	S_{Rx} [dBm]	1889	-60.7	-1.11	0.06
Tx RF1	S_{Tx} [dBm]	2004	-71.3	5.50	0.60
Tx RF2	S_{Tx} [dBm]	1132	-943	117	6.87

**Figure E.8:** Example of common parameters for the transmitter.

lines, where Tx RF1 is valid for $-30 \text{ dBm} \leq S_{\text{Tx}} \leq 10 \text{ dBm}$ and Tx RF2 accounts for $10 \text{ dBm} < S_{\text{Tx}} \leq 23 \text{ dBm}$. Because each model has been based on a measurement with one varying parameter there is an overlap in predicted power, when e.g. P_{TxBB} and P_{TxRF} are combined, because they both include the power the UE consumes when actively transmitting. The measurements were made such that the BB and RF functions share one common set of parameters (same MCS index and power level) as illustrated in figure E.8. The blue line illustrates the power consumption as a function of the UL data rate for a fixed UL Tx power (figure E.5), and the red curve illustrates the power consumption as a function of the UL Tx power for a fixed UL data rate (figure E.6). The power P_{Tx} was then defined as:

$$P_{\text{Tx}} = [P_{\text{TxRF}}(5 \text{ dBm}) + P_{\text{TxBB}}(\text{MCS3})] / 2 - P_{\text{con}} \quad [\text{W}] \quad (\text{E.3})$$

The polynomials are scaled to result in ≈ 0 Watt in the common point. By using modified p_0 's as $p_{0\text{-mod}} = p_0 - P_{\text{Tx}} - P_{\text{con}}$ this is obtained. In this way the polynomial models comply with equation (E.1) when they are added together with P_{Tx} and P_{con} . A similar approach was used on the receiver models, and the results are given in table E.2 and E.3. The offset $P_{\text{Rx+Tx}}$ was based on measurement where both Rx and Tx were active.

E.5 Verification

To verify the model two methods are applied. First the fits in figures E.3-E.6 are evaluated individually by examining the residuals. Next the model is examined empirically,

Table E.4: Verification, downlink.

P_{Rx}	DL MCS	P_{model}	P_{meas}	Error
-40 dBm	5	1.93 W	1.94 W	-0.5 %
	12	1.96 W	1.98 W	0.8 %
	20	2.02 W	2.04 W	-1.0 %
-80 dBm	5	1.98 W	1.98 W	-0.3 %
	12	2.01 W	2.02 W	-0.7 %
	20	2.06 W	2.09 W	-1.3 %

Table E.5: Verification, uplink.

UL PRB	P_{Tx}	UL MCS	P_{model}	P_{meas}	Error
50	-10 dBm	0	1.98 W	1.92 W	3.5 %
		12	1.99 W	1.91 W	4.1 %
	15 dBm	0	2.93 W	3.00 W	-2.3 %
		12	2.94 W	3.00 W	-2.0 %
100	-10 dBm	0	1.99 W	1.92 W	3.1 %
		12	2.00 W	1.92 W	3.9 %
	15 dBm	0	2.93 W	3.03 W	-3.4 %
		12	2.95 W	3.03 W	-3.0 %

i.e. the power consumption of the transmitter and receiver is compared with verification measurements. These measurements are made for power and data rate pairs, which were not used when fitting the models. This approach is shown in figure E.8 where the green crosses indicate the settings of the verification measurements on the transmitter. An identical approach is used for verification of the receiver model.

The polynomial fits' residuals are given in table E.3. The residuals for Tx RF1 and especially Tx RF2 are larger since the two functions span a larger power consumption range than the other BB and RF functions. The range for Tx RF2 is e.g. 2.1 W to 3.8 W as shown in figure E.6. Based on the residuals it is concluded that good and valid fits have been obtained.

The results of the comparison between the model and the verification measurements are given for DL in table E.4, UL in table E.5, and for the combination of UL and DL in E.6. The average error for the DL verification is 0.8 % hence a good fit has been achieved. The verification of the UL model resulted in an average error of 3.2 %. The UL model is a bit more inaccurate because the Tx RF model is the most power consuming part, hence an error in its fit will affect the overall result more. The average error for the combined verification is 2.6 % and the maximum error is 6.0 %.

Table E.6: Verification, uplink and downlink.

P_{Rx}	DL MCS	P_{Tx}	UL MCS	P_{model}	P_{meas}	Error
-40 dBm	0	15 dBm	3	2.99 W	3.10 W	-3.4 %
			12	3.01 W	3.09 W	-2.9 %
	12	-20 dBm	3	2.00 W	1.98 W	0.6 %
			12	2.01 W	1.99 W	1.0 %
	12	15 dBm	3	3.04 W	3.19 W	-4.9 %
			12	3.06 W	3.19 W	-4.5 %
12	-20 dBm	3	2.04 W	2.05 W	0.1 %	
		12	2.06 W	2.04 W	0.6 %	
-57 dBm	0	15 dBm	3	3.01 W	3.17 W	-5.4 %
			12	3.03 W	3.17 W	-4.9 %
	12	-20 dBm	3	2.01 W	2.02 W	-0.3 %
			12	2.03 W	2.02 W	0.2 %
	12	15 dBm	3	3.06 W	3.25 W	-6.0 %
			12	3.07 W	3.25 W	-5.8 %
12	-20 dBm	3	2.06 W	2.08 W	-0.7 %	
		12	2.08 W	2.08 W	-0.2 %	

E.6 Discussion

The goal with the described work was to develop a UE power consumption model for system level optimization. Because the model is based on measurements on one dongle and focused on major power consumption trends it cannot be used to optimize power consumption in individual UE components. The presented model only covers the LTE radio modem, but if a user wishes to get a complete overview of UE power consumption it is important to include statistics for the display, general purpose processor, and other radios.

A critical limitation is that the power consumption in each of the blocks in figure E.1 cannot be separated because of the integrated circuit design. This entails that when a DL parameter is examined, contributions from UL, e.g. transmission of ACK/NACK, will also be included and vice versa.

During the measurements we experienced that the absolute power level depends on which USB port the UE is connected to. This does not affect the relative trend, but entails that the absolute values vary about $\pm 10\%$. Furthermore the implementation architecture, choice of components, and component tolerance will be different for every UE model. The most important is however the trend and not the absolute value.

It is important to note the measured UE is of the first LTE generation. This means

the UE may not be as optimized and adaptive as future UEs from a power consumption point of view. One important feature the UE is missing is the Discontinuous Reception mode [184], consequently this is not included in the model.

E.7 Conclusion

A LTE user equipment power consumption model was presented. The model is designed to assist in system level simulations, e.g. optimization of network parameters, by providing knowledge of how the settings affect the user equipment (UE). This is important because the network set up is critical for the UE power consumption.

The model is based on a review of how radio frequency and baseband power consumption depends on signal power levels and data rates. The model was fitted to measurements performed on a commercial LTE USB dongle. The measurements show uplink transmit power and downlink data rate greatly affect the power consumption, while uplink data rate and downlink receive power has little affect.

Verification measurements on the LTE USB dongle show that the proposed model results in an average error of 2.6 % and a maximum error of 6 %.

In future work we expect to modify the proposed model to include multiple power amplifiers in order to examine LTE Advanced proposals such as carrier aggregation, and multiple transceiver chains to examine MIMO. Furthermore the model shall be updated to model the next generation of LTE UEs, which are expected to be more energy optimized.

Acknowledgement

We would like to thank Agilent Technologies for supplying the measurement equipment and the LTE USB dongle.

The work is partly funded by the Danish National Advanced Technology Foundation and the 4th Generation Mobile Communication and Test Platform (4GMCT) project.

Appendix F

Empirical LTE Smartphone Power Model with DRX Operation for System Level Simulations

Mads Lauridsen, Laurent Noël, and Preben Mogensen

The paper has been published in the
VTC Fall 2013

© 2013 IEEE
The layout has been revised.

Abstract

An LTE smartphone power model is presented to enable academia and industry to evaluate users' battery life on system level. The model is based on empirical measurements on a smartphone using a second generation LTE chipset, and the model includes functions of receive and transmit data rates and power levels. The first comprehensive Discontinuous Reception (DRX) power consumption measurements are reported together with cell bandwidth, screen and CPU power consumption.

The transmit power level and to some extent the receive data rate constitute the overall power consumption, while DRX proves to be a very efficient method to prolong the battery life.

F.1 Introduction

Today smartphone users experience limited battery lifetime, and the trend is not expected to improve in the future. This is due to an increasing gap between smartphone battery capacity and the energy required to power a smartphone, [187, 196], using complex telecommunication standards, such as the UTRAN Long Term Evolution (LTE) standard [197]. This is a major issue because User Equipment (UE) battery life is key to achieve high user satisfaction [13]. The UE energy consumption depends on the mobile network setup and therefore a comprehensive smartphone power consumption model is needed, when system level designers adjust key network parameters.

In previous work smartphone power consumption was examined by running an application on the phone, which logs battery discharge [48] or, by measuring the power drain using external monitoring equipment [196, 109]. All measurements were made in a live network entailing the authors could not control and record network settings. However, network trace analysis was applied to estimate some parameters in [45].

In this work we apply network emulators to perform conducted tests and measure the power consumption using a battery dummy. This entails full control and easy logging of network parameters missing in the previous work. Furthermore, there is no power footprint when using external monitoring equipment as opposed to the logging application.

The general approach to smartphone modelling is to apply submodels covering the screen, network modem, CPU and other components. In [196, 48] the screen power consumption as a function of general and pixel brightness, and the CPU power consumption as a function of utilization, and in [48] also as a function of clock frequency, is examined. Each study briefly examines WiFi but completely disregard the cellular modem. In this work we show a smartphone's LTE modem is a major power consumer, hence it is important to model and optimize.

In [109, 45] measurements on LTE modems are presented, but the power consumption is only reported as a function of receive and transmit data rates. This is problematic because the power amplifier (PA), as shown in this article, is the LTE modem part which consumes the most power, when transmitting at maximum output power. The PA also exhibits the largest power variation and therefore constitutes big potential energy savings. In addition, [109] claims that switching to a low power idle state will not reduce

the power consumption significantly. In this study we present what we believe is the first comprehensive Discontinuous Reception (DRX) power consumption measurements. The results clearly show that DRX is an important method to prolong UE battery life. In [45] DRX power consumption is measured, but they report the DRX power consumption to be 1.1 W, where we measure 0.03 W. Furthermore, they do not evaluate how the DRX power consumption depends on the main DRX parameters On Duration and Long Period [184]. The only existing detailed DRX model was proposed by Nokia [61], but based on arbitrarily selected values, which we show do not match well with current LTE modems. We therefore believe our model can be used on system level to get a more accurate and realistic view of DRX's applicability. The work in [25] covers the basic LTE parameters, but also has its limitations: the UE is a USB dongle, which is a non-power optimized device, and also uses a first generation LTE chipset, for which neither the impact of DRX nor that of cell bandwidth (BW) were captured.

First we present the power model design, then we discuss our measurement setup and results, which mainly focus on the LTE modem. Next, we fit the model to the measurements and validate it. Finally, we discuss the limitations and present a conclusion and outlook for future work.

F.2 Design of the Smartphone Power Model

In this section, the smartphone power model is designed. It is based on [25] but updated to include cell BW and DRX in addition to the functions of Transmit (Tx) and Receive (Rx) power levels (S) and data rates (R) as shown in fig. F.1.

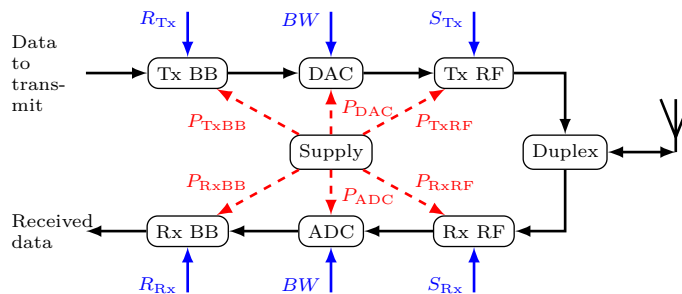


Figure F.1: LTE smartphone modem power model. Red dashed lines indicate power consumption and blue solid lines are input parameters.

The modem power consumption P_{modem} is defined as

$$P_{\text{modem}} = m_{\text{idle}} \cdot P_{\text{idle}} + m_{\text{DRX}} \cdot P_{\text{DRX}} + m_{\text{act}} \cdot P_{\text{act}} \quad [\text{W}] \quad (\text{F.1})$$

where m are Boolean variables used to activate certain UE modes. The power consumption variables P are functions of relevant input parameters as defined in the following section.

The active power consumption model includes transmit and receive Base Band (BB),

Radio Frequency (RF), and BW power consumption as shown in fig. F.1. Each component has an input parameter defining the power consumption:

$$P_{\text{act}} = P_{\text{con}} + m_{\text{Rx}} \cdot [P_{\text{Rx}} + P_{\text{RxBB}}(R_{\text{Rx}}) + P_{\text{RxRF}}(S_{\text{Rx}})] + m_{\text{Tx}} \cdot [P_{\text{Tx}} + P_{\text{TxBB}}(R_{\text{Tx}}) + P_{\text{TxRF}}(S_{\text{Tx}})] + P_{\text{BW}}(BW) \text{ [W]} \quad (\text{F.2})$$

The RRC_idle mode power consumption depends on the length of the paging cycle t_{pc} , because the modem will power on once each period to check if it is paged by the network.

$$P_{\text{idle}}(t_{\text{pc}}) = (t_{\text{iA}} \cdot P_{\text{iA}} + (t_{\text{pc}} - t_{\text{iA}}) \cdot P_{\text{iS}}) / t_{\text{pc}} \text{ [W]} \quad (\text{F.3})$$

where iS and iA indicate the sleep and active parts of the paging cycle. By measuring the two power parameters P_{iS} , P_{iA} and the active time t_{iA} the average idle power is estimated.

The DRX power model is a function of DRX Long Period t_{LP} and On Duration t_{onD} , [184]. The parameters are defined in the sketch of a DRX period fig. F.2. The DRX

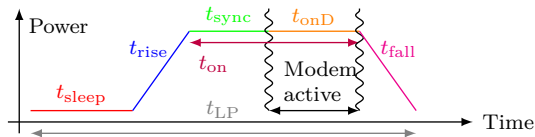


Figure F.2: DRX timing parameters.

sleep power P_{DRX} is defined to be the average of the power consumed during the sleep t_{sleep} , rise t_{rise} and fall t_{fall} stages and the part of the active period t_{on} , where frequency synchronization t_{sync} is acquired:

$$t_{\text{on}}(t_{\text{LP}}) = t_{\text{sync}}(t_{\text{LP}}) + t_{\text{onD}} \text{ [s]} \quad (\text{F.4})$$

As explained in sec. F.3 the P_{DRX} , t_{rise} , t_{fall} , and t_{sync} depend on whether $t_{\text{LP}} \leq 40$ ms. The sleep time is

$$t_{\text{sleep}} = t_{\text{LP}} - t_{\text{rise}}(t_{\text{LP}}) - t_{\text{fall}}(t_{\text{LP}}) - t_{\text{on}}(t_{\text{LP}}) \text{ [s]} \quad (\text{F.5})$$

hence the average DRX sleep power is

$$P_{\text{DRX}}(t_{\text{LP}}, t_{\text{onD}}) = \frac{t_{\text{sleep}} \cdot P_{\text{sleep}} + E_{\text{R/F+sync}}(t_{\text{LP}})}{t_{\text{LP}} - t_{\text{onD}}} \text{ [W]} \quad (\text{F.6})$$

where $E_{\text{R/F+sync}}$ is the energy consumed during t_{rise} , t_{fall} , and t_{sync} stages. The P_{DRX} does not include the power consumed in t_{onD} , this value should be calculated using P_{act} in eq. (F.2).

Average power consumption values are used because the model is made for system level simulations where average parameters are often used instead of Transmission Time Interval (TTI) level values. If TTI time traces are used P_{act} is still applicable, but the average values of P_{idle} and P_{DRX} are not.

Table F.1: Device Under Test (DUT) main physical characteristics.

	UE1	UE2	UE3
Android OS version	2.3.6	4.0.4	4.0.4
Launch date	May '12	June '12	Nov '12
Modem & CPU CMOS node	45 nm	28 nm	28 nm
RF transceiver CMOS node	65 nm	65 nm	65 nm
RF transceiver	Part #A	Part #B	Part #B
Band 4 PA	Part #C	Part #C	Part #D
LTE bands	4,17	4,17	2,4,5,17

Table F.2: Measurement test plan. Cell bandwidth 20 MHz, carrier frequency 2145 MHz. Downlink tests made for 1 & 2 CW.

Test case	DL parameters			UL parameters		
	MCS	PRB	S_{Rx}	MCS	PRB	S_{Tx}
Rx BB 1	[0,28]	100	-25	6	100	-40
Rx BB 2	0	[0,100]	-25	6	100	-40
Rx RF 3	0	100	[-25,-90]	6	100	-40
Tx BB 4	0	3	-25	6	[0,100]	-40
Tx BB 5	0	3	-25	[0,23]	100	-40
Tx RF 6	0	3	-25	6	100	[-40,23]

F.3 Conducted Smartphone Measurements

To obtain realistic values for the smartphone power model measurements were carried out on 3 LTE smartphones. UE2 was selected as the basis for the model. All measurements are performed in a conducted test environment, each UE being placed in a Faraday cage to ensure adequate shielding from the surrounding laboratory basestations. UEs are connected to an Anritsu 8820C eNodeB emulator, according to GSMA TS09 battery life test guidelines, using a dummy battery. UEs are supplied with a linear, low noise DC power supply, and the UE instantaneous power consumption is recorded over at least 30 seconds per test point. The UE average power consumption is then post processed. The power measurement accuracy of the test setup, including repeatability of the collected data is estimated at $\pm 10\text{mW}$. UEs are modern, Android based touchscreen smartphones whose relevant hardware characteristics can be found in tab. F.1. RF cable insertion losses are calibrated for each UE for both uplink (UL) and downlink (DL) carrier frequencies. Measurements are performed in band 4 (AWS band) on DL carrier frequency 2145 MHz. The strategy to derive the UE power consumption model is based upon [25], i.e. estimate Rx BB, Rx RF, Tx BB, and Tx Rf contributions by varying one variable, shown in brackets, at a time in respective test cases (TC) in tab. F.2. For the sake of simplicity, only the results collected in 20MHz cell BW are presented. Measurements collected for 15 and 10 MHz cell BW are used to validate the derived UE power consumption model accuracy.

Out of the numerous baseband receiver tasks, for a given cell BW, Turbo decoding

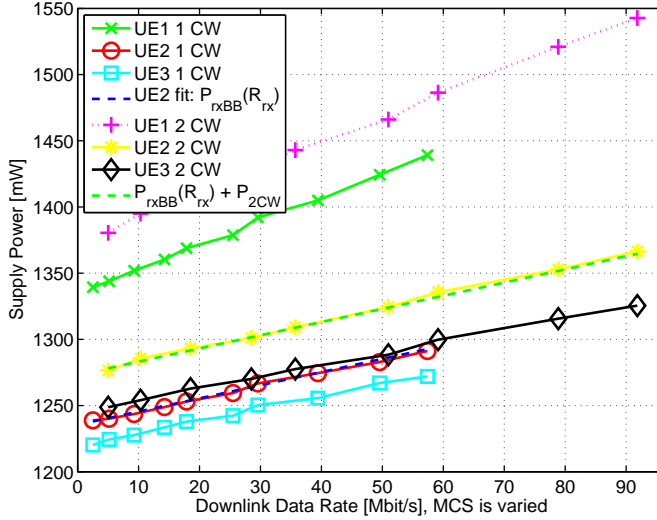


Figure F.3: Receive BB, test case 1.

activity scales in a linear fashion with the DL data rate [198, Ch.14]. Fig. F.3 clearly illustrates the linear power consumption increase vs. DL data rate: TC1 stresses the turbo decoder by varying the PDSCH MCS, while TC2 operates at constant MCS and increases DL data rate by varying the allocated DL PRB. The TC2 result is omitted since it has a trend similar to TC1. In both TCs, the Tx contribution is minimised by using a low R_{Tx} and transmitting at minimum power S_{Tx} . Using 2 code words (CW) adds a constant offset.

Fig. F.4 shows that the Rx RF chain power consumption increases as the DL carrier power is decreased, with either one or two sudden power consumption steps. The gain steps are believed to be caused by Low Noise Amplifier (LNA) gain control. Modern RF CMOS transceivers [199] implement discrete gain steps in the LNA to deliver the best compromise between linearity and power consumption. The LNA may be implemented with two (UE1 & UE2) or three gain (UE3) modes. The gain step may entail a sudden phase jump, which, if toggled frequently by the Automatic Gain Control loop, may degrade the BB demodulation performance. One mitigation technique often used consists in applying hysteresis on the LNA gain step control. This was observed by decreasing and increasing the received power during the measurements, but is not shown here for the sake of simplicity, and since hysteresis won't dramatically impact the UE power consumption model. Fig. F.5 shows the Tx BB power consumption vs. the UL data rate. The Tx BB power consumption is nearly independent of the PUSCH data rate, hence a constant value can be added to the model. Power consumption steps can be seen in UE1 (12mW) and UE2 (10mW) when UL modulation toggles from QPSK to 16QAM. It is believed that these are due to PA bias settings to deliver the best compromise between Adjacent Channel Leakage Ratio (ACLR) and power consumption performance under the higher Peak-to-Average Power Ratio (PAPR) of the 16QAM modulation scheme. The Rx chain power consumption is minimised by selecting a low DL data rate and maximum DL RF input power. In [109, 45] the power per Mbps is

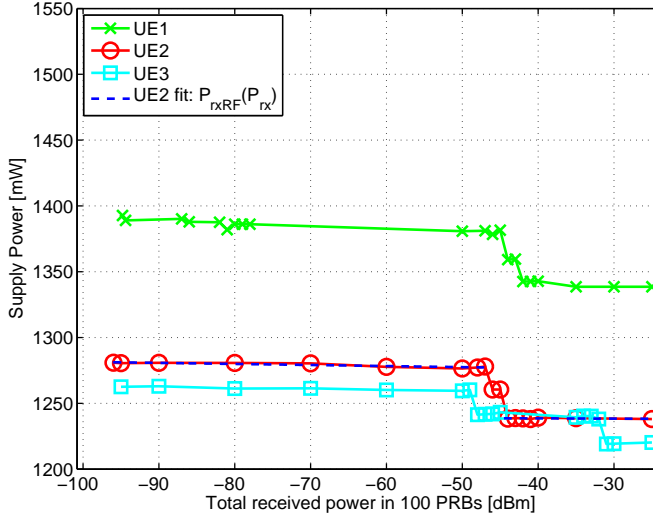


Figure F.4: Receive RF, test case 3.

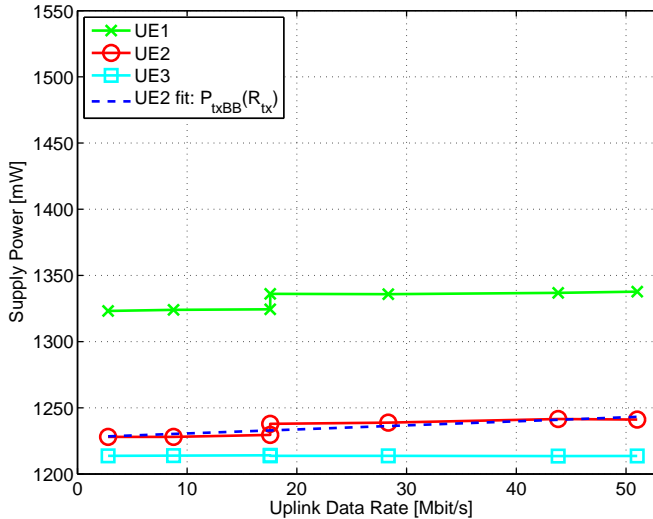


Figure F.5: Transmit BB, test case 4 & 5.

reported to be higher for transmission than reception, but fig. F.3 & F.5 clearly show this is not the case.

Fig. F.6 shows modem power consumption is dominated by the PA when $S_{Tx} > 10$ dBm. The ACLR power consumption trade-off is handled differently between UEs: the PA of UE1 & UE2 uses 2 gain modes, while UE3 PA uses 3 gain modes. The ACLR performance is out of the scope of this study.

While UE2 and UE3 only differ by their PA and front-end architecture, UE1 & UE2 use the same PA and differ by the BB CMOS process and front-end architecture, tab.

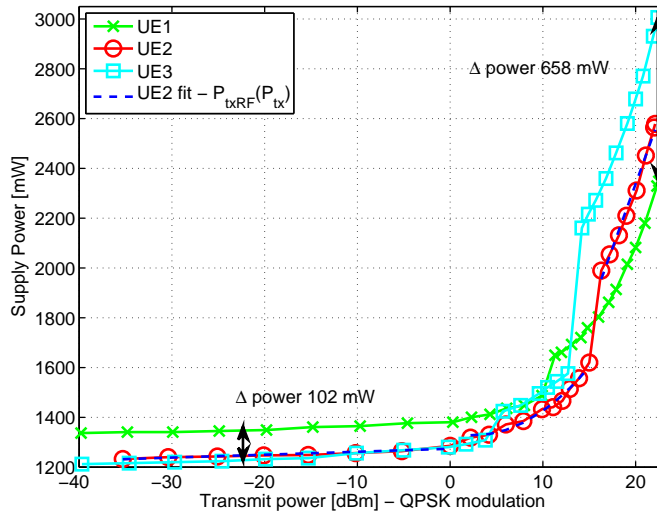


Figure F.6: Transmit RF, QPSK modulation, test case 6.

F.1. Inspection of the PCB layout indicates a lower component count and PCB area for UE1 than UE2, but it is believed that the PA to antenna port insertion losses are within a fraction of a dB from one another. It is therefore assumed that UE1 & UE2 power consumption difference is dominated by CMOS process shrink. At transistor level, CMOS 28 nm can save between 35 to 40 % power vs. CMOS 45nm [200]. From a system performance perspective, our measurements show a moderate 7 to 11 % savings at low and high data rates respectively.

F.3.1 Connected Mode DRX

Connected mode DRX measurements were made for long period t_{LP} of 32-2048 ms, and one result is shown in fig. F.7. The UE was not scheduled during t_{onD} to prevent triggering of the Inactivity Timer. When $t_{LP} \leq 40$ ms the UE powers down fast to a 0.57 W light sleep mode. When $t_{LP} \geq 80$ the UE enters a deep sleep mode consuming only 29 mW, which is close to the modem being powered off. The reason is that the UE can disable BB & RF including the Local Oscillator, and instead utilize a low precision oscillator to maintain time synchronization. When the modem awakes it takes longer to reboot, and in addition it needs an LTE frame (10 ms) to achieve proper frequency synchronization. This is done by receiving Synchronization and Reference Signals. Hence when $t_{LP} \geq 80$ ms both t_{rise} and t_{fall} are increased, but also t_{on} due to the re-synchronization.

The measurements were performed for t_{onD} of 1-200 ms, and obviously a long t_{onD} prevents the UE from reaching the deep sleep mode. If the t_{onD} is selected properly the time and power values are however independent of the t_{onD} , and the results are given in tab. F.3.

When $t_{LP} = 64$ the UE will almost reach the deep sleep mode if $t_{onD} = 1$ ms, while

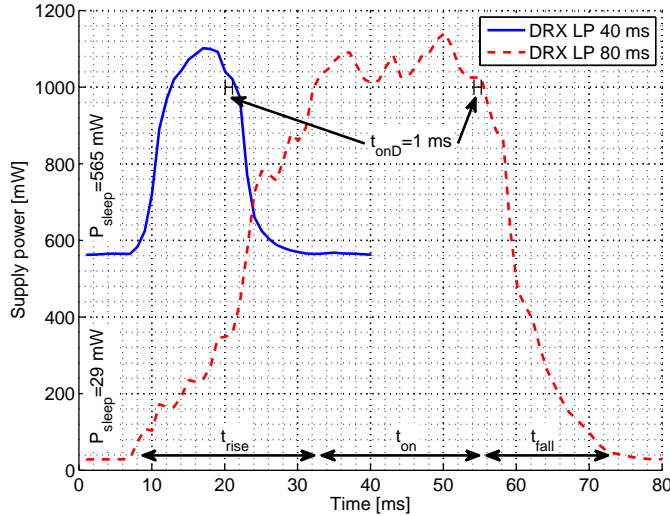


Figure F.7: DRX for long periods 40 & 80 ms.

Table F.3: Measured DRX Parameters. Based on t_{onD} of 1 and 6 ms.

t_{LP}	P_{sleep}	t_{rise}	t_{fall}	t_{sync}	$E_{\text{R/F+sync}}$
≤ 40 ms	570 mW	6 ms	9 ms	8 ms	19.2 mJ
≥ 80 ms	29 mW	26 ms	21 ms	21 ms	41.4 mJ

Table F.4: Average power difference compared to 20 MHz cell BW.

Cell BW	Rx BB	Rx RF	Tx BB	Tx RF	Global
10 MHz	146 mW	151 mW	137 mW	148 mW	145 mW
15 MHz	40 mW	45 mW	44 mW	42 mW	43 mW

for longer t_{onD} it only utilizes the light sleep mode. Measurements on other LTE UEs have shown similar power consumption trends, but the rise, fall and on times are varying among the UEs and depending on t_{LP} and t_{onD} . When $t_{\text{LP}} \leq 20$ ms the UE does not sleep at all and therefore measurements with DRX Short Period were not performed.

F.3.2 Cell Bandwidth Dependency

To determine the power consumption dependency on cell BW, TC 1, 3, 5, and 6 in tab. F.2 were repeated for cell BWs of 10 and 15 MHz. Next each measurement point of the TCs, made using 10 and 15 MHz, was compared with the measurement point of the corresponding 20 MHz TC, and the average power difference per TC was determined. The results are given in tab. F.4. The global average is used as a basis for the cell BW dependency in the power model.

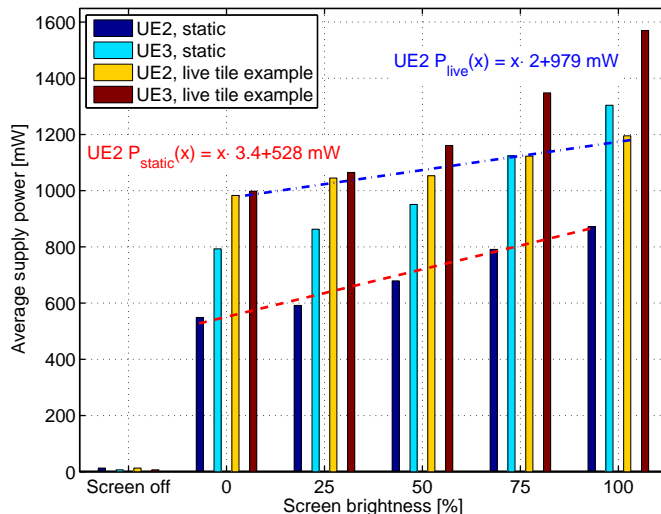


Figure F.8: Screen power consumption, UE in flight mode.

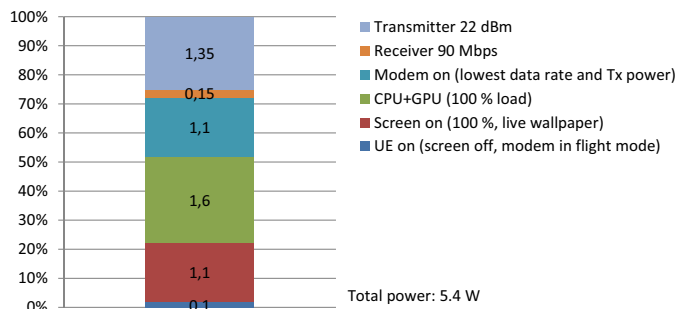


Figure F.9: UE2 smartphone power consumption. Components are fully loaded.

F.3.3 Other Smartphone Components

The screen power consumption was measured, when the UE was in flight mode and using both a static and an example of a live tiles background. The result is shown in fig. F.8, and the power consumption as a function of screen brightness is almost linear. Turning the screen on costs $\sim 0.5 \text{ W}$ and if the screen is set to full brightness another 0.35 W is consumed.

To examine the relative contribution from the major power consuming components in a smartphone, measurements were also made to evaluate the CPU and GPU. They were loaded 100% by using the Android app StabilityTest v.2.7, and the combined result is shown in fig. F.9. When all components are fully loaded, which is highly unrealistic, the LTE modem consumes about half of the total power. A scenario where the modem and CPU+GPU is less loaded is more realistic and in that case the screen, which in the full load scenario only accounts for 20%, will become more dominant. The figure however indicates that it is important to continue working on the LTE modem, especially the transmit PA.

Table F.5: Idle and basic model parameters.

P_{con}	t_{iA}	P_{iA}	P_{iS}	P_{Tx}	P_{Rx}
1169 mW	35 ms	290 mW	102 mW	28 mW	38 mW

Table F.6: Polynomial fits. Powers are in mW.

Part	Function	Comments
P_{RxBB}	$1.00 \cdot R_{\text{Rx}} - 3.51$	$P_{2\text{CW}} = 37.8$
P_{RxRF}	$-0.08 \cdot S_{\text{Rx}} + 34.5$	$S_{\text{Rx}} \leq -45.5$ dBm
P_{RxRF}	$-0.02 \cdot S_{\text{Rx}} - 1.23$	$S_{\text{Rx}} > -45.5$ dBm
P_{TxBB}	5.93	
P_{TxRF}	$1.18 \cdot S_{\text{Rx}} + 43.5$	$S_{\text{Tx}} \leq 1.1$ dBm
P_{TxRF}	$1.77 \cdot S_{\text{Rx}}^2 - 8.96 \cdot S_{\text{Rx}} + 109$	$1.1 < S_{\text{Tx}} \leq 15.6$ dBm
P_{TxRF}	$103 \cdot S_{\text{Rx}} - 962$	$S_{\text{Tx}} > 15.6$ dBm
P_{B}	0 mW=20 MHz, -43 mW=15 MHz, -145 mW=10 MHz	

WiFi was out of scope in this study, but in [47] measurements on a smartphone with a widely used WiFi chipset are presented. The receive power consumption is reported to never exceed 750 mW even for as high data rate as 49 Mbps, hence WiFi power consumption is not a major contributor.

F.4 The Smartphone Power Consumption Model

In this section the model in sec. F.2 is fitted to the data from sec. F.3. The target is to capture the trend of the smartphone modem and not implementation specific techniques.

The RRC_idle mode power consumption was measured using $t_{\text{pc}} = 320$ ms, and the derived parameters are given in tab. F.5.

Based on the measurement results polynomial fits are made for each of the 4 functions in eq. (F.2) by minimizing the least square error. The Rx BB is modelled as a 1st order linear fit with an offset $P_{2\text{CW}}$ if 2 CWs are used. The Rx RF function is divided into two 1st order fits due to the observed gain adjustments. The Tx BB is modelled as a constant due to the minor dependency on data rate. The Tx RF is divided into three fits to model the PA behaviour. The parameters are given in tab. F.6. The measurements in tab. F.2 were made with only one varying parameter e.g. S_{Rx} , but the other Rx parameter R_{Rx} still contribute to the total power consumption when the model is used. Therefore a common receive point (MCS0, 100 PRB, -25 dBm) was identified and the average value subtracted from the y-intercept point of the Rx fits. A similar approach was used on the transmitter. Finally $P_{\text{Tx}} = 28$ mW and $P_{\text{Rx}} = 38$ mW were estimated by comparing the first and second test points of TC 2 and 4 i.e. the UE being allocated either 0 PRBs or transferring with the lowest data rate.

An empirical verification of the modem power model was made by comparing the measured power consumption of TCs 1, 3, 5, and 6 of tab. F.2 for cell BWs of 10, 15, and 20 MHz with the power predicted by the model, which applies the average values

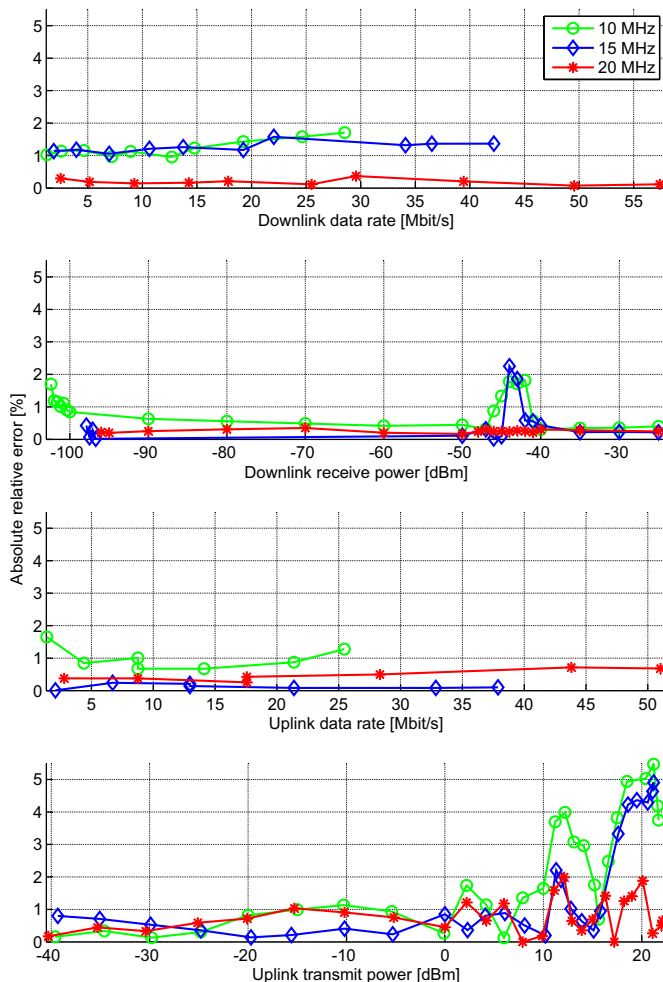


Figure F.10: Model validation using test case 1,3,5,6 in 10,15,20 MHz BW.

and polynomial fits of tab. F.6. The relative error between the measurements and the predicted power for each of the 3 cell BWs and 4 TCs is presented in fig. F.10. They show an average error of 1.0% and a maximum error of 5.5%, which we believe is sufficient for reasonable assessment of UE power consumption. The DRX and idle parameters have not been verified by additional measurements.

F.5 Discussion

The presented model is based on UE2, but as the included results on UE1 and UE3 show the power consumption trends are similar for the 3 smartphones. It is however important to remember that the model is meant for system level simulations and not examination of individual UE components.

An important limitation is that the measurements are conducted hence circumventing

the UE's antennas. Due to lossy antennas the power consumption may differ in real life, but Over-The-Air measurements are complicated and expensive.

Comparing our DRX measurements with Nokia's estimated numbers [61], which have been used extensively in 3GPP and academia, it is interesting to note that Nokia estimated the sleep power to be 1/50 of the "active with no data reception"-state. Our measurements show the ratio is 1/1.8 to 1/35 depending on whether the light or deep sleep mode is used respectively. Furthermore, [61] estimate the UE can transition from sleep mode to being active within 1 ms. Our measurements show this transition takes considerably longer (up to 21 ms for $t_{LP} \geq 80$ ms). This entails the benefits of DRX have been overestimated in previous work, but on the other hand our measurements also confirm that DRX sleep is key to achieve long battery life.

The comparison with screen and CPU+GPU clearly showed the LTE modem is a major contributor to the total power consumption, which makes the presented model relevant for future work. Especially because the modem can actively be affected by mobile network operators by adjusting data rates and power levels via scheduling and power control.

An interesting topic for future work is an assessment of the minimum number of measurement points per TC needed to achieve the level of accuracy, which we have obtained with our model. If only a few measurement points are needed the test time can be kept short, hence the model can easily be updated using new generations of phones. Based on the measurements in this study and [25] it is obvious that the power consumption is almost linearly dependent on downlink data rate, and therefore the receive BB power consumption trend can be captured with as little as 3 measurement points. The receive RF exhibits UE specific power consumption steps and therefore 5-6 points will be needed. The transmit BB power consumption is linear besides minor steps, when the modulation scheme is changed. Since it is known when the modulation scheme changes 4-5 measurement points will be sufficient. The transmit RF is the most power consuming component, and also the one which requires the most detailed analysis, because it is very non-linear for transmit powers above 0 dBm. Finally the DRX measurements require quite a few points to determine the behaviour and number of sleep modes used.

F.6 Conclusion

In this work an LTE smartphone power model was presented. The model can be applied by academia and industry in system level simulations to determine UE energy consumption. This can be an important aid, when selecting one set of network parameters or another. The model is based on empirical measurements on an LTE smartphone, and includes comprehensive LTE Connected Discontinuous Reception (DRX) measurements and also a detailed examination of second generation LTE chipsets. The measurements show that DRX can help achieve longer battery life because the deep sleep mode power consumption is less than 1/35 of the active mode power consumption.

Furthermore, a discussion of the chipset evolution is presented. As expected the power consumption has decreased due to the more efficient transistor technology in 2nd generation chipsets.

Future work can include measurements on LTE Carrier Aggregation and other vendors'

chipsets.

Acknowledgements

Thanks to Frank Laigle, Vidéotron, Taehee Song, Anritsu Canada, and Janus Faaborg, Agilent Technologies Denmark for supporting this work. The work is partly funded by the Danish National Advanced Technology Foundation and the 4GMCT project.

Appendix G

An Empirical LTE Smartphone Power Model with a View to Energy Efficiency Evolution

Mads Lauridsen, Laurent Noël, Troels B. Sørensen and Preben Mogensen

The paper has been published in the
Intel Technology Journal, volume 18, issue 1, 2014

© 2014 Intel
The layout has been revised.

AN EMPIRICAL LTE SMARTPHONE POWER MODEL WITH A VIEW TO ENERGY EFFICIENCY EVOLUTION

Contributors

Mads Lauridsen

Aalborg University, Denmark

Laurent Noël

Vidéotron, Quebec, Canada

Troels B. Sørensen

Aalborg University, Denmark

Preben Mogensen

Aalborg University, Denmark

“The smartphone power consumption model includes the main power consumers in the cellular subsystem as a function of receive and transmit power and data rate...”

“...the combination of high data rates and long sleep periods is the optimal combination from a user equipment energy-saving perspective.”

Smartphone users struggle with short battery life, and this affects their device satisfaction level and usage of the network. To evaluate how chipset manufacturers and mobile network operators can improve the battery life, we propose a Long Term Evolution (LTE) smartphone power model. The idea is to provide a model that makes it possible to evaluate the effect of different terminal and network settings to the overall user equipment energy consumption. It is primarily intended as an instrument for the network engineers in deciding on optimal network settings, but could also be beneficial for chipset manufacturers to identify main power consumers when taking actual operating characteristics into account. The smartphone power consumption model includes the main power consumers in the cellular subsystem as a function of receive and transmit power and data rate, and is fitted to empirical power consumption measurements made on state-of-the-art LTE smartphones. Discontinuous Reception (DRX) sleep mode is also modeled, because it is one of the most effective methods to improve smartphone battery life.

Energy efficiency has generally improved with each Radio Access Technology (RAT) generation, and to see this evolution, we compare the energy efficiency of the latest LTE devices with devices based on Enhanced Data rates for GSM Evolution (EDGE), High Speed Packet Access (HSPA), and Wi-Fi*. With further generations of RAT systems we expect further improvements. To this end, we discuss the new LTE features, Carrier Aggregation (CA) and Enhanced Physical Downlink Control Channel (EPDCCH), from an energy consumption perspective.

Not surprisingly, the conclusion is that having the cellular subsystem ON, and in addition, transmit powers above 10 dBm, have the largest effect on UE power consumption, and that the combination of high data rates and long sleep periods is the optimal combination from a user equipment energy-saving perspective.

Introduction

The battery life of smartphones has become shorter as smartphones have become more advanced, both due to slow battery capacity evolution, but also due to bigger displays, faster and more processor cores, and more complex Radio Access Technologies (RATs).

The power consumed due to use of various RATs depends on the hardware and software within the device, and in addition on the RAT network setup. To analyze and minimize the power consumption caused by suboptimal

network setup, the responsible network engineers require a model that describes the smartphone power consumption as a function of relevant parameters.

In recent literature the smartphone power consumption has been studied either by running a meter application on the phone^{[1][2]} or by using a dummy battery^{[3][4][5]}, which logs the current drain. The latter option seems to be the best because it does not introduce any additional signal processing and hardware routines in the smartphone. In some articles, the authors^{[4][2]} have connected the smartphone to a live, commercial network, while others have performed conducted tests using a base station emulator in a laboratory.^{[3][5]} The emulator setup is preferable because it provides the full control and logging of all relevant network parameters such as resource allocation and power levels, while also being a realistic “live” connection.

Few public measurements of LTE smartphones are available, and most of the literature unfortunately only reports power consumption for a limited number of parameters. One article^[4] provides the power consumption as a function of data rates, but with no information about the transmit (Tx) and receive (Rx) power levels, while another^[5] only reports power consumption as a function of Tx power. Therefore we decided to provide a new model, which includes the most relevant network parameters, that is Tx and Rx power levels and data rates. Our first LTE power model^[6] was based on commercial Universal Serial Bus (USB) dongles, which were not optimized for low power consumption, but the model did not include DRX and cell bandwidth. Therefore we presented an updated model^[3] where the power consumption of three different LTE smartphones, commercially available in fall 2012, was examined. Comparing our dongle and smartphone measurements, it is clear that the cellular subsystems develop fast and that the power consumption improves with each generation. Therefore it is of interest to examine how it has evolved with the launch of the latest LTE chipsets.

In this article we present our recent measurements on LTE smartphones and compare with the previous generations.^{[3][6]} We also discuss the observed energy efficiency (EE) improvement and compare it with other wireless RATs. Finally we discuss how the LTE power consumption can be lowered in the future by use of micro sleep and Carrier Aggregation.

The article is organized as follows: in the next section we introduce our smartphone power consumption model, and in the following section, “Experimental Assessment,” we present the measurement campaign we have carried out to assign meaningful values to the model. Then we define energy efficiency (EE) and provide a comparison of EE in wireless RATs in the section “Energy Efficiency Evolution,” and in connection with this we discuss micro sleep and carrier aggregation as future power optimization possibilities in the section “Energy Efficiency Improvements.” In the last section we present our conclusions.

“The emulator setup is preferable because it provides the full control and logging of all relevant network parameters...”

“...it is clear that the cellular subsystems develop fast and that the power consumption improves with each generation”

“The power consumption model of RRC_connected mode is divided into Transmit and Receive Base Band and Radio Frequency functional blocks...”

“...the power consumption can be measured independently of the other blocks’ contributions by varying the block-specific parameter.”

Smartphone Power Consumption Model

In this section the smartphone power consumption model, originally developed for the dongle measurements^[6] but also applicable here, is presented.

The model covers the LTE cellular subsystem and the overall power consumption is defined as:

$$P_{\text{cellular}} = m_{\text{con}} \times P_{\text{con}} + m_{\text{idle}} \times P_{\text{idle}} + m_{\text{DRX}} \times P_{\text{DRX}} \text{ [W]} \tag{1}$$

where m is a binary variable describing whether the UE is in RRC_connected (con), RRC_idle (idle), or DRX mode. The associated P value describes the power consumption in the given mode as a function of mode specific parameters.

The power consumption model of RRC_connected mode is divided into Tx and Rx Base Band (BB) and Radio Frequency (RF) functional blocks, which each define the power consumption as a function of either Tx or Rx power levels (S) and data rates (R). The model, sketched in Figure 1, was divided into those blocks^[6] because they each have a distinct parameter, for example, transmit power S_{Tx} in the Tx RF, which primarily affects the power consumption of that block. Therefore the power consumption can be measured independently of the other blocks’ contributions by varying the block-specific parameter. Our empirical measurements^{[3][6]} have consolidated this division.

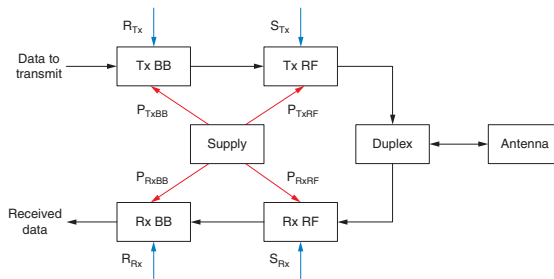


Figure 1: LTE smartphone cellular subsystem power model (Source: Mads Lauridsen, Aalborg University, 2013)

The RRC_connected mode power consumption is:

$$P_{\text{con}} = P_{\text{on}} + m_{\text{Rx}} \times (P_{\text{Rx}} + P_{\text{RxBB}}(R_{\text{Rx}}) + P_{\text{RxRF}}(S_{\text{Rx}})) + m_{\text{Tx}} \times (P_{\text{Tx}} + P_{\text{TxBB}}(R_{\text{Tx}}) + P_{\text{TxRF}}(S_{\text{Tx}})) \text{ [W]} \tag{2}$$

The constants P_{on} , P_{Rx} , and P_{Tx} describe the power consumed when the cellular subsystem is ON, the receiver is actively receiving, and the transmitter is actively transmitting, respectively.

In RRC_idle mode the UE is mainly in a low-power sleep mode. It wakes up periodically to see whether there is an incoming paging message from the network. The period is defined by the network-controlled paging cycle t_{pc} . This behavior resembles the DRX power consumption, and therefore the DRX model, which is presented in the next section, is used to calculate RRC_idle mode power consumption P_{idle} of Equation 1. This is however an approximation because the number of tasks required in RRC_idle is far less compared to RRC_connected.

DRX Power Consumption Model

Sleep modes are one of modern RATs’ most important methods to achieve high EE. The Connected Mode DRX sleep mode is standardized in LTE, and has also been included in recent versions of 3G. The idea is that the UE is scheduled periodically by the network, hence it knows when to be active and when it can sleep. The LTE DRX allows for periods of 10–2560 ms, so the period can be well adjusted to the data type. Furthermore the network can specify how long the UE must remain ON during each period, known as the On Duration t_{onD} , and whether it must remain active for a certain period after successfully decoding data. The UE power consumption as a function of time, when using DRX, could therefore be expected to look as sketched in Figure 2.

There are however multiple tasks that prevent the phone from performing as in Figure 2. They include but are not limited to^[7]:

- The use of different clocks. In deep sleep mode the UE typically uses a low-power low-precision 32 kHz crystal to keep track of the System Frame Number (SFN), whereas it needs to power on a high-precision clock to achieve a proper phase reference for all clocks used when the cellular subsystem is ON.
- The wakeup phase. To enable demodulation, the UE obviously needs a phase lock of the BB Phase Locked Loop (PLL) synthesizer, but also a stable RF subsystem. The latter entails phase-locked RF PLL, stable Automatic Gain Control (AGC), programming of channel filters, and possibly a calibration of certain components.
- The synchronization phase. This requires demodulation of LTE’s primary and secondary synchronization signals, which are sent every 5 ms, and possibly also decoding the Physical Broadcast Channel to get the SFN and other basic information. While this is being performed, channel estimation is also carried out.
- Power-down phase. In this phase the UE does not need to perform decoding, calibration, or any other time-consuming tasks, but powering down the components also takes time, and therefore the phase is included.

Due to the aforementioned tasks, the LTE DRX UE power consumption is as illustrated in Figure 3.

Comparing Figure 3 with Figure 2, you can see that the standardized t_{onD} remains the same while the sleep time t_{sleep} is shortened due to the introduction of the wakeup (t_{wup}), synchronization phase (t_{sync}), and power-down phase (t_{pd}), all of which are functions of the DRX period t_{LP} because it is the deciding

“Sleep modes are one of modern RATs’ most important methods to achieve high energy efficiency.”

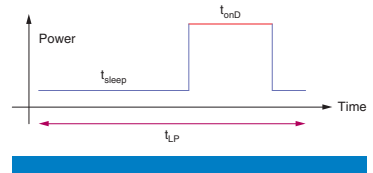


Figure 2: Ideal LTE DRX behavior
(Source: Mads Lauridsen, Aalborg University, 2013)

“...the UE is scheduled periodically by the network, hence it knows when to be active and when it can sleep. The LTE DRX allows for periods of 10–2560 ms...”

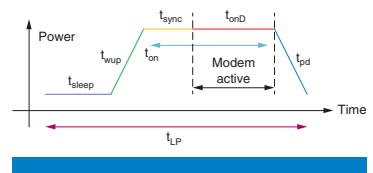


Figure 3: Realistic LTE DRX behavior
(Source: Mads Lauridsen, Aalborg University, 2013)

factor for which sleep power level is used. The shorter sleep time means that the average power consumption is increased.

The sleep time is calculated as

$$\tau_{\text{sleep}}(\tau_{\text{LP}}, \tau_{\text{onD}}) = \tau_{\text{LP}} - (\tau_{\text{wup}}(\tau_{\text{LP}}) + \tau_{\text{sync}}(\tau_{\text{LP}}) + \tau_{\text{pd}}(\tau_{\text{LP}}) + \tau_{\text{onD}}) [\text{s}] \quad (3)$$

Combining it with the energy consumed during the wakeup, synchronization, and power-down phases $E_{\text{wup/pd+sync}}(\tau_{\text{LP}})$, the average DRX power consumption, excluding the power consumed in the On Duration, is

$$P_{\text{DRX}}(\tau_{\text{LP}}, \tau_{\text{onD}}) = (\tau_{\text{sleep}}(\tau_{\text{LP}}, \tau_{\text{onD}}) \times P_{\text{sleep}} + E_{\text{wup/pd+sync}}(\tau_{\text{LP}})) / (\tau_{\text{LP}} - \tau_{\text{onD}}) [\text{W}] \quad (4)$$

Combining this value with the power consumption and length of the On Duration, the total power and energy consumption of a DRX period can be calculated and applied in system level simulations.

The DRX model uses average power, and therefore the results cannot be used for Transmission Time Interval (TTI) simulations, but only system-level simulations with a longer time perspective. Note however that P_{con} is applicable on the TTI level.

“The DRX model uses average power, and therefore the results cannot be used for Transmission Time Interval simulations, but only system-level simulations with a longer time perspective”

Experimental Assessment

Each of the proposed model's functional blocks depend on one specific parameter, and in this section it is described how the functions are derived using experimental measurements.

The assumption is that a given block's function can be assessed experimentally by varying the function-specific parameter, such as the R_{Tx} of the Tx BB, while keeping the other parameters S_{Tx} , R_{Rx} , and S_{Rx} constant and at a level where they will influence the measurement the least.

The parameters are varied by adjusting the Modulation and Coding Scheme (MCS), number of Physical Resource Blocks (PRBs), and Rx and Tx powers S . For example the receive data rate R_{Rx} can be varied by adjusting the Downlink (DL) MCS and the number of DL PRBs.

A least one test case (TC) is then designed for each of the model's four functions (see Table 1), and to enable a comparison with our previous work^[3] the same TCs are used. The varied parameter is shown in brackets. We have previously^[3] applied the TCs in 10, 15, and 20 MHz cell bandwidth. The measurements showed a very linear relationship with bandwidth and therefore the TCs are only performed in 20 MHz cell bandwidth in this study.

The TCs in Table 1 are furthermore designed such that a common point exists. The point uses DL MCS 0, DL PRB 3/4, Uplink (UL) MCS 5/6, UL PRB 100, and constant powers. In addition TC 2 and 4 have an initial test point using 0 PRBs in either DL or UL. By comparing these three points the cellular subsystem ON power P_{on} , and the power consumption of having active reception P_{Rx} and transmission P_{Tx} can be determined.

Test Case		Downlink parameters			Uplink parameters		
		MCS	PRB	S_{Rx}	MCS	PRB	S_{Tx}
Rx BB	1	[0,28]	100	-25	6	100	-40
	2	0	[0,100]	-25	6	100	-40
Rx RF	3	0	100	[-25,-90]	6	100	-40
Tx BB	4	0	3	-25	6	[0,100]	-40
	5	0	3	-25	[0,23]	100	-40
Tx RF	6	0	3	-25	6	100	[-40,23]

Table 1: Measurement parameters. Tests are made for cell bandwidth of 20 MHz. In DL both 1 and 2 code words (CWs) are tested.

(Source: Lauridsen, Mads et al.^[3], 2013)

Measurement Setup

In this study, measurements on two LTE Release 8 category 3 smartphones were performed to obtain updated and realistic values for the smartphone power model. The main characteristics of the Device Under Test (DUT) are listed in Table 2. They are both touchscreen phones running the Android® OS, and are connected to LTE band 4 with carrier frequency 2145 MHz (DL UARFCN 2300).

“In this study, measurements on two LTE Release 8 category 3 smartphones were performed to obtain updated and realistic values for the smartphone power model.”

	UE1	UE2
OS	Android 4.0.4	Android 4.1.2
Launch date	June 2012	April 2013
Modem & CPU	Part #A	Part #B
Modem & CPU CMOS node	28 nm	28 nm
RF transceiver	Part #C	Part #D
RF transceiver CMOS node	65 nm	65 nm
Band 4 PA	Part #E	Part #F
LTE bands	4, 17	1, 2, 4, 5, 17

Table 2: DUT main characteristics

(Source: Laurent Noël, Vidéotron, 2013)

UE2 is one generation newer than UE1, which we previously have examined^[3], and therefore the UEs do not share modem and RF transceiver components as indicated in the table.

“UE2 is one generation newer than UE1 and therefore the UEs do not share modem and RF transceiver components...”

Power consumption measurements are performed under conducted test conditions, that is, the DUT is connected to an Anritsu 8820c eNodeB emulator via a pair of RF coaxial cables. A Faraday cage is used to ensure adequate DUT RF isolation from surrounding commercial LTE and HSPA+ networks. An Agilent N6705B power supply is connected to the DUT via the OEM’s respective dummy batteries. Both supply voltage and current consumption are logged with microsecond time accuracy over at least 30 seconds per measurement point. Each power consumption log is then post-processed on a computer to determine the average power consumption. The accuracy of the measurement is estimated at +/- 10 mW in cell-connected mode. The setup is illustrated in Figure 4.

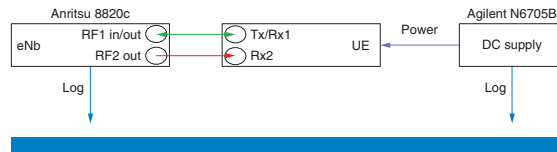


Figure 4: Measurement setup using the eNodeB emulator
(Source: Mads Lauridsen, Aalborg University, 2013)

Note that the use of a dummy battery, and especially the length and diameter of the connecting wires, have a non-negligible effect on the accuracy of the DRX time measurements, which is difficult to prevent.

Uplink Characterization

The main contributor to cellular subsystem power consumption is the transmitter, and in this section the power consumption as a function of the two UL parameters in Equation 2 is reported.

“The PA’s high gain mode is activated when the required transmit power exceeds a certain limit, and it entails a major increase in power consumption.”

A transmitter is usually composed of a single chip RF transceiver and one external power amplifier (PA). The PA’s high gain mode is activated when the required transmit power exceeds a certain limit, and it entails a major increase in power consumption. We have however previously shown^[8] that transmitting with high power and high data rates may be the most energy-efficient solution, depending on the type of data and propagation scenario.

Previous measurements^{[3][6]} on older generations of LTE UEs, including UE1 of this study, have revealed a major power consumption increase when the transmit power exceeds 10 dBm. As illustrated in Figure 5, based on TC 6, this is also the case for the new UE2. Comparing the power consumption of UE1 and UE2, it is clear that the baseline power consumption has improved considerably in UE2. For transmit powers below 0 dBm the improvement is in the order of 35 percent. On the other hand, the PA used in UE2 is not as efficient as the one used in UE1, since the power consumption gap decreases for transmit powers above 10 dBm. This means the energy savings are reduced for high transmit power, but this may not be the case for other UEs because the PA is a component, which is available in many versions and designs, and because many tradeoffs are possible when specifying PA performance. For further information refer to the discussion in Holma et al.^[7] on PAs.

The blue dotted line in Figure 5 represents the model fit for the functional Tx RF block. The design of the fit and the function’s values are presented in the subsection “Model Parameterization.” Observe the blue dotted line is present in the following measurement results as well, and that it covers the related functional block fit.

“...the UE2 power consumption is completely independent of the UL data rate.”

The 35 percent power reduction between UE1 and UE2 is also observed when examining the power consumption as a function of UL data rate as in TC 4 and 5, where the transmit power and DL parameters are kept constant. The result of TC 5 is shown in Figure 6, and it illustrates that the UE2 power consumption is completely independent of the UL data rate. In some UEs,

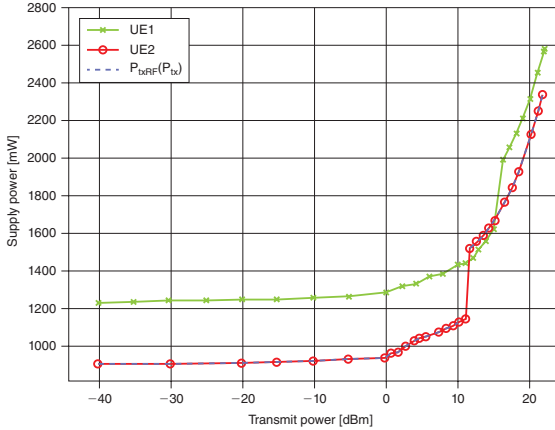


Figure 5: Supply power consumption as a function of transmit power
 (Source: Mads Lauridsen, Aalborg University, 2013)

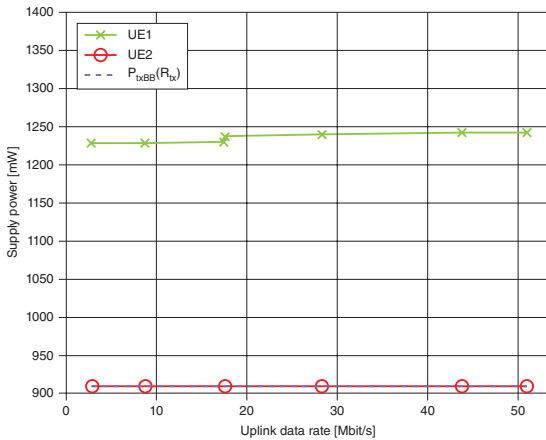


Figure 6: Supply power consumption as a function of UL data rate
 (Source: Mads Lauridsen, Aalborg University, 2013)

including the UE1, a step is observed when the modulation scheme is changed from QPSK to 16QAM. The reason is believed to be that certain PAs require a different bias/linearity setting to deliver the best compromise between power consumption and PA spectral emissions.

“... certain PAs require a different bias/linearity setting to deliver the best compromise between power consumption and PA spectral emissions.”

“...network designers can aim for the highest UL data rate without affecting UE power consumption, but that transmit powers above 10 dBm must be avoided when possible.”

“...increasing the data rate by a factor 10, for example from 5 to 50 Mbit/s, only increases the power consumption about 5 percent.”

Comparing the common point (UL MCS 6, UL PRB 100, Tx P -40 dBm) of Figure 5 and Figure 6, a maximum difference of 3.3 mW is observed, so there is good consistency between the measurements.

The UL parameter results illustrate how the new UE2 have improved the power consumption approximately 35 percent, but also that the choice of PA greatly affects the overall power consumption and that it can eliminate the advantage obtained by switching to a newer transceiver.

The results furthermore show that network designers can aim for the highest UL data rate without affecting UE power consumption, but that transmit powers above 10 dBm must be avoided when possible.

Downlink Characterization

As opposed to the UL, the DL of LTE Release 8 allows for use of Multiple Input Multiple Output (MIMO) antenna configuration, more specifically 2x2. Actually all UEs are required to have two Rx antennas, and therefore Rx diversity can be expected to be applied for all single-stream receptions. Furthermore spatial multiplexing, using two streams, is applicable in favorable channel conditions. This can greatly improve the DL data rate, but since the examined UEs are category 3, the DL data rate is limited to 100 Mbit/s.^[9]

Figure 7 shows the power consumption as a function of received power, based on TC 3, and as expected the improvement from UE1 to UE2 is at least 30 percent. Furthermore observe that UE2 applies a different gain adjustment scheme. The insert of Figure 7 highlights how the scheme adjusts the gain of the Low Noise Amplifier in multiple steps in order to ensure a good compromise between the amplifier's linearity and power consumption.

The result of TC 1, used to examine the DL data rate's effect on power consumption, is shown in Figure 8. The Turbo decoding complexity is known to scale linearly with DL data rate^[10], and this is clearly observable in the figure. The decoder power consumption does however not scale with the same proportion because increasing the data rate by a factor 10, for example from 5 to 50 Mbit/s, only increases the power consumption about 5 percent. This implies it is much more energy-efficient to run at high data rates. This is good for high data rate applications such as file transfers and high quality video streaming. Finally it is interesting to observe that the use of two CWs only add a constant offset to the power consumption.

Comparing the common point (DL MCS 0, DL PRB 100, Rx P-25 dBm) of Figure 7 and Figure 8, good consistency is again observed because the maximum difference is 1.4 mW.

The measurements on DL parameters showed the same 30–35 percent power consumption improvement as in UL, and that high data rates, similar to UL, results in the best EE.

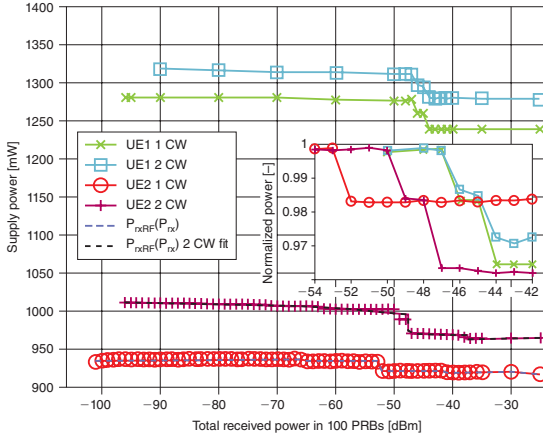


Figure 7: Supply power consumption as a function of receive power
(Source: Mads Lauridsen, Aalborg University, 2013)

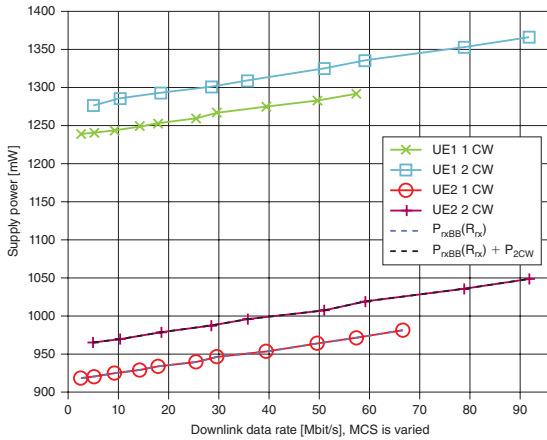


Figure 8: Supply power consumption as a function of DL data rate
(Source: Mads Lauridsen, Aalborg University, 2013)

“When LP is less than 32 ms the UE does not enter a sleep mode at all and therefore DRX Short Period was not examined.”

DRX Characterization

To examine DRX power consumption, the UEs were connected to the base station emulator and Connected Mode DRX was initiated. The DRX Long Period (LP) was varied from 32 ms to 256 ms, while the On Duration was set to 1 ms. When LP is less than 32 ms the UE does not enter a sleep mode at all and therefore DRX Short Period was not examined. Figure 9 shows two measurements on UE2 using DRX LP of 40 and 64 ms.

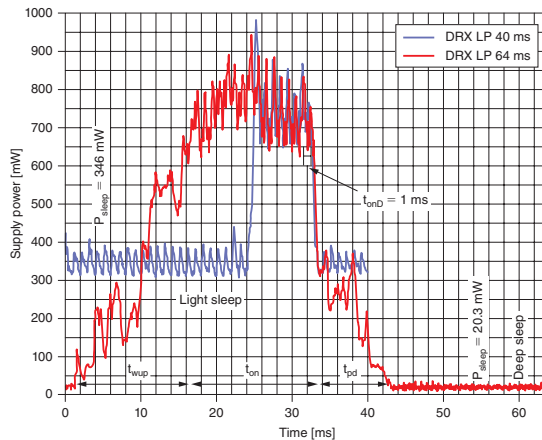


Figure 9: UE2 power consumption for DRX LPs 40 and 64 ms (Source: Mads Lauridsen, Aalborg University, 2013)

Based on the DRX measurements, values for power consumption and duration of each phase have been derived. The results are given in Table 3

Device	t _{LP}	P _{sleep}	t _{wup}	t _{pd}	t _{sync}	E _{wup/pd+sync}
UE1	≤ 40 ms	570 mW	6 ms	9 ms	8 ms	19.2 mJ
UE2	≤ 40 ms	346 mW	0.7 ms	0.6 ms	6.7 ms	6.45 mJ
Improvements		39%	88%	93%	16%	66%
UE1	≥ 80 ms	29 mW	26 ms	21 ms	21 ms	41.4 mJ
UE2	≥ 64 ms	20 mW	16 ms	10 ms	16 ms	19.3 mJ
Improvements		31%	38%	52%	24%	53%

Table 3: Measured DRX parameters. On Duration is 1 ms (Source: Mads Lauridsen, Aalborg University, 2013)

“The ratio between power consumed in the active and sleep mode has improved to 39.9 for deep sleep...”

The light and deep sleep power has improved 31–39 percent. This is as expected since similar improvements were noted in the previous sections. The ratio between power consumed in the active and sleep modes has however also improved from 1.8 to 2.2 and 35.6 to 39.9 for light and deep sleep respectively. This means the use of the sleep modes is even more effective.

In addition the wakeup and power-down times have also become shorter in the new UE2. In particular, the mode change times for light sleep have improved about 90 percent, which means it is much more applicable for short sleep periods. Previously it was discussed^[3] how Nokia's widely used LTE DRX power model^[11] does not correspond well with reality because the active-to-sleep ratio was assumed to be 50 and the transition time 1 ms, but the current results at least indicate the UEs are approaching Nokia's estimates. The sub-millisecond transition time has now been achieved for light sleep, but in this case the active to sleep ratio is far from 50. Still the conclusion remains that DRX is a key method to improve smartphones' battery life.

The synchronization time has also improved, but not as substantially as the aforementioned times, and the reason is the inherent limitation given by LTE's synchronization structure, where the synchronization signals only appear every 5 ms. Examining the synchronization phase after exiting deep sleep, it seems like there is room for improvement, but it must also be noted that achieving proper AGC and a valid channel estimate becomes more difficult when the UE has been sleeping for longer, because the old settings and estimates will be outdated.

The 40 and 64 ms LPs were selected for Figure 9 because they represent the switching point where UE2 is applying either light or deep sleep. The light sleep is used when the LP is short or the On Duration is long, in either way eliminating the use of longer sleep periods. Furthermore the use of light sleep also represents the lowest energy consumption. This is illustrated in Figure 10, where the energy consumption as a function of DRX LP and sleep mode has

“...DRX is a key method to improve smartphones' battery life.”

“...the inherent limitation given by LTE's synchronization structure, where the synchronization signals only appear every 5 ms.”

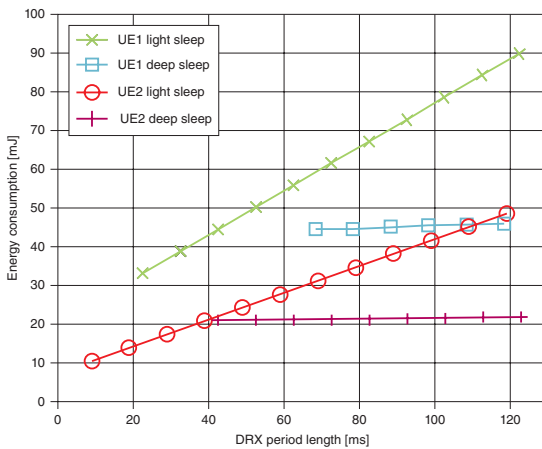


Figure 10: Energy consumption when using DRX sleep modes as a function of DRX LP length
 (Source: Mads Lauridsen, Aalborg University, 2013)

“when developing an empirical model it is important to evaluate how easy it is to update with new measurements.”

“...the cellular subsystem contributes to 30–50 percent of the total power consumption depending on transmit power, screen brightness, and CPU load.”

been calculated using Table 3. The figure clearly illustrates that deep sleep is more energy-efficient for $LP \geq 64$ ms, hence the UE sleep settings are well chosen in terms of energy consumption.

Model Parameterization

When developing an empirical model it is important to evaluate how easy it is to update with new measurements. In our work more specifically the required number of measurement points per TC needed to achieve a proper fit. We previously discussed it^[3], but now suggest the Tx BB is modeled using three points, since it is linear apart from the minor steps related to modulation scheme change. One point at each end of the data rate range is therefore sufficient, while a point in between is necessary as a sanity check. The Rx BB is also linear as a function of DL data rate and therefore three points should be sufficient. The Rx RF always includes UE-specific gain adjustments, which affect the power consumption, and therefore 5–6 points will be required to detect and model the steps of this piecewise linear function. The Tx RF exhibits a linear relation up to 0 dBm, thus the first part can be modeled using three points. For higher transmit powers, one measurement point per dB increase in transmit power is suggested. The reason for this accurate modeling is that the PA is the dominant power consumer.

Based on the above discussion it is clear how the functional blocks of the model in Figure 1 must be fitted to the measured data presented in the earlier subsections on uplink and downlink characterization. Each fit, representing one function in Equation 2, is based on adjusting a polynomial to the measured data by minimizing the least square error. The function of transmit power is divided into three piecewise linear sections due to its nonlinear behavior, while the function of UL data rate is a constant. The function of receive power is also divided into two sections due to the observed gain adjustment steps. The DL data rate function is a first order linear polynomial.

As mentioned earlier, the TCs in Table 1 are designed to have a common point, and the mean value of the four TCs in this point is 908 mW. By comparing this point with the 0 PRB point of TC 2 and 4, the cellular subsystem ON power, the active reception, and transmission power consumption were calculated. These values were then subtracted from the previously determined polynomials such that they can be applied in Equation 2 without contributing multiple times. The estimated polynomials are given in Table 4 and can be directly applied in Equation 2.

For information on how the UE cellular subsystem compares with the power consumption of screen, central processing unit (CPU), and graphics processing unit (GPU), refer to our previous measurements.^[3] We concluded that the cellular subsystem contributes to 30–50 percent of the total power consumption depending on transmit power, screen brightness, and CPU load.

The accuracy of the model fit is examined by comparing each of the measurement results with the model's estimated value. The relative error for each test point in each TC is illustrated in Figure 11. The maximum relative error is 3.3 percent hence a good fit has been achieved.

Part	Polynomial	Comment
P_{TxRF}	$0.78 \times S_{Tx} + 23.6$	$S_{Tx} \leq 0.2$ dBm
P_{TxRF}	$17.0 \times S_{Tx} + 45.4$	0.2 dBm $< S_{Tx} \leq 11.4$ dBm
P_{TxRF}	$5.90 \times S_{Tx}^2 - 118 \times S_{Tx} + 1195$	11.4 dBm $< S_{Tx}$
P_{TxBB}	0.62	
P_{RxRF}	$-0.04 \times S_{Rx} + 24.8$	$S_{Tx} \leq -52.5$ dBm
P_{RxRF}	$-0.11 \times S_{Rx} + 7.86$	$S_{Tx} > -52.5$ dBm
P_{RxBB}	$0.97 \times R_{Rx} + 8.16$	
ON	853, 29.9, 25.1	Cellular subsystem, Tx, Rx active

Table 4: Polynomial fits in mW for the UE2-based model
(Source: Mads Lauridsen, Aalborg University, 2013)

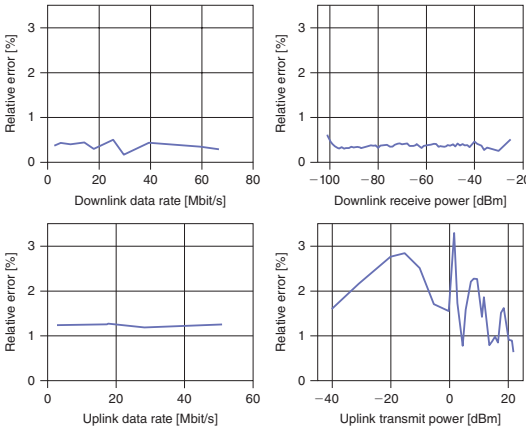


Figure 11: Relative error between estimated and measured power
(Source: Mads Lauridsen, Aalborg University, 2013)

Energy Efficiency Evolution

The measurements, presented in the previous sections, clearly showed the power consumption of LTE UEs have improved with each new chipset generation. The question is how the improvement compares with other modern RATs. We use the metric EE defined as the number of joules required to transfer one bit. In most articles the instantaneous power consumption is given as a function of data rate, but this is equal to EE:

$$P [W] / R [\text{bit/s}] > W \times s/\text{bit} = J/\text{bit}$$

“The measurements clearly showed the power consumption of LTE UEs have improved with each new chipset generation.”

“The downlink energy efficiency has improved with each RAT generation, as a result of improvements in CMOS node and devices in general, but also due to changes in the technologies used in the RATs ...”

Our study is based on a review of power consumption measurements reported in recent literature; EDGE, HSPA, and Wi-Fi* 802.11g (Wi-Fi) has been reported for an HTC Hero by Wang and Manner^[12], Friedman et al.^[13] analyzed Bluetooth* (BT) 2.0 and Wi-Fi power consumption in a Samsung i900*, while Perruci et al.^[14] covered BT 2.0, GPRS, HSDPA, and Wi-Fi using a Nokia N95. Xiao et al.^[15] examined Wi-Fi using both a Nokia N95* and a Nexus S*. Our measurements on LTE dongles^[6] and smartphones^[3] are also included. In addition Texas Instruments have reported the power consumption of their standalone Bluetooth 4.0 Low Energy (BT LE)* chip.^[16] Finally System-on-Chip measurements on BT LE and ZigBee are reported for UL by Siekkinen et al.^[17] The latter two studies obviously differ because they only cover the RAT chip and not a fully functional phone.

The DL EE is shown in Figure 12 for the examined devices. Usually the power consumption is reported as a function of increasing data rate, and therefore Figure 12 includes the dependency on both low and high data rates.

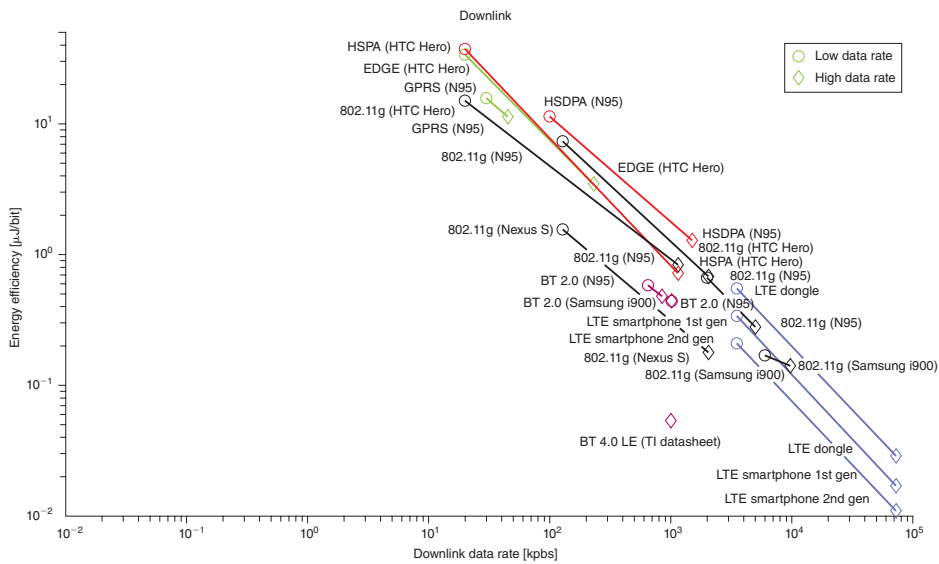


Figure 12: Downlink energy efficiency for modern RATs
(Source: Mads Lauridsen, Aalborg University, 2013)

The DL EE has generally improved with each RAT generation, as a result of improvements in complementary metal–oxide–semiconductor (CMOS) node and devices in general, but also due to changes in the technologies used in the RATs, such as switching from CDMA to OFDMA.^[18]

LTE achieves both the highest data rates and the best EE, while Wi-Fi is number two in both categories. One interesting observation is that the slope between the low and high data rate points is similar for all technologies.

If the target is Machine Type Communications (MTC), with low data rate, none of the systems seem optimal, because the EE rapidly decreases as the data rate is lowered. Currently the 3rd Generation Partnership Project (3GPP)^[19] is running a study on MTC for LTE, which includes reducing the bandwidth and peak data rates, together with a single RF chain and lower transmit power to make LTE cost competitive and energy efficient.

Comparing the EE for UL transmission is more complicated because the transmit power and the general range of the system plays an important role.

The result of the literature review is shown in Figure 13. As in Figure 12, low and high data rates are reported, when available, and additionally the transmit power of the device is included.

“If the target is Machine Type Communications, with low data rate, none of the systems seem optimal, because the energy efficiency rapidly decreases as the data rate is lowered.”

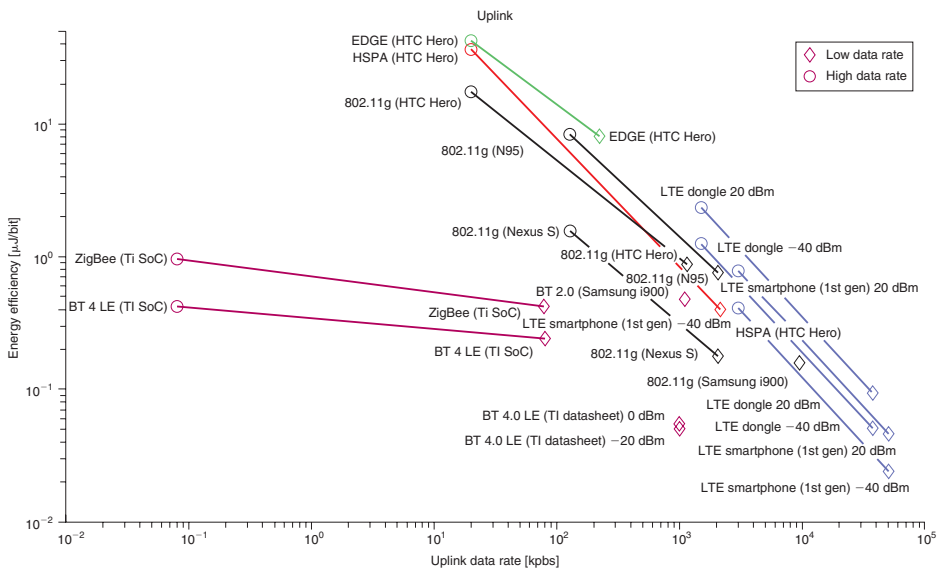


Figure 13: Uplink energy efficiency for modern RATs
(Source: Mads Lauridsen, Aalborg University, 2013)

Again LTE proves to be the most energy-efficient RAT at high data rates, both for low and high transmit powers. The LE version of BT, based on TI’s datasheet^[16], is almost as efficient at a data rate approximately two orders of magnitude lower. This means it is very useful for MTC, but one could

“...LTE has proven to be the currently most energy-effective RAT for transferring data...”

have expected the BT LE to be even more efficient because it was developed specifically for low power purposes. The limiting factor is the low data rate, which prevents the EE from improving significantly. The chip implementations of BT and ZigBee^[17] are a little less efficient, but at data rates below 100 kbps, no other RAT can compare with them in terms of EE. The authors^[17] furthermore mention BT can be made even more efficient using another protocol stack.

It is important to note that the “communication range” of the RATs differs a lot. The mobile communication systems, such as HSPA and LTE, can have a range of several kilometers, whereas Wi-Fi and BT are limited to 10–100 m. This affects their applicability in certain MTC scenarios, and therefore the 3GPP work on LTE for MTC^[19] is important.

To conclude, LTE has proven to be the currently most energy-effective RAT for transferring data, and based on our new measurement and the observed trend it is not expected to change. It is for further study to evaluate how tail energy^[4], which covers the energy consumed after the actual data transmission is completed and is due to network and RAT dependent timeouts, affect each RAT.

Energy Efficiency Improvements

The device maturity may not be enough to guarantee user satisfaction with regards to the battery life and therefore researchers are investigating methods that do not affect the current LTE standard, but decrease the power consumption. In the following subsections we discuss the micro sleep concept and how CA may affect the battery life.

Micro Sleep

One issue in LTE is that the UE is forced to receive and buffer the Physical Downlink Data Channel (PDSCH) while it is decoding the Physical Control Format Indicator Channel (PCFICH) and Physical Downlink Control Channel (PDCCH), which carry scheduling information about PDSCH.^[9] This occurs every subframe and if the UE is not scheduled it will be receiving and buffering PDSCH for no purpose.

To deal with this issue the Fast Control Channel Decoding^[20] concept has been proposed. The idea is to perform a fast decoding of the control channels, stop buffering the PDSCH if the UE is not scheduled, and then power down specific RF and BB components. The UE has to wake up and receive the next subframe, meaning the sleep period is no longer than 7–9 symbols (0.47–0.60 ms) hence the label “micro sleep.” The concept is illustrated in Figure 14. The cost is that the UE will not receive the Reference Signals (RS) in the latter part of the subframe. In literature^[20] this has been described as an SNR loss, which was simulated to result in a throughput degradation of 1–4 percent. On the other hand potential energy savings of 5–25 percent were reported and therefore the concept was deemed valuable.

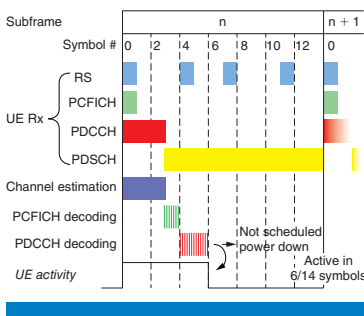


Figure 14: Micro sleep in LTE Release 8
(Source: Lauridsen et al. 2012^[20])

Further advantages of the micro sleep concept include the fact that it can complement DRX, and it fits all types of traffic scenarios as opposed to DRX, which require a periodic pattern to be effective. In addition there is no increase in control message overhead as in DRX where configuration parameters are transferred. Finally the network scheduler will not be affected, because the concept is applied autonomously and individually by each UE.

Comparing the assumptions in the micro sleep literature^[20] with current smartphones' DRX capabilities, as presented in the section "DRX Characterization," it is clear that the instantaneous power consumption cannot be lowered as much as initially expected. The reason is the wakeup and power-down times caused by powering ON and OFF of UE components, which was measured to be 0.6–0.7 ms. Table 3 does however show great improvements in wakeup and power-down times from UE1 to UE2 and therefore UE manufacturers may be able to apply the micro sleep concept in future LTE generations.

Unfortunately the introduction of the Enhanced PDCCH (EPDCCH) in LTE Release 11 has precluded the use of micro sleep. The reason is that the E-PDCCH is spread across the whole subframe time-wise, as illustrated in Figure 15, in order to obtain a frequency diversity gain by only using selected resource blocks in the frequency domain.

In a recent proposal^[21] for a next generation RAT, the control and data channel position has however been reordered such that the control data is a whole frame ahead of the data as illustrated in Figure 16. This allows for efficient pipelining and micro sleep.

Carrier Aggregation

Carrier Aggregation is included in LTE Release 10 to improve user throughput and coverage. The standardization of CA entails a more complicated transceiver design, because the UE needs to be able to receive at least two (up to five) carriers simultaneously each up to 20 MHz wide. The additional hardware can potentially lead to increased UE power consumption, hence the search for even higher data rates may worsen the users' battery life.

To examine this issue we proposed a narrow and a wideband UE power model^[22] and calculated the energy consumption in a heterogeneous network (HetNet) scenario using macro and small cells. The narrowband model applies two RF front ends and two analog-to-digital converters (ADCs), while the wideband model applies a single RF front end and ADC, but with double bandwidth capability.

The users were set to receive a file either via single carrier LTE Release 8 or using two carriers. The narrowband CA UE was estimated to consume 20 percent more power on average as compared to the Release 8 UE, but as illustrated in the simulation results in Figure 17, the energy consumption is approximately the same for both UEs. The reason is that with CA the

“Further advantages of the micro sleep concept include the fact that it can complement DRX, and it fits all types of traffic scenarios as opposed to DRX...”

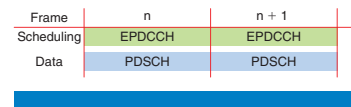


Figure 15: Control and data channel position in LTE Release 10 (Source: Lauridsen et al. 2014^[18])

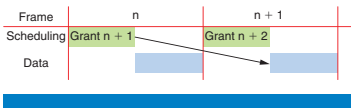


Figure 16: Control and data channel position in a 5G concept^[21] (Source: Lauridsen et al. 2014^[18])

“Carrier Aggregation is included in LTE Release 10 to improve user throughput and coverage, but entails a more complicated transceiver design...”

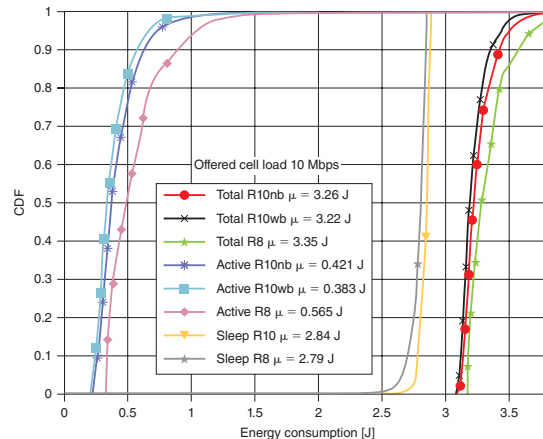


Figure 17: Carrier Aggregation energy consumption in a HetNet scenario (Source: Lauridsen et al. 2013^[22])

“If the throughput does not increase at least 20 percent, Carrier Aggregation will lead to decreasing energy efficiency.”

throughput increased more than 50 percent in the simulated scenario, and therefore the UE can receive the file faster with little penalty on the power consumption of the Rx BB as illustrated in Figure 8. Then the UE can enter a low power sleep mode and achieve high EE. If the throughput does not increase at least 20 percent^[22], CA will lead to decreasing EE.

When the work was performed there was no knowledge about how fast the transition to sleep mode could be made, but the measurements in the section “DRX Characterization” have made it clear that shifting to DRX sleep mode takes a considerable amount of time. Therefore CA will mainly be effective for very large file transfers, where the time difference between CA and Release 8 UEs, including the transition time, is large. Otherwise the penalty on the user may be heavy due to the increased instantaneous power consumption.

As mentioned, the work^[22] was based on a theoretical extension of the existing power model^[6], but recently a vendor has launched a CA device^[23], which could help clarify if the assumptions were correct.

Conclusion

In this work an empirical smartphone power model was presented. The model covers the cellular LTE subsystem and is based on measurements on the newest generation of LTE smartphones. By comparing with our previous measurements on older LTE generations, power consumption improvements of approximately 35 percent were noted and attributed to device maturity. The LTE Discontinuous Reception feature was also examined and the results

“The model covers the cellular LTE subsystem and is based on measurements on the newest generation of LTE smartphones.”

show the deep sleep power is now as low as 1/40 of the active mode power. Furthermore the new smartphone is able to enter and exit the sleep modes at least 30 percent faster, which makes DRX more applicable in a real network and enhances the possibility for use of micro sleep.

The cellular subsystem model is intended for use in system level simulations to evaluate how specific network settings affect user equipment power consumption. The measurements show that the power consumption is dominated by the subsystem being ON, consuming about 0.9 W, and also very affected by transmit powers above 10 dBm, consuming an additional 0.6–1.5 W. The power consumption is almost independent of uplink and downlink data rates, and therefore the combination of high data rates and long sleep periods must be the target of an energy-efficient network setup.

The work also surveys the energy efficiency, in terms of number of joules required to transfer one bit, of multiple radio access technologies. For high data rates, LTE is superior to older technologies such as EDGE, HSPA, and 802.11g Wi-Fi.

Finally it was evaluated that Carrier Aggregation, which is a prominent new LTE feature, will affect the energy efficiency positively if the throughput can be increased 20 percent as compared to conventional single-carrier LTE UEs.

“...the power consumption is dominated by the subsystem being ON, consuming about 0.9 W, and also very affected by transmit powers above 10 dBm, consuming an additional 0.6–1.5 W.”

“...the combination of high data rates and long sleep periods must be the target of an energy-efficient network setup.”

Acknowledgements

Thanks to Frank Laigle, Vidéotron, Taehee Song, Anritsu Canada, and Janus Faaborg, Agilent Technologies Denmark for supporting this work. The work is partly funded by the Danish National Advanced Technology Foundation and the 4GMCT project.

References

- [1] Murmura, R., J. Medsger, A. Stavrou, and J. M. Voas, “Mobile Application and Device Power Usage Measurements,” IEEE Sixth International Conference on Software Security and Reliability, 2012.
- [2] Wang, C., F. Yan, Y. Guo, and X. Chen, “Power Estimation for Mobile Applications with Profile-Driven Battery Traces,” IEEE ISLPED, 2013.
- [3] Lauridsen, M., L. Noël, and P. Mogensen, “Empirical LTE Smartphone Power Model with DRX Operation for System Level Simulations,” VTC, Fall 2013.
- [4] Huang, J., F. Qian, A. Gerber, Z. M. Mao, and S. Sen, “A Close Examination of Performance and Power Characteristics of 4G LTE Networks,” MobiSys’12, 2012.
- [5] Dusza, B., C. Ide, L. Cheng, and C. Wietfeld, “An Accurate Measurement-Based Power Consumption Model for LTE Uplink Transmissions,” INFOCOM 2013.

- [6] Jensen, A. R., M. Lauridsen, P. Mogensen, T. B. Sørensen, and P. Jensen, "LTE UE Power Consumption Model – For System Level Energy and Performance Optimization," VTC Fall 2012.
- [7] Holma, Harri, Antti Toskala, and Pablo Tapia (eds.), *HSPA+ Evolution to Release 12: Performance and Optimization* (Wiley, 2014), ISBN: 9781118503218.
- [8] Lauridsen, M., A. R. Jensen, and P. Mogensen, "Reducing LTE Uplink Transmission Energy by Allocating Resources," VTC Fall 2011.
- [9] Holma, Harri and Antti Toskala (eds.), *LTE for UMTS: OFDMA and SC-FDMA Based Radio Access* (Chichester, UK: Wiley, 2009) ISBN 9780470994016.
- [10] Holma, Harri and Antti Toskala, *LTE for UMTS: Evolution to LTE-Advanced*, 2d Ed (Chichester, UK: Wiley, 2011), ISBN 9780470660003.
- [11] Nokia, DRX Parameters in LTE – 3GPP R2-071285, 2007.
- [12] Wang, L. and J. Manner, "Energy Consumption Analysis of WLAN, 2G and 3G interfaces," IEEE GreenCom 2010.
- [13] Friedman, R., A. Kogan, and Y. Krivolapov, "On Power and Throughput Tradeoffs of Wi-Fi and Bluetooth in Smartphones," IEEE Infocom 2011.
- [14] Perrucci, G.P. and F. Fitzek, "Measurements campaign for energy consumption on mobile phones," Technical report, Aalborg University 2009.
- [15] Xiao, Y., Y. Cui, P. Savolainen, M. Siekkinen, A. Wang, L. Yang, A. Ylä-Jääski, and S. Tarkoma, "Modeling Energy Consumption of Data Transmission over Wi-Fi," *IEEE Transactions on Mobile Computing*, 2013.
- [16] Texas Instruments, CC2541, 2.4-GHz Bluetooth low energy and Proprietary System-on-Chip. Datasheet, 2012.
- [17] Siekkinen, M., M. Hienkari, J. K. Nurminen, and J. Nieminen, "How Low Energy is Bluetooth Low Energy? Comparative Measurements with ZigBee/802.15.4," WCNC Workshop 2012.
- [18] Lauridsen, M., G. Berardinelli, T. B. Sørensen, and P. Mogensen, "Ensuring Energy-Efficient 5G User Equipment by Technology Evolution and Reuse," Submitted for VTC Spring 2014.
- [19] 3rd Generation Partnership Project, "Study on provision of low-cost Machine-Type Communications (MTC) User Equipments (UEs) based on LTE," TR 36.888 v.12.0.0, 2013.

- [20] Lauridsen, M., A. R. Jensen, and P. Mogensen, "Fast Control Channel Decoding for LTE UE Power Saving," VTC Spring 2012.
- [21] Mogensen, P., K. Pajukoski, B. Raaf, E. Tirola, E. Lahetkangas, I. Z. Kovacs, G. Berardinelli, L. G. U. Garcia, H. Liang, and A. F. Cattoni, "B4G local area: High level requirements and system design," IEEE Globecom Workshops 2012.
- [22] Lauridsen, M., H. Wang, and P. Mogensen, "LTE UE Energy Saving by Applying Carrier Aggregation in a HetNet Scenario," VTC Spring 2013.
- [23] Qualcomm, "World's First Mobile Device with LTE Advanced Carrier Aggregation Powered by the Qualcomm Snapdragon 800 Processor," <http://www.qualcomm.com/media/blog/2013/06/26/worlds-first-mobile-device-lte-advanced-carrier-aggregation-powered-qualcomm>, 2012.

Author Biographies

Mads Lauridsen received his MSc EE from Aalborg University in 2009 and is currently pursuing a PhD at Aalborg University in the Radio Access Technology Section. His work focuses on user equipment energy consumption in LTE and future radio access technologies. He can be reached at ml@es.aau.dk.

Laurent Noel received a degree in mathematics and physics from the University of Montpellier II, France, in 1991, and a degree as a microelectronics engineer at the Institut des Sciences de l'Ingenieur (ISIM: now Polytech-Montpellier) in 1994. From 1994 to 2000 he worked at British Telecom (VT) Research Laboratories. From 2000 to 2010, he worked at Philips Semiconductors. He became Senior Principal System Architect at ST-Ericsson and worked on reconfigurable multimode, multiband, digital RF solutions for LTE, FDD-WCDMA, EGPRS. He currently works in the mobile phone certification team at Videotron, Montreal (Canada). He can be reached at Laurent.Noel@videotron.com.

Troels B. Sørensen graduated in 1990 (MSc EE) from Aalborg University and received his PhD degree from the same university in 2002. He has had experience in industry (telecom operator) and academia since 1997. He holds a position as associate professor in the Radio Access Technology Section at Aalborg University, Department of Electronic Systems, where his primary involvement is in the supervision of Master and PhD students and research related to wireless communication. He can be reached at tbs@es.aau.dk.

Preben Elgaard Mogensen received his MSc EE and PhD in 1988 and 1996 from Aalborg University, Denmark. He is currently Professor at Aalborg University leading the Radio Access Technology Section. Preben Mogensen is also associated with Nokia Siemens Networks. His current research work is related to heterogeneous network deployment, cognitive radio, and beyond 4G. He can be reached at pm@es.aau.dk.

Appendix H

Fast Control Channel Decoding for LTE UE Power Saving

Mads Lauridsen, Anders Riis Jensen, and Preben Mogensen

The paper has been published in the
VTC Spring 2012

© 2012 IEEE
The layout has been revised.

Abstract

This work examines the energy saving potential of powering down RRC_connected but unscheduled User Equipment (UE). The idea is to power down energy consuming circuits in RF and BB, when it is determined by Fast Control Channel Decoding (FCCD) that the UE is not scheduled to receive downlink data in the current TTI. The cost is that some reference signals are not received leading to a degraded channel estimate. Calculations show that this causes an SINR degradation of approximately 0.5 dB, which will result in maximum 4% throughput loss. Comparing this with energy saving potentials of 5%-25% it is concluded that the FCCD method is a valuable aid to prolong LTE phones' battery lifetime.

The results are generated using a two state Markov chain model to simulate traffic and scheduling, and verified mathematically. The work also includes an examination of various data traffic types' on/off relation and an evaluation of how the relation affects power consumption. The FCCD method can complement DRX sleep mode since it is applicable when the signal is too aperiodic or fast switching for DRX.

H.1 Introduction

Today mobile phone users are experiencing limited battery lifetime, and the situation is not improving because the gap between mobile phone complexity and battery capacity increases [187, 201]. One reason is that the users run more power and data demanding applications. The Third Generation Partnership Project developed the Long Term Evolution (LTE) standard [197] to deal with the demand for higher data rates and lower latency, but this caused the phones to become even more complex in terms of number of antennas and processor speed [59]. During the standardization process less attention was paid to how long the phones can utilize LTE before the battery is discharged, and therefore we now deal with a problematic relationship between required and available energy.

In previous work researchers have tried to maximize the available energy, minimize the energy consumption, [202], and harvest energy [201]. Minimizing the phone's energy consumption requires optimization of the hardware (HW) and/or software (SW). A less obvious minimization option is to adjust network controlled parameters that affect the phone's modem as described in [29]. The energy consumption of the phone's HW can be reduced by developing energy efficient components and by applying power management. In LTE Discontinuous Reception (DRX) [184] have been standardized to enable energy saving sleep modes [73]. The problem is that DRX requires a data traffic pattern with periodic trends, and furthermore it increases the control message overhead of the network and complicates the scheduling. In this work a micro-sleep mode, [74], which can be applied in traffic that does not fit DRX, is examined. The idea is to perform Fast Control Channel Decoding (FCCD) and then power down energy consuming circuits, when the phone is RRC_connected in the current TTI, but not scheduled. The objective is to determine whether the FCCD is feasible for various data traffic patterns, and if energy can be saved, but it is out of scope to present a specific power down implementation.

First we describe LTE control channel decoding, the inherent SINR degradation, the UE power model and the Markov chain traffic generator. Then we present simulation results, a mathematical verification, and finally the conclusion.

H.2 Applying FCCD to Save Energy

H.2.1 Fast Control Channel Decoding

The Physical Downlink Shared Channel (PDSCH) carries individual user data and is configured on a Transmit Time Interval (TTI) basis. The channel is shared among the users and therefore the network notifies the users of when and where in time and frequency their data is located. This procedure is known as resource block allocation. A Resource Block (RB) consists of 12 subcarriers, each 15 kHz wide, spanning one TTI, which is 1 millisecond i.e. 14 symbols, when the normal cyclic prefix is applied, [71].

The UE will initially receive one of seven different Downlink Control Information (DCI) data blocks on the Physical Downlink Control Channel (PDCCH). The DCIs are contained in Control Channel Elements (CCE) and used to determine the PDSCH's modulation format and the assigned RBs. The UE is required to blindly decode several CCEs in each TTI to check if it contains a relevant DCI, [74]. Therefore the Physical Control Format Indicator Channel (PCFICH) indicates the number of OFDM symbols, used for PDCCH in the current TTI. The PCFICH is located in the first OFDM symbol of a TTI while the PDCCH occupies the first 1-3 symbols.

Usually the UE buffers PCFICH & PDCCH, and while it decodes those channels it buffers PDSCH to ensure that it does not lose any data. Buffering PDSCH, when the user is not scheduled is a waste, because the decoding will fail since the data was not intended for the UE. The proposed idea is thus to power down energy consuming circuits in Radio Frequency (RF) and Base Band (BB), when it is determined by decoding of PCFICH & PDCCH that the UE is not scheduled to receive downlink data in the current TTI, as illustrated in figure H.1. Note that a fast decoding of the two control channels is crucial. The DCIs are transmitted on PDCCH using CCEs composed of 9 Resource Element Groups, which again are composed of 4 Resource Elements (RE), [59]. A RE is one subcarrier and one symbol, and since PDCCH is QPSK modulated a CCE is $9 \cdot 4 \cdot 2 \text{ bit} = 72 \text{ bit}$. Note that the DCIs only comprise 40-50 bit. The DCI search space is composed of 16 UE specific and 6 common CCE candidates, [72] thus the UE must Viterbi decode $2 \cdot (16 + 6) \cdot 72 \text{ bit} = 3168 \text{ bit}$ to determine if it is scheduled. The factor of 2 is due to the UE decoding both UL and DL DCI formats, but it is an estimate since some DCIs have equal size, hence they can be decoded together. The number is low compared to the 150 kbit the UE can Turbo decode per TTI and therefore the FCCD is deemed plausible. The FCCD is compared with a regular method, where the entire subframe is buffered. Here the UE decodes the control channels later and is therefore unable to power down. Instead it discards data and saves energy by not processing useless, not decodable data as illustrated in figure H.2.

The FCCD method has several advantages as compared to DRX. First of all it is much more flexible than DRX since it does not require a periodic data traffic pattern. Furthermore the network does not need to schedule sleep mode users and transmit control messages regarding the sleep mode settings i.e. the overhead is reduced because

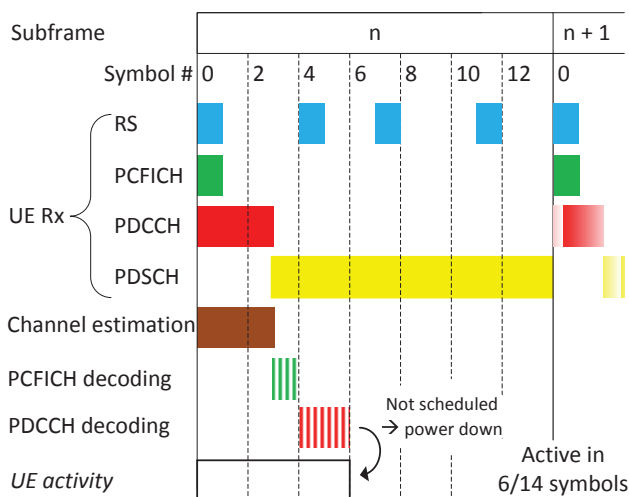


Figure H.1: Power down based on Fast Control Channel Decoding (FCCD).

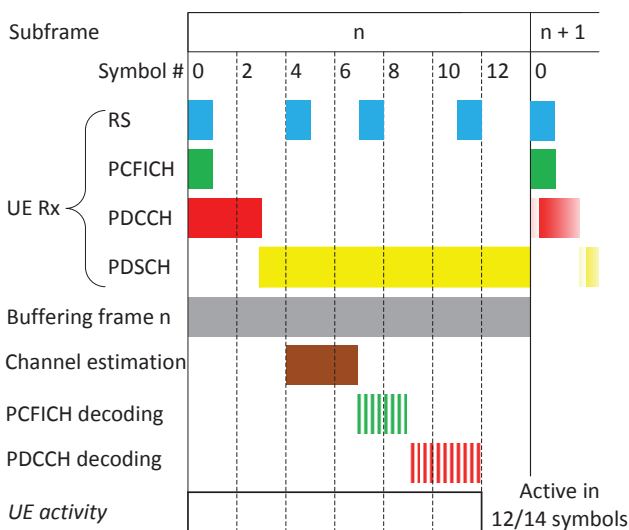


Figure H.2: Power down based on full frame buffering.

the method is applied individually by each UE. Actually the method is fully independent of DRX, which means they can co-exist.

H.2.2 SNR Degradation due to fewer Reference Signals

The Reference Signals (RS), which are transmitted in symbol 0, 4, 7, and 11 of every subframe, as shown in figure H.1, and spread across the subcarriers according to a mapping scheme, consist of a predefined symbol sequence enabling the UE to estimate the transmission channel(s), [71]. Using the power down technique in figure H.1 will entail that the RS in frame n are not available for channel estimation if the UE is

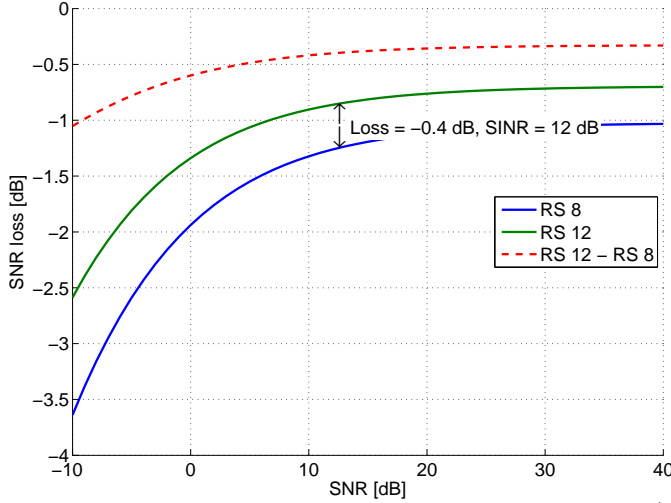


Figure H.3: SNR loss as a function of downlink Reference Signals (RS).

scheduled in frame $n+1$ as compared to figure H.2. This is interpreted as a Signal-to-Noise Ratio (SNR) degradation and therefore also a throughput loss.

In LTE the number of RS per RB's effect on the SNR was examined to determine a reasonable relationship between channel estimation quality and overhead. The effective SNR based on channel estimation is [75]

$$\text{SNR}_{\text{ch.Est}} = \frac{\text{SNR}}{1 + \frac{1}{d} + \frac{1}{d \cdot \text{SNR}}} \quad (\text{H.1})$$

where SNR is with perfect channel estimation, and d is the number of RS used to generate the channel estimate. The assumption is that the channel is flat in frequency and time during one resource block.

The UE will receive 8 RS per antenna port per RB, [71] and if the UE is active in consecutive frames it is furthermore assumed that it can utilize the last half (time wise) of the RS in the previous TTI, achieving a total of 12 RS. Figure H.3 illustrates the SNR loss, which is the difference between the original SNR and $\text{SNR}_{\text{ch.Est}}$ for 8 and 12 RS. Furthermore the loss caused by using 8 instead of 12 RS is also plotted.

To comply with the assumption that the RB is flat in time the maximum UE speed is calculated. As a rule of thumb we set the wave length λ to $1/20$ of the original wave length λ_c :

$$\lambda = \frac{\lambda_c}{20} = \frac{1}{20} \cdot \frac{c}{f} = \frac{3 \cdot 10^8 \text{ m/s}}{20 \cdot 2 \cdot 10^9 \text{ Hz}} = 0.0075 \text{ m} \quad (\text{H.2})$$

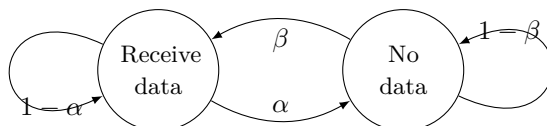
$$v_{\text{UE}} = \lambda/t = 0.0075 \text{ m}/0.001 \text{ s} = 7.5 \text{ m/s} = 27 \text{ km/t} \quad (\text{H.3})$$

where c is the speed of light, f is the carrier frequency, and t is 1 TTI. Most users are indoor hence v_{UE} is high enough for the SNR degradation assumptions to be applicable.

Note it is assumed that PDCCH is encoded so well that it can be received properly even though some RS are missing.

Table H.1: UE power model, [61]. Values are relative to P_{active}

Description	Variable	Relationship
Active with data reception	$P_{\text{active}} = 500 \text{ mW}$	1
Active, FCCD power down	P_{ccd}	[0.4,0.5,0.6]
Active, full buffering	P_{buf}	[0.7,0.8,0.9]

**Figure H.4:** Two-state Markov chain model.

H.2.3 UE Power Model

The structure of the subframe allows the UE to decode the control channels and then power down if data is not scheduled. As mentioned earlier this work introduces the FCCD method, but not a specific implementation. Implementing the method should however not pose problems, because a phone utilizes power domains i.e. it can power down circuits individually. Furthermore most circuits can power down/up fast, and in [73] the wakeup time is estimated to $2 \mu\text{s}$. This excludes the synthesis which requires $\approx 300 \mu\text{s}$ to settle. Among the envisioned sleeping circuits are Low Noise Amplifiers, Programmable Gain Controls, mixers, and analog-to-digital converters.

To evaluate the energy saving potential the UE power model from [61] is applied. The model is based on relative values and one arbitrary power level. In [61] and the DRX focused article [203], there is no sensitivity analysis of the relative values, but as shown in table H.1 this work includes such an analysis to give a broader perspective of the energy saving potential.

Because the FCCD power down happens after the 6th symbol, as shown in figure H.1, the power consumption is estimated to be half of P_{active} . Using the full buffering method is not as efficient because the decoding occurs later, and processing first stops after the 12th symbol, see figure H.2.

Note that the power model does not include uplink transmission and state transition power consumption.

H.2.4 Traffic Generation & Packet Scheduling

One of the main objectives is to evaluate the energy saving potential for various traffic patterns. The traffic is generated using a two-state Markov chain [204], where the two states represent the UE's mode. In the first mode the UE is scheduled and receiving data, and in the second mode it is RRC_connected, but not scheduled as illustrated in figure H.4. The Markov chain, which only depends on the previous state, has two parameters α & β . The probability to change from a state where the UE is receiving data to not receiving is α , while the probability to continue being in a receiving data

Table H.2: Receive patterns. H/L indicates high/low probability.

α	β	AF	Receive pattern examples	
H	H	50%	1	Rx data No data 
L	L	50%	2	Rx data No data 
L	H	> 50%	3	Rx data No data 
H	L	< 50%	4	Rx data No data 

state is $1 - \alpha$. Likewise with β for the state "no data". Small α & β results in a pattern with long consecutive blocks whereas large α & β will result in a rapidly switching pattern. Table H.2 contains four examples of the relationship between α , β and the resulting receive pattern. The ratio between "receive data" and "no data" in figure H.4 is defined as the Activity Factor (AF), and it is estimated for the patterns in table H.2. Notice that the AF is equal for the first two patterns even though α & β are not equal. Pattern 1 results in an SNR degradation four times as often as pattern 2, hence the throughput will be different. Because of this throughput difference, simulations are made for various configurations of α & β even though they result in the same AF.

Defining the transition probability matrix P for the Markov chain in figure H.4 as

$$P = \begin{bmatrix} \text{Rx} & \text{Rx} \rightarrow \text{No data} \\ \text{No data} \rightarrow \text{Rx} & \text{No data} \end{bmatrix} = \begin{bmatrix} 1 - \alpha & \alpha \\ \beta & 1 - \beta \end{bmatrix}$$

the stationary probability mass function $\boldsymbol{\pi}$ is [205, Eq. 9.18b]

$$\boldsymbol{\pi} = \boldsymbol{\pi}P = [\pi_0 \quad \pi_1] \tag{H.4}$$

That is the probability of a given state approaches a steady state independent of the initial probability. Noting that $\sum_i \pi_i = 1$

$$[\pi_0 \quad \pi_1] = [\pi_0 \quad \pi_1] \cdot \begin{bmatrix} 1 - \alpha & \alpha \\ \beta & 1 - \beta \end{bmatrix} \tag{H.5}$$

$$\pi_0 = \frac{\beta}{\alpha + \beta} \quad \pi_1 = \frac{\alpha}{\alpha + \beta} \tag{H.6}$$

where π_0 is the probability of being in state 0 (receive state) and π_1 is the probability for state 1 (not scheduled state). Since AF equals π_0 it can be calculated using α & β .

The AF can be related to real traffic generating applications by determining the applications' data rate and latency requirements. Table H.3 gives estimated AFs for four selected applications with diverse requirements. Heartbeat applications do not impose hard time constraints, neither do they require a lot of data, and therefore the AF is estimated to be $\leq 1\%$ for all network loads. The voice applications usually generate very small packets (<40 bytes), but they have a hard real time constraint.

Table H.3: Estimated activity factors for selected applications.

		Network load			Real Time
		Low	Medium	High	Constraint
Applications	Heartbeat	≤ 1	≤ 1	≤ 1	None
	Voice	5	5	5	Hard
	H.264 film	30	50-60	80-90	Easy
	FTP	80-100	80-100	50	None

Table H.4: Simulation parameters.

Parameter	Value
Allocated PRBs	8 (180 kHz per PRB)
Simulation time	120 s
SINR	12 dB
Num. RS for first/consecutive TTI(s)	8, 12
α, β	[0.01:0.04:0.09 0.1:0.4:0.9]
Block Error Rate (BLER)	10 %
Receive patterns	100 per α & β set
Channel	TU20 SISO

Because the packets arrive every 20 ms, [59], the AF is set to 5% independently of the network load. DRX is expected to be applied to both heartbeat and voice applications.

Video is available in many different qualities and frame rates. In [206] a H.264 high quality video configuration with a frame rate equal to 25 Hz is presented. The resulting bitrate is 3.6 Mbps and since the authors mention that IP and UDP adds 30% overhead the required rate is $1.3 \cdot 3.6 \text{ Mbps} = 4.68 \text{ Mbps}$. Assuming the SINR to be 12 dB the spectral efficiency is $\approx 1.7 \text{ b/s/Hz}$ for a TU20 SISO channel. In the low network load scenario the user is estimated to get 50 PRBs resulting in a throughput equal to 15.3 Mbps. The AF is $\frac{4.68}{15.3} \approx 30\%$. The allocated bandwidth reduces as the network load increases and therefore the activity factor increases in order to maintain the frame rate. The FTP application does not impose any time constraints and therefore the activity factor solely depends on the allocated resources. When the network load is low the user can be active every TTI, but as the load increases the user may not be scheduled every TTI hence the AF decreases.

In summary table H.3 shows how diverse the AF can be for traffic generated by LTE users, and therefore the simulations are made for $1\% \leq \text{AF} \leq 100\%$.

H.2.5 Simulation Setup

The simulation parameters are given in table H.4. The simulations are initialized by

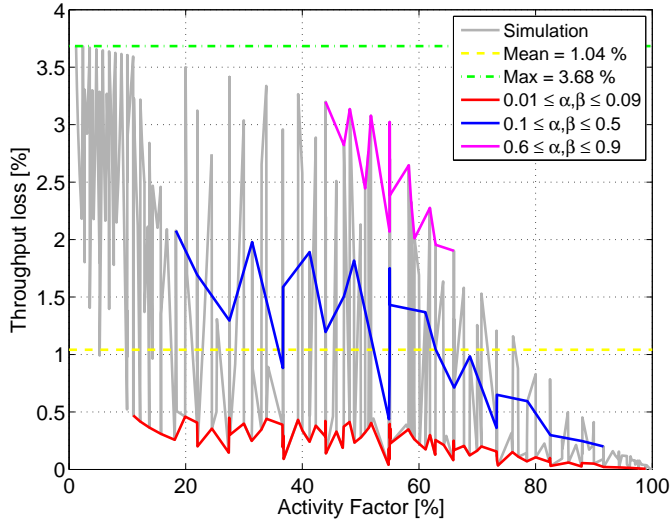


Figure H.5: Throughput loss as a function of AF.

generating a 120s receive pattern using the Markov chain and a α & β set. Then a BLER of 10% is added. This is achieved by randomly inserting 10% extra receive-periods. These periods do not add to the total throughput, but they entail that the RS are received in the given TTI. Next the throughput using 8 (FCCD) and 12 RS (full buffering) are calculated based on the SINR and the number of PRBs. Finally the energy consumption is determined using the generated pattern and the power model from section H.2.3. The simulations are made on 100 patterns per α & β set.

The simulations do not include protocol specifics such as TCP's slow start. Furthermore LTE DRX [184] is not implemented, but the authors are aware that DRX will be applied for low AFs, leading to a lower power consumption [203]. Long DRX has a minimum cycle of 10 ms, [60] and if the UE is active in one TTI the maximum AF is 10%. Short DRX has a minimum cycle of 2 ms i.e. the maximum AF is 50%.

H.3 Simulation Results

The SNR degradation described in section H.2.2 will entail a reduced throughput. The loss is calculated as the achieved throughput, when the UE is always active, minus the achieved throughput, when the UE is using FCCD. The simulated result is plotted in figure H.5 and the average loss is 1.04% and the maximum loss is 3.68%. These are negligible numbers hence FCCD is applicable for all AFs from a throughput point of view. The loss decreases as the AF increases because the FCCD is applied less and less. The loss fluctuates because the simulations are made for different combinations of α & β . If e.g. the AF is 50% the two set of probabilities [0.9, 0.9] and [0.01, 0.01] are applicable, but they will result in different patterns. When α & β are large the UE will change state rapidly leading to a larger SNR degradation as compared to smaller α & β which will entail a slowly changing pattern with minimal SNR degradation.

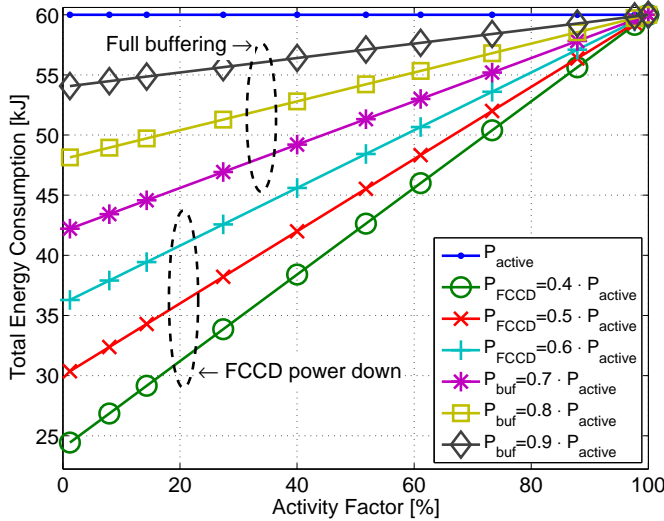


Figure H.6: Energy consumption as a function of AF.

The simulated energy consumption for the three UE modes is illustrated in figure H.6. The power model sensitivity analysis (table H.1) is represented in this plot by the three lines per sleep mode. As expected the average energy consumption is constant for the always active mode, while it decreases for decreasing AF for the two other modes. The reason is that the number of "no data" periods increase, when the AF decreases and therefore the UE is able to be in a sleep mode more often.

Figure 7 shows the energy saving when using FCCD relative to full buffering. Notice that the FCCD method is applicable for AFs that are too high for DRX. The biggest energy savings are obviously obtained for lower AF and for AF= 20% they are between 10% and 45%. When $AF \geq 80\%$ the energy savings are below 10% for all combinations. The result for $P_{ccd} = 0.5 \cdot P_{always\ active}$, $P_{buf} = 0.7 \cdot P_{always\ active}$ shows savings between 5% and 25% in the applicable AF interval. Note that there is a throughput loss when using FCCD as compared to full buffering, but as shown in figure H.5 it is less than 4%.

H.4 Verification

In this section the energy saving and the throughput loss are verified mathematically by equations that only depend on the time period T and the AF. Since the Markov chain's α and β are not used, the equations are based on periodic patterns. The average power consumption of pattern 1 (50% AF) and 3 (75% AF) in table H.2 is

$$\begin{aligned}
 P_1 &= (P_{active} \cdot 4 TTI + P_{FCCD} \cdot 4 TTI) / (8 TTI) \\
 P_3 &= (P_{active} \cdot 6 TTI + P_{FCCD} \cdot 2 TTI) / (8 TTI) \\
 &\Downarrow \\
 P_{avg} &= P_{active} \cdot AF + P_{FCCD} \cdot (1 - AF)
 \end{aligned} \tag{H.7}$$

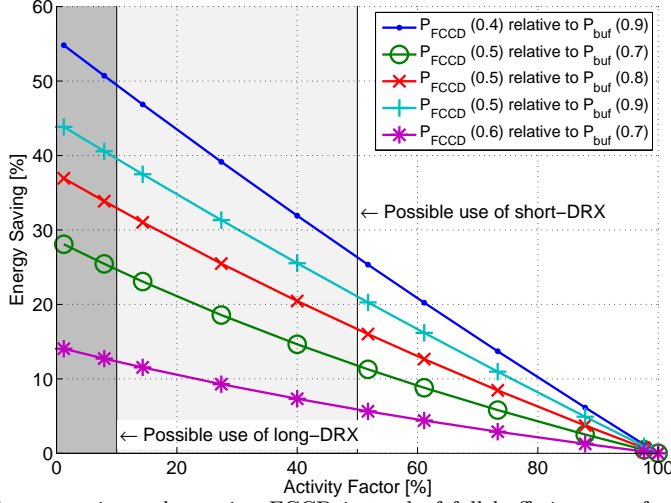


Figure H.7: Energy savings when using FCCD instead of full buffering as a function of AF. The values in () denotes the power relative to the always active power. The grey areas indicate possible DRX use based on [60].

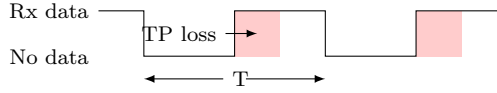


Figure H.8: Receive pattern defining T and throughput loss.

Using the power values from table H.1 the total energy consumption for $AF=40\%$ is

$$\begin{aligned} E_{\text{tot}} &= t_{\text{sim}} \cdot P_{\text{avg}} = t_{\text{sim}} \cdot (P_{\text{active}} \cdot AF + P_{\text{FCCD}} \cdot (1 - AF)) \\ &= 120 \text{ s} \cdot (0.5 \text{ W} \cdot 0.4 + 0.25 \text{ W} (1 - 0.4)) = 42 \text{ kJ} \end{aligned}$$

Similar calculations can be made for the other AFs and they are in accordance with the results in figure H.6, which thereby is verified. By replacing P_{FCCD} with P_{buf} the energy saving using the buffering method can be calculated.

The throughput loss occurs in the first receiving TTI after a period, where the UE has not been scheduled, as shown in figure H.8 and therefore the loss is determined by

$$\text{loss} = (b_{\text{active}} - b_{\text{noRS}}) / (AF \cdot T \cdot b_{\text{active}}) \quad (\text{H.8})$$

where T denotes one period i.e. a single receive period and the corresponding no data period as illustrated in figure H.8. The upper bound is $AF \cdot T = 1$. Using the PRB, SINR, and RS parameters in table H.4 $b_{\text{active}} = 2267$ bit and $b_{\text{noRS}} = 2183$ bit meaning that the throughput loss is 3.7%. This corresponds well with the simulation results shown in figure H.5.

H.5 Conclusion

In LTE scheduling information is transmitted in the Physical Downlink Control Channel on a subframe basis. The channel's format is declared in the same subframe using

the Physical Control Format Indicator Channel. By fast decoding of the two control channels the receiver can be powered down within the subframe, if it is not scheduled for data reception in that subframe. In this work a Fast Control Channel Decoding method is proposed and the results show an energy saving potential of 5%-25%, when compared with a regular buffering method in which the control channels are decoded slower and power down is not possible. The cost is that some Reference Signals are not received thus the channel estimate is less good, but calculations show it only entails a throughput degradation of 1%-4%.

The LTE Discontinuous Reception (DRX) sleep mode technique will be applied when the downlink data traffic activity factor is below 10% and 50% for long and short DRX respectively. The proposed method can however complement DRX, when the traffic is too aperiodic or rapidly switching for DRX and furthermore it is applicable for all activity factors. Contrary to DRX the method is applied individually in each UE thus it does not introduce a control message overhead and affect the network scheduling.

Acknowledgement

The work is partly funded by the Danish National Advanced Technology Foundation and the 4th Generation Mobile Communication and Test Platform (4GMCT) project.

Appendix I

Reducing LTE Uplink Transmission Energy by Allocating Resources

Mads Lauridsen, Anders R. Jensen, Preben Mogensen

The paper has been published in the
VTC Fall 2011

© 2011 IEEE

The layout has been revised.

Abstract

The effect of physical resource block (PRB) allocation on an LTE modem's transmit power and total modem energy consumption is examined. In this paper the uplink resource blocks are scheduled in either a Frequency Division Multiple Access (FDMA) or Time Division Multiple Access (TDMA) manner, to determine if low transmission power & long transmission time or high transmission power & short transmission time is most energy efficient. It is important to minimize the LTE modem's energy consumption caused by uplink transmission because it affects phone battery time, and because researchers rarely focus on energy consumption when they optimize network controlled uplink transmission power parameters.

Simulations based on a simple traffic model and a power consumption model show the TDMA scheme, where one user is allocated all 48 PRBs in a 10 MHz channel, is at least 24 % more energy efficient than the FDMA like approach with 8 PRBs per user. Furthermore the TDMA scheme decreases the average transmission time with minimum 24 %.

I.1 Introduction

The gap between mobile phone complexity and battery capacity is increasing year by year, leading to limited and continually decreasing battery lifetime. The problem is evident for smartphones, where power and data demanding applications, such as video streaming to and from YouTube, online gaming, and social applications like Facebook, have emerged.

To cope with the requirements for higher data rates, lower latency, and higher spectral efficiency, the Third Generation Partnership Project (3GPP) developed the Long Term Evolution (LTE) standard [197]. Unfortunately the new standard leads to more complex phones requiring more physical antennas and faster processors, [59]. Meanwhile less attention is paid to the amount of time the smartphone can run the aforementioned applications before the battery is discharged, leading to a problematic relationship between required and available energy.

Previous work on solving the battery gap problem has focused on maximizing the available energy and minimizing the energy consumption, [202]. The available energy can obviously be increased by improving the battery capacity, but this is not sufficient. A new potential solution is to utilize surrounding energy sources, such as kinetic, thermal, and solar energy, [15].

The smartphone's energy consumption can be minimized by optimizing the hardware (HW) and software (SW). The HW energy consumption can be reduced by choosing power efficient components and by performing power management e.g. by applying sleep modes to power down inactive HW parts. In LTE Discontinuous Reception and Transmission (DTX) [184] have been standardized to enable energy saving sleep modes [203]. Furthermore the energy consumption can be reduced by adjusting the phone's resources, e.g. display brightness and processor speed, to the individual applications. By combining and/or reducing the transmitted data from each application via SW control, energy savings are also possible. Finally, the phone's energy consumption can

be minimized by adjusting the network controlled parameters which affect the User Equipment (UE) modem.

In this study UE transmission power and Physical Resource Block (PRB) allocation in uplink are examined. Both are network controlled and much effort has been put into adjusting the parameters to increase channel capacity, throughput and coverage. In literature focus is however rarely on how the parameters affect UE power consumption. Therefore the effect of PRB allocation on transmit power and total modem energy consumption is examined in the present paper.

First the Uplink Power Control (UPC) and the system analysis including assumptions are introduced together with the simulation setup in sections I.1.1 to I.1.3. Then simulation results are presented in section I.2, and finally conclusions and guidelines are given in section I.3.

I.1.1 Uplink Power Control

The LTE UE's transmission power P_{Tx} in a subframe of the Physical Uplink Shared Channel is [72]

$$P_{Tx} = \min(P_{MAX}, P_0 + \alpha \cdot PL + 10 \log_{10}(M) + \Delta_{TF} + f) \quad [\text{dBm}] \quad (\text{I.1})$$

where P_{MAX} is the maximum transmission power, which is 23 dBm ± 2 dB for a class 3 UE [207], P_0 is a power offset [dBm], $\alpha \in \{0, 0.4, 0.5, 0.6, 0.7, 0.8, 0.9, 1\}$ is the path loss compensation factor [72], PL is the downlink path loss estimate [dB], M is the number of assigned Physical Resource Blocks, Δ_{TF} is a closed loop UE specific parameter which is based on the applied Modulation and Coding Scheme (MCS), and f is another closed loop UE specific parameter.

In literature several closed loop schemes such as Interference Based Power Control [76] and Load Adaptive Power Control [208, 77] have been presented. The schemes are often compared and combined with the open loop Fractional Power Control (FPC), where $\alpha < 1$, e.g. [209, 210, 211]. The FPC was examined in [68]. Usually the focus is on cell capacity i.e. average cell throughput versus coverage. The problem is that the effect on the UE power consumption is rarely examined hence an energy inefficient UPC scheme may be selected. In this study the open loop FPC is used and the values of P_0 and α are broadcasted i.e. they are identical for all UEs. Based on a review of the literature concerning FPC and macro1 propagation scenario simulations the set [$P_0 = -54.5$ dBm, $\alpha = 0.6$] is used.

I.1.2 System Analysis

To calculate the UE's transmit power a downlink path loss estimate PL is required. In this study the estimates are based on the macro1, [76, 208, 77] propagation distribution illustrated in figure I.1. Each user is assigned one path loss value from the distribution for the entire transmission. In the simulations, path loss values above

$$PL_{\max} = \frac{P_{MAX} - P_0 - 10 \log_{10}(1)}{\alpha} = \frac{24 + 54.5 - 0}{0.6} = 130.8 \text{ dB}$$

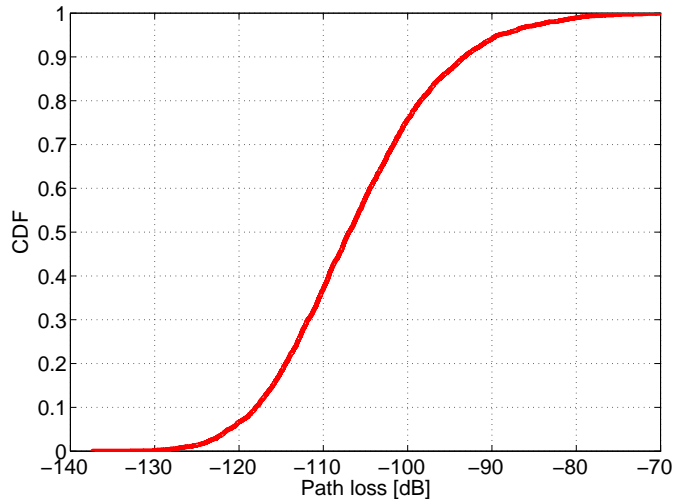


Figure I.1: CDF for the Macro1 propagation scenario.

are removed because the UE will be power limited i.e. $P_{\text{Tx}} > P_{\text{MAX}}$ even for $M = 1$ with the selected P_0, α . Usually the UE will reduce M one-by-one until $P_{\text{Tx}} \leq P_{\text{MAX}}$ but that is not possible when M is already at its lowest value.

The number of allocated PRBs M depends on the cell channel bandwidth, the number of users, and the allocation scheme, which is determined by the network operator. The channel bandwidth is 10 MHz and as in [79] 48 PRBs are available to the users, because 2 PRBs are used for control signaling such as the Sounding Reference Signals. The maximum number of simultaneously active uplink users is set to 10 based on the limitations imposed by the Physical Downlink Control Channel as described in [212]. Furthermore simulations are made where the maximum is 6 and 8 users as in [79]. The PRB allocation is based on an equal opportunity turn-based scheme. The scheme allocates PRBs user by user, who then either will be limited by UE transmission power or maximum allowable PRBs per user, until all PRBs in the Transmission Time Interval (TTI) are allocated or the maximum number of simultaneous users (SU) is reached. In the following TTI the next user in the queue is scheduled and so forth. It is assumed that there is no packet loss i.e. no retransmissions.

When P_0 , α , M , and PL for the current user have been determined the transmit power P_{Tx} is calculated using (I.1) without the closed loop parameters Δ_{TF} and f , and then the spectral efficiency for the user is determined via the Signal-to-Interference-and-Noise Ratio (SINR) as illustrated in figure I.2. If the SINR is below -3 dB, transmission cannot occur because the spectral efficiency is equal to 0 bit/S/Hz. Interference is assumed to be non-existent within the cell, because of the orthogonal structure of LTE uplink SC-FDMA signals. The same UPC scheme is assumed to be used in the neighbor cells. If e.g. the transmit power in a cell increases it will cause an increase in inter-cell interference, but likewise the transmit power will have increased in the neighbor cells. This means the relative signal-to-interference ratio will remain the same independently of the maximum PRBs and users. Based on this reasoning the interference is set to a constant (0) in the simulations even though the users' relative positions in a real live

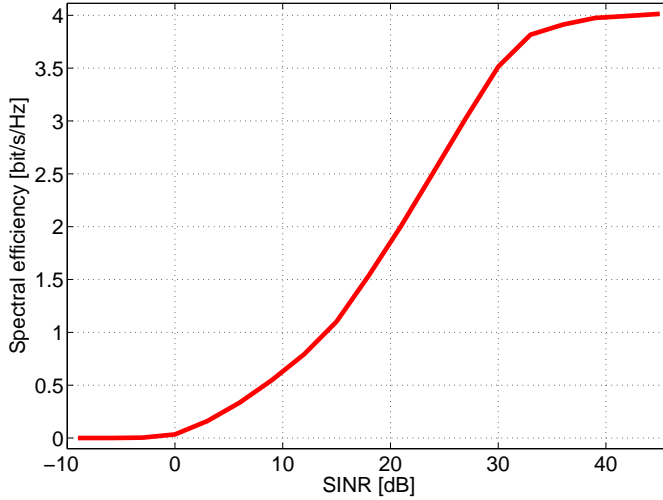


Figure I.2: SINR vs. spectral efficiency. Based on a simulation of single input single output uplink transmission, where adaptive MCS is applied to achieve a BLER target of 10 %. The channel model is ITU's Typical Urban 20 paths.

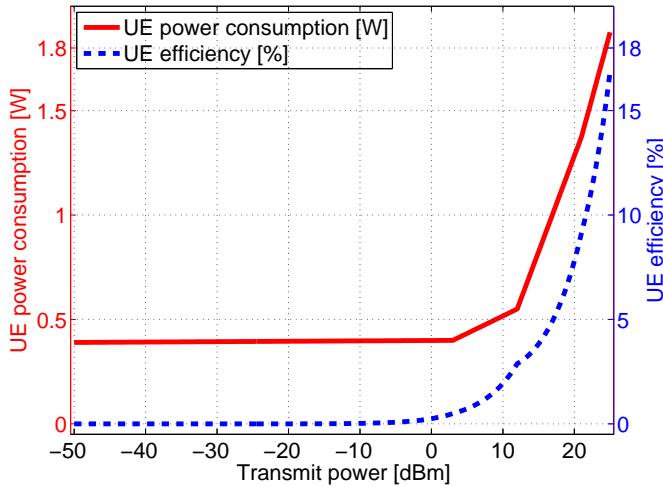


Figure I.3: Transmission power versus total UE power consumption & efficiency. The total consumption covers RF including power amplifiers, base band, power management units and external memory. Based on a polynomial fit to the '2011 UE model' curve in [78, Fig. 20.30].

network would entail the instantaneous inter-cell interference to fluctuate.

When the transmit power has been calculated the total energy consumption is determined via the curve in figure I.3. The curve predicts the power consumption of a year 2011 WCDMA UE, but it is believed to approximate an LTE UE as well. When the UE is active, but not scheduled, in the current TTI its idling power is set to 255.5 mW based on the LTE UE power consumption model presented in [203]. Before and after the UE conducts the uplink transmission it is considered to be in a DTX light

sleep mode, which based on [203] is set to 11 mW. The i 'th user will be in DTX mode for $t_{\text{DTX},i}$ seconds to ensure that all users are compared over the same time interval

$$t_{\text{DTX},i} = \max_{j \in [1, N]} (t_{\text{tx},j}) - t_{\text{tx},i} \quad [\text{s}] \quad (\text{I.2})$$

where $t_{\text{tx},j}$ is the transmission time for the j 'th user and N is the total number of simulated users.

In this study the traffic model is a single video file with a constant data rate equal to 400 kbps and a duration of 200 seconds. The values are based on the results in [213, 214], where the authors have used web crawlers on the Youtube site.

I.1.3 Simulation Setup

To analyze the total UE energy consumption's dependency on the number of PRBs two simulation methods are applied. In the first simulations only one user exist. The user is assigned a path loss value from the CDF and then allocated a pre-specified number of PRBs every TTI until the user finishes uploading the video file. The number of PRBs are only changed (in this case reduced) if the user is power limited i.e. exceeding P_{MAX} . This simulation will provide insight into transmit power distributions, maximum achievable throughput and energy consumption, and each PRB setting is simulated 50.000 times. In the second batch of simulations an upper limit is again imposed on the number of allocated PRBs, but furthermore the users now exist and transmit simultaneously. New users arrive according to a pre-specified probability and the target is 4 active users per TTI on average. The probability is based on an iterative examination of the average number of users. In total 5.000 users are simulated in the second batch.

The maximum number of PRBs are in the range 2 to 48 in the single user simulations. If the user only get 2 PRBs the transmission channel will look like Frequency Division Multiple Access (FDMA), where many users are active concurrently but allocated a few resources in the frequency domain. If the user is allocated up to 48 PRBs the transmission channel changes towards Time Division Multiple Access (TDMA), where the users are active in a short time frame and occupying a large amount of the available bandwidth. In the simultaneous users simulation the minimum number of PRBs is increased to 8 in order to fully utilize the 10 MHz channel (48 PRBs), when the maximum number of simultaneous users is set to 6. If one or more users are power limited and unable to utilize all 8 PRBs, channel capacity is wasted, but then it is caused by user limitations. Table I.1 contains the simulation parameters.

I.2 Simulation Results

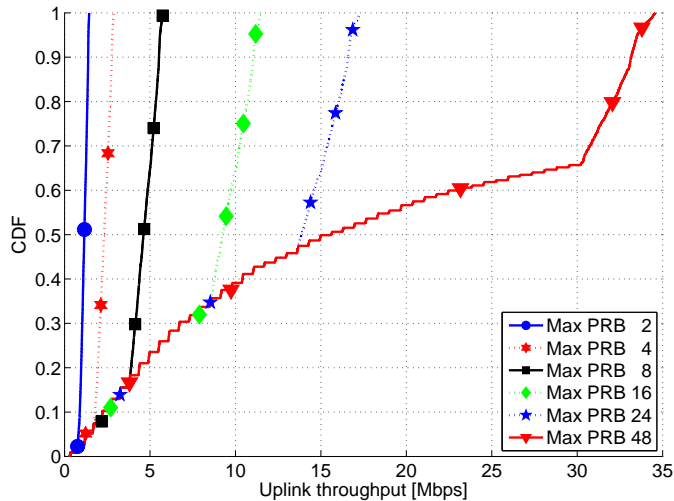
Figure I.4 illustrates the single user throughput and as expected it increases when the number of PRBs increases because the larger bandwidth enables the user to transmit more data per TTI. The curves' continuous part is caused by the user's SINR, which affects the spectral efficiency hence the capacity per PRB. The curves' step-like bottom part indicate that the user is power limited i.e. transmitting P_{MAX} and forced to reduce the number of PRBs one-by-one as the path loss increases. The transmission power distributions in figure I.5 consolidates this point, because they illustrate that

Table I.1: Simulation parameters.

Parameter	Value
Propagation scenario	Macro1
Network size	1 cell
System bandwidth	10 MHz
PRB size	180 kHz
PRBs available to the users	48 (2 are used for control signaling)
Traffic model	1 file (200 s · 400 kbps = 80 Mb)
Maximum simultaneous users	[6,8,10]
Maximum number of PRBs/user	[2,4,8,16,24,48] ^a , [8,12,16,24,48] ^b
Max transmission power P_{MAX}	24 dBm
P_0	-54.5 dBm
Path loss compensation α	0.6
Antenna gain	UE Tx 0 dB, eNodeB Rx 14 dB
Interference	0
Noise	-174 dBm/Hz (thermal)
Noise figure	10 dB

^a PRBs per user in single user simulations

^b PRBs per user in simulations with several simultaneous users

**Figure I.4:** Single user uplink throughput.

e.g. the ~35 % of the users with 16 PRBs, who had a step-like throughput curve, are power limited. The transmit distributions are based on the UPC formula, (I.1).

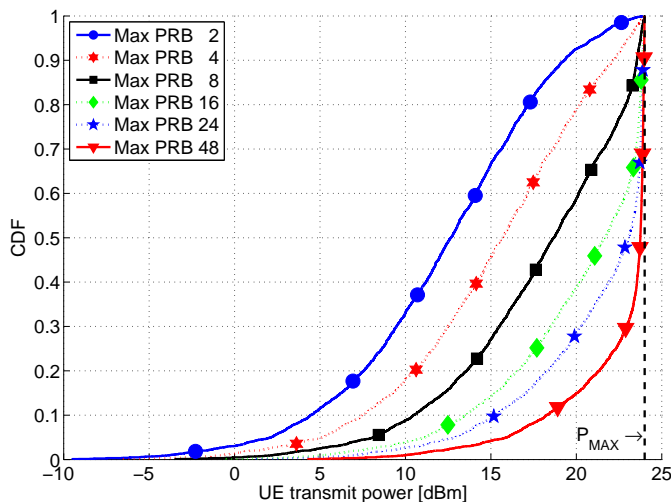


Figure I.5: Single user uplink transmission power.

Note that doubling the bandwidth, e.g. from 4 to 8 PRBs causes a 3 dB increase in transmission power and that the curves' slopes are equal because of the common path loss compensation factor α .

Figure I.6 shows the users' individual energy consumption. Since the simulations are made for one user at a time the user is scheduled every single TTI, hence the energy consumption can be directly based on the numbers from figure I.5 and the transformation from transmit power to total power in figure I.3. The energy consumption curves show that it is more energy efficient to allocate many PRBs even though it leads to a higher transmission power as shown in figure I.5. The reason is that the transmission time is shorter for a user with many PRBs and high transmission power than for a user with few PRBs. Furthermore the UE is more efficient when transmitting with higher power as illustrated in figure I.3. Analyzing figure I.6 in further detail it is evident that users with either 16 or 24 PRBs do not consume much more energy than users with 48 PRBs, and the benefit is that using 16 or 24 instead of 48 PRBs will leave resources for triple and twice as many users respectively. The top part of the curves combine because they are constituted of the users, who experience large path loss. This means they are forced to reduce the number of PRBs because of transmit power limitations, effectively leading to users with the same low number of PRBs no matter how many they were initially allocated.

Having established that allocating as many PRBs as possible is more energy efficient for the single user case, it is interesting to examine the results where users exist simultaneously and the equal opportunity turn-based scheduler is applied.

The simultaneous user throughput is shown in figure I.7 and as expected the resource sharing amongst the users reduces the throughput. The conclusion however remains the same i.e. more allocated resources per user lead to higher transmission throughput. Again the step-like pattern, which was discussed for figure I.4, where users are power limited, can be identified. Simulations were performed for a maximum of 6, 8, and 10 simultaneous users, but as the three curves for 48 PRBs show, the difference between

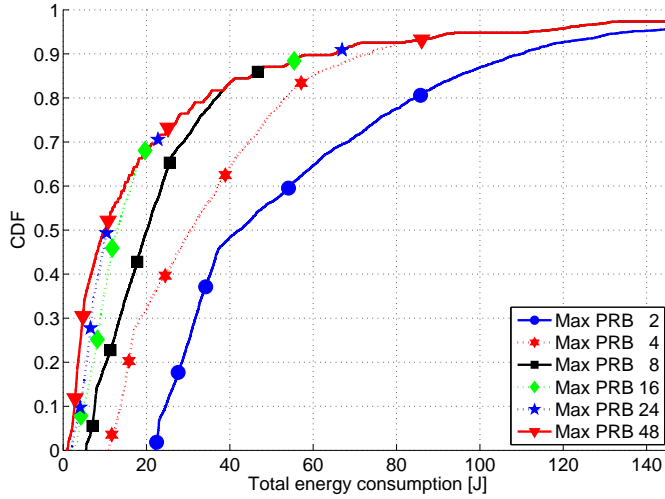


Figure I.6: Single user total energy consumption.

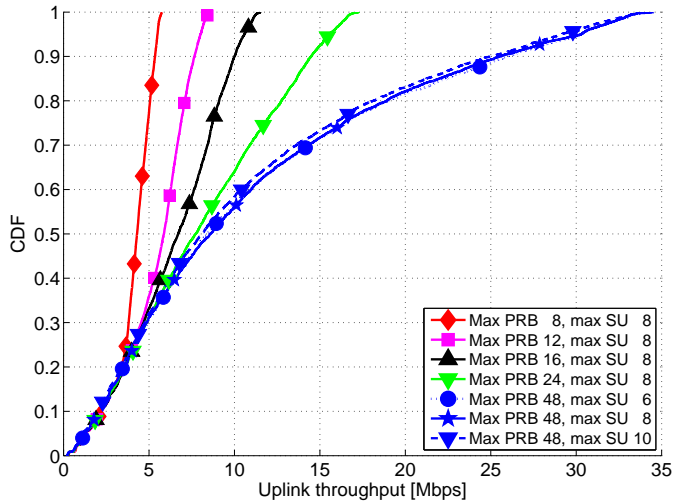


Figure I.7: Simultaneous users' (SU) uplink throughput.

the three setups is small and therefore the results for 6 and 10 users are not plotted for other PRBs. The cell throughput for all simulations was ~ 15 Mbps.

Table I.2 contains the average transmission time for the combinations of maximum simultaneous users and maximum number of PRBs. The average transmission time decreases at least 24 %, when the maximum number of PRBs is changed from 8 to 48. The advantage decreases as the number of users increases because more users lead to longer waiting time for the individual user. The transmission time for 6 users and 8 PRBs is significantly higher than any other setup. The reason is the low probability of allocating all 48 PRBs in each TTI because of power limited users. Therefore a new resource block scheduler is suggested for future work. The idea is to frequently allocate

Table I.2: Average user transmission time.

		Maximum PRBs					ΔT^\dagger
		8	12	16	24	48	
Max. SU	6	30.1 s	21.8 s	20.5 s	19.4 s	18.8 s	38 %
	8	25.2 s	21.8 s	20.5 s	19.5 s	18.9 s	25 %
	10	25.7 s	22.1 s	21.0 s	20.2 s	19.5 s	24 %

$^\dagger \Delta T$ denotes the time difference between 8 and 48 PRBs

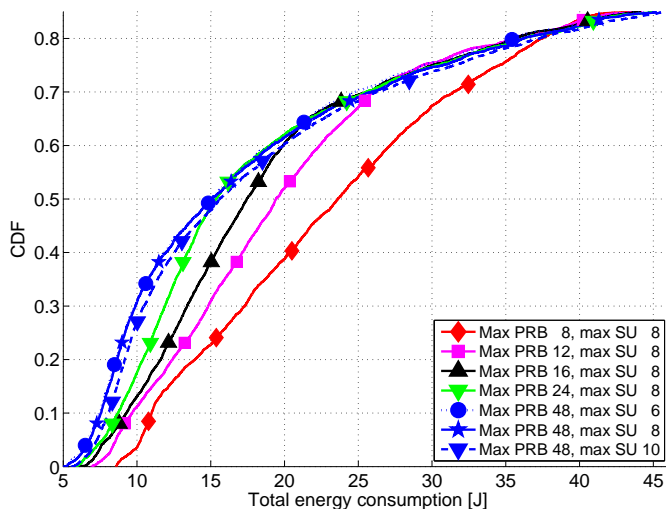


Figure I.8: Simultaneous users' total energy consumption.

large path loss users to mitigate the effect of them only being able to use a few PRBs per TTI because of transmit power limitations. Increasing the maximum number of users from 6 to 10 increases the average transmission time with $\sim 4\%$, when the results for 8 PRBs are excluded.

Figure I.8 illustrates the simultaneous users' total energy consumption while transmitting the video file. The conclusions from the single user simulation are still valid i.e. more PRBs per user lead to lower energy consumption because the UE is more energy efficient, when it transmits with high power, and because the transmission time decreases. The 15 % most energy consuming users show the same trend independently of the PRB and user settings and are therefore not plotted. The average energy consumption is given in table I.3 and the results consolidate that more PRBs lead to reduced energy consumption. At least 24 % energy can be saved if the users are allocated 48 PRBs instead of 8. Based on table I.2 it was discussed that an increase in the number of users does not increase the average transmission time with more than $\sim 4\%$ and examining table I.3 it is concluded that the average energy consumption similarly only increases $\sim 6\%$, but because the cell throughput is the same for all simulations there is no incentive to allow more than 6 simultaneous users.

Table I.3: Average energy consumption for 85 percentile users.

		Maximum PRBs					ΔE ‡
		8	12	16	24	48	
Max. SU	6	23.1 J	18.8 J	17.6 J	16.9 J	16.0 J	31 %
	8	22.0 J	19.1 J	17.9 J	17.0 J	16.3 J	26 %
	10	22.2 J	19.4 J	18.1 J	17.2 J	16.9 J	24 %

‡ ΔE denotes the energy difference between 8 and 48 PRBs

I.3 Conclusion

Physical Resource Block (PRB) allocation effects on LTE UE transmission power and energy consumption were examined. The simulation results, based on a mapping from transmission power to energy consumption, show that it is more energy efficient to allocate as many PRBs as possible to a single user instead of assigning several users less PRBs. On average at least 24 % energy can be saved if a user is allocated an entire 10 MHz channel (48 PRBs) instead of 8 PRBs. LTE's Uplink Power Control entails that users with more PRBs will transmit with higher power, but the throughput increases concurrently and therefore energy can be saved. Furthermore the applied power consumption model entails that the UE's efficiency increases when the transmit power increases.

An equal opportunity turn-based PRB scheduler was implemented to evaluate how scheduling of maximum 6, 8, and 10 simultaneous users affect the energy consumption. The results show scheduling maximum 10 users instead of 6 increases the average transmission time with ~4 % and the average energy consumption with ~6 %. Yet there is no incentive to allow more than 6 users because the cell throughput is independent of the number of users. The conclusion is that one user should be allocated as many PRBs as possible, while limiting the number of simultaneous users to reduce the average waiting time.

The findings are valuable to network operators since the presented conclusion provides insight into how the network can be adjusted to prolong the users' battery time.

Future work can focus on other traffic types, UPC parameters, and modeling of interference and packet loss.

Acknowledgement

The authors would like to thank Frank Frederiksen, Claudio Rosa, Jens Steiner, & Jeroen Wigard, Nokia Siemens Networks for valuable discussions. The work is partly funded by the Danish National Advanced Technology Foundation and the 4th Generation Mobile Communication and Test Platform (4GMCT).

Appendix J

LTE UE Energy Saving by Applying Carrier Aggregation in a HetNet Scenario

Mads Lauridsen, Hua Wang, and Preben Mogensen

The paper has been published in the
VTC Spring 2013

© 2013 IEEE

The layout has been revised.

Abstract

In this work it is examined if downlink Carrier Aggregation (CA) can be used to save UE energy. A dual-receiver LTE release 10 UE is compared with a single-receiver LTE release 8 UE. The models are based on scaling of an existing LTE release 8 UE power model. The energy consumption of the UEs is examined in a Heterogeneous Network scenario consisting of macro and small cells. The unexpected conclusion is that CA UEs can save energy, compared to LTE release 8 UEs, if they, depending on cell load, experience a throughput gain of 20%. However if the UE throughput is unaltered the energy consumption can increase up to 20%.

J.1 Introduction

Carrier Aggregation (CA) has been standardized in LTE release 10, and it entails that the CA UE can connect to more than one component carrier (CC) in the downlink. Previously research has shown that CA can be used to provide better coverage and average throughput if carefully adjusted, [80]. Unfortunately little attention has been paid to how the increasingly complex requirements, [215], to the UE transceiver potentially can increase the energy consumption. Neither has it been examined if operators can adjust their LTE network, using CA, to help the CA UEs save energy.

In previous work Wang et al. [216], discussed CA UE structures and estimated the current consumption based on RF components' data sheets, but the energy consumption was not evaluated in a realistic scenario. The energy consumption of CA capable UEs was discussed in the 3GPP, [217, 218], when CA was proposed, but there are no accurate evaluations of how CA will affect the UE energy consumption. Deactivating the Secondary Cell [82], i.e. the UE does not receive or transmit from that cell, was however standardized to save UE energy.

In this work a novel CA UE power consumption model is proposed and it is shown that CA can actually prolong UE battery life if the network is configured properly. This novel conclusion is based on a comparison of LTE release 8 and 10 UEs' energy consumption in a Heterogeneous Network (HetNet) scenario consisting of macrocells and small cells.

First we propose a CA UE power consumption model, and then we describe the considered HetNet scenario. By combining the statistics from the HetNet simulation with the UE model the energy consumption is calculated and discussed. Finally the paper is concluded with recommendations for network operators who utilize CA.

J.2 Downlink CA UE Power Model Design

To evaluate the energy consumption of downlink CA UEs a power model is required. Currently only Qualcomm has announced a CA chip set [219], but because it is not yet commercially available an empirical model cannot be established. Therefore a CA model is derived from the existing LTE release 8 (R8) power model in [25]. The block diagram of the R8 model is shown in Fig. J.1. The model is defined in Eq. (J.1) using

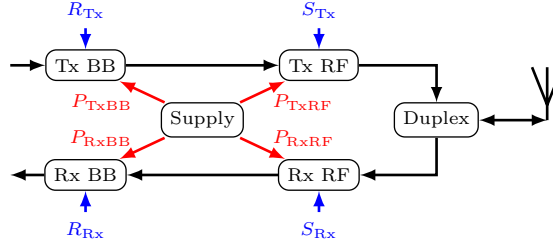


Figure J.1: LTE UE release 8 power model, [25, Fig.1]

Table J.1: First Order Polynomial Parameters, [25, Tab.3]

Part	Variable	p_0	p_1
Rx BB	R_{Rx} [Mbit/s]	-26.6 mW	2.89 mW/Mbit/s
Tx BB	R_{Tx} [Mbit/s]	34.5 mW	0.87 mW/Mbit/s
Rx RF	S_{Rx} [dBm]	-60.7 mW	-1.11 mW/dBm
Tx RF1 ^a	S_{Tx} [dBm]	-71.3 mw	5.50 mW/dBm
Tx RF2 ^b	S_{Tx} [dBm]	-943 mw	117 mW/dBm

^a valid for -30 dBm $\leq S_{Tx} \leq 10$ dBm

^b valid for 10 dBm $< S_{Tx} \leq 23$ dBm.

Table J.2: Constant Parameters, [25, Tab.2].

Part	P_{idle}	P_{con}	P_{Rx}	P_{Tx}	P_{Rx+Tx}	P_{2CW}
Mode [-]	m_{idle}	$\overline{m_{idle}}$	m_{Rx}	m_{Tx}	$m_{Tx} \cdot m_{Rx}$	m_{2CW}
Value [W]	0.50	1.53	0.42	0.55	0.16	0.07

the parameters in Tables J.1 and J.2. Descriptions of how the parameters were defined and measured are given in [25].

$$\begin{aligned}
 P_{tot} = & m_{idle} \cdot P_{idle} + \overline{m_{idle}} \cdot \{P_{con} + m_{Tx} \cdot m_{Rx} \cdot P_{Rx+tx} + \\
 & m_{Rx} \cdot [P_{Rx} + P_{RxRF}(S_{Rx}) + P_{RxBB}(R_{Rx}) + m_{2CW} \cdot P_{2CW}] \\
 & + m_{Tx} \cdot [P_{Tx} + P_{TxRF}(S_{Tx}) + P_{TxBB}(R_{Tx})]\} \quad [\text{W}]
 \end{aligned} \tag{J.1}$$

The four functions in Eq. (J.1) are evaluated using Table J.1 and:

$$P_{part}(\text{variable}) = \text{variable} \cdot p_1 + p_0 \quad [\text{mW}] \tag{J.2}$$

This work focuses on downlink CA and hence the transmitter part of the UEs is disabled in the following, i.e. $m_{Tx} = 0$.

In 3GPP three band combinations have been defined, [81]:

1. Intra-band with contiguous component carriers (CCs)
2. Intra-band with non-contiguous CCs
3. Inter-band with non-contiguous CCs

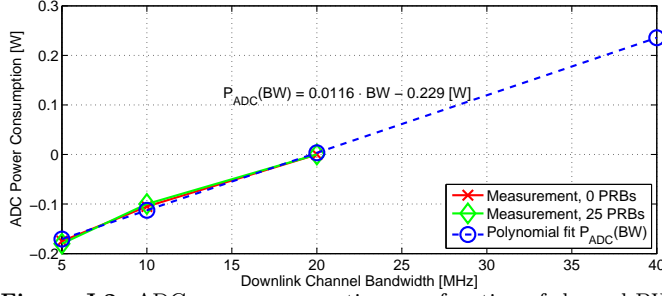


Figure J.2: ADC power consumption as a function of channel BW.

together with two Release 10 UE receiver architectures [81]

- a) Single Radio Frequency (RF) front-end with single wideband Analog-to-Digital Converter (ADC) and dual base band (BB) processor
- b) Dual RF with dual narrowband ADCs and dual BBs

Architecture (a) is only applicable in scenario 1, because it cannot filter undesired frequency content between non-contiguous CCs. Architecture (a) is however of interest because the hardware is less complicated and because scenario 1 will be used by some operators.

The R8 model was made for a 20 MHz downlink channel, but measurements were also performed for 5 and 10 MHz channels as shown in Fig. J.2. The measurements were made using the Downlink Fixed MAC Padding for 0 and 25 DL PRBs, see [25] for further information. Based on those measurements a linear function of channel bandwidth is implemented in the R8 model and the receiver’s power consumption is:

$$P_{R_x, R8} = P_{R_x} + P_{R_xRF}(S_{R_x}) + P_{R_xBB}(R_{R_x}) + P_{ADC}(BW) + q_{2CW, R8} \cdot P_{2CW} \quad [W] \quad (J.3)$$

The probability of using 2 codewords is q_{2CW} , and calculated by the simulator. Architecture (a), called release 10 wideband (R10wb), is defined as

$$P_{R_x, R10wb} = P_{R_x} + P_{R_xRF}(S_{R_x}) + P_{ADC}(BW) + [q_{2CW, cc1} + q_{2CW, cc2}] \cdot P_{2CW} + P_{R_xBB1}(R_{R_x1}) + P_{R_xBB2}(R_{R_x2}) \quad [W] \quad (J.4)$$

and (b), called release 10 narrowband (R10nb), is defined as:

$$P_{R_x, R10nb} = 2 \cdot P_{R_x} + P_{R_xRF1}(S_{R_x1}) + P_{R_xRF2}(S_{R_x2}) + P_{R_xBB1}(R_{R_x1}) + P_{R_xBB2}(R_{R_x2}) + P_{ADC1}(BW1) + P_{ADC2}(BW2) + [q_{2CW, cc1} + q_{2CW, cc2}] \cdot P_{2CW} \quad [W] \quad (J.5)$$

The receivers’ linear power functions are given in Table J.1 and the ADC function is shown in Fig. J.2. The ADC of rel10wb can handle two contiguous 20 MHz bandwidths while the rel8 and rel10nb are limited to 20 MHz per ADC.

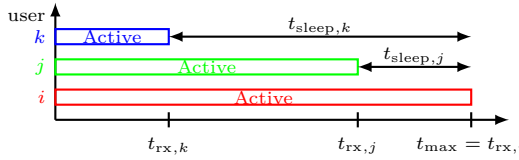


Figure J.3: Active and sleep time example for UEs i , j , and k .

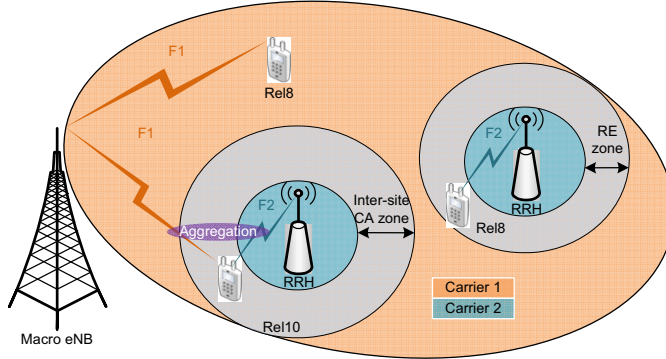


Figure J.4: Considered HetNet scenario with dedicated carrier deployment.

The proposed CA power models are scaled versions of the published R8 model, because we believe the linear scaling is currently the best estimation available. The models do not include DRX [62] or micro-sleep, which is a method where a connected, but unscheduled UE can sleep during parts of a subframe [28], because the R8 model also does not include the methods. The idle mode power consumption P_{idle} , given in Table J.2, is therefore used as the UEs optimal low power mode. We anticipate DRX and micro-sleep will be of benefit in CA, because both receivers will not always be active.

The simulations are made such that when UE i has finished receiving the payload it will sleep for (using P_{idle} Watts)

$$t_{sleep,i} = \max_{j \in [1,N]} (t_{rx,j}) - t_{rx,i} \quad [s] \quad (J.6)$$

where $t_{rx,j}$ is the receive time for UE j and N is the total number of UEs. The purpose is to compare all UEs over the same period of time as shown in Fig. J.3. For later reference note that $t_{max} = \max_{j \in [1,N]} (t_{rx,j})$.

J.3 The HetNet Scenario

HetNets are expected to be the next big leap in cellular system performance improvement by changing the topology of traditional networks which will bring the network closer to end users. In a HetNet, a mixture of macrocells combined with low-power nodes such as picocells, femtocells, and remote radio heads (RRHs) are used. The placement of macrocells is generally based on careful network planning to maximize the wide area coverage and control the inter-cell interference, while low-power nodes

are deployed to either eliminate coverage holes in the macrocell or improve capacity at hotspot areas. In this paper, we focus on dedicated carrier deployment. Two contiguous CCs, each with 10 MHz bandwidth, are configured. One carrier frequency (CC1) is allocated to macro eNB whereas the other one (CC2) is allocated to small cells. The small cells are implemented as RRHs and are connected to macro eNBs via high bandwidth, low latency fibers. Thus, all baseband signal processing for the small cells (RRHs) could be placed in the macro eNB, allowing the aggregation of CCs between the macrocell (configured as primary serving cell (PCell)) and the small cell (configured as secondary serving cell (SCell)). Referring to the 3GPP terminology, the dedicated carrier deployment with macro and RRHs is denoted CA scenario 4 [82]. The R8 UEs can only connect to either the macro eNB or the RRH on the corresponding CC, based on downlink signal strength and the range expansion (RE) offset which is used to increase the footprint of small cells by adding a positive bias to the signal strength of low-power nodes during cell association [220]. The R10 UEs configured to operate with CA can connect to both the macro eNB and the RRH using CA so that they can benefit from larger transmission bandwidth, and therefore opportunities to be served at higher data rates. The corresponding example of the considered deployment scenario is presented in Fig. J.4.

It is worth mentioning that as the packet scheduler for the small cells (RRH) is physically located in the macro eNB, joint multicell packet scheduling [221] for those UEs configured with CA is feasible. The difference between independent and joint proportional fair (PF) scheduler lies in the calculation of the scheduling metric. In joint PF scheduler, the denominator of the PF metric is updated as the sum of the average scheduled throughput over all cells where the UE has been scheduled in the past. It simply requires information exchange on the average scheduled throughput between the scheduler for macro and small cells. In that way, the scheduler can essentially offer fast and efficient load balancing between macro and small cells, thereby allowing for more equitable distribution of radio resources among UEs. The comparisons between independent and joint PF scheduling across multiple CCs can be referred to [221] in the context of CA.

J.4 Simulation Assumptions and Energy Consumption Results

The performance of the considered HetNet deployment scenarios is evaluated in a quasi-static downlink multi-cell system-level simulator that follows the LTE specifications, including detailed modeling of major radio resource management (RRM) functionalities. The network topology consists of 7 hexagonal macrocells transmitting at 40W with 3 sectors per cell. 4 RRHs transmitting at 1W are randomly placed within each sector. 2×2 MIMO with rank adaptation and interference rejection combining is configured. A bursty traffic model is considered where the call arrival follows a homogeneous Poisson process with fixed payload size per call. The average offered load per macrocell area is calculated as the product of the user arrival rate and the payload size. We assume hotspot UE distribution, where $2/3$ of the UEs are dropped within a 40 m radius of the small cells while the remaining UEs are uniformly distributed within the macrocell

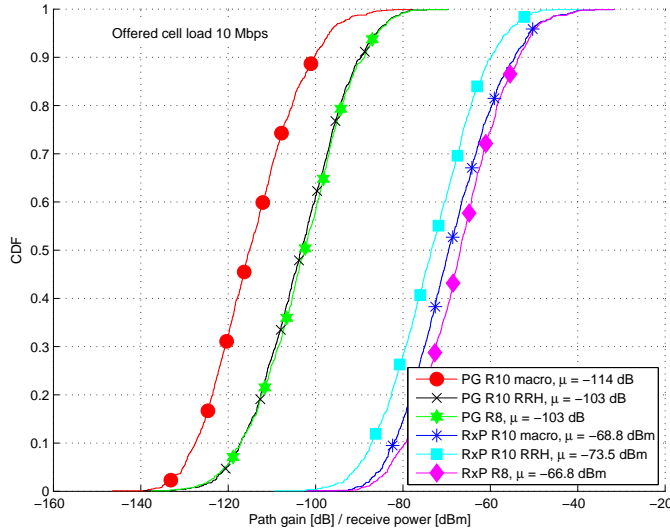


Figure J.5: Path gain (PG) & receive power (RxP). OCL=10 Mbps, μ is the mean.

area. The results in this section are for an offered cell load (OCL) of 10 Mbps and a UE payload of 10 Mb. Simulations were also performed with 20 Mb payload, but they do not affect the overall conclusions, and therefore the results are omitted. The scheduling granularity is 1 PRB. The UEs are mainly located around the small cells, and therefore the path gain to the small cell is lower as compared to the macrocell as shown in Fig. J.5. For R10 UEs, it is assumed that they are always connected to both the macro and the most dominant RRH so that they can benefit from potential larger transmission bandwidth and fast inter-cell load balancing. This however does not entail that R10 UEs will always be scheduled on both CCs, as the scheduling of each CC is based on the channel quality and the cell load. For R8 UEs, different RE offsets are simulated. Only the optimal RE offset that maximizes the cell edge (5-percentile) throughput is used (RE=1.5dB with RSRQ cell selection for 10 Mbps OCL). Note R10 and R8 UEs are simulated separately.

Fig. J.6 shows the UEs' average throughput. The CA UEs achieve similar throughput on both CCs and $\sim 56\%$ higher throughput than the R8 UEs. This is due to the CA UE on average is allocated 95 PRBs while the R8 UE gets 48 PRBs. The CA UEs' higher throughput entail they receive the payload faster hence they can be in sleep mode for a longer duration.

The power consumption for each of the architectures is shown in Fig. J.7. The R10nb on average uses 20% more power than the R8 because the CA UE utilizes two receivers. Fig. J.8 shows the total energy consumption of the UEs. The R10wb is the most energy efficient solution and on average 4% can be saved, while the R10nb entails a saving of 3%. The savings may not seem impressive, but it is of interest that CA does not introduce an energy consumption penalty on the UE given the model and scenario assumptions. The figure also contains a breakdown of the energy consumption in active and sleep mode. The R8 UE consumes more than 25% extra energy in active mode compared to the CA UEs even though the actual power consumption of the R8 UE is

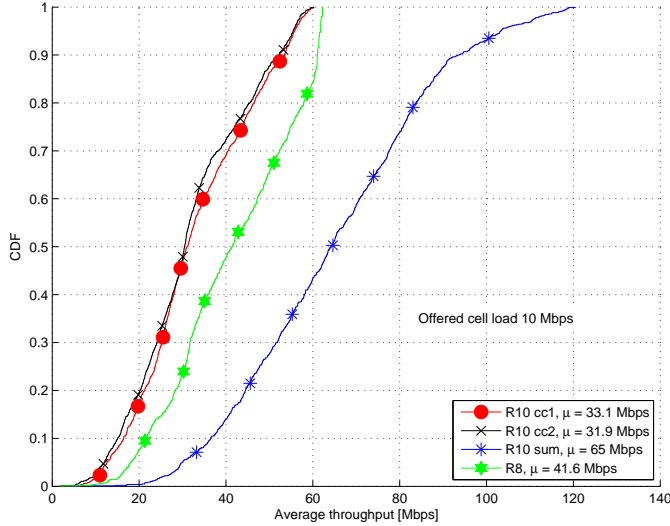


Figure J.6: Throughput. OCL = 10 Mbps, μ is the mean.

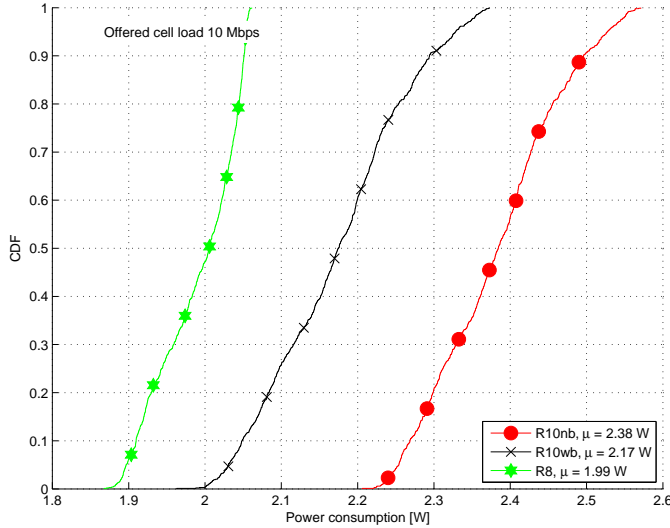


Figure J.7: Power consumption. OCL = 10 Mbps, μ is the mean.

20% lower as shown in Fig. J.7. This is due to the lower throughput which entails the UE has to remain active for a longer time in order to receive the same amount of data. Given the major difference in active mode energy consumption major overall savings could be expected, but due to the sleep mode definition in Eq. (J.6) the UEs on average spend less than 10% of the total time in active mode, hence the sleep mode energy consumption is dominant. The reason is that a single UE with low throughput prolongs the sleep time via t_{\max} .

The simulations were also performed for other cell loads, and the mean values of

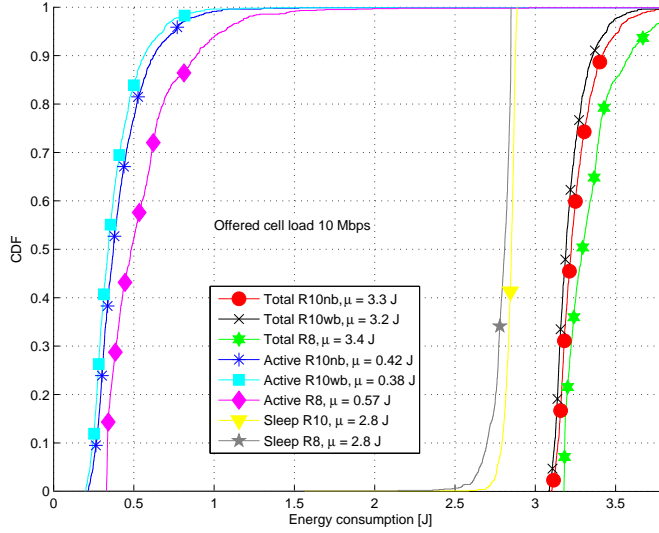


Figure J.8: Energy consumption. OCL = 10 Mbps, μ is the mean.

Table J.3: Mean data rate and receive power.

Load [Mbps]	R_{R8} [Mbps]	$R_{R10\ cc1}$ [Mbps]	$R_{R10\ cc2}$ [Mbps]	$R_{R10\ sum}$ [Mbps]	S_{R8} [dBm]	$S_{R10\ cc1}$ [dBm]	$S_{R10\ cc2}$ [dBm]
10	42	33	32	65	-71	-69	-73
30	32	22	24	45	-72	-70	-73
50	24	15	17	31	-73	-72	-74
70	18	10	11	21	-74	-73	-75

these results are shown in the following Tables. Table J.3 contains the results for mean throughput rate R and receive power S as a function of the cell load. The CA throughput gain decreases as the cell load increases because each UE is allocated less PRBs less often. Table J.4 contains the associated results for mean receive time t and energy consumption E . The first thing to observe is that the receive time difference between R8 and R10 decreases as the cell load increases. Furthermore the ratio between the longest receive time and average R10 receive time decreases as the load increases because the average throughput approaches the minimum throughput i.e. the throughput spread is much smaller, when the cell load is high. This means the sleep time is very significant for all loads hence the sleep energy is the major contributor to the total energy consumption. The relative energy consumption difference between R8 and R10 is almost constant. The reasons are that the active time ratio is almost constant and that the sleep mode, which consumes the same amount of energy for both releases, is dominating.

Due to the sleep time definition in Eq. (J.6) a slowly downloading UE will entail all other UEs experience long sleep times. In the previous results this meant the sleep energy was dominating and therefore an artificial simulation campaign was made, where UEs with a throughput below 5 Mbps were excluded from the statistics. This results in a lower maximum receive time as shown in Table J.5. The 5 Mbps throughput limit

Table J.4: Mean receive time and energy consumption.

Load [Mbps]	t_{R8} [s]	t_{R10} [s]	t_{max} [s]	$\frac{t_{R8}-t_{R10}}{t_{R8}}$ %	$\frac{t_{max}}{t_{R10}}$	E_{R8} [J]	E_{R10nb} [J]	E_{R10wb} [J]	$\frac{E_{R8}-E_{R10nb}}{E_{R8}}$ %
10	0.29	0.18	5.9	38	33	3.4	3.3	3.2	3
30	0.4	0.27	6.3	33	23	3.7	3.6	3.5	3
50	0.61	0.42	7	30	16	4.3	4.2	4.1	3
70	0.96	0.68	9.2	29	13	5.9	5.7	5.6	3

Table J.5: Mean values using a minimum throughput limit of 5 Mbps.

Load [Mbps]	t_{R8} [s]	t_{R10} [s]	t_{max} [s]	$\frac{t_{R8}-t_{R10}}{t_{R8}}$ %	$\frac{t_{max}}{t_{R10}}$	E_{R8} [J]	E_{R10nb} [J]	E_{R10wb} [J]	$\frac{E_{R8}-E_{R10nb}}{E_{R8}}$ %
10	0.28	0.18	1.6	37	9	1.2	1.1	1.1	7
30	0.39	0.27	2	32	7	1.5	1.5	1.4	6
50	0.56	0.42	2	25	5	1.8	1.7	1.6	3
70	0.76	0.65	2	15	3	2	2.1	2	-2

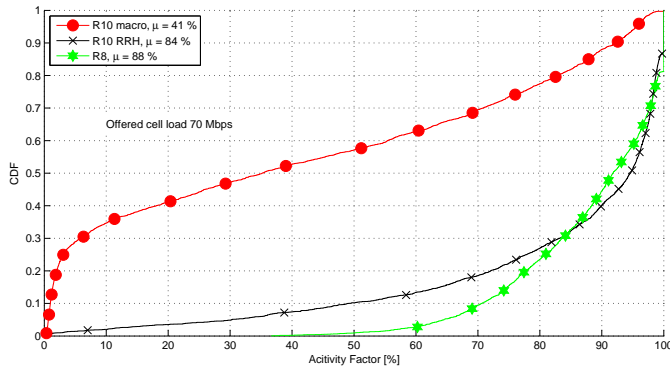


Figure J.9: Activity Factor. OCL = 70 Mbps, μ is the mean.

affects all scenarios, and it is clear that CA has an advantage in low cell load scenarios where the energy savings now are 5-7%. When the cell load is increased the difference between R8 and R10 receive times decreases. This means the active energy consumption of the R8 UE becomes smaller than the CA UE hence the CA energy advantage is lost.

As discussed in section J.2 CA can obtain even higher energy savings by the use of DRX and/or micro-sleep, because the CA UE is scheduled less often when it is in RRC_connected mode. Fig. J.9 shows the UE activity factor, which is the ratio between scheduled time and connected mode time, of the simulated 70 Mbps cell load scenario. When the UE is connected to the macrocell it is scheduled less than 50% of the time, and based on the assumptions in [28], where it is estimated that the energy consumption in micro-sleep mode is half of the active mode, the energy consumption can be reduced by ~25%. One reason for the low activity factor is due to the CA UE always being connected to both CCs even though one of the CCs may experience so low path gain that it cannot serve the UE.

Table J.6: Mean power values and break-even points for 10 Mb payload.

Load [Mbps]	P_{R8} [W]	P_{R10nb} [W]	P_{R10wb} [W]	$1 - x_{nb}$ %	$1 - x_{wb}$ %
10	2	2.4	2.2	21	11
30	2	2.3	2.1	19	9
50	1.9	2.3	2	19	8
70	1.9	2.2	2	19	7

J.5 Energy Break-Even

The results in the previous section showed that CA can be used to save UE energy. The savings are possible when the UE, using CA, receives a certain file faster than it would have without CA. In this section the break-even point i.e. the required increase in throughput to make CA energy efficient, is calculated. The energy consumed by a R8 UE is:

$$E_{R8} = P_{R8} \cdot t_{rx} + P_{sleep} \cdot (t_{max} - t_{rx}) \quad [\text{J}] \quad (\text{J.7})$$

The receive time t_{rx} is scaled by x so the CA UE consumes

$$E_{R10} = P_{R10} \cdot t_{rx} \cdot x + P_{sleep} \cdot (t_{max} - t_{rx} \cdot x) \quad [\text{J}] \quad (\text{J.8})$$

The break-even point i.e. the scaling factor x is

$$\begin{aligned} E_{R8} &= E_{R10} \quad [\text{J}] \\ P_{R8} \cdot t_{rx} - P_{sleep} \cdot t_{rx} &= P_{R10} \cdot t_{rx} \cdot x - P_{sleep} \cdot t_{rx} \cdot x \quad [\text{J}] \\ x &= \frac{P_{R8} - P_{sleep}}{P_{R10} - P_{sleep}} \quad [-] \end{aligned} \quad (\text{J.9})$$

The break-even point is calculated for the simulated cell loads and shown in Table J.6. The sleep power is 0.50 W for all UEs. The power consumption decreases as the load increases because the UE throughput also decreases meaning that the baseband processor is less loaded. When the R10nb is applied a throughput increase of 19-21% is required to break even. If the R10wb is used the increase shall be as little as 7-11%. The conclusion that the throughput must be increased in order to enter sleep mode fast and save energy e.g. by scheduling one UE continuously is similar to the conclusion that was reached for uplink transmission in [29]. Therefore it is expected that the same conclusion can also be applied to uplink CA.

J.6 Conclusion

Carrier Aggregation (CA) is standardized in LTE release 10 to improve throughput and coverage. However this entails a more complicated transceiver design, hence a potential increase in UE energy consumption. In this study it was shown that CA can actually be used to save UE energy if the downlink throughput is increased 20%, hence this is what network operators should aim for.

In this work two CA UE architectures were mapped to a power model, and the energy consumption of the new UEs were compared with an existing LTE release 8 UE in a Heterogeneous Network scenario. The reason why energy can be saved is that the CA UE can enter sleep mode faster, and this low-power state is the key to save energy in current UE architectures. If the LTE network using CA is implemented to improve the coverage the throughput gain may be small. This can entail the CA UEs experience an increased energy consumption of up to 20%. Discontinuous Reception and the micro-sleep concept can add to the CA's advantage because the CA UE is likely to be scheduled less often, when it is in connected mode and receiving finite buffer traffic.

To summarize CA can be used to increase the throughput, and moreover decrease UE energy consumption, both key performance indicators leading to a better user experience.

Acknowledgement

Thanks to Nokia Siemens Networks Aalborg for providing comments and statistics. The work is partly funded by the Danish National Advanced Technology Foundation and the 4th Generation Mobile Communication and Test Platform project.

Appendix K

Current Consumption Measurements with a Carrier Aggregation Smartphone

Rafael Sanchez-Mejias, Yu Guo,
Luis A. Maestro Ruiz de Temiño, Mads Lauridsen, and Preben Mogensen

The paper has been published in the
VTC Fall 2014

© 2013 IEEE
The layout has been revised.

Abstract

Carrier Aggregation (CA) is introduced in LTE release 10 to improve data rates by allowing the User Equipment (UE) to receive data on more than one LTE carrier. The related increased complexity is expected to affect the UE current consumption, but yet no empirical evaluation has been published on this topic. Currently there are only theoretical expansions of LTE release 8 power models available, but this article presents the first publicly available current consumption measurements on a commercial CA-capable UE.

In this work it is examined how the activation and use of CA (10 + 10 MHz) affects the UE current consumption with different traffic profiles such as FTP or web browsing. For a large FTP download the average CA current consumption is reduced 13% compared to single-carrier 10 MHz due to increased data rate and extended idle time, which allows the UE to enter a low-current sleep mode. For small data bursts, such as keep-alive messages, configuring CA results in 17 mA average current increase during RRC connected state inactivity periods. Depending on the UE background activity, this could translate into 3% to 8% reduction of the UE's stand-by battery life.

K.1 Introduction

Downlink (DL) Carrier Aggregation (CA) has been introduced in 3GPP Long Term Evolution (LTE) release 10 [80]. This feature allows the User Equipment (UE) to receive data from up to five different Component Carriers (CCs). While each CC is backwards compatible with previous LTE releases, a CA-capable UE can potentially aggregate the CCs to achieve a total bandwidth of up to $5 \times 20 \text{ MHz} = 100 \text{ MHz}$. This obviously helps increase the data rates, but it can also bring additional benefits in terms of frequency diversity by aggregating CCs on different frequency bands with different propagation properties such as band III (1.8 GHz) and band V (850 MHz). Finally, the use of CA can also be beneficial in scenarios with fragmented spectrum since the CA-capable UEs can aggregate those spectrum chunks to boost the data rates.

Supporting CA will induce a more complex UE design both in terms of receiver and transmitter RF [222], but also increased baseband processing due to channel estimation over a larger bandwidth or different CCs, higher data rates, etc.. So far little work has been published on how this will affect the UE battery life, which is crucial for user satisfaction [223]. When CA was standardized in 3GPP some contributions, such as [217, 218], discussed the effect on UE complexity and battery life, but without quantifying the current consumption. Since then researchers have estimated the current consumption of CA UEs by extending empirical models based on measurements on LTE release 8 UEs. In [30] DL CA current consumption was studied by increasing the bandwidth and number of RF chains of a previously established single-chain model, while [224] presented a similar study for uplink (UL) CA by combining measurements on multiple release 8 power amplifiers. Both studies showed that if CA provides a significant throughput increase then energy can be saved, but until now the conclusions have not been validated by real measurements.

Since no commercial CA devices have been available, the verification of the theoretic

models has not been possible until recent dates. This, however, changed with the launch of the first commercial CA-capable device in summer 2013 [83] and therefore we present, to our best knowledge, the first independent current consumption and throughput measurements on a commercial CA UE.

Our objective is to provide a detailed analysis on how CA affects UE throughput and current consumption in relevant scenarios such as FTP file transfer and web browsing sessions, but also examine how CA may affect UE current consumption when CA is configured but unused. This information can also be useful for network operators to determine how to setup their network to ensure longer UE battery life, and thereby improve user satisfaction.

The article is structured as follows: section K.2 presents an overview of CA in LTE, and discusses how it impacts the UE's current consumption. In section K.3 the measurement setup is described, and in section K.4 the related results are presented. Finally a discussion and conclusion is given in sections K.5 and K.6 respectively.

K.2 Carrier Aggregation in LTE

Two main scenarios are defined for LTE CA: intra-band, with either contiguous or non-contiguous CCs, and inter-band in which the CCs belong to different frequency bands. Each CC is backwards compatible, which means the control and data signaling complies with release 8 and has the same numerology. Consequently a release 8 UE is still able to use a single CC of a network that also supports CA. The bandwidth of each CC is also limited to what was specified for the single-carrier band, for example maximum 20 MHz for band III and 10 MHz for band V [225].

The inter-band scenario is the most challenging from a UE perspective, because the multiple separated bands require multiple receive and transmit chains, each with a Local Oscillator (LO) tuned to the band's carrier frequency. The large number of frequency bands specified in 3GPP LTE (more than 20 for single-carrier FDD) entails that there are numerous combinations for inter-band CA. The number of standardized combinations has already increased from 1 to 21 between release 10 (version 10.13) and release 11 (version 11.7) [225] causing major challenges for chipset designers, who have to deal with a multitude of coexistence issues and coupling of LOs [222]. This affects both cost and current consumption of the UE. From a baseband processing perspective the CA scenario has little effect on the current consumption [222], because the throughput is the defining metric for the current consumption regardless whether single-carrier or a CA scenario is considered. Furthermore, the UE's energy consumption per transferred bit actually decreases when incrementing DL and UL throughput in regular release 8 devices [26]. This is also expected to be the case for CA UEs.

When the CA UE is switched ON and performs the network selection procedure, it will connect to a single CC, known as Primary Cell (PCell), following normal release 8 procedures as illustrated in Figure K.1. After the UE has become RRC_Connected the network will request the UE's capabilities, and then configure a certain number of additional CCs to the UE. The CC configuration depends among other things on the UE capabilities and Quality-of-Service requirements [80]. These additional CCs are called Secondary Cells (SCells) and when they are configured the UE may have

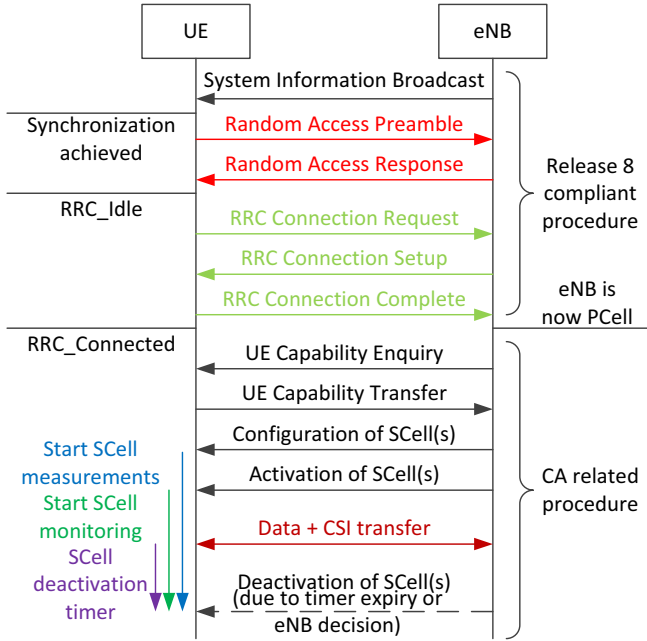


Figure K.1: Procedure for connecting a CA UE to an eNodeB.

to periodically monitor the receive power level of the SCell(s) causing an increase in current consumption. Once configured, the SCells may be activated by the network, using an “Activation/Deactivation MAC Control Element” [226], when e.g., a certain data buffer threshold is met. The exact activation algorithm is not standardized and therefore vendor specific. For each active CC, the UE continuously monitors the control channels and reports channel state information (CSI) needed for scheduling purposes. Monitoring and reporting SCells is costly power wise due to the additional RF chains and baseband processing required. Therefore 3GPP standardized a timer-based deactivation mechanism for SCells [226]. The timer, known as “sCellDeactivationTimer”, is restarted whenever the UE receives an UL grant or DL assignment, and upon expiration the UE must deactivate the SCell, discontinue the control channel monitoring and the CSI reporting. The SCell can also be deactivated by the network using the aforementioned MAC Control Element. Finally, the network can command the UE to release a specific SCell.

K.3 Measurement Setup

The test environment for this study was designed to measure both performance and battery usage of a commercial device under emulated realistic network conditions in a laboratory environment. A commercial CA-capable smartphone, and a state of the art LTE end-to-end network including eNodeB and Enhanced Packet Core (EPC) equipment were used. The eNodeB included two radio modules transmitting in band III

(1.8 GHz) and band V (850 MHz) respectively, which enabled 10+10 MHz downlink inter-band carrier aggregation, i.e. configuration CA_3-5 [225], or single-carrier configurations up to 20 MHz in band III or 10 MHz in band V. Intra-band CA configurations were not tested due to lack of support from the UE. All the tests were done using open loop 2x2 Multiple-input Multiple-Output (MIMO) in both bands. Over the air transmission was done by combining the signals from each band through two general purpose antennas, as described in Figure K.2. Furthermore, each of the four radio paths (two for each band) was connected to an independently configurable attenuator which allowed setting up different path loss imbalance between carriers.

The current consumption was measured with an external, constant 4 V DC supply

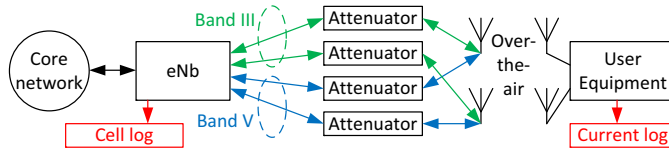


Figure K.2: Block diagram of the measurement setup.

which was connected directly between the battery and the input power pins of the UE. Additionally, cell logs with sub frame resolution (1 ms) were collected for throughput and packet scheduling analysis.

For most of the tests, based on file data transfer, the display was switched OFF after the application was initiated in order to reduce the impact of current consumed by the display. However, when testing more interactive services such as web browsing or YouTube, the display was kept on during the duration of the test.

The scope of the testing was divided in four scenarios:

K.3.1 Impact of carrier aggregation activation

This test was designed to analyze the impact of having CA configured or activated when there is no active data transmission. I.e. current consumption was monitored during the time where the RRC inactivity timer is running after a file download finishes. The percentage of time spent on RRC inactivity timer becomes relevant when there are a high number of short transmissions, such as keep-alive messages, during long stand-by periods. Connected mode Discontinuous Reception (cDRX) was used in all the measurements.

K.3.2 Large data transmission

This test was based on the download of a 1 GB file using FTP. Two different current consumption measurements were taken. The first one considered only the active download time, while the second was measured during a constant time window given by the slowest download. The purpose of the latter was to make a fair comparison between 10 MHz, 20 MHz and 10+10 MHz CA by capturing the current consumption of both the active reception and the following idle period.

K.3.3 Multiple application performance

Different application traffic profiles were tested with and without CA in order to identify the likelihood that certain traffic patterns will trigger CA usage. The multi-application profile includes web browsing across different web sites, a Skype video call and watching standard quality and high definition (HD) YouTube videos.

K.3.4 Impact of radio conditions

The final step in the analysis consisted in studying how different radio conditions on each CC affect the probability of CA being used, and how a coordinated packet scheduler and carrier selection algorithm can dynamically use both CCs in an efficient manner.

K.3.5 Theoretical Current Consumption Estimation

To estimate what can be expected from the measurements the power model from [30] is applied to scenario B presented above. In this scenario the UE is receiving a 1 GB file via FTP. The receiver current consumption depends mainly on the channel bandwidth and the throughput, and therefore an increase of 12-22% is estimated; see Table K.1, for the 20 MHz and 10+10 MHz cases compared to the 10 MHz. When the UE is not receiving data it can enter a low-current sleep mode which is the key to save energy. Because of the increased data rate in the 20 MHz and 10+10 MHz cases the UE is able to enter the sleep mode faster and therefore the power model predicts that energy consumption over a period, defined as the longest time it took in all the setups to receive the file, will be reduced 28-30%.

Table K.1: Estimated single-carrier (SC) and CA current consumption using the power model from [30].

Setup	SC 10 MHz	SC 20 MHz	CA 10+10 MHz
Throughput ¹	51.0 Mbps	92.0 Mbps	96.7 Mbps
Receive current consumption	398 mA	445 mA	487 mA
Current difference		11.8 %	22.4 %
Energy (1 GB, 185 s)	391 J	282 J	275 J
Energy difference		-27.8 %	-29.7 %

¹ Throughput numbers are based on the measurement results in Figure K.5.

Note that the absolute values are not realistic because the devices have improved significantly since the model was proposed. Furthermore, the idle current value does not match the one measured later because it depends on the paging cycle settings and UE implementation details. In section K.4 the actual current consumption is measured and in section K.5 compared with the simulated predictions.

K.4 Measurement Results

In this section the average current consumption and throughput measurement results for the four scenarios defined in section K.3 are presented.

K.4.1 Impact of carrier aggregation activation

The current consumed by the UE during RRC inactivity periods with 320 ms DRX cycle is shown in Figure K.3. When CA was activated the average current increased by 79% (21mA) compared to single-carrier 10 MHz, since the UE has to monitor the PDCCH and transmit periodic CSI reports for both carriers. The increment was reduced to 65% (17 mA) when CA was configured but not activated. In this case the UE only has to monitor the PDCCH and send CSI reports of the PCell. The higher current level compared to single-carrier measurements seems to indicate that during DRX cycles, the UE is actually switching ON and OFF radio capabilities for both bands, although it is only required to monitor the PCell.

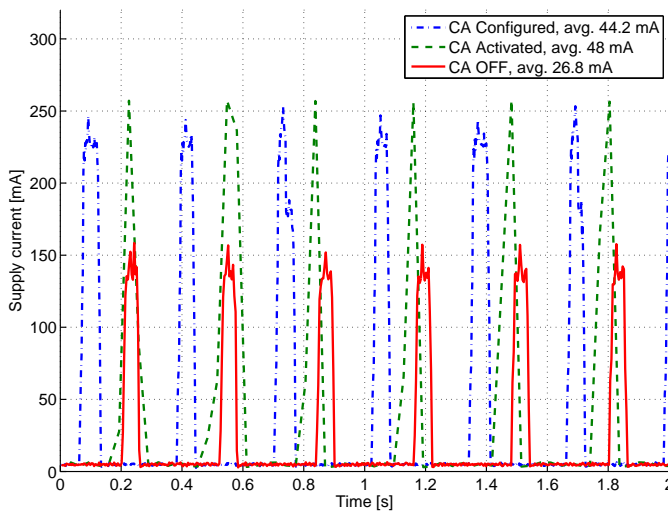


Figure K.3: Average current consumption during RRC inactivity timer with DRX.

K.4.2 Large data transmission

Figure K.4 presents the UE current consumption for a 1 GB FTP transfer. The red bar shows that with CA, the current consumption during the active transmission time, i.e. while the file was downloaded, increased by 61% compared to 10 MHz single-carrier. Furthermore, a similar increase was observed for 20 MHz single-carrier, indicating that current consumption increase is mainly related to the amount of resource blocks used. In other words, the baseband processing load seems to have a higher impact on the current consumption than the use of multiple RF chains.

However the higher throughput achieved when using CA allowed finalizing the data transfer and moving to RRC idle state approximately twice as fast, as illustrated in Figure K.5. The green bar in Figure K.4 represents the average current during a constant time window of 185 s, which is given by the slowest file download (the 10 MHz, No CA case). The averaged results over the time window show 13% energy efficiency improvement compared to single-carrier 10 MHz, because the UE can enter a low-current

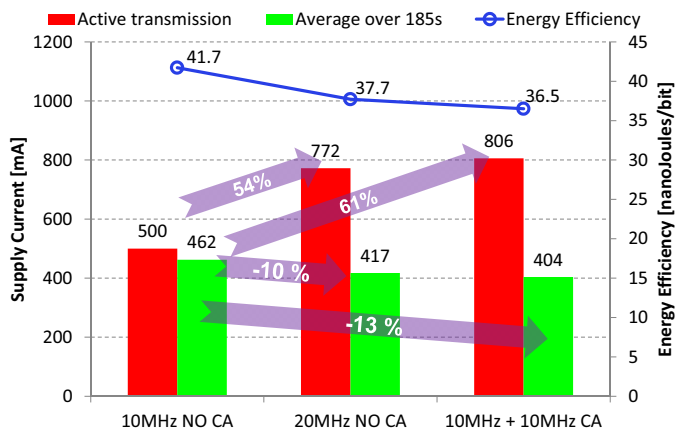


Figure K.4: Average current during 1 GB FTP download.

sleep mode while in RRC idle.

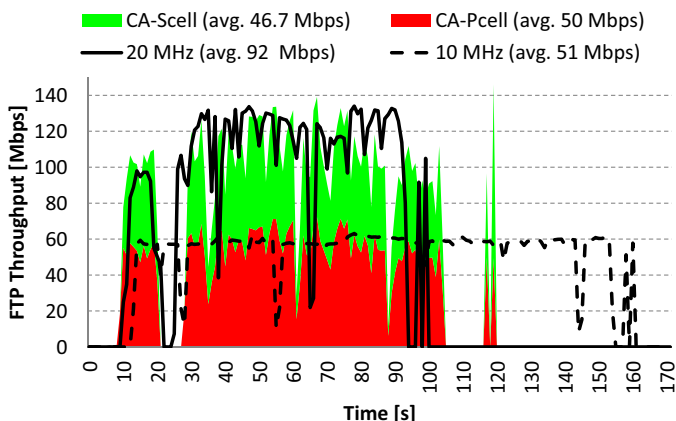


Figure K.5: Throughput vs. Time during 1 GB FTP download.

K.4.3 Multiple application performance

In this scenario popular applications were executed on the UE to see if they would trigger the usage of CA. It was observed that relatively low bit rate applications such as web browsing, Skype video call or even standard quality YouTube videos (750 kbps) were unlikely to trigger the activation of CA when UE was in good radio conditions and there was low load in the cell. CA was still configured at RRC level, but if the amount of buffered data was small, it was generally transmitted using only the PCell. Only HD YouTube video (2 Mbps) seemed to trigger the usage of CA in some occasions.

K.4.4 Impact of radio conditions

The same YouTube HD video was downloaded in good and bad radio conditions. Additionally, two cases were tested where the PCell was either stronger or weaker than the SCell. Bad radio conditions were generated by attenuating both PCell and SCell by 30 dB. Asymmetric conditions implied a 9 dB additional attenuation on either of the CCs. Figure K.6 shows the throughput and Physical Resource Block (PRB) allocation on both PCell and SCell in bad radio conditions. In this scenario both CCs were used by the packet scheduler, allocating up to an aggregated number of 100 PRBs during the initial video buffering time, and achieving a peak rate of 6 Mbps. After that, the PRB share among the PCell and SCell was approximately 50%. Even with a similar allocation of resources, the throughput achieved in the PCell was higher due to better quality experienced in band III, which allowed the usage of higher modulation and coding scheme.

Table K.2 summarizes the throughput and PRB usage on the PCell and SCell dur-

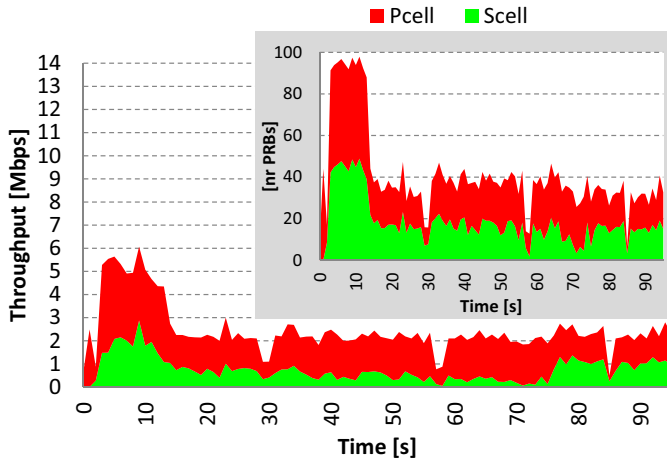


Figure K.6: HD YouTube video throughput and PRB usage in bad radio conditions. Note the results of the two cells are stacked.

ing the HD YouTube video playback. It can be observed how the stronger CC provides the higher throughput, even if that CC is the SCell. This represents the ability of the packet scheduler and carrier selection algorithm to assign resources dynamically and efficiently on each CC depending on the given channel conditions. Examining the last row of Table II it can be seen that with HD YouTube video the current consumption increased between 12% and 21% when 10+10 MHz CA was used, compared to single-carrier 10 MHz. The increase was more significant in bad radio conditions as a higher number of PRBs were used to cope with the video bit-rate requirements. In general, the total current consumption highly depends on the radio conditions of each CC.

Table K.2: Average throughput, PRB usage and current consumption per CC for HD YouTube video streaming.

	Good RF			Bad RF			Asymmetric RF	
	10 MHz band III	10 MHz band V	10+10 MHz CA	10 MHz band III	10 MHz band V	10+10 MHz CA	Pcell band V weaker band III	Pcell band V stronger band III
Average Throughput [Mbps]								
PCell	2.7	2.1	2.2	2.0	2.1	1.7	2.5	0.4
SCell			1.0			0.8	0.0	2.2
Total	2.7	2.1	3.2	2.0	2.1	2.5	2.5	2.6
Average PRB Usage [# of PRBs]								
PCell	2.9	1.8	1.5	22.3	33.5	22.7	13.8	2.4
SCell			0.7			18.2	1.1	2.2
Total	2.9	1.8	2.3	22.3	33.5	40.9	14.9	4.6
Average Supply Current [mA]								
	450	476	502	773	831	936	726	735

K.5 Discussion

LTE DL CA provides higher peak data rates, improves scheduling flexibility and brings inherent inter-carrier load balancing in multi-carrier LTE deployments.

In this analysis it was evaluated how CA is capable of reducing the average UE current consumption over a period of time when transferring large files. This enables network operators to use fragmented spectrum (10 + 10 MHz) instead of a contiguous 20 MHz band without harming the UE battery life.

However, with bursty traffic which doesn't benefit from the larger peak throughput, the additional cost of activating two (or more) receivers and monitoring different carriers may have a negative impact on the UE's stand by time. This increase is however not very different of what is observed when using 20 MHz of contiguous spectrum. An advantage of CA over 20 MHz single-carriers could come from intelligent decision on whether configuring CA can provide the most benefit.

Figure K.7 shows an estimation of the average current consumption and the battery life compared to single-carrier 10 MHz for an UE in stand-by mode with varying number of keep-alive events. The model assumes that one keep-alive event consists of a short 1 s transaction of only a few packets, followed by 10 s where the inactivity timer is running, and finally, the transition to the RRC_idle state. The current consumption in idle state is set to 6 mA based on measurements on the test UE, while the other current consumption values are based on Figure K.3.

The amount of background traffic that one UE generates depends significantly on

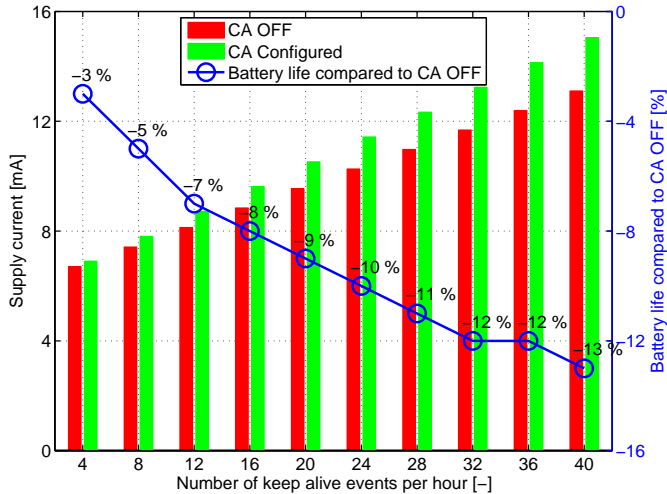


Figure K.7: Stand-by current estimation vs. keep-alive activity.

the operating system and the applications which are installed and running on that UE. Based on our internal studies, a much optimized smartphone with only basic services configured may generate as few as 2 to 4 events per hour, which would translate into a 3% battery life reduction, while an average smartphone with multiple applications installed may have 15 or more events per hour, yielding an 8% stand-by battery life reduction. Note the calculations are based on a 2600 mAh battery.

Finally the 1 GB FTP download measurements showed that the power model from [30] is too optimistic when compared to the measurements on the selected commercial device. The model predicted a current consumption increase of 22% when using CA, but the measurements showed the instantaneous increase is more than 60% and therefore an updated power model is proposed future work. Fortunately the measurements also confirmed that CA can provide higher data rates, and therefore the conclusion stating that the battery life can be prolonged due to increased sleeping opportunities is still valid.

It is also important to note that receiver's current consumption previously has been reported to contribute with less than 10% of the total UE current consumption [26], and therefore an increase even as big as 60% may not be as significant in the total perspective. This is however a very device specific observation because the total current depends heavily on the choice of the power amplifier and display components.

K.6 Conclusion

In this study we presented the first current consumption measurements on a commercial Carrier Aggregation (CA)-capable smartphone, and showed that CA can decrease the average current consumption thanks to increased data rates. Comparing 10 MHz

single-carrier and 10+10 MHz CA we observed a 90 % data rate increase in the given conditions, which resulted in 13 % lower current consumption when normalizing measurements over a common time window. The main reason is that the CA smartphone can move faster to a more energy efficient state as the data reception ends earlier with the provided higher data rates.

Our results also showed that configuring and activating CA can result in up to 21 mA current consumption increase compared to single-carrier transmission during RRC inactivity periods. For small data transactions, such as keep-alive message transmissions, this can result in up to 8 % battery lifetime reduction with typical keep-alive patterns.

Other studied traffic types, such as web browsing, or VoIP/video call are unlikely to trigger CA usage, especially in good radio conditions and empty cells since these applications are not too demanding in terms of data rates.

Finally, CA performance with a YouTube video streaming application was also evaluated. Results showed that downloading a high-definition video can increase the current consumption between 12 % and 21 % compared to 10 MHz single-carrier transmission depending on the radio conditions. It was also observed that the ability of the packet scheduler and carrier selection algorithm to efficiently allocate resources on each CC maximizes the performance.

Acknowledgement

The work is supported by Nokia and partly funded by the Danish National Advanced Technology Foundation and the 4th Generation Mobile Communication and Test Platform Project.

Appendix L

Ensuring Energy Efficient 5G User Equipment by Technology Evolution and Reuse

Mads Lauridsen, Gilberto Berardinelli, Troels B. Sørensen, Preben Mogenssen

The paper has been published in the
VTC Spring 2014

© 2014 IEEE

The layout has been revised.

Abstract

Research on fifth generation (5G) radio access technology (RAT) is ramping up, with the goal of significantly improving user data rates and latency compared to previous RAT generations. While energy efficiency (EE) of the user equipment (UE) was not a key optimization parameter for the current wireless standards, it is anticipated to become a distinguishing factor for 5G.

In this paper, we analyze established and emerging technological solutions for features such as waveform, frame structure, duplexing and multiple antenna transmission from an EE perspective. Our contribution is to identify and discuss the features' pros and cons in achieving high performance in terms of data rate and/or latency while limiting their effect on the UE power consumption.

Based on the discussion we give general recommendations for an energy efficient 5G design in the context of a previously proposed RAT concept.

L.1 Introduction

The large improvements in terms of data rate and latency from 2nd generation (2G) to 4th generation (4G) RAT have led to a significant increase in UE power consumption [13]. Recent measurements [26] showed a modern smartphone's cellular subsystem can consume half of the total power, and therefore a new energy efficient 5G RAT design may significantly improve the UE battery life.

Energy efficiency (EE), defined as the amount of energy required to transfer one byte of data, was identified as a key 5G requirement in [90], but until now little research has been devoted to UE EE. Current 5G projects such as METIS [93] and 5GNow [96] are following a clean slate approach to RAT design, and since EE is a significant design motivation for 5G it justifies a novel disruptive design. Conversely backwards compatibility requirements prohibit substantial changes to standards like Long Term Evolution (LTE), which is partly in a deadlock with several releases, providing limited EE improvements. For instance the LTE release 11 Enhanced Physical Downlink Control Channel (EPDCCH) even has a negative effect on EE.

The EE of existing RAT standards have been discussed in a few contributions. In [227], the impact of Radio Resource Management, deployment strategies, Multiple Input Multiple Output (MIMO) antenna technologies and Multiple Access (MA) schemes on the EE of the network was analyzed, but recommendations for future 5G designs were not provided. The impact of the EE improvement on other significant parameters such as bandwidth and network delay was discussed in [228]. However, [228] only focused on network power consumption due to its effect on global CO₂ emissions and operators expenditure, while omitting the effect on UE battery life.

In this paper, we provide concrete recommendations on the design of an energy efficient 5G RAT. We base our recommendations on a discussion, made with the UE EE perspective, of the main technology features of the previous RAT generations and emerging solutions. We then compare our recommendations with a 5G RAT, proposed in a conceptual form in [87]. The RAT design is still under research and therefore our EE recommendations, which among others include suggestions for choice of waveform,

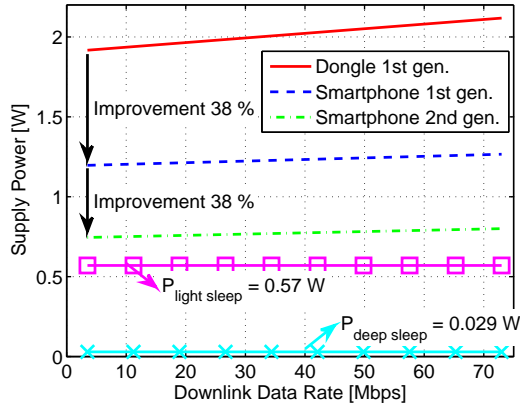


Figure L.1: UE power consumption based on [26, 25].

duplexing scheme, frame structure and interference management, are useful inputs to the researchers, such that their design can fulfil the 5G UE EE requirements.

The paper is structured as follows: sec. L.2 presents a discussion on the technology features adopted by the current RAT standards, with particular focus on their pros and cons from an UE EE perspective. The recommendations for an energy efficient 5G design are given in sec. L.3. Finally, sec. L.4 presents the conclusions and ideas for future work.

L.2 Energy Efficiency of existing RATs

This section presents a discussion on the most significant technology features of the existing RAT standards, with the aim of identifying their pros and cons in terms of UE EE. We refer to GSM release 7 as 2G, HSPA+ release 8 as 3G, and LTE release 11 as 4G, hence mature versions of the standards [95]. Tab. L.1 displays the main technology features of which we will discuss a selection in the following subsections.

L.2.1 Bandwidth and Data Rate

The downlink (DL) demodulation complexity has increased steadily with the introduction of each RAT generation due to higher order modulations and increased bandwidth; 200 kHz (2G), 5 MHz (3G), 20 MHz (4G). The possibility of boosting the data rate enabled by the larger bandwidth induces a faster baseband processing at both transmitter and receiver, hence higher power consumption. Fig. L.1 illustrates the evolution of the supply power as a function of the DL data rate for three generations of LTE devices. The dongle measurement is from our first LTE measurements made in 2011 [25], while the measurements on the smartphone 1st generation [26] and on the recently released smartphone 2nd generation were made in 2012 and 2013, respectively. Increasing the data rate by a factor of 10 only increases the power consumption by 10%. This entails the UE can receive a data file much faster and then turn off its receive chain i.e. enter a

Table L.1: Overview of key Radio Access Technology Parameters. (cl refers to the UE class)

Method	2G	3G	4G	5G
Specification	GSM rel. 7, band 850/900	HSPA+ rel. 8	LTE rel. 11	5G concept [87]
Duplex	FDD, HD	FDD, FD (some TDD exist)	FDD, FD (some TDD exist)	TDD (synchronization needed)
Multiple access	TDMA/FDMA	CDMA	OFDMA	OFDMA
Bandwidth	200 kHz	5 MHz	1.4-20 MHz	10-200 MHz
Frame/subframe size	4.615 ms (comprising 8 slots) / -	10 ms / 2 ms	10 ms / 1 ms	- / 0.25 ms
Equalizer	Time	Time	Frequency	Frequency
Antennas	2 Rx, 1 Tx	2 Rx, 1 Tx	4 Rx, 4 Tx	4 Rx, 4 Tx
Control/data pos.	Initial paging, then fixed BW	One slot spacing	No gap	One frame offset
Sleep mode	CM DTX	CM DTX+DRX	CM DTX+DRX	CM DTX+DRX
Frequency reuse	3 (varying)	1	1	1
DL modulation	GMSK, 8PSK, 16QAM, 32QAM	QPSK, 16QAM, 64QAM	QPSK, 16QAM, 64QAM	LTE like
Multiple carriers	2	2	5	Possible
Link Adaptation	AMC using RxQual	AMC using CQI	AMC using CQI	AMC
UL modulation	GMSK, 8PSK, 16QAM, 32QAM	QPSK, 16QAM	QPSK, 16QAM, 64QAM	LTE like
UL PAPR	3.2 dB	6-8 dB	11 dB	LTE like
Max. UL transmit power (sum of antennas)	33 dBm (cl4) +/-2 dB, -3 to -9 dB if 2-8 time slots are allocated	24 dBm +1/-3 (cl3), additionally CuM-1 for some channels	23 dBm +/-2 dB (cl3), -1 to -2 dB depending on MCS and #PRBs	10-15 dBm per antenna
Min. UL power	5 dBm +/- 5 dB	-50 dBm	-40 dBm	-20 dBm
Dynamic range	28 dB	74 dB	63 dB	~30 dB
UL power control	2 dB step, 16.67 Hz	1, 2, 3 dB step, 1500 Hz	FPC, open+closed loop, ≤1000 Hz	Not yet specified

low power sleep mode to conserve energy. The EE of the 2nd generation 4G smartphone is $\sim 0.8 \text{ W}/10 \text{ Mbps} = 80 \text{ nJ/bit}$, whereas 2G achieves $3.5 \mu\text{J/bit}$ and 3G 450 nJ/bit [229, Fig.8], hence the increased data rate has a positive effect on UE EE.

This is also the case when using multiple carriers as shown in [30]. Downlink Dual Carrier (2G), Dual Cell (3G) and Carrier Aggregation (4G) have been defined to enable the UE to connect to multiple carriers and achieve a load balancing gain, resulting in improved capacity and data rates. The cost, which affects the power consumption, is the need for a second receiver and an extra Local Oscillator if the multiple carriers operate in different frequency bands.

Fig. L.1 also shows that, when moving from one generation to another, the power consumption is reduced by a factor of $\sim 38\%$. This is partly due to technology node scaling, i.e. voltage scaling and reduction of switched capacitance, which according to Intel [230] will continue. Previously, [78] has predicted a similar power reduction of 30-40% per node change. The reduction is also due to device maturity i.e. the chipset design is optimized throughout the standard's lifetime.

L.2.2 Sleep Modes

In the previous section it was discussed how higher data rates allows the UE to power off its receive chain and enter sleep mode. Several types of sleep mode have been defined in the RAT standards. They can be divided into two groups where the UE is either in Idle or Connected mode.

In Idle mode the UE is unable to receive or transmit data. Instead it performs measurements on neighbor cells and monitors system information and a periodic paging channel, which notifies it about incoming calls. To save energy the UE only monitors a subset of the channels and sleeps for the rest of the period. This sleep mode is called Idle mode Discontinuous Reception (DRX), and is available in all the RAT generations.

The 2G standard includes the Connected mode Discontinuous Transmission (CM-DTX), because 2G was mainly designed for voice calls where silent periods are frequent. To save energy the UE can choose not to transmit any information during these silent periods that are identified by a Voice Activity Detection mechanism [231]. The CM-DTX also reduces the interference footprint in the network.

The initial 3G specifications did not include CM-DTX, thus forcing the UE to transmit the control channel even when no user data was available. However, later 3G releases re-introduced this feature. Later Connected mode DRX (CM-DRX) was implemented with the aim of saving energy in the receiver, because the need for receive energy savings became apparent as the amount of DL data increased.

The 4G standard includes both CM-DRX and CM-DTX, because it is focused on packet switched data, which can handle the inherent delays introduced by sleeping. Different CM-DRX settings may lead to light or deep sleep modes; measurements [26] on LTE UEs using CM-DRX have shown that the deep sleep power consumption is 30 mW (see fig. L.1), which corresponds to $1/35$ of the active mode power. The 4G frame structure also allows for micro sleep, see sec. L.2.6.

L.2.3 Duplexing

The term duplexing describes a point-to-point system where communication can flow in both directions. The duplexing method affects the energy consumption due to hardware requirements and the impact on data rate and latency.

The 2G RAT utilizes Frequency Division Duplexing (FDD) and Half Duplexing (HD); i.e. communication can only flow in one direction at a time, and different carrier frequencies are used for the DL and the uplink (UL). Therefore the duplexer in the Radio Frequency (RF) Front End (FE) can be removed, resulting in a lower component cost and a lower attenuation between the antenna and the RF FE [103]. Lower attenuation allows the Power Amplifier (PA) to reduce its transmit power, with benefits in terms of overall power consumption. The drawback of HD is the need for guard time to avoid power leakage of the transmitter into the receive slot. The guard time is pure overhead and therefore has a negative effect on EE. The 3G RAT is mostly deployed as FDD but utilizes full duplexing (FD) i.e. simultaneous transmission and reception, and therefore a duplexer is needed. Conversely, the guard time is substituted with a guard band in frequency. Furthermore the combination of FDD and FD entails strict Third-Order Intercept Point (IP3) requirements, because the UE's transmit signal can be mixed with external signals leading to a blocker in the receive band. Improving the IP3 performance leads to increased UE power consumption. In 4G both FDD and Time Division Duplexing (TDD) have been specified; TDD is by default HD since UL and DL transmissions are scheduled in different time slots, while the FDD design allows for FD.

L.2.4 Uplink Waveform

The UL modulation scheme choice impacts the Peak to Average Power Ratio (PAPR), which affects the obtainable PA efficiency. High PAPR forces the PA to operate far from its saturation point; this increases the dissipation of DC supply power and therefore impacts the EE as illustrated in fig. L.2. If the PA is saturated the signal is distorted and out-of-band harmonics occur, which impacts the Adjacent Channel Leakage Ratio (ACLR). Increased ACLR affects data rates negatively and thus the EE due to decreased sleeping opportunities.

In the first version of 2G the Gaussian Minimum Shift Keying (GMSK) modulation was used. Since the GMSK pulse has a constant envelope [103] the PA can operate close to the saturation region, where the EE peaks as shown in fig. L.2. However, the GMSK waveform suffers from low spectral efficiency since only 1 bit/symbol is supported. In current 2G RAT versions higher level PSK is used to increase the data rate. The cost is increased sensitivity to distortion and therefore Output Back Off (OBO) is applied to ensure operations in the linear region as shown in fig. L.2.

Initially, the 3G waveforms had PAPR properties similar to the 2G waveforms, but later releases have led to a higher PAPR due to the introduction of more advanced UL channels as shown in fig. L.3. Furthermore, the Code Division MA (CDMA) scheme used in 3G is often coupled with the Rake receiver whose complexity increases with the number of multipath components and antennas. This increases the baseband processor power consumption [78]. As in 2G, the bandwidth is not scaled with respect to the needed data rate.

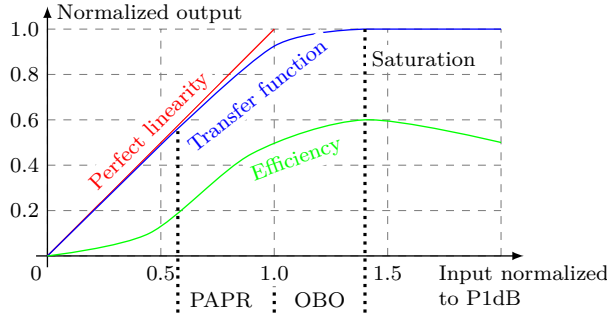


Figure L.2: Power amplifier operation, based on [103, Fig. 2.30].

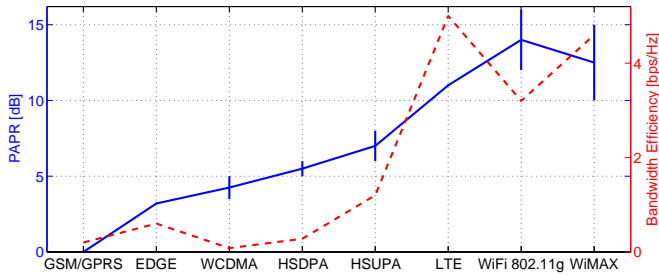


Figure L.3: UL PAPR evolution, based on data from [103].

In 4G DL, the usage of Orthogonal Frequency Division Multiplexing (OFDM) has led to significant computational complexity reduction due to the efficient single-tap equalization in the receiver [59]. However, OFDM has a large PAPR due to the possibility of co-phasing multiple narrowband signals in the time domain. The usage of Single Carrier-Frequency Division Multiplexing (SC-FDM) in 4G UL decreases the PAPR compared to OFDM up to 4 dB. Unfortunately SC-FDM suffers from noise enhancement at the receiver which degrades the link performance [105] thus lowering the data rate and EE as discussed in sec. L.2.1. Furthermore, the PAPR of SC-FDM increases with high order modulations such as 64QAM, but a significant improvement over OFDM is preserved.

L.2.5 Transmit Power and Control

The UE transmit power obviously affects the overall UE power consumption, because the PA is the major power consumer in the UE cellular subsystem [26].

The high transmit power of 2G (33 dBm) is necessary because the UE is active only in one out of eight slots [231]. In later releases the UE was allowed to occupy a larger set of time slots, and therefore reduce its transmit power to achieve the same detection performance as shown in tab. L.1.

In 3G the transmit power is 24 dBm, but since the RAT is FDD and FD the average transmit energy is the same as for 2G. Due to the mentioned PAPR increase from WCDMA to HSUPA, see fig. L.3, the maximum transmit power was reduced in order to

enable reuse of the previous releases' PAs. The reduction is based on the Cubic Metric (CuM) [232] which represents a measure of the expected intermodulation distortions introduced by the PA. This can lower the PA power consumption because the transmit power may be reduced by 1 dB, for $0 \leq \text{CuM} \leq 3.5$ dB, [233].

The maximum transmit power of 4G is 1 dB lower than 3G. The allowed transmit power reduction is 0-2 dB [145] and it depends on the Modulation and Coding Scheme (MCS) and the number of allocated resource blocks in the channel.

If the transmit power is not adjusted to a specific scenario's needs energy is wasted and the battery time reduced; an UL power control (UPC) technique is therefore critical for EE. Slow UPC is applied in 2G because the Time Division MA (TDMA) / Frequency Division MA (FDMA) + FDD structure ensures zero intra-cell interference. Slow UPC lowers the control overhead, but may result in high transmit power because it only adapts to pathloss and shadow fading. Furthermore excessive transmit power increases inter-cell interference.

The near-far CDMA problem in 3G leads to the necessity of using a faster UPC; its rate is fixed at 1500 Hz with steps of 1, 2, and 3 dB. By using a fast UPC the UE can track the channel conditions (fast fading) at the expense of a large control overhead. The UPC is closed loop because for FDD the channel is not reciprocal, hence the UE needs to inform the base station (BS) of the channel condition perceived in the DL and vice versa for the UL.

In 4G the UPC can update every ms, but the average rate is estimated to be 50-200 Hz depending on the channel type and conditions. The UPC consists of an open loop, where the UE compensates for a fraction of the experienced pathloss based on parameters which are set by the network, and a closed loop where the network dictates power adjustments until a certain Signal-to-Interference-plus-Noise-Ratio (SINR) is achieved.

L.2.6 Frame Structure

The frame duration, more specifically the time domain scheduling granularity, has been reduced with the introduction of every new RAT generation from 4.615 ms (2G) to 1 ms (4G). Shorter frame size entails a lower latency, but may also result in a larger overhead in case each frame preserves the same amount of control information. As described in sec. L.2.1 it is beneficial to transfer data as fast as possible, and therefore it is important to minimize the control overhead.

The relative position of control and data channels affects the control channel decoding procedure, which is used to determine if the UE is scheduled or can power down.

Initially 2G was designed as a circuit switched RAT, where a certain amount of resources was allocated to the user for the entire call duration even though the user might not need such resources in every slot. Later releases introduced packet switched data while preserving dedicated channels for each session. For instance, the UE can be allocated slots 0-3 of every TDMA frame, but they may be unused causing excessive power consumption due to reception of useless data.

In 3G, the High-Speed Shared Control Channel (HS-SCCH) is used to provide information to the UE on how to demodulate the High-Speed Downlink Shared Channel (HS-DSCH) [78]. The HS-SCCH is located in slot n and $n+1$, while data is in slot $n+2$ and onwards as illustrated in fig. L.4a. The first part of slot n indicates the modulation

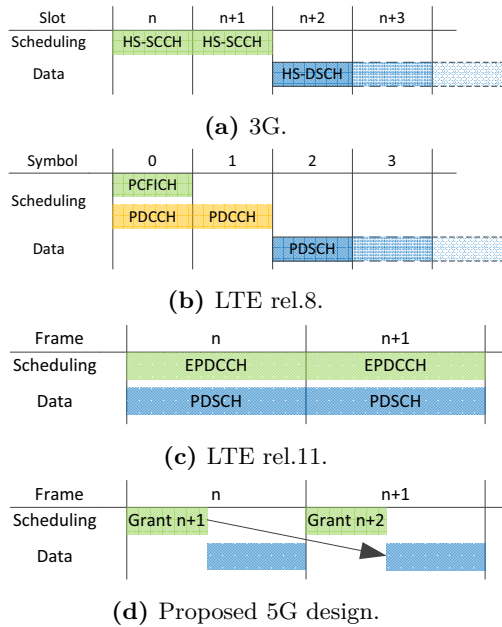


Figure L.4: Control/data channel position.

format and which data codes the UE must despread. The second part, in slot $n+1$, contains redundancy information, Automatic Repeat Request (ARQ) process number and a retransmission indicator. This design is beneficial from an energy consumption perspective, because it informs the UE of the necessity of decoding the data mapped in slot $n+1$ and onwards upon detection of slot n . This eliminates the buffering of unused data.

In 4G the UE decodes the Physical Control Format Indicator Channel (PCFICH), which indicates the number of symbols used for the Physical Downlink Control Channel (PDCCH) [59]. Simultaneously, the UE receives and decodes the PDCCH which reports the used MCS and the location of the potentially allocated resources. The PDCCH is immediately followed by the Physical Downlink Shared Channel (PDSCH), which carries data. The UE needs to buffer PDSCH because there is no time available for decoding between the allocation indication and the actual data, as illustrated in fig. L.4b. The micro sleep concept [28] has been introduced with the aim of minimizing the energy waste in case of unused buffered data. The main idea of the micro-sleep is to perform fast decoding of the control channel, and then power down the receiver in case the UE has no scheduled data. The cost is that the Reference Signals which are allocated at the end of the subframe are not received. This may lead to a degradation in the channel estimation, which may affect the throughput.

In LTE release 11 the EPDCCH has been standardized. The idea is to achieve a frequency selective scheduling gain by allocating the EPDCCH across an entire frame (see fig. L.4c) and limit it to the frequency subcarriers which experience the most advantageous channel conditions. However, the expected SINR improvement comes at the

expense of higher power consumption, since the usage of micro sleep is made impossible.

L.2.7 MIMO

The usage of multiple receive antennas entails the UE can exploit receive diversity to improve the link budget, but also enhances the interference cancellation/mitigation capability. Furthermore the BS can transmit multiple data streams to boost the data rate. The power consumption will increase with the introduction of the extra RF circuitry which is needed to accommodate multiple transmit/receive chains. Furthermore MIMO requires larger baseband processing capabilities to deal with multiple data streams. However, as explained in sec. L.2.1 the increased data rate leads to longer, efficient sleep modes.

In 2G the UE receive diversity is specified, while 3G and 4G allow for both receive diversity and DL multistream MIMO. Even though a maximum of 4 streams is specified in 4G, the number of codewords is limited to 2; this enables the implementation of Successive Interference Cancellation (SIC) receivers with feasible complexity. Newer versions of 4G also include transmit diversity and UL multistream MIMO.

L.2.8 Frequency Reuse and Interference

Frequency Reuse is a widely used technique for dealing with inter-cell interference. The presence of interference may severely limit the data rate, thus also affecting the energy consumption since UEs need longer active time for transmitting/receiving their data as discussed in sec. L.2.1.

In 2G a frequency reuse factor of 3 or more is used. This allows for significant reductions of the inter-cell interference experienced by the cell edge users at the cost of a lower spectral efficiency from a system perspective. Intra-cell interference can also occur if the frequency channels are not properly filtered; since the potential improvement in SINR translates to higher data rates, interference cancellation techniques have been proposed. The widely used Single Antenna Interference Cancellation method has feasible complexity [234].

In 3G reuse factor 1 is applied, hence the users can experience interference from neighbor cells. Since the spreading codes adopted by neighbor BSs are not completely orthogonal, the users may experience Multiple Access Interference (MAI). UEs can apply interference cancellation/mitigation methods, which estimate and subtract the interference from the desired signal. As in 2G, these methods have high complexity, but also significant advantages when the MAI is high [78].

The 4G RAT primarily applies a frequency reuse factor of 1 and therefore cell edge users may experience inter-cell interference. Methods such as soft and fractional frequency reuse have been proposed [59] along with the previously discussed power control strategies.

L.3 Recommendations for EE 5G

A 5G RAT shall be designed with the aim of minimizing the power consumption at the UE while maintaining high performance in terms of data rate and latency. In the

light of the discussion on the technology features presented in the previous section, we now provide our recommendations, summarized in tab. L.1, for an energy efficient 5G design.

Our target 5G RAT was proposed in a conceptual form in [87]; since the envisioned design has not yet been finalized, we believe that our EE recommendations can significantly influence it. The concept aims at peak data rates of 10 Gbps, short latency below 1 ms and wake-up time from inactive to active in the order of 10 ms. The ambitious data rate requirement is to be achieved by using a 200 MHz bandwidth, TDD mode, a frame of 0.25 ms and multistream transmission, as well as established technology features such as Adaptive Modulation and Coding (AMC), Hybrid ARQ (HARQ), and efficient time/frequency scheduling. Since most of the data traffic is expected to be generated in an indoor environment, the 5G RAT will be optimized for a local area (LA) scenario rather than for macro area as is the case for the 4G RAT.

TDD has clear cost advantages over FDD as duplex mode for 5G as it allows for a flexible spectrum assignment (no need for paired spectrum as in FDD), flexible duplexing of UL and DL, which is beneficial for asymmetric data, and simple support for backhauling and device-to-device communication. Its drawback is the need for a tight time synchronization to avoid mutual interference among UEs due to a misaligned UL/DL switching point. From an energy consumption perspective, TDD allows for discarding of the duplexer, which reduces the insertion loss in the RF FE by up to 3 dB (in both directions). Furthermore, in TDD mode the UE's transmit signal is not present during reception, hence the IP3 requirements can be relaxed since the undesired harmonics will not interfere the reception, with benefits in terms of power dissipated in the mixer. In addition, the possibility of exploiting the channel reciprocity between UL and DL may avoid the transmission of channel feedback from the UE to the BS, thus also saving transmit power.

Research on novel modulation/MA schemes for 5G is ongoing. For instance Non-Orthogonal MA, which combines Superposition Coding and OFDM [106], has drawn attention. This scheme requires a complex SIC receiver as baseline detector, and its EE properties are still unclear. Moreover, the Superposition Coding principle works best when the channel gain difference between UEs is large, which may not be the case in the LA scenario targeted by 5G [87]. The Filter Bank Multicarrier (FBMC) modulation [235] can be seen as a generalization of OFDM where the simple square window which is applied at each subcarrier, is replaced by a filter. FBMC allows removing the Cyclic Prefix and significantly reduces the out-of-band emissions. However, the computational complexity and thus the power consumption is significantly larger due to the time domain processing; moreover, the extension to MIMO is not as straightforward as in OFDM.

The usage of OFDM on both link directions allows for efficient resource allocation and UE implementation. The high PAPR, which represents the main drawback of OFDM modulation, should not be considered a significant limitation in the future. The reason is that novel techniques for the supply of PAs have gained attention and could considerably improve PA efficiency. One technique is Envelope Tracking (ET), which adjusts the PA supply voltage in accordance with the input signal (the modulated low power signal) to allow the PA to operate closer to the saturation region. According to [141] 20 MHz bandwidth is already supported, but it is an open question when and how

the 200 MHz 5G bandwidth can be accommodated. If ET is realisable, the PAPR effect on the PA power efficiency is minimal hence OFDM can be implemented in an energy efficient manner.

When considering the benefits in terms of complexity and flexibility of OFDM and the reduced impact of its PAPR drawback, we believe OFDM modulation is the strongest candidate for energy efficient 5G.

While the 5G RAT is expected to be similar to the 4G standard for what concerns multiplexing and modulation format, the major difference is the 10 times increase in bandwidth. Moreover, 256QAM modulation is intended to be included to boost the spectral efficiency in favorable channel conditions. The larger bandwidth is not believed to impose a complexity problem. The reason is that the complexity of LTE scales linearly with the bandwidth [59], and the same is expected for an OFDM-based 5G RAT. Furthermore, the turbo decoding complexity is a linear function of the data rate [59]. The complexity of the 5G RAT is therefore expected to be 10 times higher, but if Moore's law continues to be valid the performance is supposed to increase by a factor of 10 – 30 within the next decade, i.e. the complexity can be handled. Similarly, the power consumption is not expected to be affected due to Gene's law [132], which states the power dissipation per Million Instructions Per Second is halved every 18 months.

Note that, as the bandwidth becomes larger, the attenuation of the adjacent channels decreases. The reason is that wideband analog filters have a larger transition bandwidth with respect to narrowband filters. The related out-of-band emissions on the adjacent channels affect the dynamic range of the Analog to Digital Converter (ADC), which may cause it to consume more power. The baseband complexity is also increased because better digital filters are needed to remove the unwanted signals. Conversely, the wider bandwidth is not expected to have a significant effect on the RF power consumption.

A potential reduction of the maximum transmit power to the range 10-15 dBm, has to be taken into consideration given the LA scenario targeted by 5G. This would lead to huge power savings, and possibly to the removal of the external amplifier stage in current UE transmitters. In addition to the power savings this could entail less costly and less bulky UEs. We believe the UPC for 5G should be similar to 4G, because it represents a good tradeoff between control overhead and SINR control, with no significant penalty on the power consumption.

Clearly the control data channel design of 3G results in better energy efficiency when compared to 4G (as shown in fig. L.4a and L.4b), since useless data is not buffered. Therefore the 5G frame structure should be designed such that the scheduling information for frame $n+1$ arrives in frame n as illustrated in fig. L.4d. This allows the UE to determine in adequate time whether it is scheduled or not, hence it can power down and save energy when possible. The cost is an increased delay, but due to the short frame size this is not a major issue. The CM-DRX and CM-DTX sleep modes should also be included given their obvious power reduction benefits. It is worth to mention that the usage of deep sleep modes may however increase the latency since the UE needs to spend some time waking up, before tight synchronization can be re-acquired. The design of energy efficient wake up and re-synchronization methods are important further studies.

When 5G is ready for deployment it is expected that the technological evolution allows for 4x4 MIMO implementation in the UE. The multistream transmission boosts the data rate, and therefore increases the sleeping opportunities. We foresee that the

low power sleep will compensate the extra power consumed by the extra RF circuitry and baseband processing.

The 5G RAT envisioned in [87] targets LA scenarios with uncoordinated deployment of small cells; in such scenarios inter-cell interference is a significant limiting factor. In case neighbor cells are time synchronized, such interference can be suppressed/cancelled by using Interference Rejection Combining (IRC) or SIC receivers. The usage of advanced receivers obviously leads to increased complexity, which however translate again to the possibility of boosting the data rate and then increase the sleeping opportunities. This can also be accomplished by autonomous interference coordination techniques; 5G BSs can sense interference from neighbor cells and select their frequency resources accordingly, as well as notify their neighbors about the interference they may generate.

Based on this discussion we conclude that a future 5G RAT can be made energy efficient, and that the proposed concept [87] is beneficial from UE EE perspective. It is however important that UE EE is included as a design parameter in the clean slate designs, and not only as a buzz word.

L.4 Conclusions and future work

The 5th generation (5G) radio access technology aims at increased user data rates and lower latency compared to the previous generations, while reducing the user equipment (UE) power consumption. In this work existing technology features, generally recognized as necessary for achieving the 5G requirements, have been discussed considering their effect on UE energy efficiency. Based on that we gave recommendations for an energy efficient design of a previously proposed 5G concept, which is still under research.

We foresee significant advantages in the usage of TDD mode given the related simple and low power hardware design. Multiple access based on OFDM has several advantages such as low computational complexity and considering the ongoing improvements in power amplifier efficiency, the large PAPR can be handled with good UE energy efficiency. We further predict that the local area scenario targeted by 5G allows for a significantly lower transmit power, with obvious benefits on the overall power consumption. Features like MIMO antenna schemes and multiple carrier transmission allow shortening the active time of the device; this leads to higher energy efficiency, by use of low power sleep modes, despite of the increased computational complexity. Finally, a novel control channel design allows for effective micro sleep, which has to be supplemented with Discontinuous Reception and Transmission sleep modes.

We predict that the main key to achieve high UE energy efficiency in 5G is the combination of high data rates and low power sleep modes.

Future open problems, from an energy efficiency perspective, include the design of low complexity interference cancellation receivers, sleep mode and synchronization procedures, as well as the analysis of the wide bandwidth's effect on the power consumption of Analog to Digital Converters and filters.

Acknowledgement

The work is partly funded by the Danish National Advanced Technology Foundation and the 4th Generation Mobile Communication and Test Platform project.